Senescence-associated P_4-type ATPases in the model plant *Arabidopsis thaliana*

Dissertation

zur Erlangung des akademischen Grades des

Doktors der Naturwissenschaften (Dr. rer. nat.)

eingereicht im Fachbereich Biologie, Chemie, Pharmazie

der Freien Universität Berlin

vorgelegt in englischer Sprache von

Tilbert Kosmehl

geboren in Weissenfels

März 2010

1. Gutachter: Prof. Dr. Reinhard Kunze

2. Gutachter: Prof. Dr. Bernd Müller-Röber

Tag der Disputation: 29. Juni 2010

生活的禅意生命的教育

Results of this thesis are being prepared for publication:

“ALA1 a plastid localized P_4-type-ATPase in *Arabidopsis thaliana*”
T. Kosmehl and R. Kunze.

Index

Figures

Tables

Abbreviations

°C	degree Celsius
A	ampere, also adenine
ABC	ATP-binding cassette
A. thaliana	*Arabidopsis thaliana*
A. tumefaciens	*Agrobacterium tumefaciens*
AB	antibody
ADP	adenosine diphosphate
ALA	aminophospholipid ATPase
ALIS	ALA interacting subunit
app.	approximately
ASG	acylated steryl glucoside
ATP	adenosine triphosphate
ATPase	adenosine triphosphatase
BAP	benzyl aminopurine
bp	base pair
BSA	bovine serum albumin
c	centi
C	cytosine
CAB	chlorophyll a/b binding protein
cDNA	copy deoxyribonucleic acid
CER	ceramide
CIAP	calf intestine alkaline phosphatase
CoA	coenzyme A
CSPD	disodium 3-[4-methoxyspiro{1,2-dioxetane-3,2'-(5'-chloro)tricyclo [3.3.1.1]decan}-4-yl]phenyl phosphate
CT	cycle number (reaching a de fined threshold)
CTAB	cethyl trimethyl ammonium
CTP	cytidine triphosphate
d	day, also deoxy
Da	dalton
DAG	days after germination, also diacylglycerol
ddH2O	double distilled water
DEPC	diethyl pyrocarbonate
DGD	digalactosyldiacylglycerol
dGTP	deoxyguanosine triphosphate
di-17:0	1,2-diheptadecanoyl-sn-glycero-3-phospho-
DIG	digoxygenin
DMSO	dimethylsulfoxide
DNA	deoxyribonucleic acid
DNase	deoxyribonuclease
dNTP	deoxynucleotide triphosphate
DTT	dithiothreitol
E. coli	*Escherichia coli*
e.g.	*exempli gratia*; for example
EDTA	ethylenediamine tetraacetic acid
eGFP	enhanced GFP
ER	endoplasmatic reticulum
et al.	*et alii*; and others
F_0	minimum fluorescence
FA	fatty acid
FACS	fluorescence-activated cell sorting
FAME	fatty acid methyl ester
FID	flame ionization detection
F_{max}	maximum fluorescence
F_v	variable fluorescence
FW	fresh weight
g	gravity, also gram
G	guanidine
GAL	galactose
GC	gas chromatography
GFP	green fluorescent protein
GL	glycolipid
GLU	glucose
GUS	β-glucuronidase
h	hour
HDL	high-density lipid protein
HEPES	4-(2-hydroxyethyl)-1-piperazine-ethanesulfonic acid
His	histidine
Hz	hertz
i.e.	*id est*; that is
IPTG	isopropyl β-D-1-thiogalacto pyranoside
k	kilo
kb	kilo base (pair)
kDa	kilodalton
KOH	potassium hydroxide
l	liter
LB	left border, also Luria-Bertani
LDL	low-density lipid protein
LP	left primer

m	meter, also mili
M	molar
MES	2-(N-morpholino) ethanesulfonic acid
MGD	monogalactosyldiacylglycerol
min	minute
MOPS	3-(N-morpholino) propanesulfonic acid
mRNA	messenger RNA
MS	Murashige-Skoog
MTBE	methyl tertiary butyl ether
MW	molecular weight
n	nano, also number
N	normality
N. benthamiana	*Nicotiana benthamiana*
NaOH	sodium hydroxide
NBD	2-(6-[7-nitrobenz-2-oxa-1,3-diazol-4-yl]-amino)hexanoyl
nt	nucleotide
ø	diameter, also mean
OD	optical density / extinction
ORF	open reading frame
P	probability
PA	phosphatidic acid
PAGE	polyacrylamide gel electrophoresis
PAM	pulse amplitude modulation
PBS	phosphate buffered saline
PC	phosphatidylcholine
PCR	polymerase chain reaction
PE	phosphatidylethanolamine
PEG	polyethylene glycol
PG	phosphatidylglycerol
pH	power of hydrogen
P_i	(inorganic) phosphorus
PI	phosphatidylinositol, also propidium iodide
PL	phospholipid
PM	plasmamembrane
PMSF	phenylmethylsulphonyl fluoride
PS	phosphatidylserine
PVDF	polyvinylidine difluoride
PVP	polyvinylpyrrolidone
QRTPCR	quantitative real-time PCR
QY	quantum yield
RCB	Rubisco-containing body
RNA	ribonucleic acid
RNase	ribonuclease
RP	right primer
rpm	rounds per minute
rRNA	ribosomal RNA
RT	reverse transcription, also room temperature
Rubisco	ribulose-1,5-bisphosphate carboxylase oxygenase
RVB	Rubisco-vesicular body
S	sedimentation coefficient
S. cerevisiae	*Saccharomyces cerevisiae*
S.D.	standard deviation
SAG	senescence-associated gene
SATP	senescence-associated transporter
SAV	senescence-associated vacuole
SDS	sodium dodecyl sulphate
sec	second
SG	steryl glucoside
SM	sphingomyelin
SQD	sulfoquinovosyldiacylglycerol
T	thymine
Taq	*Thermophilus aquaticus*
TBS	Tris buffered saline
T-DNA	transfer-DNA
TEM	transmission electron microscopy
TF	transcription factor
TLC	thin layer chromatography
TM	transmembrane domain
TP	tonoplast
Tris	tris(hydroxymethyl)aminomethane
TTP	thymidine triphosphate
u	unit
USA	United States of America
UTP	uridine triphosphate
UV	ultraviolet
V	volt
v/v	volume per volume
vol	volume
w/v	weight per volume
WT	wild type
X-Gluc	5-bromo-4-chloro-3-indolyl-β−D-glucoronid
µ	micro

1 INTRODUCTION

Aging and death thrilled humans ever since. Questions of how and why humans age have great intellectual appeal and major societal implications. To investigate and, thus, understand the aging process is of great importance. Researchers are drawing the intention not only to humans but also to other living beings, such as plants, in order to obtain insights in aging processes of other living systems. Senescence, the process of aging, defines biological changes related to age. Examination of senescence and its molecular background is fundamental in order to understand more about life as such.

1.1 Senescence

Senescence is an important phase within plant development leading to death of single cells, tissues, organs and in the end the whole organism. The process can be described as transdifferentiation rather than deterioration (Thomas *et al.*, 2003). Due to the high complexity and tight regulation, senescence is distinct from programmed cell death although finally leading to death (Gan and Amasino, 1997; van Doorn and Woltering, 2004; Zimmermann and Zentgraf, 2005; Lim *et al.*, 2007). Programmed cell death describes rather fast cell death (e.g. hyper-sensitive response) that is limited to single cells or certain cell types (e.g. tracheary elements), whereas senescence occurs at an organ-wide level with much lower speed (Lim *et al.*, 2007). Several forms of senescence exist: monocarpic senescence (senescence followed after completion of the reproductive phase of a monocarpic plant), fruit ripening, and senescence of cotyledons, flower organs and specialized tissues. Leaf senescence represents the best-studied and most obvious form and is described as follows.

1.2 Leaf senescence

The last phase of leaf development constitutes leaf senescence, which has evolved as a process to salvage nutrients from older leaves and thus increasing plant fitness (Leopold, 1961; Bleecker, 1998). It is a genetically regulated developmental program involving sequential events at the molecular, physiological and morphological level

(Figure 1). The result of this recycling process is the coordinated degradation of macromolecules and the subsequent mobilization of nutrients like nitrogen, phosphorus, sulfur and minerals from senescing tissues into other developing parts of the plant (Noodén, 1988; Buchanan-Wollaston and Ainsworth, 1997; Himelblau and Amasino, 2001).

Natural senescence is endogenously controlled by the developmental status, plant age, phytohormones, the sugar status and some yet unknown factors (Hensel *et al.*, 1993; Dai *et al.*, 1999; Quirino *et al.*, 2000; Noodén and Penney, 2001; Guo and Gan, 2005; Jing *et al.*, 2005). Among phytohormones ethylene, brassinosteroids, jasmonic acid, salicylic acid and abscisic acid have inducing effects on senescence, whereas cytokinin has an inhibitory effect (Gan, 2003). Additionally, environmental factors including temperature, nutrient and water supply, light availability, wounding, ozone and pathogens can induce senescence (Thomas and Stoddart, 1980; Noodén, 1988; Gan and Amasino, 1997). The initiation and progression of leaf senescence is a flexible process (Thomas and Donnison, 2000) and the conversion of chloroplasts during senescence is reversible in leaves of many, perhaps all, species until a certain threshold and time point (point of no return) is exceeded (Zavaleta-Mancera *et al.*, 1999a; Zavaleta-Mancera *et al.*, 1999b).

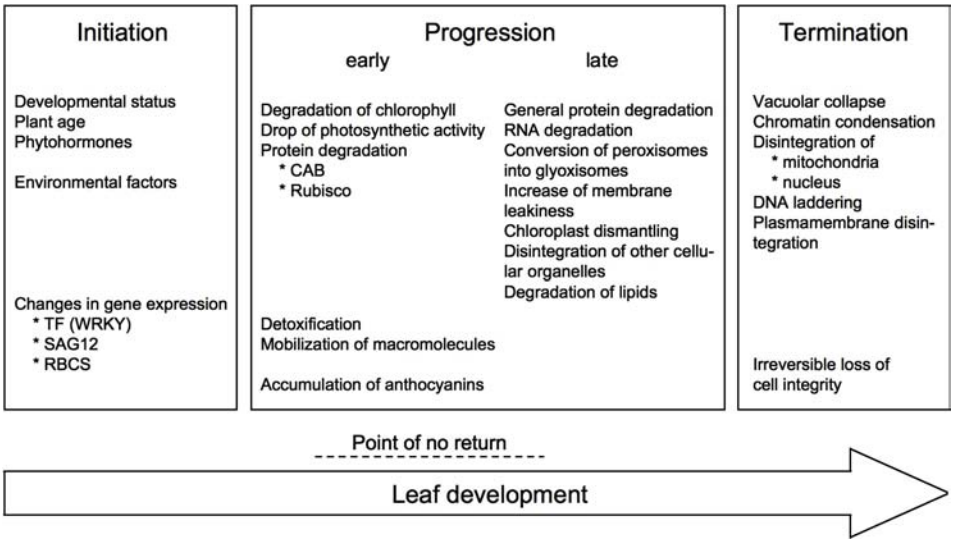

Figure 1: Phases of leaf senescence and their characteristic features (modified after Zimmermann and Zentgraf, 2005).

Natural leaf senescence occurs in a coordinated manner, usually starting from the tips or the margins of a leaf toward the base (Lim *et al.*, 2007). During senescence cells are submitted to biochemical and physiological changes: Photosynthetic activity and chlorophyll content drop, chloroplasts are dismantled and chlorophyll, proteins and RNA

are degraded (Gepstein, 2004). Later in the senescence process peroxisomes are converted into glyoxisomes, other cellular organelles are disintegrated and lipids are degraded (Zimmermann and Zentgraf, 2005). Mitochondria and nuclei are maintained intact until very late in senescence assuring sufficient energy supply and effective gene expression and thus orderly control of the senescence process (Thomas and Stoddart, 1980; Quirino *et al.*, 2000; Lee and Chen, 2002). Vacuolar collapse, chromatin condensation, DNA laddering and disintegration of the plasma membrane characterize the final stage of senescence (Cao *et al.*, 2003).

1.2.1 Chlorophyll breakdown

Chloroplasts contain 75-80% of the total leaf nitrogen mainly as proteins (Makino *et al.*, 1991) representing the major source of nitrogen for new growth (Friedrich and Huffacker, 1980). One main feature and visible symptom of senescence is leaf yellowing caused by the degradation of chlorophyll and other complex proteins such as light-harvesting molecules, chlorophyll binding proteins and Rubisco (Thomas and Stoddart, 1980; Smart, 1994; Gan and Amasino, 1997). Additionally, anthocyanins accumulate during senescence within chloroplasts (Diaz *et al.*, 2005). Free chlorophyll, which is toxic to cells, is released during the degradation of chlorophyll binding proteins (CAB). As a detoxification program chlorophyll is metabolized over chlorophyllide, pheophorbide, red-fluorescent chlorophyll catabolites, fluorescent chlorophyll catabolite to the nontoxic and nonfluorescent chlorophyll catabolite (Hörtensteiner, 2006). A part of these reactions occur in the senescing chloroplast, whereas the final reactions occur in the central vacuole (Hörtensteiner, 2006). However, when leaf yellowing becomes obvious, total leaf chlorophyll content has already declined to 50% (Hanfrey *et al.*, 1996).

1.2.2 Plastid conversion

Chloroplasts are the first cellular organelles affected by catabolic processes during senescence (Quirino *et al.*, 2000). They gradually shrink and are transformed into gerontoplasts displaying reduced disintegrated thylakoid membranes and accumulated plastoglobuli (globular structures of lipids within the stroma of plastids; Sitte, 1977; Thomas *et al.*, 2003). This conversion is often reversible in leaves of many, perhaps all, species (Zavaleta-Mancera *et al.*, 1999b; Zavaleta-Mancera *et al.*, 1999a). Plastids of senescent leaf tissue are characterized by grana unstacking, swelling of intrathylakoid space and loss of photochemical reactions, whereby the outer plastidial mem-

brane remains intact until late within the senescence process (Grover, 1993; Biswal *et al.*, 2003). Due to the decrease in chlorophyll content, the breakdown of Rubisco and the disintegration of membranes, photosynthetic activity drops and membrane ion leakage rises (Fan *et al.*, 1997; Oh *et al.*, 1997).

1.2.3 Protein degradation

Protein degradation is one of the most prominent features of leaf senescence and accompanied by an increase in the quantity of amino acids (Quirino *et al.*, 2000). Ammonia is released by the deamination of amino acids and to a smaller extent by the catabolism of nucleic acids and converted to glutamine representing the major phloem transport form of nitrogen (Pourtau *et al.*, 2006). Sugars are formed from degenerated macromolecules via TCA-cycle and gluconeogenesis and long-distance transported via the phloem (Hinderhofer and Zentgraf, 2001; Lim *et al.*, 2007). In order to achieve the massive protein breakdown during senescence ubiquitin-mediated protein degradation is assisted by the *de novo* synthesis of proteolytic enzymes (Woo *et al.*, 2001; Yoshida, 2003). On the other side, general protein synthesis is decreasing (Woolhouse, 1984). Genes representing proteases and protein kinases are upregulated during senescence indicating that these proteins play an important role within this process, although their function is in many cases unknown (Buchanan-Wollaston *et al.*, 2003). One prominent example is the senescence-associated gene *SAG12*, which encodes a cysteine protease. The expression occurs not only in leaves but also in other aging tissues, like stems and flower organs (Grbic, 2003). However, *sag12* mutants do not display any noticeable phenotypic differences, including the progression of senescence (Otegui *et al.*, 2005) and the exact function of the protein remains to be determined. Since *SAG12* is expressed exclusively during senescence, it is used as a molecular marker (Weaver *et al.*, 1998). Rubisco, the predominant protein of chloroplasts (representing approximately 50% of the soluble total protein content) is rapidly degraded during senescence serving as the main source of nitrogen (Makino *et al.*, 1991). At the same time, the number of chloroplasts remains constant (Wada *et al.*, 2009). Mechanisms of intra-chloroplastic Rubisco degradation are still unknown, however, chloroplast proteases that might degrade intra-chloroplastic proteins have been identified (Nair and Ramaswamy, 2004; Feller *et al.*, 2008).

The central vacuole is vital for the recycling and degradation of cytosolic proteins (Canut *et al.*, 1985). Most proteins degraded during senescence come from chloroplasts and catabolites released from the senescing chloroplast are further metabolized in the central vacuole (Hörtensteiner and Feller, 2002). Nutrient recycling and removal of dam-

aged or unnecessary organelles during senescence occurs mainly by autophagy (Thompson and Vierstra, 2005; Bassham *et al.*, 2006). Direct invagination of the tonoplast into the central vacuole in senescing cells has been reported (Thompson *et al.*, 1997; Inada *et al.*, 1998). However, the exact role of autophagy in the degradation of chloroplast proteins is still unclear. It is now known that senescing plastid-containing leaf cells show smaller senescence-associated vacuoles (SAV) specialized for the degradation of plastidial proteins (Matile, 1997; Otegui *et al.*, 2005). In contrast to the central vacuole SAV are more acidic and possess an intense proteolytic activity. Furthermore, cellular structures containing plastidial Rubisco were found in wheat (*Triticum aestivum*), soybean (*Glycine max*) and *Arabidopsis* (Chiba *et al.*, 2003; Otegui *et al.*, 2005). These Rubisco-containing bodies (RCB) seem to be released from the senescing chloroplast. Similar structures, called Rubisco-vesicular bodies (RVB), were observed in senescing tobacco leaves (*Nicotiana tabacum*; Prins *et al.*, 2008). In contrast to RCB, the structures possess double membranes and seem to be derived from the chloroplast envelope.

1.2.4 Lipid degradation

Membranes represent the major source of lipids and their breakdown is another characteristic feature of senescence (Thompson *et al.*, 1998). Lipid-degrading enzymes hydrolyze and metabolize membrane lipids in senescing leaves and lead to an enrichment of free fatty acids and sterols (Fan *et al.*, 1997; Thompson *et al.*, 1998; Thompson *et al.*, 2000). Subsequently, fatty acids are either metabolized to phloem-mobile sugars or, as in *Arabidopsis*, oxidized to provide energy for the senescence process due to the decline in photosynthesis causing sugar deficiency (Thompson *et al.*, 1998; Graham and Eastmond, 2002; Hörtensteiner and Feller, 2002). Increased membrane permeability or ion leakage is a convenient physiological marker that accompanies senescence (Woo *et al.*, 2001). The catabolism of membranes during senescence leads to a decreased function of key membrane proteins such as ion pumps (Thompson *et al.*, 1998).

1.2.5 Regulation

The initiation and progression of senescence is accompanied by changes in gene expression indicating that this process is highly regulated and genetically programmed (Buchanan-Wollaston *et al.*, 2003; Gan, 2003; Guiamét, 2004). The alteration in gene

expression is subsequently leading to complex metabolic and finally morphological changes (Thomas and Stoddart, 1980). Over 1900 of these so-called senescence-associated genes (*SAG*) were identified in *Arabidopsis thaliana* (He *et al.*, 2001; Hinderhofer and Zentgraf, 2001; Buchanan-Wollaston *et al.*, 2003; Guo *et al.*, 2004; Lin and Wu, 2004; Buchanan-Wollaston *et al.*, 2005; van der Graaff *et al.*, 2006). Transcription factors (TF) are responsible for genetic regulation and 185 TF genes with differential expression were identified during leaf senescence of *Arabidopsis thaliana* (Balazadeh *et al.*, 2008) representing over 20 different TF families (Lim *et al.*, 2007). The two largest groups of senescence-associated TF are WRKY and NAC, which exist exclusively in plants. The most prominent examples are NAC2 (alternatively named NAP), NAC1 and WRKY53 that display increased transcript amounts during senescence (Miao *et al.*, 2004; Guo and Gan, 2006).

1.3 Biological membranes

Although knowledge related to leaf senescence has increased rapidly in the past, the underlying biochemical properties and regulatory mechanisms are only rudimentarily understood. The main purpose of senescence is nutrient recycling following degradation of macromolecules and their mobilization out of the senescing cell across membranes (Hörtensteiner and Feller, 2002). Considering this, one can assume that specific transmembrane proteins or transporters are involved within this process. It is obvious that biological membranes are indispensable for transmembrane proteins as they are a part of their vital environment. Membranes comprise natural barriers of the cell and its organelles and accomplish a variety of essential tasks. They are responsible for im- and export of nutrients and metabolites but also for signaling between cells and their environment as well as their intracellular compartments. Membrane lipid composition affects not only its physical properties such as fluidity but also cellular processes such as signaling, transport activity and vesiculation (Balasubramanian and Schroit, 2003).
Biological membranes consist of two leaflets that can differ in their lipid bilayer composition according to their subcellular localization and functional tasks (Bretscher, 1972). Asymmetry of the plasma membrane is a characteristic feature of eukaryotic cells. The plasma membrane external leaflet is enriched in choline-containing lipids such as phosphatidylcholine (PC) and sphingomyelin (SM), whereas the luminal leaflet consists of more amine-containing lipids like phosphatidylethanolamine (PE) and phosphatidylserine (PS; Figure 2; Williamson and Schlegel, 1994; Daleke, 2003). The Golgi network

represents another example of membranes with different lipid bilayer composition in eukaryotic cells (Daleke, 2003; Pomorski *et al.*, 2004).

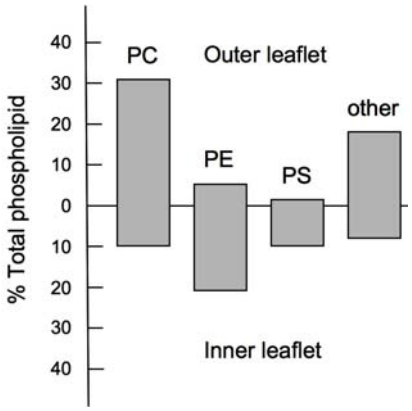

Figure 2: Membrane lipid asymmetry in eukaryotic cells. Depicted are proportions of the main phospholipids of the inner and outer plasma membrane leaflet as percentages (after Balasubramanian and Schroit, 2003). PC phosphatidylcholine, PE phosphatidylethanolamine, PS phosphatidylserine.

1.3.1 Biosynthesis of fatty acids and lipids

Lipids consist of fatty acids (FA) of various lengths and saturation degrees fused to a glycerol backbone carrying different head groups. FA biosynthesis in plants is primarily conducted within plastids and to a smaller extent in the cytosol (Ohlrogge and Kuo, 1985). Therefore plants possess two biosynthetic pathways to generate lipids: A prokaryotic pathway occurring in plastids and a eukaryotic pathway present in the cytoplasm. In both pathways acetyl-CoA deriving from glycolysis and amino acid degradation is converted to malonyl-CoA, which is then metabolized through a series of reduction and dehydration to palmitic acid (16:0; Somerville *et al.*, 2000). Most of the palmitic acid is elongated to stearic acid (18:0) and then desaturated in the chloroplast stroma so that 16:0 and 18:1 (oleic acid) fatty acids are the primary product of the prokaryotic synthesis pathway (McKeon and Stumpf, 1982; Shanklin and Somerville, 1991). Subsequently, these are either used for the synthesis of plastidial glycerolipids or released into the cytoplasm for further modification, such as elongation, desaturation or incorporation into glycero- or sphingolipids (Moore, 1982; Millar *et al.*, 2000).

The lipid phosphatidic acid (PA) is synthesized via a multi-step reaction in which α-glycerophosphate is sequentially acylated of position *sn*-1 and *sn*-2 with two acyl-CoA derivatives of FA chains. The prokaryotic pathway localized at the inner envelope of chloroplasts results in PA with 18:1 at the *sn-1* position and 16:0 fatty acids at the *sn-2* position (Roughan *et al.*, 1980). In contrast PA formed by the eukaryotic pathway located at the ER consists mainly of 16:0/18:1 and 18:1/18:1 fatty acids at the *sn-1* and *sn-2* position (Frentzen, 1990).

In chloroplasts PA is used for the synthesis of phosphatidylglycerol (PG) and diacylglycerol (DAG), which is the precursor for the synthesis of other major chloroplast lipids:

The transfer of different head groups to DAG leads to the formation of glycolipids like monogalactosyldiacylglycerol (MGD), digalactosyldiacylglycerol (DGD) and sulfoquinovosyldiacylglycerol (SQD; Browse and Somerville, 1991; Joyard *et al.*, 1993). FA bound to these glycolipids can further be modified by membrane bound desaturases (Heinz, 1993). The synthesis of glycolipids is exclusively exerted within the plastid envelope but can include PA and DAG derived from the ER (Browse and Somerville, 1994).
On the other side, synthesized PA in the ER gives rise to phospholipids (PL) such as PC, PE and phosphatidylinositol (PI) resulting in PL rich membranes distinct to plastidial membranes (Moore, 1982; Mudd and Datko, 1989). In addition PC is returned to the chloroplast envelope where it contributes to the production of thylakoid lipids (Roughan and Slack, 1982; Browse *et al.*, 1986).
PS is synthesized in the ER by the exchange of serine with the headgroup of PC or PE (Nishijima *et al.*, 1986) and subsequently transported to mitochondria where PE is synthesized (Vance and Shiao, 1996). Additionally, PE is synthesized in the Golgi network (Voelker, 2000). Finally, lipid transport proteins in the cytoplasm, such as HDL (high-density lipoprotein) and LDL (low-density lipoprotein), deliver fatty acids, cholesterol, and PL to the plasma membrane and other cellular compartments (Balasubramanian and Schroit, 2003).

1.3.2 Establishment of membrane asymmetry

Asymmetry of the plasma membrane must be established as the membrane flows from the ER through the Golgi network to the plasma membrane, and/or by delivery of lipids from intracellular sites of synthesis to the plasma membrane via vesicular transport (reviewed in Graham, 2004; Liu *et al.*, 2008). The major *de novo* synthesis of PL occurs on the cytosolic side of the ER and this lipid class represents the major component of cellular membranes (Bell *et al.*, 1981). ER membranes possess specialized proteins, so-called scramblases that are Ca^{2+}-dependent but energy-independent non-specific lipid transporters which facilitate a rapid and bidirectional equilibration of PL between both membrane leaflets (Bishop and Bell, 1985; Burton *et al.*, 1996; Menon *et al.*, 2000; Nicolson and Mayinger, 2000).
Within the Golgi network sphingolipids are synthesized at the luminal side. The production of sphingolipids may have an important role in the sorting of membrane proteins and lipids between the ER and the plasma membrane (reviewed in van Meer *et al.*, 2008). At the same time lipid transporters (P_4-type ATPases) shuffle PS and PE to the cytoplasmatic leaflet, thus, generating membrane asymmetry in the late Golgi network. Vesicles budding from the Golgi fuse with the plasma membrane and contribute to its

specific lipid composition and bilayer asymmetry. The mechanism by which aminophospholipids (PL that contain an amine or an amino acid as head group) are transported from their sites of synthesis to the plasma membrane has not been completely established but probably involves both vesicular and cytosolic protein-mediated transfer mechanisms (Sprong *et al.*, 2001). As PL diffusion across the bilayer occurs over the course of several hours (Kornberg and McConnel, 1971), selective ATP-dependent transporters must operate to maintain (and/or establish) the asymmetric distribution of lipids within two membrane leaflets (Zachowski, 1993; Daleke, 2003; Pomorski *et al.*, 2004). Various types of these transporters must exist: ATPases of class 4 are supposed to act as flippases transporting lipids from the outer to the inner membrane leaflet whereas some ABC-transporters represent floppases and transport lipids from the inner to the outer membrane leaflet (Seigneuret and Devaux, 1984; Pomorski *et al.*, 2004; Daleke, 2007).

The inward movement of PL from the exoplasmatic leaflet to the cytoplasmic leaflet was first described in human erythrocyte membranes (Seigneuret and Devaux, 1984). The ATP-dependent translocation is specific for PS and induces substantial changes in membrane structure (Daleke and Huestis, 1985). ATP-dependent PL translocation was subsequently detected in a wide range of eukaryotic cell types such as yeast, bovine chromaffin granules and human platelets (Seigneuret and Devaux, 1984; Sune *et al.*, 1987; Devaux, 1991; Kean *et al.*, 1993; Zachowski, 1993; Bevers *et al.*, 1999). Members of the P_4-type ATPase family are thought to be involved in the translocation process (Daleke, 2003) and are therefore essential for any membrane where the maintenance of a PL asymmetry between the two leaflets is required.

1.3.3 Membrane changes during senescence

PL are the major membrane lipids in young tissue. Advancing senescence is paralleled by a decline in structural and functional integrity of cellular membranes as fatty acids are oxidized to provide energy for the senescence process (Thomas and Stoddart, 1980; Thompson *et al.*, 1998). A loss of PL has been demonstrated for senescing flower petals, leaves, cotyledons and ripening fruits (Mckersie and Thompson, 1975; Borochov *et al.*, 1982; Thompson, 1988). Lipid metabolites accumulate between the two membrane leaflets and cause lipid phase separations and packing imperfections (Döbereiner *et al.*, 1993). Consequently, bilayer fluidity and conformation of membrane proteins are negatively affected (Leigh, 1979; Barber and Thompson, 1980). Under non-senescing conditions membrane lipid catabolites form domains that bud subsequently into the cytosol as lipid-protein particles (Yao *et al.*, 1991a; Hudak *et al.*, 1995).

The formation of these particles (called blebbing) becomes impaired during advanced senescence resulting in a loss of membrane function that is a characteristic feature of aging (Barber and Thompson, 1980; Woodson and Handa, 1987; Starling *et al.*, 1995). Membrane blebs are derived from all cellular membranes, i.e. the plasma membrane, the tonoplast, the ER and membranes of the Golgi network as well as plastidial and mitochondrial membranes (Yao *et al.*, 1991b; Yao *et al.*, 1991a; Hudak *et al.*, 1995). In contrast to microvesiculation, membrane blebs are bilayered (Murphy, 1990; Huang, 1992; Murphy, 1993; Hudak and Thompson, 1996). Lipid translocators such as P_4-type ATPases might facilitate or contribute to the formation of these structures by accumulating lipids in the cytosolic leaflet of the membrane.
Mathematical models show that the translocation of a few lipids from one monolayer to the other in a lipid bilayer triggers membrane deformations, which resemble vesicle budding (Devaux *et al.*, 2008). This suggests that lipid translocators / P_4-type ATPases drive membrane bending towards the cytosol by expanding the cytoplasmatic leaflet of the bilayer while reducing the PL number in the exoplasmatic or luminal leaflet. Subsequently, P_4-type ATPases might contribute to vesicular trafficking by facilitating the generation of membrane curvature inherent in this process or establishing a membrane environment permissive for vesicle budding (Devaux, 1991; Chen *et al.*, 1999).

1.4 P_4-type ATPases

ATPases represent the largest group of active transport systems within cells and can be grouped into four distinct types, P-, F-, V-type ATPases and ABC transporter (Pedersen and Carafoli, 1987; Pedersen, 2007). Their common feature is the hydrolysis of ATP driving the transport of a wide range of cations and molecules across membranes against their electrochemical gradient. V-type ATPases transport protons across the membrane and thus affect the pH in vesicles and vacuoles by establishing a proton gradient. By contrast, F-type ATPases function in the opposite direction using a proton gradient to synthesize ATP. ABC transporters move a diverse set of macromolecules across biological membranes. P-type ATPases transport mainly ions and differ fundamentally in structure and reaction mechanisms from the three other groups. They share a DKTGTXX motif and are characterized by a phosphorylation step during their reaction cycle where the γ-phosphate group of ATP is reversibly transferred to an aspartic acid residue (D) within the motif (Axelsen and Palmgren, 1998; Apell, 2004).
According to their substrate specificity and evolutionary similarity, P-type ATPases are subgrouped into five subfamilies (P-type ATPase database; http://www.patbase.kvl.dk/;

Axelsen and Palmgren, 1998): Type-I comprises heavy metal pumps (transported ions: K^+, Cu^+, Ag^+, Cu^{2+}, Cd^{2+}, Zn^{2+}, Pb^{2+} and Co^{2+}), proteins of type II are Ca^{2+} pumps and Na^+/K^+; H^+/K^+ antiporters and type III includes Mg^{2+} and H^+ pumps. Type IV ATPases exist ubiquitously in eukaryotes but only little information is available on the substrate specificity and biochemical function of the proteins. It is assumed that P_4-type ATPases are involved in the transport of phospholipids while the substrate of type V ATPases remains to be identified (reviewed in Poulsen *et al.*, 2008a).

Characteristic features of P_4-type ATPases are three conserved protein domains. The first domain is associated with the ATP hydrolysis and substrate transport (actuator domain), the second domain contains the DKTGTXX motif including the reversibly phosphorylated aspartic acid residue (phosphorylation domain) and the third domain is probably involved in ATP-binding (nucleotide-binding domain; Tang *et al.*, 1996). Based on analogy to the crystal structure of the sarco-/endoplasmatic reticulum localized Ca^{2+} P-type ATPase SERCA1, the N-terminal tail and the loop between transmembrane segments 2 and 3 might form the actuator domain, and the large cytoplasmatic loop between membrane segments 4 and 5 might form the phosphorylation and nucleotide-binding domains (Kühlbrandt, 2004; Toyoshima and Mizutani, 2004). Based on hydropathy plots ten transmembrane domains (TM) are predicted for P_4-type ATPases (Figure 3; Aramemnon database; http://aramemnon.botanik.uni-koeln.de; Schwacke *et al.*, 2003). N- and C-termini as well as a smaller and a larger loop (between the 2nd and 3rd and the 4th and 5th transmembrane region, respectively) are cytoplasmatically located (Tang *et al.*, 1996; Daleke, 2003).

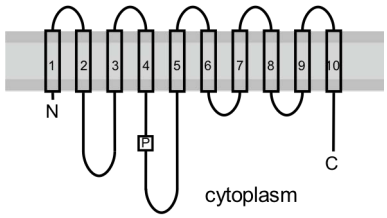

Figure 3: Schematic P_4-type ATPase protein model. The proteins are membrane located and predicted to possess ten transmembrane regions with N- and C-termini reaching into the cytoplasm. They display a small and a large cytoplasmatic loop containing the phosphorylation site (P) at an aspartic acid residue.

1.4.1 P_4-type ATPases in *Saccharomyces cerevisiae*

Most of the information on the identity of P_4-type ATPases has been generated by research in yeast and cells from a patient suffering from a congenital bleeding disorder

termed Scott syndrome (Balasubramanian and Schroit, 2003). Five P_4-type ATPases were identified in the model organism *Saccharomyces cerevisiae* (Figure 4; Costanzo *et al.*, 2001). Dnf1p and Dnf2p are located at the plasma membrane (PM), Drs2p and Dnf3p at membranes of the trans-Golgi network and Neo1p at endosomal membranes as well as membranes of the trans-Golgi network (Chen *et al.*, 1999; Gall *et al.*, 2002; Hua *et al.*, 2002; Pomorski *et al.*, 2003; Wicky *et al.*, 2004).

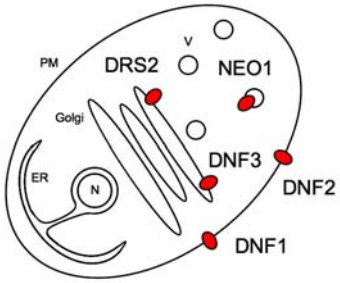

Figure 4: P_4-type ATPases in *Saccharomyces cerevisiae*. Sketch of a yeast cell with its identified P_4-type ATPases. ER endoplasmatic reticulum, Golgi Golgi network, N nucleus, PM plasma membrane, V vesicles/endosomes.

The yeast deletion mutant strain *Δdrs2* is sensitive to temperatures below 23 °C and displays furthermore sensitivity to heavy metals that cannot be explained (Ripmaster *et al.*, 1993). Additionally, cells of the *Δdrs2* mutant strain have a defect in ribosomal assembly of the 40S subunit (Ripmaster *et al.*, 1993) and defects in polarized cell growth at temperatures below 23 °C (Saito *et al.*, 2004). In experiments with fluorescently labeled PL analogs, *Δdrs2* cells internalized exogenously applied PS and PE analogs (Saito *et al.*, 2004). A mutation of the catalytically important aspartic acid residue of Drs2p perturbs the formation of clathrin-coated vesicles targeted to the plasma membrane (Gall *et al.*, 2002). Furthermore, there is evidence that Drs2p is directly involved in the interaction with the components Arf1p (ADP-ribosylation-factor, a GTP-binding protein) and Gea2p (guanidine exchange factor or ARF exchange factor) responsible for the formation of clathrin-coated vesicles (Chantalat *et al.*, 2004; Pomorski *et al.*, 2004; Wicky *et al.*, 2004).

Removal of the P_4-type ATPases Dnf1p and Dnf2p abolishes inward translocation of fluorescently labeled PS, PE and PC across the plasma membrane of the *Δdnf1Δdnf2* strain and causes cell surface exposure of endogenous PE (Pomorski *et al.*, 2003; Liu *et al.*, 2008). Similar to *Δdrs2* cells the *Δdnf1Δdnf2* strain is sensitive to temperatures below 23 °C and heavy metals and shows a cold-sensitive defect in the uptake of endocytosis markers (Pomorski *et al.*, 2003). Phenotypes of the *Δdrs2* and the *Δdnf1-Δdnf2* mutant strains are intensified in the triple mutant *Δdrs2Δdnf1Δdnf2*. The strain displays exposition of endogenous PE at the extracellular leaflet of the plasma membrane and endocytosis defects at temperatures greater than 23 °C (Pomorski *et al.*, 2003). These findings indicate that P_4-type ATPase are involved in PL flipping from the outer to the inner membrane leaflet and are required for the maintenance of a lipid

asymmetry in membranes (Pomorski *et al.*, 2003; Saito *et al.*, 2004; Alder-Baerens *et al.*, 2006).

1.4.2 Interacting partners of P_4-type ATPases

Proteins of the Cdc50 family were found to complex with P_4-type ATPases in yeast: Drs2p interacts with Cdc50p, Dnf1p and Dnf2p with Lem3p and Dnf3p with Crf1p (Saito *et al.*, 2004). No interaction partner was found for Neo1p. While the formation of these complexes is required for the ATPase to exit from the endoplasmic reticulum, little is known about the functional role of the Cdc50 subunits (Saito *et al.*, 2004; Lenoir *et al.*, 2009). Interaction of P_4-type ATPases with a β-subunit was also shown in other organisms: LdRos3p the Lem3p homologue in the parasite *Leishmania donovani* is necessary for the transport activity and additionally required for correct export from the ER to the PM of the LdMTp P_4-type ATPase (Pérez-Victoria *et al.*, 2006). In humans the P_4-type ATPase Atp8b1 requires a Cdc50p homologue in order to leave the ER and reach the PM (Paulusma *et al.*, 2008).
In *Arabidopsis* five members of Cdc50-homologs that may represent β-subunits for the P_4-type ATPases were reported and named ALIS 1 to 5 (ALA interacting subunit; Poulsen *et al.*, 2008b). ALIS proteins possess two transmembrane spans and a large extracellular loop of approximately 75% of the protein (Poulsen *et al.*, 2008b).
Most P-type ATPases in yeast are monomeric and only members of type II pumps (Na^+/K^+-ATPase and the closely related H^+/K^+-ATPase) are oligomeric requiring β-subunits that are similar to Cdc50 proteins (Geering, 2001). Besides assisting as a chaperone in the functional maturation of the catalytic α-subunit (P-type ATPase), the β-subunit also contributes specifically to intrinsic transport properties of the Na^+/K^+ pump. However, Cdc50 subunits possess only one transmembrane region and are post-transcriptionally modified by glycosylation (Geering, 2001; Morth *et al.*, 2007). Cdc50 proteins in yeast and its homologues in humans and plants display conserved glycosylation sites within the extracellular loop predicted by bioinformatic tools. The glycosylation is confirmed *in vivo* for the yeast protein Lem3p (Kato *et al.*, 2002). Based on the similarities between P_4-type and P_2-type ATPase subunits one can assume similar function of these proteins.

1.4.3 Reaction cycle

P_4-type ATPases are believed to act as a flippase, catalyzing the transport of PL from the outer membrane bilayer leaflet to the inner (Devaux *et al.*, 2006; Pérez-Victoria *et*

al., 2006; Lenoir *et al.*, 2007; Paulusma *et al.*, 2008). In contrast to the PL transporting P_4-type subgroup all other P-type ATPases pump much smaller substrates like cations or metal ions. However, atomic structures revealed a conserved transport mechanism throughout the entire P-family (Lenoir *et al.*, 2009).

Interaction with a β-subunit might lead to the specific lipid transport, however the primary role of the additional polypeptide and the lipid transport mechanism itself are yet unknown. Additionally, P_4-type ATPases expose hydrophobic residues in the region where cation transporters expose negatively charged residues supporting the hypothesis that these proteins have an amphipathic substrate such as PL (Tang *et al.*, 1996; Chen *et al.*, 1999).

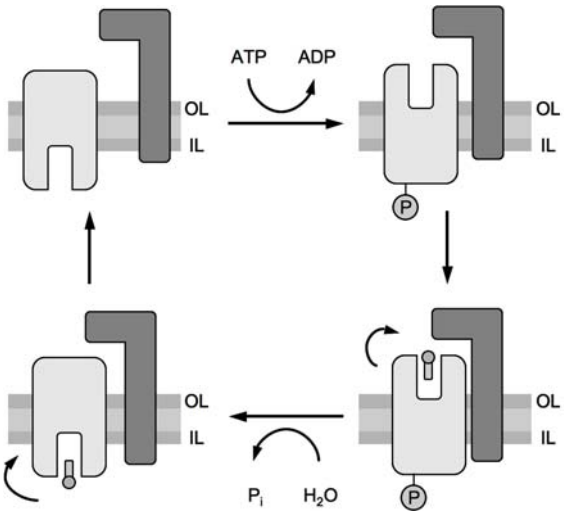

Figure 5: Scheme of the reaction cycle of P_4-type ATPases displaying the dynamic interaction between the yeast Drs2p ATPase, its Cdc50p subunit and lipid substrate. ATPase in light grey, subunit in dark grey. OL outer membrane leaflet, IL inner membrane leaflet (adapted from Lenoir *et al.*, 2009).

Based on interaction studies with the yeast P_4-type ATPase Drs2p and its partner Cdc50p, a reaction cycle scheme of P_4-type ATPases was suggested (Figure 5; Lenoir *et al.*, 2009). The affinity between P_4-type ATPases and subunits is likely to be dynamic during the transport reaction: Phosphorylation is the crucial step in a P_4-type ATPase reaction cycle, whereby the enzyme is subjected to a conformational change exposing its ligand-binding pocket at the outer membrane leaflet allowing a substrate to enter the enzyme. Subsequently, the binding affinity of the ATPase interacting subunit increases reaching the highest point when the enzyme is associated with its substrate. Dephosphorylation leads again to a conformational change exposing the ligand-binding pocket at the inner membrane leaflet, thus, releasing the substrate and decreasing the binding affinity between ATPase and subunit. These findings suggest β-subunits as integral components of the P_4-type ATPase transport machinery and the acquisition of these subunits may have been a crucial step in the evolution of lipid flippases from a family of cation pumps (Lenoir *et al.*, 2009).

1.4.4 P_4-type ATPases in *Arabidopsis thaliana*

Only a few members of the P_4-type ATPase family have been identified genetically in other organisms apart from yeast: Examples are the bovine ATPase II and the mammalian Atp8a1 that are both closely related to Drs2p and the rice blast fungus PDE1 that is most similar to Dnf3p (Ding *et al.*, 2000; Balhadere and Talbot, 2001; Soupene *et al.*, 2008). Homologs of the yeast Drs2p ATPase and the bovine ATPase II were also found in plants. 12 P_4-type ATPases were identified in *A. thaliana* (Gomès *et al.*, 2000). The ALA called proteins (aminophospholipid ATPase) can be divided into five groups based on sequence alignments and intron positions (Figure 6; Baxter *et al.*, 2003). ALA1, 2 and 3 are separated from each other and the clusters consisting of ALA4-6 and ALA 8-12.

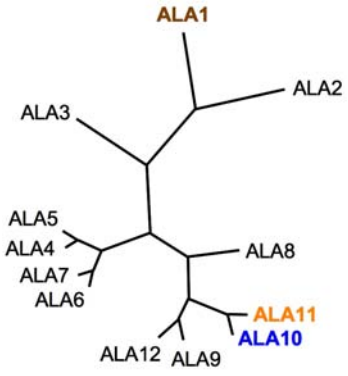

Figure 6: Phylogenetic tree of *Arabidopsis thaliana* P_4-type ATPases. Depicted are all 12 ALA proteins (aminophospholipid ATPase). Bootstrap values are expressed in percentages. Colors indicate investigated ALA proteins within this work.

Knowledge on P_4-type ATPases in *Arabidopsis* is limited and so far investigations focused on ALA3, the closest homolog of the yeast protein DRS2p, and ALA1 (Gomès *et al.*, 2000; Poulsen *et al.*, 2008b): *Arabidopsis thaliana ALA1*-antisense plants with reduced *ALA1* transcripts are cold sensitive. When grown at 12 °C, the plants display reduced growth resulting in smaller rosette leaves, shorter inflorescences with less siliques compared to wild type (Gomès *et al.*, 2000). When expressed in the yeast *Δdrs2* mutant strain, ALA1 complements the cold sensitivity of the strain. Additionally, reconstituted membrane vesicles from *Δdrs2* cells expressing ALA1 show increased internalization of PS and to a lesser extent of PE (Gomès *et al.*, 2000).

These lines of evidence suggest that ALA1 is involved in the generation of membrane lipid asymmetry and probably encodes an aminophospholipid translocase. Furthermore, the data suggest a link between regulation of transmembrane bilayer lipid asymmetry and the adaptation of plants to cold.

Poulsen *et al.* (2008b) reported on ALA3 and localized the protein to the Golgi apparatus. The authors described T-DNA insertion lines displaying reduced growth of roots

and shoots. The effect is probably caused by an impaired proliferation of slime vesicles containing polysaccharides and enzymes for secretion in the root cap, which are essential for an efficient root interaction with the environment. In fact, *ala3* mutants show few vesicles in root tip cells and possess large vacuole-like structures. Consequently, due to the impaired secretion of slime vesicles columella cells in the root tip are not degraded and stick to the root tip and inhibit proper growth. Furthermore, the authors showed that ALA3 alone is not able to complement the cold-sensitivity of the Δ*drs2*-Δ*dnf1*Δ*dnf2* yeast mutant strain, however when co-expressed with ALIS subunits 1, 3 or 5 the wild type phenotype is recovered. A co-expression of *ALA3* and *ALIS1* in yeast Δ*drs2*Δ*dnf1*Δ*dnf2* cells leads to an inward transport of the fluorescent phosphatidylethanolamine and phosphatidylcholine analogs NDB-PE and PBD-PC. The inward transport is not detected, when an *ala3* mutant version is co-expressed with *ALIS1*. The authors confirmed an interaction of both proteins *in vivo*, and additionally showed similar expression patterns for *ALA3* and *ALIS1*.
These experiments indicate an important role for the P_4-type ATPase ALA3 in the formation of vesicles within the Golgi network and underline the importance of its subunit ALIS1 for proper performance of the lipid translocation process.

1.5 Expression of P_4-type ATPases during leaf senescence of *Arabidopsis thaliana*

Arabidopsis thaliana is often used as a model for the molecular genetic study of leaf senescence due to the fact that extensive genomic resources are available for the plant (Lim *et al.*, 2007). The identification of genetic mutants that control leaf senescence in *A. thaliana* opened up new possibilities for genetically analyzing leaf senescence in a model system (Nam, 1997). Furthermore, *Arabidopsis* rosette leaves undergo distinguishable developmental stages and show a well-defined and reproducible senescence program facilitating the analysis of leaf senescence (Lim *et al.*, 2003). Senescence as a nutrient recycling program implies the involvement of senescence-associated transporters (SATP) that export degraded macromolecules across biological membranes. Thus, senescence-associated transporters are very important to understand the biochemical properties and regulatory mechanisms of this nutrient recycling process. However, even with the advantage of genetic tools, only a few SATP have been reported (Himelblau and Amasino, 2001; Quirino *et al.*, 2001). Via genome-wide expression profile analyses attempts were made to identify more SATP (Buchanan-Wollaston *et al.*, 2003; Guo *et al.*, 2004; Lin and Wu, 2004; Buchanan-Wollaston *et al.*,

2005; van der Graaff *et al.*, 2006). These analyses indicate the involvement of many previously uncharacterized transmembrane proteins within the senescence process.

Van der Graaff *et al.* (2006) distinguished in their analyses between naturally occurring (developmental) senescence and artificially induced senescence and were able to show overlapping but also unique sets of SATP for these types of senescence. Thus, genes coding for SATP specific for developmental senescence were identified with an accuracy that had not been possible before.

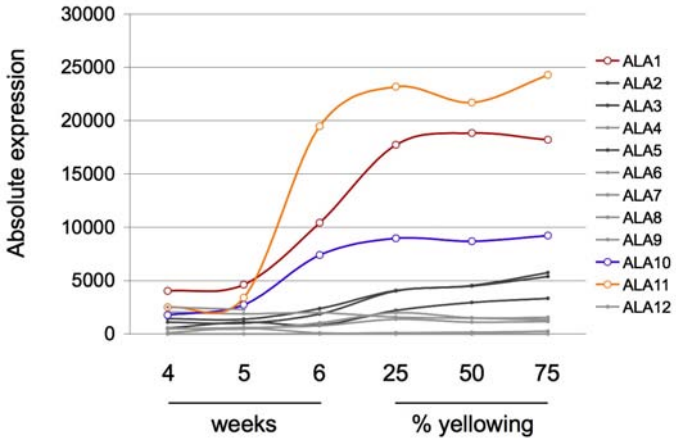

Figure 7: Expression of *ALA* (aminophospholipid ATPase) genes during natural development in leaves of *Arabidopsis thaliana* wild type Col-0. Depicted are absolute expression values obtained from gene chip hybridization with pooled material from 5th and 6th rosette leaves at 4, 5 and 6 weeks and when displaying 25%, 50% and 75% yellowing of the leaf blade. (Data from van der Graaff *et al.*, 2006).

Strikingly, most of the genes coding for P_4-type ATPases (*ALA* in *Arabidopsis thaliana*) were significantly affected suggesting an important role of these proteins within developmental senescence. Nine of twelve *ALA* genes displayed at least a 2-fold increase in transcript amount in leaves during natural aging-induced senescence of *Arabidopsis thaliana* (*ALA1*, *ALA2*, *ALA3*, *ALA4*, *ALA5*, *ALA7*, *ALA9*, *ALA10* and *ALA11*). Among these, three *ALA* genes displayed a transcript level induction of 4.5 or greater (Figure 7; *ALA11*: 9.7-fold, *ALA10*: 5.3-fold and *ALA1*: 4.7-fold). The association of P_4-type ATPases to the senescence program might indicate their role in the maintenance of membrane asymmetry, membrane reorganization or lipid bilayer modification during this developmental process.

1.6 Aim of the project

Manipulation of leaf senescence can potentially greatly improve crop yield. Considering the potential future food shortage and the use of plants as a source of energy this area of research is getting more and more important. However, key issues of plant senescence still need to be elucidated.

Goal of this investigation is to contribute to a better understanding of plant senescence, especially the knowledge on P_4-type ATPases (ALA, aminophospholipid ATPase). Yet existing expression analyses indicate that ALA proteins are putatively involved in the senescence program of *Arabidopsis thaliana*. Within the *ALA* gene family the majority of its members shows increased transcript levels during natural occurring senescence pointing out their importance during this developmental process. *ALA1*, *ALA10* and *ALA11* display the strongest induction in senescence-associated gene expression and were investigated in this work.

Information on P_4-type ATPases in plants is still rudimentary. Tissue-specific expression is partly known for ALA1. ALA3 represents the only P_4-ATPase with an identified tissue-specific expression as well as a subcellular localization of the protein. To gain knowledge of more plant P_4-type ATPases in these aspects, the tissue-specific expression of the three senescence-associated *ALA* genes (*1*, *10* and *11*) as well as the subcellular localization of the proteins are aimed.

The relation and contribution of P_4-type ATPases to plant senescence is not understood at present. The role of ALA1, ALA10 and ALA11 within the senescence program of *Arabidopsis thaliana* should be pointed out for the first time with the help of T-DNA insertion lines. The focus is on the physiological and morphological description of these insertion lines with a special emphasis on the senescence process.

P_4-type type ATPases are thought to alter the characteristics of biological membranes via lipid flipping. Only the cellular ultrastructure of *ala3* mutants is available to date. To gain additional insights into the specific function of other P_4-type ATPases and their relevance for biological membranes, cellular ultrastructure of the identified and generated *ala* mutant lines is targeted. In order to reveal effects on the lipid composition, caused by the proteins, the investigation of cellular membranes of *ala* plant mutants is aimed because the exact lipid composition of any plant or yeast P_4-ATPase mutant is still undetermined.

It is known that ALIS proteins (ALA interacting subunit) interact with ALA3. For that reason, the subunit specifications of ALA1, ALA10 and ALA11 are aimed. Furthermore, the evidence of phospholipid translocating activity and substrate preferences for ALA1, 10 and 11 are aimed completing the yet existing knowledge on P_4-type ATPases.

2 MATERIAL AND METHODS

2.1 Chemicals

Chemicals were purchased from Bio-Rad (Munich, Germany), Biozym (Oldendorf, Germany), Carl-Roth (Karlsruhe, Germany), Difco Laboratories (Detroit, MI, USA), Duchefa (Haarlem, The Netherlands), Fluka (Buchs, Switzerland), GE Healthcare Europe (Munich, Germany), Merck (Darmstadt, Germany), Peqlab (Erlangen, Germany), Qiagen (Hildesheim, Germany), Roche Applied Science (Mannheim, Germany), Serva (Heidelberg, Germany), Sigma-Aldrich (Taufkirchen, Germany), Thermo Fisher Scientific (Bonn, Germany), if not mentioned otherwise. All media for yeast handling were ordered from ForMedium (Hunstanton, England).
If not mentioned otherwise water indicated as ddH_2O refers to twice-purified water via reverse osmosis (Milli-Q Water System, Millipore, Schwalbach, Germany). Buffers and solutions used in this work were either autoclaved for 15 min at 120 °C (Fedegari Autoclave, Tecnomara, Fernwald-Steinbach, Germany) or sterile filtered using a pore diameter of 0.2 µm (Schleicher & Schuell, Dassel, Germany).
Commonly used buffers and solutions for molecular biology were prepared according to Sambrook *et al.* (1989).

2.2 Oligonucleotides and plasmids

Oligonucleotides used in this work were purchased from Invitrogen (Karlsruhe, Germany). To provide a better summary, primers are listed in this section (Table 1 – 9) if not mentioned otherwise.
Plasmids utilized in this work are listed in Table 10 and Table 11.

Table 1 (continued on next page): Gene and T-DNA specific primer pairs for T-DNA identification. LP left primer, RB right primer, LB left border primer.

Line name	Primer	Nucleotide sequence	Amplicon size [bp]
ala1-1	LP	5'-TCTGCGATACTCTGCTGCCG-3'	
	RP	5'-CAGGTTCATTTCAACTCCCACG-3'	1016

Line name	Primer	Nucleotide sequence	Amplicon size [bp]
ala10-1	LP	5'-CCAATGGCTGCAATATACCAC-3'	
	RP	5'-AACTCGCTTACTTATCAGCTCCC-3'	873
ala10-2	LP	5'-TCTGTTTTGTTCTGTTCTCACTCTG-3'	
	RP	5'-AGAGATCCCATTTTGTGTCCG-3'	904
ala11-1	LP	5'-ATGCGCAGGTTTATCATTCTC-3'	
	RP	5'-TACCTCTCACCTTCGTCATCG-3'	1070
ala11-2	LP	5'-GAGTGAAGCGAACCCTTTTTG-3'	
	RP	5'-CGTTTTCTTCTCTTCGCTTCC-3'	954
GABI	LB	5'-CCATTTGGACGTGAATGTAGACAC-3'	
SALK	LB	5'-TGGTTCACGTAGTGGGCCATCG-3'	

Table 2 (continued on next page): Primer pairs for RTPCR of *ala* mutant lines. LP left primer, RB right primer.

Line name	Gene	Primer	Nucleotide sequence	Amplicon size [bp]
ala1-1	*ALA1*		5' of T-DNA insertion	
		LP	5'-TCACTGGCAGCTTGCAATAC-3'	
		RP	5'-TTGTCACCAGTCAAGACCCA-3'	638
	ALA1		spanning T-DNA insertion	
		LP	5'-TGCAGGGATAAAAGTCTGGG-3'	
		RP	5'-TGTCAATTGTACTGCCCCAA-3'	878
	ALA1		3' of T-DNA insertion	
		LP	5'-CAACTGCCATCACAGAATGG-3'	
		RP	5'-GTTCATTTCAACTCCCACGG-3'	623
ala1-10	*ALA10*		5' of T-DNA insertion	
		LP	5'-TATTCCGGCAAGAAGAATGG-3'	
		RP	5'-GCGAAATCGGGATGAAGTAA-3'	690
	ALA10		spanning T-DNA insertion	
		LP	5'-TCATCCCGATTTCGCTTTAC-3'	
		RP	5'-GACAACAGCAAGAGCTTCCC-3'	662
	ALA10		3' of T-DNA insertion	
		LP	5'-CAATGAAGCTAAGGCTTCCG-3'	
		RP	5'-CTGCTTGCATTCCTTCAACA-3'	718
ala11-1	*ALA11*		5' of T-DNA insertion	
		LP	5'-GAGGACCTGGTTTCTCACGA-3'	
		RP	5'-TTCGTTTCTCCGTCGAGATT-3'	502
	ALA11		spanning T-DNA insertion	
		LP	5'-GAGGACCTGGTTTCTCACGA-3'	
		RP	5'-CCAGTGAAGACAACAACTCCA-3'	736

Line name	Gene	Primer	Nucleotide sequence	Amplicon size [bp]
ala11-1	*ALA11*		3' of T-DNA insertion	
		LP	5'-ACAAAAGGCATTGGTTACGC-3'	
		RP	5'-CAAAGCGAAGAACATCACGA-3'	850
	ACT2 (At3g18780)			
		LP	5'-AACTCTCCCGCTATGTATGTCGC-3'	
		PR	5'-TTCCATCTCCTGCTCGTAGTCAAC-3'	303 / (382 including intron)

Table 3: Primer pairs for QRTPCR. LP left primer, RB right primer.

Gene	Primer	Nucleotide sequence	Amplicon size [bp]
ALA1	LP	5'-CAAGACATGGATGTTCTGGTTC-3'	
	RP	5'-AAACTTGATGGCGAATCTAGGA-3'	76
ALA10	LP	5'-GCTCACGACTCTCTTTGTGATG-3'	
	RP	5'-TAGGGAAAAACCTCATTTGCAC-3'	80
ALA11	LP	5'-TGAAGCTAAGAACTCGGTGACA-3'	
	RP	5'-TCAAATCACGTTCCATCTGTTC-3'	77
SAG12	LP	5'-TCTGGTGTGTTCACTGGAGAGT-3'	
	RP	5'-ATCCGTTAGTAGATTCGCCGTA-3'	82
RBCS1a	LP	5'-GACCAAAGCACTAGACCAAACC-3'	
	RP	5'-CCATAGTAGCGGAAGAGAGCAT-3'	84
WRKY53	LP	5'-CAAGACACCAGAGTCAAACCAG-3'	
	RP	5'-TTCGAACGGTTAAGTTGGATTT-3'	82
UBQ10 (At4g05320)			
	LP	5'-GCAGTTCTGCGAAACTTGTAAA-3'	
	RP	5'-AGAACCCAACAGCTCAACACTT-3'	81
CTRL (At5g65080)			
	LP	5'-TTTTTTGCCCCCTTCGAATC-3'	
	RP	5'-ATCTTCCGCCACCACATTGTAC-3'	68 (only on genomic DNA)

Table 4: Primer pairs for generation of DIG-labeled probes (for GABI and SALK generated T-DNA insertion lines). LP left primer, RB right primer.

vector	Primer		Nucleotide sequence	Amplicon size [bp]
pAC161 (GABI)	o9525	LP	5'-CCACACGTGGATCGATCCGTCG-3'	
	o10706	RP	5'-GAACCCTAATTCCCTTATCTGGG-3'	1181
pROK2 (SALK)	nptIIf	LP	5'-GAAGAACTCGTCAAGAAGG-3'	
	nptIIr	RP	5'-ATGATTGAACAAGATGGATTGCAC-3'	791

Table 5: Primer pairs for amplification of upstream regions of *ALA1*, *ALA10* and *ALA11*. Major cases represent priming sequences, minor cases represent non-priming sequences/added overhangs, underlined nucleotides represent *Sma*I endonuclease restriction sites.

Region	Primer	Nucleotide sequence	Amplicon size [bp]
ALA1	forward	5'-ccccccgggAATATTAAAACCAATACTCGATCGATAATG-3'	
	reverse	5'-ccccccgggTTCCCGGGTCCAGGAATTG-3'	1997
ALA10	forward	5'-ccccccGGGTTAGTGAAATTTTCATTATCCAAG-3'	
	reverse	5'-ccccccgggAGCTTTTTTAGTTTAGTTCTTTGTCTGAAA-3'	2004
ALA11	forward	5'-ccccccggGCCTTTCCTTTTCTATCAGCGT-3'	
	reverse	5'-ccccccgggTGTTTGTCTGAAAATCCTCTGTAAAGTT-3'	1998

Table 6: Primer pairs for amplification N-terminal regions of *ALA1*, *ALA10* and *ALA11* (*ALA*$_{TM1-4}$-fragments). Major cases represent priming sequences, minor cases represent non-priming sequences/ added overhangs, underlined nucleotides represent endonuclease restriction sites.

Region	Primer	Nucleotide sequence	Restriction site	Amplicon size [bp]
ALA1	forward	5'-gctctagaATGGATCCCAGGAAATCAATTG-3'	*Xba*I	
	reverse	5'-aactgcagcAGGGACACCACGCTGCAAT-3'	*Pst*I	2182
ALA10	forward	5'-gctctagaATGGCTGGTCCAAGTCGGA-3'	*Xba*I	
	reverse	5'-aactgcagaCATTCTCTTCCTAGTGCTATTGAATTCA-3'	*Pst*I	1797
ALA11	forward	5'-gctctagaATGACAAAGTGTCGGAGAAGAA-3'	*Xba*I	
	reverse	5'-aactgcagtCTCCCGTTTTTGGCTAGTCTTTC-3'	*Pst*I	2050

Table 7: Primer pairs for amplification of *ALA1*, *ALA10* and *ALA11* open reading frames. Major cases represent priming sequences, minor cases represent non-priming sequences/added overhangs, underlined nucleotides represent endonuclease restriction sites or start/stop codons.

Region	Primer	Nucleotide sequence	Restriction site	Amplicon size [bp]
ALA1	forward	5'-gctctagaAAATGGATCCCAGGAAATCAATT-3'	*Xba*I	
	reverse	5'-cgacctcgagTATCATCTCCGTGGAGGATCCT-3'	*Xho*I	4064
ALA10	forward	5'-tccccgcg*gctagc*GCTATGGCTGGTCCAAGTCG-3'	*Sac*II, *Nhe*I	
	reverse	5'-cgggatcCTTTAGACACCGACAAGATCCTTATAG-3'	*BamH*I	4417
ALA1	forward	5'-gctctagaCAATGACAAAGTGTCGGAGAAG-3'	*Xba*I	
	reverse	5'-cgggatcCTTCAGAAAGCAATGAAATTCTTG-3'	*BamH*I	4527

Table 8: Primer pairs for amplification of *ALA1*, *ALA10* and *ALA11* open reading frames in two halves. Major cases represent priming sequences, minor cases represent non-priming sequences/added overhangs, underlined nucleotides represent endonuclease restriction sites or start/stop codons.

Region	Primer	Nucleotide sequence	Restriction site	Amplicon size [bp]
	ALA1			
1)	forward	5'-gctctagaAAATGGATCCCAGGAAATCAATT-3'	*Xba*I	
	reverse	5'-ggacGAGCTCCATCGATATGTAG-3'	*Sac*I	1245
2)	forward	5'-gatgGAGCTCGTCCGTATTGG-3'	*Sac*I	
	reverse	5'-cgacctcgagTATCATCTCCGTGGAGGATCCT-3'	*Xho*I	2833
	ALA10			
1)	forward	5'-tcccgcgg*ctagc*GCTATGGCTGGTCCAAGTCG-3'	*Sac*II, *Nhe*I	
	reverse	5'-aaaAGTACTAGAGTCCTTAGACCTGCATCTG-3'	*Sca*I	2340
2)	forward	5'-aaaAGTACTTGCATACCGTGAGGTTG-3'	*Sca*I	
	reverse	5'-cgggatcCTTTAGACACCGACAAGATCCTTATAG-3'	*BamH*I	2883
	ALA11			
1)	forward	5'-gctctagaCAATGACAAAGTGTCGGAGAAG-3'	*Xba*I	
	reverse	5'-ttgaGCTAGCTTGTCGATACAATC-3'	*Nhe*I	2592
2)	forward	5'-acaaGCTAGCTCAAGCAGGG-3'	*Nhe*I	
	reverse	5'-cgggatcCTTCAGAAAGCAATGAAATTCTTG-3'	*BamH*I	1949

Table 9: Primer pairs for the conversion of *ALA1*, *ALA10* and *ALA11* clones to the GATEWAY cloning system. Major cases represent priming sequences, minor cases represent non-priming sequences/added overhangs, underlined nucleotides represent start codons, bold letters represent (parts of) the attB1 and attB2 GATEWAY specific cloning sites.

Clone	Primer	Nucleotide sequence
		First reaction
ALA1	attB1-forward1	5'-**aaaaagcaggct**tcATGGATCCCAGGAAATCAATTG-3'
	attB2-reverse1	5'-**agaaagctgggt**cTCTCCGTGGAGGATCCTTCAT-3'
ALA10	attB1-forward10	5'-**aaaaagcaggct**tcATGGCTGGTCCAAGTCGGA-3'
	attB2-reverse10	5'-**agaaagctgggt**cGACACCGACAAGATCCTTATAGATC-3'
ALA11	attB1-forward11	5'-**aaaaagcaggct**tcATGACAAAGTGTCGGAGAAGAAGAT-3'
	attB2-reverse11	5'-**agaaagctgggt**cGAAAGCAATGAAATTCTTGTTGAG-3'
		Second reaction
	attB1 F	5'-**gtttgtacaAAAAAGCAGGCT**-3'
	attB2 R	5'-**ctttgtacaAGAAAGCTGGGT**-3'

Table 10: Plasmids used in this work.

Plasmid	Function/Description	Resistance (b: bacteria, p: plants)
pAC161	binary T-DNA vector for generation of T-DNA mutagenized plants Rosso *et al.* (2003)	ampicillin (b), sulfadiazine (p)
pB7WGF2	GATEWAY binary T-DNA vector for expression of eGFP fusion constructs under control of *35S* promoter Karimi *et al.* (2002)	spectinomycin (b), phosphinotricin (p)
pBIN20	binary T-DNA vector for expression of mCherry-organelle marker fusions Hennegan and Danna (1998)	spectinomycin (b), kanamycin (p)
pBlueScript II KS+	cloning and sequencing vector MBI Fermentas (St. Leon-Rot, Germany)	ampicillin (b)
pDONR221	cloning and sequencing vector Invitrogen (Karlsruhe, Germany)	kanamycin (b)
pGTkan3	binary T-DNA vector for expression of eGFP fusion constructs Hajdukiewicz *et al.* (1994)	spectinomycin (b), kanamycin (p)
pSTBlue-1	cloning and sequencing vector MBI Fermentas (St. Leon-Rot, Germany)	ampicillin or kanamycin (b)
pUTkan	binary T-DNA vector for GUS expression under control of promoter of choice Yoo *et al.* (2005)	spectinomycin (b), kanamycin (p)
pUC18	expression vector MBI Fermentas (St. Leon-Rot, Germany)	ampicillin (b)
pROK2	binary T-DNA vector for generation of T-DNA mutagenized plants Baulcombe *et al.* (1986)	ampicillin (b), kanamycin (p)

Table 11 (continued on next page): Used plasmids obtained from the Palmgren laboratory (University of Copenhagen, Denmark).

Plasmid	Function/Description	Resistance/Auxotrophy
pMP1872	yeast expression vector pRS423-GAL1-10(-His) Poulsen *et al.* (2008b)	ampicillin/histidine
pMP2127	pMP1872 containing ALIS1-RGSH$_6$	ampicillin/histidine
pMP2129	pMP1872 containing ALIS3-RGSH$_6$	ampicillin/histidine
pMP2130	pMP1872 containing ALIS5-RGSH$_6$	ampicillin/histidine
pMP2432	pMP1872 containing ALA1-HA	ampicillin/histidine
pMP2435	pMP1872 containing ALA1-HA & ALIS1-RGSH$_6$	ampicillin/histidine
pMP2436	pMP1872 containing ALA1-HA & ALIS3-RGSH$_6$	ampicillin/histidine

Plasmid	Function/Description	Resistance/Auxotrophy
pMP2437	pMP1872 containing ALA1-HA & ALIS5-RGSH$_6$	ampicillin/histidine
pMP3229	pMP187 containing ALA10 (untagged)	ampicillin/histidine
pMP3230	pMP187 containing ALA10 & ALIS1-RGSH$_6$	ampicillin/histidine
pMP3231	pMP187 containing ALA10 & ALIS3-RGSH$_6$	ampicillin/histidine
pMP3232	pMP187 containing ALA10 & ALIS5-RGSH$_6$	ampicillin/histidine
pMP1869	yeast expression vector	
	pRS423-GAL1-10(-Leu)	ampicillin/leucine
pMP2284	pMP1869 containing ALIS1-RGSH$_6$	ampicillin/leucine
pMP2285	pMP1869 containing ALIS3-RGSH$_6$	ampicillin/leucine
pMP2286	pMP1869 containing ALIS5-RGSH$_6$	ampicillin/leucine
pMP3210	pMP1869 containing ALA11 (untagged)	ampicillin/leucine
pDRS2	pMP1872 containing yeast DRS2	ampicillin/histidine
pMP2061	cloning vector	
	pBlueScript SK- containing ALA11 (incl. stop codon)	
	MBI Fermentas (St. Leon-Rot, Germany)	ampicillin
pMP3228	cloning vector	
	pENTR/D-TOPO containing ALA10 (incl. stop codon)	
	Invitrogen (Karlsruhe, Germany)	kanamycin

2.3 Enzymes and Kits

All restriction enzymes were purchased from MBI Fermentas (St. Leon-Rot, Germany) and New England Biolabs (Frankfurt, Germany).
If not indicated self-made *Taq* DNA polymerase (2.7.8.1) was used for all regular PCR. In case of unclear results commercially available *Taq* DNA polymerase (MBI Fermentas, St. Leon-Rot, Germany) was used for PCR. For generation of accurate DNA copies prior to cloning, proof-reading polymerases were used in PCR (KOD [Novagen, Gibbstown, NJ, USA] or Pfu [MBI Fermentas, St. Leon-Rot, Germany], TripleMaster [Eppendorf, Hamburg, Germany]).
Furthermore, calf intestine alkaline phosphatase, DNase I, RNase A, T4-DNA ligase, Lambda DNA and the Maxima SYBR Green qPCR Mastermix were purchased from MBI Fermentas (St. Leon-Rot, Germany). RevertAid H Minus M-MuLV Reverse Transcriptase and RNA inhibitor were purchased from New England Biolabs (Frankfurt, Germany). SuperScript III reverse transcriptase as well as the BP and LR Clonase II Enzyme Mixes were ordered from Invitrogen (Karlsruhe, Germany). DIG-11-dUTP (alkali-labile) and CSPD were acquired from Roche Applied Science (Mannheim, Germany). The Perfectly Blunt Cloning Kit was purchased from Novagen (Gibbstown, NJ, USA) and the Low Viscosity Spurr Kit from Ted Pella (Redding, CA, USA).

2.4 Computer software

All sequence information was obtained from The Arabidopsis Information Resource (TAIR; http://www.arabidopsis.org; Huala *et al.*, 2001) and further analyzed using MacVector 10.0 for annotations, map generation and alignments. Restriction analyses were performed with EnzymeX 3. Sequencing data was analyzed using the 4Peaks 1.7.2 and MacVector 10.0 software. MacVector and Paup 4b10 and were used for phylogenetic analysis and tree generation. Oligonucleotides were designed using MacVector (general primer and sequencing primer) and the web-based version of Primer3 0.4.0 (http://frodo.wi.mit.edu/primer3/input.htm; Rozen and Skaletsky, 2000). Required primer for genotyping of T-DNA insertion mutants were designed using the iSect tool on the Salk Institute Genomic Analysis Laboratory web page (SIGnAL; http://signal.salk.edu/tdnaprimers.2.html). In order to predict subcellular localization and domains of proteins the collection of analysis and prediction tools from the Plant Membrane Protein Database (ARAMEMNON; http://aramemnon.botanik.uni-koeln.de) was used (Schwacke *et al.*, 2003). ImageJ 1.40g was used on pictures for area determination and object counting.

2.5 Biological material

2.5.1 Bacteria strains

Escherichia coli as well as *Agrobacterium tumefaciens* strains used in this work and listed in Table 12.

Table 12 (continued on next page): List of bacterial strains.

Escherichia coli

* XL1-Blue — Stratagene (La Jolla, CA, USA)
*rec*A1 *end*A1 *gyr*A96 *thi*-1 *hsd*R17 *sup*E44 *rel*A1
lac [F' *pro*AB *lac*I^{q}ZΔM15::Tn10 (Tet^{r})]

* DH5α — Hanahan (1983)
*rec*A1 *end*A1 λ-*gyr*A96 (Nal$_{r}$) *thi*-1 *hsd*R17 (r_{K}^{-} m_{K}^{+}) *sup*E44 *rel*A1 D(*lac*ZYA-*arg*F) U169
F-ϕ80d *lac*ZΔM15

* NovaBlue K-12 — Novagen (Nottingham, UK)
*rec*A1 *end*A1 *gyr*A96 *thi*-1 *hsd*R17 (r_{K12}^{-} m_{K12}^{+}) *sup*E44 *rel*A1
lac [F′ *pro*A^{+}B^{+} *lac*I^{q}ZΔM15::Tn10 (Tet^{r})]

Agrobacterium tumefaciens

* GV3101::pMP90 Koncz and Schell (1986)
Rif^r, Gent^r

2.5.2 Yeast Strains

Saccharomyces cerevisiae wild type strain was obtained from the *Saccharomyces Cerevisiae* Archive for Functional Analysis (EUROSCARF; http://web.uni-frankfurt.de/fb15/mikro/euroscarf/index.html, Frankfurt, Germany). The *dnf1*Δ*dnf2*Δ*drs2* triple mutant strain was previously described (Hua *et al.*, 2002) and was obtained from Thomas Pomorski's laboratory (Berlin, Germany). Yeast strains are listed in Table 13.

Table 13: List of used yeast strains.

wild type:	BY4741 (*MATa his3 leu2 ura3 met15*)
	EUROSCARF
triple mutant (Δ*drs2*Δ*dnf1*Δ*dnf2*):	ZHY709 (*MATa his3 leu2 ura3 met15 dnf1*Δ *dnf2*Δ *drs2::LEU2*)
	Hua *et al.* (2002)

2.5.3 Plants

All *Arabidopsis thaliana* single mutant lines as well as wild type (ecotype Columbia, Col-0) were either obtained from the Salk Institute Genomic Analysis Laboratory (SIGnAL; http://signal.salk.edu/; La Jolla, CA, USA) or the GABI-Kat project (Genomanalyse im biologischen System Pflanze; http://www.gabi-kat.de/; Cologne, Germany) via ordering at the Arabidopsis Biological Resource Center (ABRC, http://www.biosci.ohio-state.edu/~plantbio/Facilities/abrc/abrchome.htm, Columbus, OH, USA) and the Nottingham Arabidopsis Stock Centre (NASC; http://arabidopsis.org.uk/; Loughborough, UK; Scholl *et al.*, 2000; Alonso *et al.*, 2003; Rosso *et al.*, 2003). Used and generated mutant lines and their origins are listed in Table 14.

Table 14 (continued on next page): List of *Arabidopsis thaliana* T-DNA insertion lines.

Name	Origin
ala1-1	SALK_056947
ala10-1	GABI_785G10
ala10-2	SALK_024877
ala11-1	GABI_529G04

Name	Origin
ala11-2	SALK_107029
ala10/11	crossing of GABI_785G10 with GABI_529G04
ala1/10/11	crossing of GABI_785G10/GABI_529G04 with SALK_056947

The *ala10/11* double mutant was generated by crossing mutant lines *ala10-1* with *ala11-1*, allowing the F1 plant to self fertilize, and isolating mutant plants from an F2 population (chapter 2.6.6). The *ala1/10/11* triple mutant was generated in similar fashion by crossing *ala10/11* double mutant line with *ala1-1*.
Other transgenic plants generated by plant transformation (chapter 2.6.7) are listed in Table 15.
Tobacco plants (*Nicotiana benthamiana*) were used for transient expression of fusion proteins in epidermal leaves (chapter 2.11.1).

Table 15: List of generated *Arabidopsis thaliana* transgenic lines.

Description		Name
promoter-GUS reporter lines		pALA1::GUS
		pALA10::GUS
		pALA11::GUS
GFP reporter lines	(truncated)	*35S*::eGFP-ALA1(TM1-4)
		35S::eGFP-ALA10(TM1-4)
		35S::eGFP-ALA11(TM1-4)
	(full length)	*35S*::eGFP-ALA1
		35S::eGFP-ALA10

2.6 Handling bacteria, yeast and plants

2.6.1 Cultivation of bacteria

Bacteria were normally grown on standard LB (Bertani, 1951) if not mentioned otherwise. The media was spiked with one or more required antibiotics depending on the bacterial stain transformed plasmid (Table 16). The media (1% tryptone, 0.5% yeast-extract, 0.5% sodium chloride [w/v]; pH 7.5 with NaOH) was either used for liquid cultures or solidified with 1.5% agar (w/v) for plate cultures. Plate cultures of *E. coli* were grown over night (at least 8 h) at 37 °C, whereas cultures of *A. tumefaciens* were

grown for 2 d (at least 12 h) at 28 °C. Liquid cultures were grown under the same conditions in an incubator with constant shaking of 220 rpm.

Table 16: Antibiotics used for cultivation of bacteria.

Antibiotic	Concentration [mg/l]
kanamycin	50
rifampicin	50
gentamycin	25
ampicillin	100
spectinomycin	25

2.6.2 Transformation of bacterial cells

Heat-shock transformation

Competent *E. coli* cells (chapter 2.6.2.1) were heat-shock transformed. 1 µl plasmid preparation (chapter 2.7.1) was added to on ice thawed cells. After an incubation for 30 min on ice, the cells were incubated at 42 °C for 45 sec and immediately chilled on ice for 2 min. 500 µl 37 °C warm SOC media (2% tryptone, 0.5% yeast-extract [w/v], 10 mM NaCl, 2.5 mM KCl, 10 mM $MgCl_2$, 10 mM $MgSO_4$, 20 mM glucose; pH 7.5 with NaOH) was added to the cells, followed by an incubation for 50 min at 37 °C under shaking. Depending on the plasmid size 100-900 µl of the cells solution was plated on LB plates supplemented with the required antibiotic and incubated at 37 °C.

Electroporation

A. tumefaciens cells were transformed via electroporation based on Dower *et al.* (1988). Competent cells (chapter 2.6.2.1) were thawed on ice and 1 µl plasmid preparation (chapter 2.7.1) was added. Cells were incubated for 10 min on ice, transferred to an ice-cold electroporation cuvette (1 mm width) and shocked with 2.2 kV for 5 ms. Immediately, 1.9 ml hand-warm SOC media was added to the cells. The solution was transferred to a new reaction tube and incubated under shaking for 2 h at 28 °C. 50-100 µl were plated on a LB plate supplemented with the required antibiotics and incubated at 28 °C for 2 d.

2.6.2.1 Generation of competent cells

Escherichia coli

Chemical competent *E. coli* cells were generated using a variant of the calcium chloride method (Ausubel *et al.*, 1989) where calcium chloride was replaced by rubidium

chloride. Cells were grown in 200 ml Psi broth (2% tryptone, 0.5% yeast-extract, 0.5% magnesium sulfate [w/v]; pH 7.6 with KOH) until an OD_{600} of 0.5 was reached. Cells were incubated for 15 min on ice and pelleted by centrifugation for 10 min at 3000 g and 4 °C. The pellet was resuspended in 40 ml ice-cold transformation buffer I (100 mM RuCl, 50 mM MnCl, 30 mM CH_3COOK, 10 mM $CaCl_2$ in 15% glycerol [v/v]; pH 5.8 with acetic acid) and incubated for 15 min on ice. The cells were pelleted again, resuspended in 4 ml ice-cold transformation buffer II (75 mM $CaCl_2$, 10 mM RuCl, 10 mM MOPS in 15% glycerol [v/v]; pH 6.5 with NaOH), incubated for 10 min on ice and frozen in liquid nitrogen in 50 µl aliquots. The cells were stored at -80 °C.

Agrobacterium tumefaciens

Electrocompetent *A. tumefaciens* cells were generated based on Sambrook *et al.* (1989). Cells where grown in 500 ml SOB media (2% tryptone, 0.5% yeast-extract, 0.05% sodium chloride [w/v], 25 mM KCl, 20 mM glucose, 10 mM $MgCl_2$; pH 7.0 with NaOH) until an OD_{600} of 0.7 was reached. Cells were incubated for 15 min on ice and pelleted by centrifugation for 10 min at 3000 g and 4 °C. The pellet was resuspended in 500 ml ice-cold ddH_2O and pelleted again. Cells were then resuspended in 250 ml ice-cold water/glycerol (ddH_2O, 10% glycerol [v/v]), pelleted, resuspended in 10 ml ice-cold water/glycerol, pelleted and finally resuspended in 2 ml ice-cold water/glycerol. The cell solution was divided into 50 µl aliquots, frozen in liquid nitrogen and stored at -80 °C.

2.6.3 Cultivation of yeast

Yeast wild-type cells were grown on standard YPD media (1% yeast-extract, 2% peptone, 2% glucose [w/v]; pH 6.2 with NaOH; Sambrook *et al.*, 1989). All other yeast strains and transformed yeast was grown on SD minimal media (0.17% yeast nitrogen base, 0.5% ammonium sulfate, amino acids, 2% glucose [w/v]; pH 6.2 with NaOH; Rose and Broach, 1990). For auxotrophy selection the composition of amino acids (Table 17) within the SD media was adjusted depending on the plasmid and yeast strain. Amino acid solutions were sterile filtered and added to the sterilized SD media. Both YPD and SD were either used for liquid cultures or solidified with 2% agar (w/v) for plate cultures. Liquid yeast cell culture was maintained under constant shaking of 220 rpm at 35 °C for 1-3 d, whereas yeast cells on plates were incubated at 30 °C (if not mentioned otherwise) for 2-7 d, depending on the strain and media. Due to the cold-sensitivity of the used mutant stain all cells were maintained on plates at 35 °C.

Table 17: Amino acids used for auxotrophy selection in SD media.

Amino acid	Final concentration (w/v)
adenine sulfate	0.02%
uracil	0.02%
L-tryptophan	0.02%
L-leucine	0.1%
L-histidine HCl	0.02%
L-methionine	0.02%

2.6.4 Transformation of yeast cells

Yeast cells were transformed using lithium acetate based on Gietz and Woods (2002). 10 ml liquid culture was grown to an OD_{600} of 0.8. 2 ml cell suspension was transferred into a new reaction tube and centrifuged for 4 min at 800 g and RT. Supernatant was discarded and the cells carefully mixed with 5 µl (10 mg/ml) denatured salmon sperm DNA (Sigma-Aldrich, Taufkirchen, Germany; incubated for 5 min at 95 °C, immediately chilled on ice for 5 min) and 0.5-2 µg plasmid. The cells were then resuspended in 500 µl transformation buffer (100 mM lithium acetate, 1 mM EDTA, 36% PEG 3350 [w/v] in 10 mM Tris; pH 7.5) and 20 µl freshly prepared 1 M DTT was added. After an incubation over night at RT, cells were pelleted, resuspended in 100 µl selective SD media, plated on selective SD plates and incubated at 30 °C.

2.6.5 Cultivation of plants

2.6.5.1 Soil

A mix of P- and T-soil and sand (2:2:1 [v/v]; pH 5.5-6.0, Einheitserde, Balster Einheitserdewerk, Fröndenberg, Germany) served as soil after sterilization and drying.

Arabidopsis thaliana

Seeds were sown in pots (12 cm ø) and allowed to stratify at 6 °C for 48 h. Pots were either transferred to the greenhouse (16 h light/d, 250-300 $\mu mol*m^{-2}*sec^{-1}$ photosynthetically active radiation, 70% relative humidity, 21-24 °C) for seed production or to a climate chamber with strictly controlled conditions (16 h light/d, 120 $\mu mol*m^{-2}*sec^{-1}$ photosynthetically active radiation, 70% relative humidity, 21 °C [if not mentioned otherwise]) for phenotypical analysis. For plant analysis under short day conditions, plants were cultivated under the same conditions but light period was reduced to 8 h/d. Plants

were watered every day. 10 days after germination seedlings were transferred to single pots (6 cm ø) with fresh soil and further cultivated until first siliques ripened. If seeds were needed the entire inflorescence was put the into a paper bag at that stadium and plants were allowed to grow for 2 more weeks. Then the plants were dried for 2 weeks, the bag with the inflorescence removed and seeds harvested by separating them dried parts of the plant using a sieve. Seeds were stored at 6 °C.

Nicotiana benthamiana
Plants of tobacco were grown in pots (9 x 9 cm, a single seed/pot) in the greenhouse at 24 °C (14 h light/d, 300-350 µmol*m^{-2}*sec^{-1}, 70% relative humidity).

2.6.5.2 Seed sterilization

Seeds of *Arabidopsis thaliana* were surface sterilized when grown on plates (chapter 2.6.5.3). Approximately 500 seeds were filled in a reaction vial and incubated in 1 ml 70% ethanol for 2 min. The ethanol was removed and 1 ml 1% sodium hypochlorite solution was added. After an incubation of 5 min the seeds were washed 3 times with sterile ddH_2O, dried on sterilized filter paper and stored at 4 °C. All steps occurred under sterile conditions.

2.6.5.3 Sterile culture

Arabidopsis plants were cultivated under sterile conditions on half strength MS medium (Murashige and Skoog, 1962) supplemented with 2% sucrose (w/v), buffered with 20 mM MES; pH 5.8 and solidified with 1% agar (w/v). After sterilization the media was cooled down to app. 50 °C, sterile filtered MS-vitamins and required antibiotics were added and the media was poured into Petri dishes.

Plates
Surface sterilized seeds (chapter 2.6.5.2) were put on plates (8 cm ø) and lids were closed with tape ensuring respiration (Leucopore, Duchefa, Haarlem, The Netherlands). Plates were stratified for 2 d at 6 °C in the dark and then incubated in a growth chamber (16 h light/d, 120 µmol*m^{-2}*sec^{-1} photosynthetically active radiation, 70% relative humidity, 21 °C).

Vertical plates
In order to observe root growth, plants were grown vertically under sterile conditions in a growth chamber (16 h light/d, 70% relative humidity, 21 °C) with lateral illumination

(120 µmol*m^{-2}*sec^{-1}). Sterilized seeds were put in a row in the upper third of the plates (12 x 12 cm) using a toothpick. After 10 and 20 d root length was measured.

2.6.5.4 Hydroponic culture

In order to observe the influence of phosphorus deprivation on plant development a hydroponic growth system was chosen. Pots (10 x 10 cm) were filled with acid washed sand (incubated in 10% hydrochloric acid over night, rinsed with ddH_2O, dried at 50 °C) and were watered with Hoagland based media (Arnon and Hoagland, 1940) supplemented with MS vitamins. Standard media contained 0.5 mM phosphorus in contrast to low phosphorus media with 10 µM phosphate where potassium phosphate was reduced and the missing potassium added in form of potassium chloride. *Arabidopsis* was grown for 10 d under sterile conditions (chapter 2.6.5.3) and then transferred to the pots (5 plants per pot). The plants were then cultivated in a climate chamber (16 h light/d, 120 µmol*m^{-2}*sec^{-1} photosynthetically active radiation, 70% relative humidity, 21 °C) and the development observed compared to plants grown on standard Hoagland based media.

2.6.6 Crossing of *Arabidopsis thaliana*

The female partner was emasculated before the flower had opened and anthers were immature. The pistil was pollinated with mature stamen from the male crossing partner. A macroscope was used and assured that mature pollen was on the surface of the style.

2.6.7 Transformation of *Arabidopsis thaliana*

Stable transformation of *Arabidopsis* wild-type plants (ecotype Col-0) was achieved by floral dipping (Clough and Bent, 1998). 200 ml culture of *A. tumefaciens* transformed with the required binary vector was grown over night. The cells were pelleted for 20 min at RT and 3000 g and resuspended in an equal volume of dipping media (half strength MS supplemented with 5% sucrose [w/v], 44 nM BAP and 0.005% Silwet L-77 [v/v] [Lehle Seeds, Round Rock, TX, USA]). For each transformation the inflorescences of five singe *Arabidopsis* plants were dipped into the bacteria containing solution for app. 30 sec. The inflorescences were app. 10 cm high and first developed siliques were removed prior to dipping. In order to select antibiotic resistant transformants, the developed seeds were grown under sterile conditions on MS plates for two weeks. Developed green plants were carefully picked from the plate and put into single pots for further

cultivation in the greenhouse or a climate chamber. For the selection of phosphinotricin resistant transformants (De Block *et al.*, 1987) seeds were sown in boxes (15 x 30 cm), transferred to the greenhouse and sprayed with a 0.1% phosphinotricin solution (Basta, Agrevo, Berlin, Germany) after the first true leaves had developed (app. 1 week). The treatment was repeated after 2 and 5 d. Resistant, still green plants were picked after one week of the last treatment and planted into single pots. Independent transformants were allowed to self-pollinate for two generations. The third generation was screened for segregation events to identify homozygous transformants within the second generation.

2.6.8 Identification of T-DNA insertion mutants

A PCR-based method (description of PCR in chapter 2.7.8) was used to identify and verify homozygous mutant plants. Genomic DNA was prepared as described in chapter 2.7.1. Two PCR reactions per T-DNA insertion were performed; the first reaction gave rise on an intact gene, the second reaction detected integrated T-DNA. For these purposes two gene specific primers, homologous to the gene sequence up- and downstream of the insertion locus of the T-DNA (LP – left primer, RP – right primer) and a T-DNA specific primer, homologous to the left border sequence (LB), were generated (chapter 2.4) and are listed in Table 1. For the first reaction both gene specific primers (LP and RP) were used, for the second reaction a gene specific primer and the T-DNA specific primer (RP and LB) were combined. A touch-down PCR with a modified program (given in Table 18) was chosen to achieve better amplification results (Don *et al.*, 1991).

Table 18: PCR program for identification of T-DNA insertion lines.

2 min 94 °C
[30 sec 94 °C – 25 sec 60 °C – 1 min 72 °C] x 9 - 0.5 °C/cycle
[30 sec 94 °C – 25 sec 55 °C – 1 min 72 °C] x 21
5 min 72 °C

LP and RP were designed to give a product of app. 1000 bp. In the case a T-DNA is integrated into a gene, the amplification product is too large (app. 4-5 kb) to be amplified with the used *Taq*-DNA-polymerase and elongation time of one minute. RP and LB should give an amplification product between 600 and 1000 bp under those circumstances, depending on the position of the T-DNA. Considering the fact that *Arabidopsis thaliana* is a diploid species, only evaluation of both PCR reactions can clearly identify the insertion status of the T-DNA. As the first detection reaction should result negative for insertions in both alleles, control reactions using wild type DNA were required. Once homozygous identified mutant plants were twice backcrossed (chapter 2.6.6) with wild

type to clear the genome from eventually additional T-DNA insertions. F2 generation plants were checked again via PCR for homozygous T-DNA insertions in the corresponding genes and the T-DNA insertion number was controlled via southern hybridization (chapter 2.7.5).
The exact T-DNA integration position was confirmed by sequencing. Therefore the T-DNA specific PCR (using RP and LB primers) was performed with a proofreading DNA-polymerase (KOD, Novagen, Gibbstown, NJ, USA). The product was blunt-cloned (chapter 2.7.4) into the EcoRV digested (chapter 2.7.2) and dephosphorylated (chapter 2.7.3) vector pBlueScript II KS+. The generated plasmid was transformed into *E. coli* cells for amplification (chapter 2.6.2), extracted from the cells (chapter 2.7.1) and sent together with primers T3 5'-GCGAAATTAACCCTCACTAAAG-3' and T7 5'-GTAATAC GACTCACTATAGGGC-3' for sequencing.

2.7 Molecular biological methods

Standard protocols for molecular methods were used (Sambrook *et al.*, 1989) if not mentioned otherwise.
DNA for sequencing analysis was sent to Macrogen (Seoul, South Korea) or GATC Biotech (Konstanz, Germany) and results were downloaded from the companies' homepages.

2.7.1 DNA extraction

Genomic DNA
Genomic DNA from *Arabidopsis* leaves was isolated from either frozen or fresh material a modified CTAB method (Murray and Thompson, 1980). 50-100 µg were homogenized using either a mini-pestle or a grinding mill (addition of 0.5 mm ø steel ball) for 1.5 min at 30 Hz directly in 1.5 ml tubes with 0.2 ml extraction buffer (2% CTAB, 1% PVP MW 10.000 [w/v], 1.4 M NaCl, 20 mM EDTA, 100 mM Tris; pH 8.0). Samples were incubated at 95 °C for 1 h and 200 µl phenol/chloroform/isoamyl alcohol (25:24:1 v/v) was added and mixed, followed by centrifugation for 10 min at 13000 g. The aqueous phase was transferred to a new tube, mixed with chloroform/isoamyl alcohol (24:1 v/v) and centrifuged for 10 min at 13000 g. Again, the aqueous phase was transferred to a new tube but supplemented with 0.7 vol isopropanol to precipitate genomic DNA for 10 min at RT. After centrifugation for 10 min at 13000 g the DNA pellet was washed with 70% ethanol, air-dried and dissolved in 50 µl ddH_2O.

Plasmid DNA

The isolation of plasmid DNA from *E. coli* was performed with liquid cultures based on alkaline lysis (Birnboim and Doly, 1979; Ish-Horowicz and Burke, 1981). Cells of 2 ml liquid culture were spun down at 3000 g for 10 min and resuspended in 100 µl ice-cold buffer (50 mM glucose, 10 mM EDTA, 25 mM Tris; pH 8.0). After incubation for 2 min on ice, 200 µl lysis buffer was added (0.2 N NaOH, 1% SDS [w/v]) and the samples softly inverted and incubated for 5 min on ice. 200 µl neutralization buffer (5 M potassium acetate, 11.5% acetic acid [v/v]) was added and the samples centrifuged for 5 min at 13000 g and 4 °C. 400 µl supernatant was transferred into a new reaction tube and an equal volume of phenol/chloroform/isoamyl alcohol (25:24:1 v/v) was added. After mixing and centrifugation for 10 min at 13000 g and 4 °C, the aqueous phase was transferred to a new tube and supplemented with an equal volume of 96% ethanol to precipitate plasmid DNA for 10 min on ice. After centrifugation for 10 min at 13000 g and 4 °C the DNA pellet was washed with 70% ethanol, air-dried and dissolved in 50 µl ddH_2O.

2.7.2 Restriction digest and analysis

Restriction endonucleases were used to digest DNA according to the manufacturers' instructions (MBI Fermentas, St. Leon-Rot and New England Biolabs, Frankfurt, Germany). A standard digest was performed in a 20 µl volume (Table 19) for 1 h at the temperature optimum of the used enzyme. In the case two endonucleases were used at the same time a buffer in which both enzymes showed ≥80% performance was chosen. If no suitable buffer existed or enzymes with different *tem*perature optima were used, restriction analyses were performed successively, whereas buffer and enzyme of the first digest were removed via DNA extraction and precipitation (chapter 2.7.7.3).

Table 19: Composition of a standard DNA digest.

Reagent	Quantity/Concentration
DNA	10 ng - 1µg
enzyme	3-5 u (each)
BSA	0-0.1 mg/ml, depending on the used enzyme
in buffer	depending on the used enzyme

2.7.3 Dephosphorylation

Phosphates at the 5'-termini of DNA strands were removed in order to prevent self-ligation in a ligation reaction (2.7.4). Calf intestine alkaline phosphatase (CIAP, MBI

Fermentas, St. Leon-Rot, Germany) was used according to the manufacturer's instructions. A standard dephosphorylation was performed in 40 µl using 1 µg vector DNA. After incubation for 15 min at 37 °C and heat-inactivation at 65 °C for 10 min, dephosphorylated DNA was extracted, precipitated (chapter 2.7.7.3) and dissolved in 10 µl ddH_2O.

2.7.4 Ligation

Ligation of DNA fragments with compatible ends (sticky ends) was carried out using T4-DNA ligase (MBI Fermentas, St. Leon-Rot, Germany) according to the manufacturer's instructions. A standard ligation was performed in a 20 µl volume for 2-4 h at RT using ≤100 ng DNA. In the case DNA fragments with blunt ends were ligated 5% PEG 4000 [w/v] was added to the reaction (Zimmerman and Pheiffer, 1983). Ligation was stopped and ligase inactivated by incubation at 65 °C for 20 min.

2.7.5 Southern hybridization

2.7.5.1 Preparation of genomic DNA

Genomic DNA was isolated based on a modified method by Dellaporta *et al.* (1983). Leaf tissue of soil grown 30 d old plants was frozen in liquid nitrogen and incubated with 5 ml 65 °C warm extraction buffer (0.5 M NaCl, 50 mM EDTA, 10 mM β-mercapto ethanol, 1% SDS [w/v], 100 mM Tris; pH 7.5) for 10 min at 65 °C under shaking. Each probe was supplemented with 1.67 ml 5 M potassium acetate, carefully inverted, incubated for 20 min on ice and centrifuged for 30 min at 3300 g. The supernatant was transferred to a new reaction tube, supplemented with 3.33 ml isopropanol and nucleic acids precipitated for 10 min on ice. Nucleic acids were pelleted via centrifugation for 30 min at 3300 g and 4 °C, air-dried, dissolved in 500 µl TE (1 mM EDTA, 10 mM Tris; pH 8.0) and transferred to a new reaction tube. RNA was digested via addition of 20 µl RNase A (10 mg/ml) and incubation for 30 min at 37 °C. An equal volume of phenol/chloroform/isoamyl alcohol (25:24:1 v/v) was added, mixed and centrifuged for 10 min at 13000 g and 4 °C. The aqueous phase was transferred to a new tube, supplemented with an equal volume of chloroform/isoamyl alcohol (24:1 v/v), mixed and centrifuged for 10 min at 13000 g and 4 °C. The aqueous phase was again transferred to a new reaction tube and nucleic acids were precipitated with sodium acetate and isopropanol (chapter 2.7.7.3). Extracted genomic DNA was checked for integrity on an agarose gel

(chapter 2.7.7.1). 5 µg of intact genomic DNA were used for digestion with endonucleases in a total volume of 50 µl (chapter 2.7.2) using 50 u of each enzyme (Table 20) and an incubation time of app. 6 h: First, 30 u of each enzyme were added to the probes and incubated for 2 h, then the remaining 20 u were added.

Table 20: List of used restriction enzymes for digestion of genomic DNA from *ala* mutant lines for southern hybridization.

Line	Restriction enzyme
ala1-1	*Kpn*I
ala10-1	*Sac*I
ala11-1	*Hind*III

2.7.5.2 Southern transfer

Digested genomic DNA was electrophoretically separated on a 0.8% agarose gel at 3.5 V/cm for 6 h (chapter 2.7.7.1). Subsequently the gel was incubated in 0.2 N hydrochloric acid for 10 min, in denaturing buffer (1.5 M HCl, 0.5 N NaOH) for 30 min and twice in neutralizing buffer (1.5 M NaCl, 1 M Tris; pH 7.4 with HCl) for 20 min. The DNA was transferred to a nylon membrane (Hybond NX, Amersham Pharmacia Biotech, Freiburg, Germany) via wet capillary transfer (Southern, 1975) with 20x SSC (3 M NaCl, 0.3 M sodium citrate) over night. After transfer the membrane was washed with 2x SSC (0.3 M NaCl, 30 mM sodium citrate) and dried on blotting paper (3MM, Whatman, Maidstone, UK). DNA was cross-linked to the membrane with UV-light (1200 x100 µJ).

2.7.5.3 DIG-labeling of DNA

Probes for hybridization were generated via PCR and simultaneously DIG-labeled using *Taq* polymerase (MBI Fermentas, St. Leon-Rot, Germany). PCR for DIG-labeled probe generation (composition given in Table 21) was performed in 100 µl reaction volume (divided into 4 fractions) with DIG-dUTP (Roche Applied Science, Mannheim, Germany) using a slightly modified standard program (Table 23) with 30 cycles and 57 °C annealing temperature. Vector DNA pROK2 and pAC161 served as a template for the labeling reaction, thus, generating probes for SALK and GABI-Kat T-DNA insertion lines, respectively. The resistance gene within the T-DNA region was amplified using the primer combinations given in Table 4. PCRs were loaded onto a 1% agarose gel for quantification and purification (chapter 2.7.7.1).

Table 21: Composition of DIG-labeling PCR.

Reagent	Quantity/Concentration
DNA template	1 ng plasmid DNA
nucleotides	0.2 mM dATP, dGTP, dCTP (each)
	0.13 mM dTTP
	3.5 mM DIG-dUTP
$MgCl_2$	25 mM
primer 1	0.2 µM
primer 2	0.2 µM
polymerase	5 u
in buffer	with $(NH_4)_2SO_4$

2.7.5.4 Hybridization

Hybridization of DIG-labeled probes to membrane bound DNA was performed in hybridization tubes under rotation at 42 °C in a hybridization oven. Prior the membrane was wet with 2x SSC and incubated for 2 h at 42 °C with 10 ml 65 °C heated hybridizing buffer (Table 22). 250 ng DIG-labeled probe was added to 10 ml hybridization buffer (Table 22) and the membrane incubated with the solution at 42 °C for app. 12 h.

Table 22: Hybridization buffer.

Reagent	Quantity/Concentration
blocking reagent	3% (w/v) (Roche Applied Science, Mannheim, Germany)
sodium lauroyl-sarcosine	0.1% (v/v)
SDS	0.2% (w/v)
salmon sperm DNA	50 µg/ml (w/v), heated for 10 min at 95 °C, immediately chilled on ice
formamide	50% (v/v)
in 5x SSC	750 mM NaCl, 75 mM sodium citrate
for hybridization:	
DIG-labeled probe	25 ng/ml, heated for 10 min at 95 °C, immediately chilled on ice

2.7.5.5 Immunodetection

Prior to immunodetection the membrane was washed in a series of buffers as follows: wash buffer I (2x SSC, 0.1% SDS [w/v]) for 10 min at RT, wash buffer II (0.5x SSC, 0.1% SDS [w/v]) for 20 min at 65 °C, wash buffer III (0.1x SSC, 0.1% SDS [w/v]) for 20 min at 65 °C and wash buffer IV (100 mM maleic acid, 150 mM NaCl, 0.3% Tween

20; pH 7.5 with NaOH) for 5 min at RT. Blocking of the membrane was performed for 30 min at RT using blocking buffer (100 mM maleic acid, 150 mM NaCl, 1.5% blocking reagent ([w/v], Roche Applied Science, Mannheim, Germany); pH 7.5 with NaOH). Immunological detection of DIG-labeled DNA was performed as follows: Incubation of the membrane with anti-DIG antibody (Roche Applied Science, Mannheim, Germany) diluted 1:3800 in blocking buffer for 30 min at RT. Washing of the membrane three times with wash buffer IV for 15 min at RT followed by incubation for 5 min at RT in detection buffer (50 mM $MgCl_2$, 100 mM NaCl, 100 mM Tris; pH 9.5). Visualization of detected DNA was performed via chemiluminescence using CSPD. 1 ml CSPD solution (0.1% CSPD [v/v] in detection buffer) was dropped onto the membrane and incubated for 5 min at RT. The membrane was wrapped in foil, excessive CSPD solution removed, incubated for 10 min at 37 °C and exposed to a film (XOD Retina, Fotochemische Werke, Berlin, Germany) for 3 h at RT which was subsequently developed.

2.7.6 RNA extraction

For extraction of total RNA from *Arabidopsis* the Trizol method was applied (Chomczynski and Sacchi, 1987; Weigel and Glazebrook, 2002). Per 100 mg of frozen ground plant material 0.75 ml Trizol reagent was added (Invitrogen, Karlsruhe, Germany). The samples were shaken for 30 sec until the material was melted and incubated for 15 min at RT. Cell compounds were removed through centrifugation for 10 min at 4 °C and 14000 g. The supernatant was divided and allotted into two new reaction tubes. 0.2 ml of chloroform/isoamyl alcohol (24:1 v/v) were added to each tube and softly mixed for 30 sec to separate RNA in the aqueous phase. After incubating for 5 min at RT, tubes were spun at 4 °C and 14000 g for 15 min for phase separation. RNA was precipitated through addition of 0.6 vol isopropyl alcohol and 0.1 vol 3 M sodium acetate to the upper phase in a new reaction tube. Samples were incubated for 30 min at 4 °C and then centrifuged for 10 min at 14000 g and 4 °C. The supernatant was discarded and pelleted RNA washed twice with 1 ml 70% ethanol, air-dried for 10 min at RT and content of both reaction tubes dissolved and combined in 50 µl DEPC-treated water (0.1 ml DEPC to 100 ml ddH_2O stirring over night, twice autoclaved). RNA quantity was determined photometrically (chapter 2.7.7.4) and quality controlled on integrity via gel electrophoresis (chapter 2.7.9).

2.7.7 Analysis, quantification and purification of nucleic acids

2.7.7.1 Gel electrophoresis

In order to separate nucleic acids regarding their size horizontal electrophoresis was performed using agarose gels. The method is used for analysis of PCRs and enzymatic digests of DNA as well as for concentration estimation (using a defined amount of size marker), integrity control and purification of DNA from other nucleic acids and buffers.

DNA

The gel usually consisted of 1% agarose, which was dissolved in TAE buffer (40 mM Tris, 1 mM EDTA, pH 8.0) by boiling the solution in a microwave oven. After cooling down to app. 50 °C ethidium bromide was added to a final concentration of $5*10^{-5}$% (v/v) and the gel was poured into a gel chamber of varying size applying combs with a different quantity and slot height, depending on the number and quantity of probes. The gel was transferred to an electrophoresis chamber filled with TAE buffer, nucleic acid containing probes were mixed 1:6 with loading dye (15% ficoll [v/v], 0.2% bromo-phenol blue [w/v] in water) and applied to the gel. *Pst*I digested λ-phage DNA (MBI Fermentas, St. Leon-Rot, Germany; denatured at 65 °C for 5 min after digestion, cooled on ice for 3 min and dissolved in loading dye) was used as a size marker. Typically, electrophoresis was carried out with 8 V/cm gel for 1h, depending on the gel size. Ethidium bromide intercalated in nucleic acids emits light at 556 nm when excited by UV light. For visualization of nucleic acids, the gel was laid on a transilluminator using light of 254 nm and photographed (DeVision DBox, Decon, Hohengandern, Germany).

RNA

To keep RNA denatured, formaldehyde and formamide were used. The gel consisted of 1.25% agarose in MEN buffer (20 mM MOPS, 1mM EDTA, 5mM sodium acetate; pH 7.0) supplemented with 5.5% formaldehyde (v/v). Concentration of RNA samples was determined (chapter 2.7.7.4) and 5 µg RNA adjusted to 8 µl using DEPC-treated water. The probes were treated with 12 µl RNA-loading dye (37% formamide, 5.5% formaldehyde, 6% ficoll, 1% ethidium bromide [v/v], 0.06% bromo-phenol blue [w/v] in MEN buffer), incubated for 15 min at 65 °C and immediately chilled on ice. The gel was fitted into the gel chamber and RNA probes were applied, whereas unused slots were filled up with RNA-loading dye to achieve a clean and equal separation. Then the gel chamber was filled with MEN buffer until the gel was slightly covered with buffer solu-

tion. A voltage of 4 V/cm was applied for 15 min. After migration of the RNA samples into the matrix additional MEN buffer was poured into the chamber. Electrophoresis was carried out with 8 V/cm gel for 3-6 h, depending on the gel size. For documentation the gel was laid on a transilluminator in the same way as for DNA gels.

2.7.7.2 Gel extraction

Nucleic acids (PCR products or fragments of restriction digests) were extracted from agarose gels using a simple self-made device: A hole was made in the tip of a 0.5 ml plastic reaction tube using a syringe. The tube was stuffed with a small amount of plastic fiber (Filterwolle, Amtra, Rodgau, Germany) and inserted in a 1.5 ml plastic reaction tube. DNA band was cut out of the agarose gel with a scalpel on a transilluminator, the gel piece inserted in the extraction device and centrifuged for 10 min at 13000 g. The smaller reaction tube with the gel debris was removed and nucleic acids in the resulting solution were precipitated, washed and redissolved in 10 µl ddH_2O (chapter 2.7.7.3).

2.7.7.3 Purification and precipitation of nucleic acids

Phenol-chloroform extraction
Nucleic acids were extracted from solutions by addition of an equal volume of phenol/ chloroform/isoamyl alcohol (25:24:1 v/v). The solution was mixed and centrifuged for 10 min at 13000 g and 4 °C. The upper phase was supplemented with an equal volume of 96% ethanol and centrifuged for 10 min at 13000 g and 4 °C. The resulting nucleic acid pellet was washed with 70% ethanol, air-dried and dissolved in a suitable amount of ddH_2O.

Precipitation
Nucleic acids were precipitated with 0.1 vol 3 M sodium acetate (pH 5.2) and 1 vol isopropanol. After a 10 min incubation on ice, nucleic acids were pelleted by centrifugation for 10 min at 13000 g and 4 °C, washed twice with 70% ethanol, air-dried and dissolved in 10-50 µl sterile ddH_2O.

2.7.7.4 Concentration determination of nucleic acids

DNA or RNA concentrations were determined photometrically (Sambrook *et al.*, 1989). Samples were diluted in water (1:50-1:200), filled in a cuvette and measured at 260, 280 and 320 nm against a blank probe. The value at 260 nm multiplied by a correction

factor of 50 and the dilution factor yields the content of double-stranded DNA in µg/ml. In case of RNA the correction factor is 40. The absorption quotient at 260 and 280 nm indicates the purity of nucleic acids. Samples with values equal or greater than 1.8 are considered non-protein contaminated. The value at 320 nm indicates carbohydrate contamination and should not exceed 0.01.

2.7.8 PCR

The PCR method, established by Mullis *et al.* (1986), was used to amplify DNA-fragments. The reaction requires two oligonucleotide sequences (primers) complementary to the target region, dNTPs, a DNA template (vector, genomic DNA, cDNA or bacterial cells [colony PCR]), DNA-dependent polymerase and a suitable buffer. Under a cycling temperature program (Table 23), DNA strands of template and primers are physically separated (denaturing), primers are allowed to hybridize to the template (annealing) and the region in between the primers is synthesized by the polymerase (elongation). Repeating these steps the DNA target is exponentially amplified.

Table 23: Standard PCR program.

Step	Time	Temperature	Remark
1 Initial denaturing	2 min	94 °C	
2 Denaturing	45 sec	94 °C	
3 Annealing	30 sec	55 °C	
4 Elongation	1 min	72 °C	back to step 2, 32 cycles
5 Final synthesis	5 min	72 °C	

Table 24: Standard PCR composition.

Reagent	Quantity/Concentration
DNA template	genomic DNA: 100-500 ng or
	plasmid DNA: 50 pg – 1 ng
nucleotides	0.2 mM of each dNTP
primer 1	1 µM
primer 2	1 µM
polymerase	1 u
in *Taq*-buffer	20 mM $(NH_4)_2SO_4$, 2 mM $MgCl_2$, 0.01% Tween 20 (v/v), 75 mM Tris; pH 8.8

The PCR program was varied in annealing temperature (depending on the primer pair combination), elongation time (depending and the product length and polymerase processing capacity) and cycle number (depending on the template concentration and amplification rate) for each purpose individually.
Standard PCR reactions were performed in 25 µl volume using *Taq*-polymerase (chapter 2.7.8.1) and sterilized working materials. The standard reaction composition is given in Table 24. When amplifying DNA fragments prior to cloning, commercially available proofreading polymerase with 3'-5' exonuclease activity (KOD, [Novagen, Gibbstown, NJ, USA] or TripleMaster [Eppendorf, Hamburg, Germany]) was used according to the manufacturer's instructions.

2.7.8.1 Preparation of *Taq*-polymerase

DNA-polymerase from *Thermophilus aquaticus* was prepared using a method based on Desai and Pfaffle (1995). The open reading frame of the enzyme was encoded on plasmid pUC18 (MBI Fermentas, St. Leon-Rot, Germany).
Transformed *E. coli* cells were grown in 50 ml TB media (1.2% tryptone, 2.4% yeast-extract [w/v], 0.4% glycerol [v/v], 72 mM K_2HPO_4, 17 mM KH_2PO_4) until an OD_{600} of 0.6. Cell culture was IPTG induced (0.4 mM final concentration) and incubated for 3 h to allow expression of the *Taq* polymerase. Cells were then pelleted for 10 min at 4000 g and resuspended in 1 ml lysis buffer (50 mM glucose, 1 mM EDTA, 0.4% lysozyme [w/v] 50 mM Tris; pH 7.9). After incubation for 15 min at RT 1 ml extraction buffer (50 mM KCl, 1 mM EDTA, 0.5% Tween 20, 0.5% Nonidet P40 [v/v], 10 mM Tris; pH 7.9) was added to the cells followed by an60 min incubation at 75 °C under shaking. The solution was centrifuged for 15 min at 12000 g and 4 °C and the supernatant diluted drop wise with 1 vol ice-cold buffer C (100 mM NaCl, 0.1 mM EDTA, 0.5 mM DTT, 1% Triton X-100, 50% glycerol [v/v], 50 mM Tris; pH 7.9) followed by drop wise dilution with 2 vol ice-cold buffer D (100 mM NaCl, 0.1 mM EDTA, 0.5 mM DTT, 1% Triton X-100, 75% glycerol [v/v], 50 mM Tris; pH 7.9). Prepared *Taq*-polymerase (app. 5 u/µl) was aliquoted and used in standard PCR with *Taq*-buffer (20 mM $[NH_4]_2SO_4$, 2 mM $MgCl_2$, 0.01% Tween 20 [v/v], 75 mM Tris; pH 8.8).

2.7.9 RTPCR

In order to observe gene expression in *Arabidopsis* tissues RTPCR was performed. The method has a high sensitivity and is suitable for the detection of low expressed genes. mRNA transcripts are converted into cDNA and are then detected via PCR with

suitable primers. Three steps are necessary: preparation of DNA-free RNA, reverse transcription (RT) and PCR on the generated cDNA.

Preparation of DNA-free RNA

DNA-free RNA was obtained by DNase I treatment. To 1 µg of total RNA (chapter 2.7.6) 0.25 µl RNase inhibitor (10 u) and 1 µl reaction buffer containing $MgCl_2$ were added. The volume of the samples was adjusted with DEPC-treated water to 9 µl. 1 µl DNase I (1 u) was added and incubated for 30 min at 37 °C. The reaction was stopped by addition of 1 µl 25 mM EDTA and incubation for 10 min at 65 °C.

Reverse transcription

RNA was reverse transcribed into cDNA using RevertAid transcriptase, a RNA-dependent DNA-polymerase. 1 µg DNA-free total RNA (in 11 µl) was incubated with 1 µl oligo-$(dT)_{18}$ primer (0.5 µg/µl) for 5 min at 70 °C and immediately chilled on ice. A mix containing of 4 µl reaction buffer, 2 µl dNTPs (10 mM total), 0.25 µl RNase inhibitor (10 u) and 0.75 µl DEPC-treated water was added and the RNA incubated for 5 min at 37 °C. 1 µl reverse transcriptase (200 u) was added and first strand cDNA synthesis was performed at 42 °C for 1 h. The reaction was stopped by incubation for 10 min at 70 °C.

PCR

1 µl of the generated cDNA was used in a PCR (chapter 2.7.8) but with commercially available *Taq*-polymerase (MBI Fermentas, St. Leon-Rot, Germany). The program was slightly modified: 2 min 94 °C, [35 sec 94 °C, 25 sec 55 °C, 1 min 72 °C] x 30, 5 min 72 °C. Primers for RTPCR are listed in Table 2 and were designed at the 5' and 3' region at the T-DNA insertion site of the mutants as well as spanning the T-DNA insertion site. To proof that the same amounts of RNA were used in all probes (assuming that the performance of reverse transcription was equal in all probes) an additional PCR with primers for the non-regulated housekeeping gene ACT2 was performed on all generated cDNAs (An *et al.*, 1996).

2.7.10 QRTPCR

In order to quantitatively determine gene expression levels in *Arabidopsis* tissues QRTPCR was conducted. The PCR based method uses fluorescence dyes to quantify the generated DNA amount after each PCR cycle. Relative transcript ratios between different samples can be determined after normalization to an internal reference.
As for an RTPCR (chapter 2.7.9) three steps are necessary: preparation of DNA-free RNA, reverse transcription (RT) and quantitative PCR on the generated cDNA.

RNA extraction and DNase I treatment were exactly carried out as for an RTPCR. cDNA was generated with Superscript lll reverse transcriptase (Invitrogen, Karlsruhe, Germany) according to the manufacturer's instruction using 1 µg DNA-free RNA, 1 µl oligo-$(dT)_{18}$ primer (0.5 µg/µl), 0.25 µl RNase inhibitor (10 u) and 200 u of Superscript lll.

Quantitative PCR

The QRTPCR program (Table 25) varied in several steps from a standard PCR: denaturing time was reduced, primer annealing and elongation were combined in one step and cycle number was increased. An inactivation and prolonged initial denaturing step were required by the used antibody-coupled polymerase. Adjacent to the PCR the melting temperature of the amplified product was determined.

Table 25: QRTPCR program.

Step	Time	Temperature	Annotation
1 Initiation	2 min	50 °C	
2 Inactivation, Denaturing	10 min	95 °C	
3 Denaturing	15 sec	95 °C	
4 Annealing and elongation	1 min	60 °C	back to step 3, 40 cycles
5 Final synthesis	5 min	72 °C	
6 melt curve determination	10 min	95 °C	
	1 min	60 °C	
	15 sec	60 °C	increasing 1 °C/15 sec until 95 °C

PCR reactions were performed in 10 µl volume using 5 µl SYBR-Green master mix (including dNTPs, SYBR-green, ROX as internal background fluorescence dye and DNA-dependent polymerase in buffer), 2 x 1 µl primer 1 and 2 (0.5 µM final concentration, each) and 1 µl cDNA (app. 1 ng).

Generated cDNA was tested via QRTPCR for complete DNA absence of genomic origin with intron primers (CTRL). Additionally, a positive control with 1 µl genomic DNA was carried out. The cDNA was then diluted 1:10 and proofed for the same amounts of used RNA via QRTPCR with primers for the non-regulated housekeeping gene *UBQ10*. All cDNA was diluted in a manner to give a CT value (cycle number when reaching the threshold) of 20 for *UBQ10* transcripts. CT values for genes using specific primer pairs (Table 3) were recorded after reaching a certain threshold (≥ 0.1). In case the melting temperature of the product peaked at various temperatures, the result was omitted and the reaction repeated. Relative transcript rate quantification was obtained using the CT method (Guiulietti *et al.*, 2001). The difference in CT value (ΔCT) of each target gene to the reference gene (*UBQ10*) was determined. To compare probes against each oth-

er, corresponding ΔCT values were subtracted and yielded in ΔΔCT. Transcription rates in x-fold difference (diff) were calculated according to the formula: diff = $2^{-\Delta\Delta CT}$. Triplicate values were determined and averaged.

2.8 Cloning strategies

2.8.1 *ALA* promoter-GUS-fusions

DNA fragments containing 1981, 1998 and 1983 bp upstream of the open reading frame of *ALA1*, *ALA10* and *ALA11*, respectively, were amplified (chapter 2.7.8) from *Arabidopsis thaliana* wild type genomic DNA (chapter 2.7.1) using TripleMaster proof-reading polymerase (Eppendorf, Hamburg, Germany) and primer pairs given in Table 5. The fragments were gel purified (chapter 2.7.7) and cloned (chapter 2.7.4) into pSTBlue-1 blunt vector (Novagen, Gibbstown, NJ, USA) using the Perfectly Blunt Cloning Kit (Novagen, Gibbstown, NJ, USA) according to the manufacturer's instruction. The generated plasmids (pSTB1-1, pSTB1-10 and pSTB1-11) were transformed into *E. coli* cells for amplification (chapter 2.6.2), extracted from the cells (chapter 2.7.1) and sent together with primers T7 5'-GTAATACGACTCACTATAGGGC-3' and SP6 5'-ATT TAGGTGACACTATAG-3' for sequencing. Correctly copied upstream sequences were then subcloned (chapter 2.7.4) into the plant binary vector pUTkan (Yoo *et al.*, 2005; digested with A] *Kpn*I/*Xho*I or B] *Xba*I/*Pst*I, gel purified and dephosphorylated) via *Kpn*I/*Xho*I (upstream region of *ALA10*) or *Xba*I/*Pst*I (upstream regions of *ALA1* and *ALA11*) restriction sites (chapter 2.7.2) resulting in transcriptional fusions of the *ALA1*, *ALA10* and *ALA11* promoter with the β-glucuronidase (GUS) coding region. Constructed plasmids (pUTkan-P1, pUTkan-P10 and pUTkan-P11) were first transformed into *E. coli* (chapter 2.6.2), positive transformants selected on spectinomycin-containing LB medium and tested via colony PCR (chapter 2.7.8) using primers forwardMCS 5'-GTTGTGTGG AATTGTGAGCGG-3' and GUS2 5'-GAATGCCCACAGGCCGTCGAG-3'. If the cells harbored the vector with the correctly oriented *ALA* promoter region, the plasmid was extracted (chapter 2.7.1) and used for GUS-assay (chapter 2.12).

2.8.2 ALA genes

Attempts were made to amplify (chapter 2.7.8) the open reading frames of *ALA1*, *10* and *11* from *A. thaliana* Col-0 genomic DNA (chapter 2.7.1) using three different proof-reading polymerases (KOD, Novagen, Gibbstown, NJ, USA; *Pfu* DNA Polymerase,

MBI Fermentas, St. Leon-Rot, Germany; TripleMaster, Eppendorf, Hamburg, Germany) with primer pairs given in Table 7. However, PCR were negative or resulted in unspecific amplification. In contrast, PCR performed with *Taq* polymerase (chapter 2.7.8) led to amplification products of the expected sizes (Table 7).

In order to reduce the size of the amplicons and, thus, obtain positive amplification results, PCR were performed (chapter 2.7.8) using cDNA from *A. thaliana* Col-0 (chapter 2.7.9) and TripleMaster polymerase (Eppendorf, Hamburg, Germany). After a successful PCR, the fragments were gel purified (chapter 2.7.7) and blunt cloned into the pSTBlue-1 vector (Novagen, Gibbstown, NJ, USA) using the Perfectly Blunt Cloning Kit (Novagen, Gibbstown, NJ, USA) according to the manufacturer's instruction. After transformation in *E. coli* (chapter 2.6.2) positive transformants were selected on ampicillin containing LB medium, the plasmid extracted (chapter 2.7.1) and sent with T7 and SP6 primers for sequencing. However, sequencing of the generated plasmids revealed in every case base exchanges within the amplified regions caused by nucleotide substitutions during the PCR.

Due to the size of *ALA* genes and inspired by Ding *et al.* (2000), two pairs of primers were designed (Table 8) to independently clone the 5'- and 3'-halves of the open reading frames of *ALA1*, *10* and *11*. A natural occurring endonuclease restriction site was chosen (*ALA1*: *Sac*I, *ALA10*: *Sca*I and *ALA11*: *Nhe*I) to divide the *ALA* cDNA. Restriction sites were introduced via the used primer A) in the first half (5') in front of the start codon (*ALA1*: *Xba*I, *ALA10*: *Sac*II/*Nhe*I and *ALA11*: *Xba*I) and B) in the second half (3') behind the stop codon for further cloning purposes (*ALA1*: *Xho*I, *ALA10* and *ALA11*: *BamH*I; Table 8). Halves of *ALA1*, *10* and *11* were amplified (chapter 2.7.8) using *A. thaliana* cDNA (chapter 2.7.9) and KOD proofreading polymerase (Novagen, Gibbstown, NJ, USA). The fragments were gel purified (chapter 2.7.7) and blunt cloned into pSTBlue-1 resulting in vectors pSTB1.1, pSTB1.2, pSTB10.1, pSTB10.2, pSTB11.1 and pSTB11.2. Successfully cloned regions were confirmed by sequencing (with T7/ SP6 primers) ensuring no nucleotide substitutions had occurred during PCR.

To generate full-length clones, amplified pSTBlue-1 vectors containing the 5'- and 3'-halves of *ALA1*, *10* and *11* were cleaved with restriction endonucleases: *Xba*I/*Sac*I for the 5'-half of *ALA1*, *Sac*II/*Sca*I for the 5'-half of *ALA10* and *Xba*I/*Nhe*I for the 5'-half of *ALA11* as well as *Sac*I/*Xho*I for the 3'-half of *ALA1*, *Sca*I/*BamH*I for the 3'-half of *ALA10* and *Nhe*I/*BamH*I for the 3'-half of *ALA11*. The fragments were gel-purified (chapter 2.7.7) and ligated via a three-way ligation (chapter 2.7.4) into pBlueScript II KS+ (MBI Fermentas, St. Leon-Rot, Germany) that was digested with *Xba*I/*Xho*I, *Sac*II/*BamH*I and with *Xba*I/*BamH*I for *ALA1*, *10* and *11* fragments, respectively, gel purified (chapter 2.7.7) and dephosphorylated (chapter 2.7.3). The generated constructs (pSTB*1, pSTB*10 and pSTB*11) were transformed into *E. coli* (chapter 2.6.2) and positive transformants were selected on ampicillin containing LB medium. Several attempts of

ligation and transformation resulted always in no bacterial colonies for *ALA10* and *11*. However, cloning of *ALA1* was successful.

In order to make *ALA* clones compatible for the GATEWAY cloning system (Invitrogen, Karlsruhe, Germany) a two-step PCR (adaptor PCR) was performed similar to the instructions by Invitrogen: The first reaction with specific primer pairs for *ALA1*, *ALA10* and *ALA11* (Table 9) added A) two nucleotides at the 5'-end immediately in front of the ATG start codon and 12 nucleotides of the GATEWAY cloning specific attB1 site and B) removed the stop codon and, in return, added 1 nucleotide at the 3'-end and 12 nucleotides of the GATEWAY cloning specific attB2 site. The second reaction was performed with primers (attB1 F and attB2 R, Table 9) and added the missing 9 nucleotides of the specific cloning sites attB1 (5') and attB2 (3') to the ends of the *ALA* coding regions. The PCR were performed with KOD proofreading polymerase. The previously generated pSTB*1 served as a template for $ALA1_{\text{full-length}}$. Due to the cloning difficulties of *ALA10* and *ALA11*, generated vectors received from the Palmgren group (University of Copenhagen, Denmark) were used for further cloning. Vector pMP2061 (*ALA11* in pBlueScript SK- between *EcoR*V and *Sal*I restriction sites) served as a template for $ALA11_{\text{full-length}}$. $ALA10_{\text{full-length}}$ was already cloned in the GATEWAY entry vector (pENTR/D-TOPO; Invitrogen, Karlsruhe, Germany) constituting vector pMP3228 and the two PCR adding attB sites to *ALA10* were not performed. The generated attB PCR products of $ALA1_{\text{full-length}}$ and $ALA11_{\text{full-length}}$ were gel purified and cloned into pDONR221 (Invitrogen, Karlsruhe, Germany) using the BP Clonase II Enzyme Mix (Invitrogen, Karlsruhe, Germany) according to the manufacturer's instruction converting the vector into pENTR221-ALA1 and pENTR221-ALA11.
The vectors (pENTR221-ALA1, pMP3228 and pENTR221-ALA11) were transformed into *E. coli* and positive transformants selected on kanamycin containing LB medium. The plasmids were extracted from the cells (chapter 2.7.1) and used for further subcloning of the *ALA* regions via the LR Clonase II Enzyme Mix (Invitrogen, Karlsruhe, Germany) according to the manufacturer's instruction. The plasmids pB7WGF2-ALA1 and pB7WGF2-ALA10 were generated via subcloning of the *ALA* regions into the plant binary vector pB7WGF2 (Karimi *et al.*, 2002) resulting in fusions of the eGFP-coding region to the N-termini of the $ALA_{\text{full-length}}$ regions. The generated vectors were transformed into *E. coli*, the cells selected on spectinomycin containing LB medium, vectors extracted from the cells and transformed into *A. tumefaciens*, which were then used for plant transformation (chapter 2.6.7) and GFP studies (chapter 2.11). Transformation of the subcloned, gateway-compatible *ALA11* in the plant binary vector pB7WGF2 (pB7WGF2-ALA11) into *E. coli* cells failed and resulted always in no colonies on spectinomycin containing LB medium.

2.8.3 ALA-GFP-fusions

ALA_{TM1-4}-eGFP fusions

Due to the cloning difficulties of full-length *ALA* genes, transcriptional fusions of the first four transmembrane spanning regions of *ALA1*, *10* and *11* with eGFP were generated: *ALA_{TM1-4}*-fragments were amplified (chapter 2.7.8) from *A. thaliana* wild-type cDNA (chapter 2.7.9) using KOD proofreading polymerase (Novagen, Gibbstown, NJ, USA) and primer pairs given in Table 6. The N-terminal fragments covered a region beginning at the ATG start codon and reaching in the large loop between TM domain 4 and 5 resulting in a length of 2173, 1788 and 2041 bp for *ALA1*, *10* and *11* fragments, respectively. *Xba*I and *Pst*I restriction sites were introduced via PCR at the 5' and 3' end of the fragments, respectively. The generated fragments were blunt cloned into the pSTBlue-1 vector (Novagen, Gibbstown, NJ, USA) according to the manufacturers' instruction and the resulting plasmids were transformed into *E. coli* cells for amplification (chapter 2.6.2), extracted from the cells (chapter 2.7.1) and sent together with T7 and SP6 primers for sequencing. Sequence-proofed fragments were subcloned via *Xba*I/*Pst*I restriction sites in the plant binary vector pGTkan3-35S resulting in *ALA* fragments fused to the N-terminus of *eGFP*. pGTkan3-35S represents a modified version of pGTkan3 (Hajdukiewicz *et al.*, 1994), where the *35S* promoter (853 bp; Odell *et al.*, 1988) from cauliflower mosaic virus (*CaMV35S*-promoter) was introduced over KpnI/*Xba*I restriction sites in order to drive expression of the eGFP-fusion proteins. Constructed plasmids were first transformed into *E. coli* (chapter 2.6.2), positive transformants selected on spectinomycin-containing LB medium and tested via restriction analysis (chapter 2.7.2). If the cells harbored the correct vector, the plasmid was extracted and used for GFP studies (chapter 2.7.1 and 2.11, respectively).

2.9 Lipid analysis

In order to avoid auto oxidation of lipids, samples were always overlaid with argon gas. All preparatory steps occurred in glass tubes or vials and pipetting was done using glass pipettes to prevent samples from lipid and fatty acids deriving from plastic ware.

2.9.1 Extraction of lipids

Total lipids were extracted from leaves of *Arabidopsis* using MTBE according to Matyash *et al.* (2008). 100 mg ground frozen leaf material (6th leaf) was dissolved to-

gether with an internal standard in 1.5 ml methanol in a sealable 10 ml glass tube. As internal standard heptadecanoic fatty acids (17:0) were used (1 mg/ml in chloroform), depending on the measurement, i.e. for total FA: 100 µl di-17:0-PC, for total PL and GL: 30 µl di-17:0-PC and 70 µl di-17:0-MGD together and for single PL species: 15 µl di-17:0-PC, 15 µl di-17:0-PE, 1 µl di-17:0-PS, 15 µl di-17:0-PG and 1 µl di-17:0-PA together (Sigma-Aldrich, St. Louis, MO, USA). Samples were thoroughly mixed and after addition of 5 ml MTBE incubated at RT in the dark under agitation of 200 rpm for 1 h. After the incubation 1.25 ml ddH_2O was added, 10 min incubated at RT and centrifuged for 15 min at RT and 800 g. The supernatant was collected into a new glass tube, whereas the pellet was reextracted with 1.42 ml methanol/water (3:2.5 v/v) and 2.58 ml MTBE for 10 min at RT. The resulting lipid extracts were combined and dried under streaming nitrogen. They were then A) converted into FAMEs and measured via GC-FID for total FA-analysis (chapter 2.9.4 and 2.9.5) or B) solid phase separated into PL and GL (chapter 2.9.2), converted into FAMEs and measured for analysis of PL- and GL-specific FAs or C) solid phase separated into PL and GL, separated into single lipid species via TLC (chapter 2.9.3), scraped from the plate, converted into FAMEs and measured for FA composition in single PL- and GL-species.

2.9.2 Separation of lipid classes

Phospholipids and glycolipids were separated via solid phase extraction on a silica (500 mg/6 ml) column (SI-1 Silica Phenomenex, Strata, Aschaffenburg, Germany). The column was equilibrated with 1 ml chloroform; total lipid extracts were dissolved in 1 ml chloroform and loaded on the column. Neutral lipids were eluted with 14 ml chloroform, glycolipids with 15 ml acetone/isopropanol (9:1 v/v) and finally phospholipids with 15 ml methanol/acetic acid (9:1 v/v). GL- and PL-fractions were evaporated under streaming nitrogen.

2.9.3 TLC

PL and GL were separated into their single classes by TLC on silica plates. Extracted PL or GL were dissolved in 100 µl chloroform and transferred to TLC-vials. 20 µl were loaded via a robot (TLC Sampler 4, Camag, Berlin, Germany) to ammonium sulfate-impregnated silica gel plates (Si250, J. T. Baker, San Francisco, CA, USA).
GL classes were developed with app. 100 ml chloroform/methanol (85:15 v/v) on vertical incubation chambers into SQD, DGD, CER, SG, MGD and ASG (from bottom to top). The same method was applied for PL class separation. The solvent system

chloroform/methanol/acetic acid (65:25:8 v/v) was used to separate PC, PI, PE, PG and PA (from bottom to top). After incubation TLC plates were air-dried and incubated a second time. Individual lipid classes were identified according to co-migration with standard lipids on the same plate. The plates were split in half and the side with separated standard lipids was incubated in a copper sulfate solution (10 g $CuSO_4$ x 5 H_2O, 92 ml H_2O, 8 ml H_3PO_4). Heating at 180 °C for 10 min stained lipids (Dormann *et al.*, 1995b; Dormann *et al.*, 1995a). Individual PL and GL were isolated from the plate, transmethylated (chapter 2.9.4) and quantified by GC (chapter 2.9.5).

2.9.4 Acidic hydrolysis of lipids, FA methylation and FAME extraction

Transesterification (methyl ester) of lipid bound FAs to their corresponding FAMEs was accomplished in one step according to Miquel and Browse, (1992). 1 ml of a methanolic solution containing 2.75% sulfuric acid and 2% dimethoxypropan (v/v) was added to the samples already containing an internal standard in 10 ml glass tubes (either total lipid extracts dried under nitrogen or scraped silica powder from TLC). The samples were incubated for 1 h at 80 °C and cooled down. After addition of 200 µl 5 M sodium chloride FAMEs were extracted two times with 2 ml hexane. Samples were incubated for 10 min at RT and phases separated by centrifugation for 10 min at RT and 800 g. The hexane phase of both extractions was pooled dried under streaming nitrogen and redissolved in 2 ml hexane and 2 ml ddH_2O. Samples were mixed and phase separated by centrifugation. The hexane phase was filtered through a glass pipette filled with sodium sulfate soaked cotton wool to remove moisture. The sample was collected in a reaction vial, dried under nitrogen and redissolved in 10 µl acetonitrile and analyzed via GC (chapter 2.9.5) similar to Browse *et al.* (1986).

2.9.5 Identification of FAMEs by GC-FID

The analysis of FAMEs was performed with an Agilent 6890 gas chromatograph (Waldbronn, Germany) fitted with a capillary DB-23 column (15 m x 0.18 mm; 0.2 µm coating thickness; J&W Scientific, Agilent, Waldbronn, Germany) and coupled to a flame ionization detector according to Hornung *et al.* (2002). Probes were dissolved in 10 µl acetonitrile and transferred to GC-vials. Helium was used as carrier gas at a flow rate of 0.8 ml/min. The temperature gradient was 180 °C for 1 min, 180-200 °C at 20 K/min, 200-250 °C at 25 K/min and 250 °C for 2.5 min. A FAME mixture (F.A.M.E. Mix, C4-C24", Sigma, Munich, Germany) was used as retention time standard and was injected before and after every series of measurements. The injection volumes depending on

the concentration of FAMEs within in the sample and the used split-ratio on the GC machine but varied between 0.2 and 1 µl with a split-ratio of 1/15 and 1/60. FID-signals were recorded, peak areas integrated and FA-species identified via retention time of the used standard mix. Internal heptadecanoic fatty acid standards with defined concentrations added to the probes before the extraction process were used to calculate the absolute FA contents of the leaf samples via the peak area.

2.10 Physiological parameter

2.10.1 Chlorophyll fluorescence analysis

A pulse-modulated imaging fluorometer (FluorCam 800MF, Photon Systems Instruments, Brno, Czech Republic) was used for determination of minimum (F_0) and maximum fluorescence (F_{max}) of chlorophyll a according to Wingler *et al.* (2004) and Pourtau *et al.* (2006). Rosettes or single leaves were illuminated with actinic light of 150 µmol*m^{-2}*sec^{-1} and the dark-adaptation period was reduced to 15 min. Light pulses for measurement of F_m were set to 800 ms. QY was calculated using following equation: $QY_{max} = F_v/F_{max} = (F_{max} - F_0) / F_m$.

2.10.2 Protein measurements

Protein content of plants was measured using Bradford reagent (Bradford, 1976). Fresh plant material was weighted and homogenized in 1 ml chilled buffer (100 mM Tris, pH 7.5, 50 mM NaCl, 1 mM EDTA, 1% w/v PVP) using a grinding mill and 0.5 mm ø steel balls for 1.5 min at 30 Hz. The samples were spun down, 10 µl of 1:20 diluted supernatant was mixed with 990 µl Bradford reagent (Roti-Quant, Carl-Roth, Karlsruhe, Germany), incubated for 20 min at RT and measured photometrically at 595 nm. For exact protein concentration determination a diluted BSA series (1.5-0.1 mg/ml) was measured at the same time and a calibration line was generated. Absorption values were calculated against the calibration line and absolute protein levels per fresh weight determined.

2.10.3 Membrane ion leakage

Membrane ion leakage was performed on pooled 6th rosette leaf samples according to Woo *et al.* (2001) and repeated 5 times. Leaf samples were immersed in 10 ml ddH_2O

and incubated at RT for 1 h. 100 µl were removed, diluted with 10 ml ddH_2O and the conductivity (σ_1) determined (HI8633 conductivimeter, Hanna Instruments, Kehl, Germany). Samples were then boiled for 10 min, cooled down to RT and conductivity (σ_2) of a 100 µl probe diluted with 10 ml ddH_2O was measured. Ion leakage was calculated and expressed in percentage through the equation: Ion leakage = (σ_1 / σ_2) * 100.

2.10.4 Determination of chlorophyll content

Absolute chlorophyll content in *Arabidopsis* leaves was measured according to Lichtenthaler (1987). Chlorophyll of 5-50 mg ground leaf material (whole rosette or 6th leaf) was extracted with 1 ml 96% ethanol. The samples were mixed and incubated for 30 min at RT in the dark, cell debris was shortly spun down and the supernatant stored in a new reaction tube. The probes were extracted again with 1 ml 96% ethanol, incubated for 10 min at RT in the dark and pelleted. Both supernatants were pooled and measured photometrically at 649 and 664 nm. Chlorophyll a and b content was calculated using following formula (Porra *et al.*, 1989) and related to FW: Chlorophyll a+b content = (22.24 * E_{649} + 5.24 * E_{664}) * 2. Every measurement was repeated five times and the results averaged.

2.10.5 Determination of anthocyanin content

Anthocyanin content in *Arabidopsis* leaf material was performed following Neff and Chory (1998). Per 40 mg ground and frozen leaf material (whole rosette or 6th leaf) 1 ml methanol spiked with 1% hydrochloric acid was used to extract anthocyanins. The extraction was performed in the dark and under agitation of 800 rpm at RT over night. The next day 0.4 vol ddH_2O and 1 vol chloroform were added to the extractions and thoroughly mixed. Cell debris was spun down and phase separation achieved by centrifugation for 10 min at 4000 g. The upper phase was collected and measured photometrically at 530 and 657 nm. Relative anthocyanin levels were calculated using the following formula and related to FW: Anthocyanin content = E_{530} - E_{657}. Every measurement was repeated five times and the results averaged.

2.10.6 Determination of leaf and cell size

Prior to size determination of epidermal cells, *Arabidopsis* 6th rosette leaves were destained via chloral hydrate based on Yadegari *et al.* (1994). Entire leaf samples were fixated in glass vials over night at RT using ethanol/acetic acid (6:1 v/v), followed by

three wash steps of 70% ethanol. The samples were cleared over night at 4 °C using 15 M chloral hydrate in 40% glycerin. Leaf samples were directly used for light microscopy (Berleth and Jurgens, 1993). Images from entire leaves were taken with a macroscope (SZX12, Olympus, Tokyo, Japan) equipped with a camera (C-4040ZOOM, Olympus, Tokyo, Japan). Cell area (size), number and stomatal index of the abaxial leaf epidermis were determined as described by De Veylder *et al.* (2001) using a microscope (Axioskop 2plus, Zeiss, Jena, Germany). Images were acquired with an AxioCam ICc3 camera (Zeiss, Jena, Germany). Considered were regions of the leaf blade located at 25, 50 and 75% from the distance between the tip and the base halfway between midrib and leaf margin. All obtained images were analyzed using the ImageJ software.

2.11 GFP studies

Transgenic plants expressing a fusion protein consisting of the protein of interest fused to the green fluorescent protein (GFP; Chalfie *et al.*, 1994; Baulcombe *et al.*, 1995) can help to identify the subcellular localization of the corresponding protein *in vivo*. If GFP is excited by light it emits fluorescent light and thus can be observed in tissues via confocal laser scanning microscopy (chapter 2.11.2).
GFP studies were carried out with leaf probes of *Arabidopsis thaliana* and *Nicotiana benthamiana*. eGFP with enhanced fluorescence properties and mCherry were used as fluorescent reporter proteins (Shaner *et al.*, 2004). Protein fusion constructs (chapter 2.8.2 and 2.8.3) and/or marker constructs (Nelson *et al.*, 2007) were introduced into *A. tumefaciens* strain GV3101 (chapter 2.6.2) and used for either stable transformation of *Arabidopsis* plants (chapter 2.6.7) or for transient expression in tobacco epidermal cells (chapter 2.11.1).

2.11.1 Transient expression in tobacco

Transient expression of GFP fusion proteins in *Nicotiana benthamiana* epidermal cells was performed following Sparkes *et al.* (2006). *A. tumefaciens* transformed with the required binary vector were grown in 2 ml liquid culture was grown over night and cells were pelleted by centrifugation. Supernatant was removed and cells were resuspended in infiltration media (200 µM acetosyringone [3',5'-dimethoxy-4'-hydroxy acetophenone in DMSO], 10 mM MES; pH 5.6, 2% sucrose [w/v] in ½ strength MS). The cells were spun down for 10 min at 3000 g and RT and dissolved again in infiltration media. The

cell suspension culture was diluted in a way with infiltration media to obtain an OD_{600} of 0.1. Leaves of 5-week-old tobacco plants were punctured with a needle on the underside and 1-2 ml bacteria containing infiltration media was injected with a syringe in the mesophyllic air space. The infiltrated area was marked and plants were grown for 2-4 d under normal growth conditions. Small leaf samples were cut out of the infiltrated areas and observed with a confocal laser scanning microscope. For tobacco plasmolysis infiltrated 3-day-old leaf discs were incubated in 0.7 M D-sorbitol for 30 min prior to confocal microscopy.

2.11.2 Confocal microscopy

To detect expression of fluorescent proteins in biological probes a confocal laser-scanning microscope (TCS SP5, Leica Microsystems, Wetzlar, Germany) with a water-immersion objective was used. eGFP was excited by monochromatic laser light at 488 nm and its fluorescence recorded in the range of 505-525 nm. At the same time chlorophyll was excited with 561 nm and its autofluorescence detected in the interval of 670-700 nm. mCherry was excited at 561 nm, and fluorescent emissions were measured at 585-610 nm. Probes expressing eGFP and mCherry at the same time were sequential line scanned in order to record emissions of both fluorescent proteins without mutual interference. Autofluorescence of chlorophyll and cellular structures within both recording ranges (505-525 nm, 585-610 nm) was proved negligible using wild type probes and photomultiplier settings were adjusted to wild-type levels in order to exclude amplification of background signals. Image recording was performed with line and frame average of four. Z-stacks were of appoximately 10 µm thickness and consisted of ten images.

2.12 GUS assay

Transgenic plants expressing the β-glucuronidase (GUS) gene (*uidA*; Jefferson *et al.*, 1987) under transcriptional control of a promoter of interest can help to localize the expression domains of the corresponding gene. β-glucuronidase splits X-Gluc resulting in a blue colored product indication the tissue-specific expression of the used promoter. Promoter-GUS fusion constructs (chapter 2.8.1) were introduced into *A. tumefaciens* strain GV3101 (chapter 2.6.2) and stable *Arabidopsis* transformants generated (chapter 2.6.7). Between ten and twenty independent T2 transgenic lines were subjected to GUS assays. GUS-staining was carried out similar to Haritatos *et al.* (2000) and Weigel and Glazebrook (2002) but with minor variations: Tissue of *Arabidopsis* to be examined

was incubated in 90% acetone at -18 °C for 1 h before staining. No glutaraldehyde was used. After the initial step, samples were washed twice in 50 mM sodium phosphate buffer, pH 7.2 and incubated in staining solution (50 mM sodium phosphate buffer, pH 7.2, 10 mM potassium ferrocyanide, 10 mM potassium ferricyanide, 0.2% triton X-100, 0.5 mg/ml X-GlucA) at 37 °C over night. Subsequently staining the samples were washed with sodium phosphate buffer, dehydrated in a graded ethanol series (50%, 70%, 85%, 96%) and stored in 70% ethanol until observation. Images of X-Gluc-stained tissues were taken with a macroscope (Wild M3K$^+$, Leica, Wetzlar, Germany) equipped with a camera (DFC420C, Leica, Wetzlar, Germany).

2.13 Experiments with yeast

2.13.1 Complementation (drop test)

For complementation analysis transformed yeast cells were grown in 10 ml selective SD media (with glucose) until an OD_{600} of 0.5. The cultures were split into two aliquots and pelleted via centrifugation for 10 min at 800 g. The first pellet was diluted in selective SD media (with glucose) in a way to obtain 0.5 OD_{600} after 12 h of incubation. The second pellet was diluted in the same manner using selective inductive media (without glucose, supplemented with 1% galactose and 1% fructose [w/v]). After incubation five successive 1:5 dilutions starting with an OD_{600} of 0.3 were set up for each culture. Drops of 3 µl were spotted on a set of plates (selective SD plates [with glucose], selective inductive SD plates [without glucose, supplemented with 1% galactose and 1% fructose (w/v)], normal and inductive YPD plates [glucose or galactose/ fructose] as control). One set of plates was incubated at 30 °C for 2-3 days, to check for complementation of cold-sensitive phenotypes an additional plate set was incubated at 20 °C for 5-7 d.

2.13.2 Lipid uptake assey

100 ml yeast cell culture within the exponential phase (OD_{600} 0.3-0.7) grown on selective SD media (with glucose) was pelleted via centrifugation for 10 min at 800 g and dissolved in the same amount selective inductive SD media (without glucose, supplemented with 2% galactose [w/v]). Cells were incubated for 12 h under gene expression inducing conditions driven by the GAL1-10-promoter on the transformed plasmid (Johnston

and Davis, 1984). Cells transformed with an empty vector were treated the same way and used as a negative control. OD_{600} was determined and the culture split in two aliquots. Probes of the first aliquot were diluted in a way to achieve the same OD. 40 ml were pelleted and used for protein analysis (chapter 2.13.3). Probes of the second aliquot were pelleted and diluted with selective SD media (without glucose, supplemented with 4% galactose [w/v]) in a way to achieve an OD_{600} of 10.

2.13.2.1 Lipid labeling of cells

Uptake experiments with fluorescently labeled PL were performed as described by Pomorski *et al.* (2003) with the optimizations from Poulsen *et al.* (2008b). Cells were incubated 5 min at 30 °C prior to labeling. 1.5 µl 10 mM NBD-labeled phospholipids (myristoyl-[NBD-hexanoyl]-PC, -PE and -PS were tested, Avanti Polar Lipids, Alabaster, AL, USA) dissolved in DMSO were added and incubated for 30 min at 30 °C. A negative control was prepared in the same way with DMSO only. Cells were thoroughly mixed every 5 min. The reaction was stopped by addition of 1 ml ice-cold SSA/BSA (2mM NaN_3, 2% sorbitol, 3% BSA [w/v] in selective SD media) and cells were immediately chilled on ice. Cells were pelleted (5 min at 700 g and 4 °C), redissolved in 1 ml SSA/ BSA und transferred into new glass tubes. In order to remove non-internalized PL, cells were washed two times with SSA/BSA and the pellet finally dissolved in 250 µl PBS (composition given in Table 26) and kept on ice until flow cytometry measurement.

2.13.2.2 Measurement by flow cytometry

Flow cytometry was used to evaluate internalization of NBD-labeled PL of yeast cells. 50 µl cell suspension was mixed with 1 ml PBS in FACS vials. Immediately before measurement 1 µl propidium iodide (5 mg/ml [w/v]) was added under mixing to the cells. Flow cytometry was performed on a Becton Dickinson flow cytometer (San Jose, CA, USA) equipped with a 488 nm argon laser. Detection of propidium iodide (PI) stained cells was recorded at 570 nm, NBD fluorescence at 545 nm. Forward scatter indicated cell size, sideward scatters the fluorescence intensity of PI and NBD. 20000 cells, gating PI stained dead cells, were counted and the accumulation of NBD-labeled lipids was calculated as percentage compared to a negative control (cells transformed with an empty plasmid).

2.13.3 Protein analysis

2.13.3.1 Preparation of total cell lysate and membrane concentration

Cellular membranes were prepared similar to the method from Villalba *et al.* (1992). Pelleted yeast cells were resuspended in 250 µl ice-cold lysis buffer (composition given in Table 26) and transferred to a new 10 ml glass tube. 0.5 g glass beads (600 µm ø) were added to the cell suspension and cells disrupted by vigorously mixing for 5 min.

Table 26: Lysis buffer for yeast cells.

PBS containing 1% PMFS-stock and 0.1% protease inhibitor mix [v/v]

Name	Concentration	Substance
PBS	136.89 mM	NaCl
	2.68 mM	KCl
	10.14 mM	Na_2HPO_4
	1.67 mM	KH_2PO_4; pH 7.4
PMFS-stock	100 mM	PMSF in isopropanol
protease inhibitor mix	1 mg/ml	apoprotein
	1 mg/ml	leupeptin
	1 mg/ml	pepstatin
	5 mg/ml	antipain
	157 mg/ml	banzamidine in DMSO

During cell disruption, probes were shortly chilled on ice app. every 30 sec. After cell disruption the supernatant was transferred to a new reaction vial, the glass beads were washed with 250 µl ice-cold lysis buffer and the buffer combined with the previous supernatant. Cell debris and intact cells were separated via centrifugation for 5 min at 500 g and 4 °C and total cell lysate stored at -20 °C.
Membranes were concentrated from total cell lysate via ultra-centrifugation for 1 h at 100000 g and 4 °C. 25 µl of the supernatant (total lysate) was kept as a control and the membrane pellet was resuspended in 25 µl ice-cold lysis buffer.

2.13.3.2 SDS-PAGE

Electrophoretically separation of proteins was performed after Laemmli (1970) via discontinuous SDS-PAGE. Polyacrylamide gels of 0.75 mm thickness consisting of a

10% resolving gel (375 mM Tris-HCl; pH 8.8) combined with a 4.5% stacking gel (125 mM Tris-HCl; pH 6.8) were generated and run using the Mini-PROTEAN 3 cell system (BioRad, Munich, Germany) according to the manufacturer's instructions with a running buffer consisting of 25 mM Tris, 192 mM glycine and 0.1% SDS (w/v). Prior to electrophoresis 25 µl sample buffer (10% SDS, 0.0025% bromo-phenol blue [w/v], 12.5% glycerol [v/v], 100 mM DTT in 100 mM Tris; pH 6.8) was added to each probe (25 µl), followed by incubation for 15 min at 37 °C and centrifugation for 10 min at 5000 g. 15 µl of the supernatant was loaded together with 8 µl of a size marker (Prestained SDS-PAGE standard, BioRad, Munich, Germany) on an PA gel. Electrophoretical separation was performed at 180 V for 50 min.

2.13.3.3 Protein transfer

Prior to their detection proteins were transferred from the PA matrix to a membrane based on Towbin *et al.* (1979). Protein transfer occurred in a wet blot chamber (Trans Blot Cell, BioRad, Munich, Germany) onto a PVDF membrane (Hybond-P, Amersham Pharmacia Biotech, Freiburg, Germany) according to the manufacturer's instructions using 4 °C chilled transfer buffer (20% methanol [v/v], 10 mM Tris, 77 mM glycine, 0.1% SDS [w/v]) and applying an amperage of 3.5 mA/cm^2 membrane for 50 min.

2.13.3.4 Immunological protein detection

After protein transfer the membrane was incubated in TBS (150 mM NaCl, 10 mM Tris; pH 8.0) for 10 min followed by a 1% blocking solution (Western Blocking Reagent, Roche Applied Science, Mannheim, Germany) for 1 h at RT. The immunological detection of tagged proteins was performed as follows: First, the membrane was incubated with primary antibody (monoclonal mouse anti-HA 1:1000 and monoclonal mouse anti-RGSH$_6$ 1:5000 [Santa Cruz Biotechnology, Santa Cruz, CA, USA]) in 0.5% blocking solution ([v/v] in TBS) over night at 4 °C. Next, the membrane was washed twice with TBST (TBS supplemented with 0.1% Tween 20 [v/v]) for 10 min, followed by two wash steps with 0.5% blocking solution for 10 min. Then the membrane was incubated with secondary antibody (peroxidase-linked goat anti-mouse 1:5000 [Santa Cruz Biotechnology, Santa Cruz, CA, USA]) in 0.5% blocking solution for 1 h at RT. Subsequently, the membrane was washed four times 15 min with TBST. All washing and incubation steps occurred under shaking.
Visualization of detected proteins was done via chemiluminescence with ECL Plus Reagenz (Amersham Pharmacia Biotech, Freiburg, Germany) according to the manu-

facturer's instructions. Prepared reagent was carefully dropped on the wet membrane and incubated for 5 min at RT. Depending on the signal strength the membrane was exposed to a film (X-OMAT AR, Kodak, Stuttgart, Germany) for 10 sec - 5 min and subsequently developed.

2.14 Transmission electron microscopy

Plants for electron microscopy were grown on soil for 28 d. Small samples (2 x 4 mm, parallel to the midrib; in between midrib and leaf edge) were taken from 6th rosette leaves 4 h after the start of the light period and immediately immersed in a formaldehyde-glutaraldehyde mixture (Karnovsky, 1965). Samples were fixed with 2% paraformaldehyde/glutaraldehyde in 50 mM sodium cacodylate buffer (pH 7.4) for 3 d at 4 °C based on the methods by Kuroiwa *et al.* (2002) and Schulz *et al.* (1998). Specimens were washed five times for 15 min in 50 mM sodium cacodylate buffer (pH 7.4) and post-fixed first for 3 h in 50 mM sodium cacodylate buffer (pH 7.4) supplemented with 1% osmium tetroxide at RT. Specimens were washed again four times for 20 min with ddH_2O and incubated for 1 h at RT in 100 mM HEPES buffered 0.1% tannic acid (pH 7.4). Again specimens were washed three times for 10 min with ddH_2O and then contrasted with 2% uranyl acetate in 100 mM HEPES (pH 7.4) for 1.5 h at RT. After a short washing step with ddH_2O the samples were dehydrated in a graded series of ethanol (70%, 80%, 90% 2x 96%, each step for 30 min). Samples were embedded in Spurr's resin (Spurr, 1969). Therefore, samples were prepared with a mixture of propylene oxide/ethanol (1:1 v/v) for 5 min, two incubation steps with pure propylene oxide for 10 min, propylene oxide/ Spurr resin (1:1 [v/v]) for 30 min and pure Spurr resin for 2 h (Low Viscosity Spurr Kit, Ted Pella, Redding, CA, USA). The resin was changed and samples incubated again for 2 h at RT and the resin was polymerized at 60°C for 2 d. 70 nm ultra-thin section were cut with an ultramicrotome (Reichert Ultracut E, Leica, Wetzlar, Germany) and mounted on pioloform-coated electron microscopy copper grids with 200 meshes. Prior to transmission electron microscopy sections were counterstained with 2% uranyl acetate in 70% methanol for 20 sec, washed four times with, followed by lead citrate (2.6% lead nitrate and 3.5% sodium citrate; pH 12) for 20 sec and again four washing steps with ddH_2O (Reynolds, 1963). Sections were then examined on a transmission electron microscope (Tecnai Spirit, FEI, Eindhoven, The Netherlands) at 120 kV.

2.15 Hardware / Equipment

If not mentioned otherwise equipment, hardware and devices used in this work are listed in Table 27.

Table 27: Used technical equipment.

Device	Name/Type, Manufacturer
Camera	PowerShot S2 IS, Canon, Krefeld, Germany
Centrifuge	Biofuge Fresco, Heraeus Instruments, Bad Grund, Germany
	5810 R, Eppendorf, Hamburg, Germany
	Beckman Coulter, Krefeld, Germany
Climate chamber	Rumed, Rubarth Apparate, Laatzen, Germany
Crosslinker	Stratalinker 1800, Stratagene, Heidelberg, Germany
Drying oven	Heraeus Instruments, Bad Grund, Germany
Electrophoresis	ElectroPhoresis Power Supply, Biozym, Hess. Oldendorf, Germany
Electroporator	MicroPulser, BioRad, Munich, Germany
Gel documentation	DeVision DBox, Decon, Hohengandern, Germany
Grinding mill	Mixer Mill 400, Retsch, Haan, Germany
Hybridization oven	Saur, Reutlingen, Germany
Incubator	HT Minitron GFL 3032, Infors, Bottmingen, Switzerland
Lyophylizator	Leybold-Heraeus, Cologne, Germany
Probe mixer	Vortex Genie2, Scientific Industries, Bohemia, NY, USA
Quantum meter	QMSW-SS, Apogee instruments, Roseville, CA, USA
Real-time cycler	AB-7500 fast, Applied Biosystems, Foster City, CA, USA
Spectrophotometer	Genesys10UV, VWR, Darmstadt, Germany
Thermocycler	T-Gradient, Biometra, Göttingen, Germany
TLC-dipper	Immersion Device, Camag, Berlin, Germany
TLC-heater	Plate Heater, Camag, Berlin, Germany
Tube incubator	Thermomixer 5436, Eppendorf, Hamburg, Germany

3 RESULTS

3.1 Senescence-associated expression of *ALA1*, *ALA10* and *ALA11*

This thesis is based on the observations by van der Graaff *et al.* (2006) that reported a senescence-associated expression of genes of the *ALA* family (Figure 7). Expression data obtained via oligonucleotide chip hybridization technique often has low sensitivity and a narrow dynamic range. In order to validate the expression data of *ALA* genes, quantitative real-time PCR (QRTPCR) as another method for gene expression analysis was performed on *Arabidopsis thaliana* wild type leaf material (chapter 2.7.10).
The studies by van der Graaff *et al.* (2006) were performed with pooled 5th and 6th rosette leaves. Rosette leaves of *Arabidopsis* grow in a temporal succession and thus, each leaf has a specific age and progression of senescence regarding its position compared to the other rosette leaves (Zentgraf *et al.*, 2004). To obtain a very precise age-dependent status of *Arabidopsis thaliana* leaf tissue the focus in this work was set on the 6th rosette leaf (Figure 8). Leaf six has a number of advantages compared to other rosette leaves: A) It is easily identifiable due to its position in an angle of approximately 5° from leaf number one. B) It is the first rosette leaf with an elongated longish leaf shape typical for *Arabidopsis thaliana* Col-0 rosette leaves and therefore larger in size and yielding more material for experiments than leaf number 1-5. C) It emerges early within the development of the plant and D) its senescence process is completed before the entire plant life span is finalized assuring a leaf senescence unhindered by the death of the whole organism.

Figure 8: Rosette of *Arabidopsis thaliana* wild type Col-0 at 30 DAG (days after germination). Numbers indicate leaves with respect to their emergence and age. Leaf number 6, taken for many analyses, is marked in red. Scale bar: 1 cm.

Expression of genes *ALA1*, *10* and *11* was analyzed in 6th rosette leaves during a 25 d time course beginning with 25-day-old plants in order to completely cover the time

span of natural occurring leaf senescence (Figure 9). Later during development gene expression was analyzed in green (45 days after germination [DAG]) and senescing (60 DAG) cauline leaves as well as in flowers (50-60 DAG) and roots (45 DAG). Total RNA was extracted from the plant material and reverse transcribed into cDNA, which was used for subsequent QRTPCR runs. Additionally to *ALA* gene expression, expression of the senescence associated gene *SAG12*, the WRKY transcription factor gene *WRKY53* and the Rubisco small subunit gene (*RBCS1a*), important for proper photosynthesis, was analyzed as these genes represent positive and negative senescence marker genes, respectively (Weaver *et al.*, 1998; Hinderhofer and Zentgraf, 2001; Pourtau *et al.*, 2006). During the time course *ALA1* expression was found to be approximately 20-fold up-regulated in rosette leaf number 6. Expression of *ALA10* and *11* increased 6- and 225-fold during this time span, respectively. The tendency in expression increase of *ALA1*, *10* and *11* during senescence described by van der Graaff *et al.* (2006) was validated. In fact, an even higher gene expression during leaf senescence was observed for *ALA1* and especially for *ALA11* compared to the array data (*ALA1*: 4.7-fold, *ALA10*: 5.3-fold and *ALA11*: 9.7-fold increase in transcript amounts, respectively). Furthermore, the QRTPCR experiments revealed an increase in *ALA* gene expression to a smaller extent in senescing cauline leaves (*ALA1* – 6-fold, *ALA10* – 3.7-fold and *ALA11* – 32-fold) indicating a putative role for ALA proteins in the senescence process of these leaves. A lower expression increase of *ALA1*, *10* and *11* was detected in flowers. The expression increase in roots was negligible. These results indicate that leaves in general might be the main site of action of *ALA1*, *10* and *11*.

Expression of *SAG12* was detected in rosette leaves from 40 DAG on and increased 18000-fold until 50 DAG. Detectable *SAG12* expression identified the starting point (40 DAG) of senescence in wild type rosette leaves, as the gene is highly specific to senescence (Weaver *et al.*, 1998; Grbic, 2003). *SAG12* expression increased by 50,000 and 19,000 times in senescing cauline leaves and flowers, respectively. *WRKY53* expression increased during leaf development 15-fold until 40 DAG. As soon as *SAG12* transcript begun to increase, *WRKY53* transcript amounts decreased until a 2-fold increase was reached at 50 DAG. Its expression was likewise 2-fold increased in senescent cauline leaves and flower buds. In roots the expression was 4-fold decreased. The senescence-associated expression of *WRKY53* was found exactly as stated by Hinderhofer and Zentgraf (2001) especially in the onset of leaf senescence (around 40 DAG). It seems furthermore that WRKY53 plays a role in the upper part of the plant, mainly in rosette leaves, and only to a minor part in roots. In contrast to *SAG12* and *WRKY53*, *RBCS1a* expression was maintained at a high level in young non-senescent leaf tissue and decreased steadily during rosette leaf development after 40 DAG until an 800-fold reduction at 50 DAG was reached. Similarly, its expression was 400-fold reduced in senescing cauline leaves. These results are also in concor-

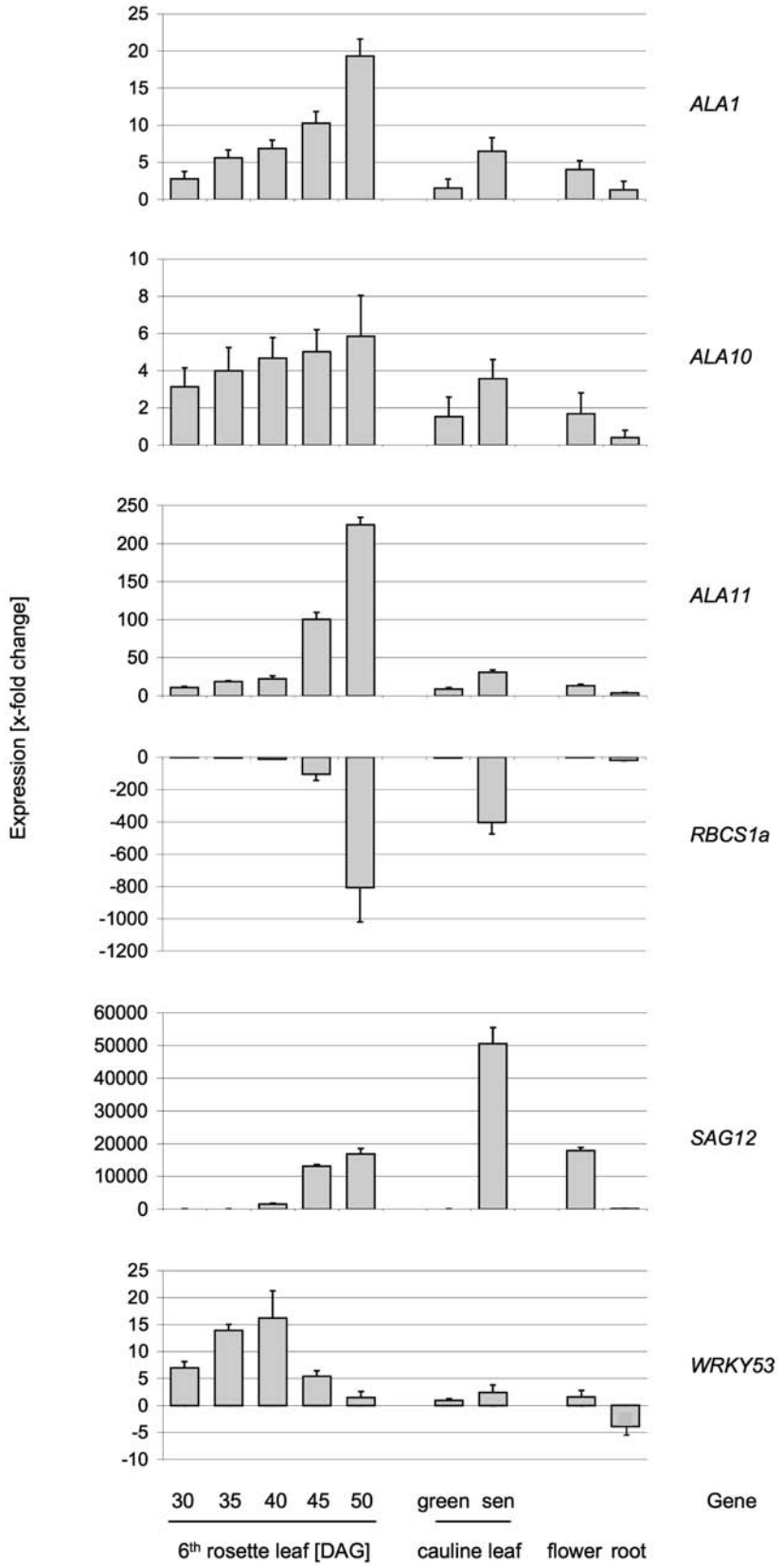

Figure 9: Expression analysis of *ALA* and marker genes via QRTPCR. Diagrams show changes in relative transcript amounts of the 6th rosette leaf during natural development as well as green and senescent (sen) cauline leaves, flowers and roots of *Arabidopsis thaliana* wild type (Col-0) compared to the 6th rosette leaf at 25 DAG. Data are means of three technical replicates ± S.D.

dance with previously described observations by Pourtau *et al.* (2006) and indicate the onset of leaf senescence as well as its ongoing progression by a steady reduction in transcript amounts.

3.2 ALA1, ALA10 and ALA11 are expressed in senescing leaves and in young seedlings

To investigate the tissue and developmental specificity of the *ALA* promoters, GUS staining was performed (chapter 2.12). Therefore, transcriptional fusions of the β-glucuronidase (*GUS*) gene and the *ALA1*, *ALA10* and *ALA11* promoter regions (2 kb region in front of the transcription start codon) were generated (chapter 2.8.1) and transformed into *Arabidopsis thaliana*, resulting in $Prom_{ALA1}$*::GUS*, $Prom_{ALA10}$*::GUS* and $Prom_{ALA11}$*::GUS* transgenic plant lines. Plants from different developmental stages were analyzed for GUS activity (Figure 10). Young seedlings (10 DAG) displayed an intense GUS staining especially in cotyledons as well as roots (Figure 10 A-C and G-I), whereby the leaf vasculature was more pronounced indicating highly active *ALA1*, *10* and *11* promoters in these tissues at that developmental stage. Staining in roots diminished with age and was found until 25 DAG (Figure 10 D-F). No GUS staining was detected in adult roots (data not shown). GUS staining in rosette leaves diminished as well with age. In mature plants leaf expression domains of the *ALA1*, *10* and *11* promoters was very similar. $Prom_{ALA1}$*::GUS* plants displayed the strongest GUS staining intensity and $Prom_{ALA10}$*::GUS* plants the weakest (Figure 10 D-F and O-Q). The GUS signal appeared in a pattern all over the leaf but was always stronger at the leaf margins (Figure 10 O-Q). Leaf GUS staining decreased with age and was observed in regions with beginning senescence. GUS staining was not detectable in regions with more advanced senescence and in fully senescent (yellow) leaves (data not shown). Cauline leaves and rosette leaves displayed the same staining patterns (data not shown). Apart from leaves, GUS staining in *Prom::GUS* plants varied only slightly: staining in the abscission zone of siliques was visible in $Prom_{ALA10}$*::GUS* and $Prom_{ALA11}$*::GUS* plants (Figure 10 K and L-M). Additionally, $Prom_{ALA10}$*::GUS* plants showed uniquely GUS staining in a region of approximately 4 cm in the upper part of the inflorescence below the first developed flowers (Figure 10 J and K). All tested *Prom::GUS* plants displayed similar promoter activity in flowers: GUS staining was observed before pollination only in the stigma (Figure 10 J as an example for $Prom_{ALA10}$*::GUS*). No GUS staining was observed after leaf wounding (after 1 h and 3 h) using 45-day-old transgenic plants (Figure 10 R-T), which excludes an involvement of the proteins in wounding-related processes.

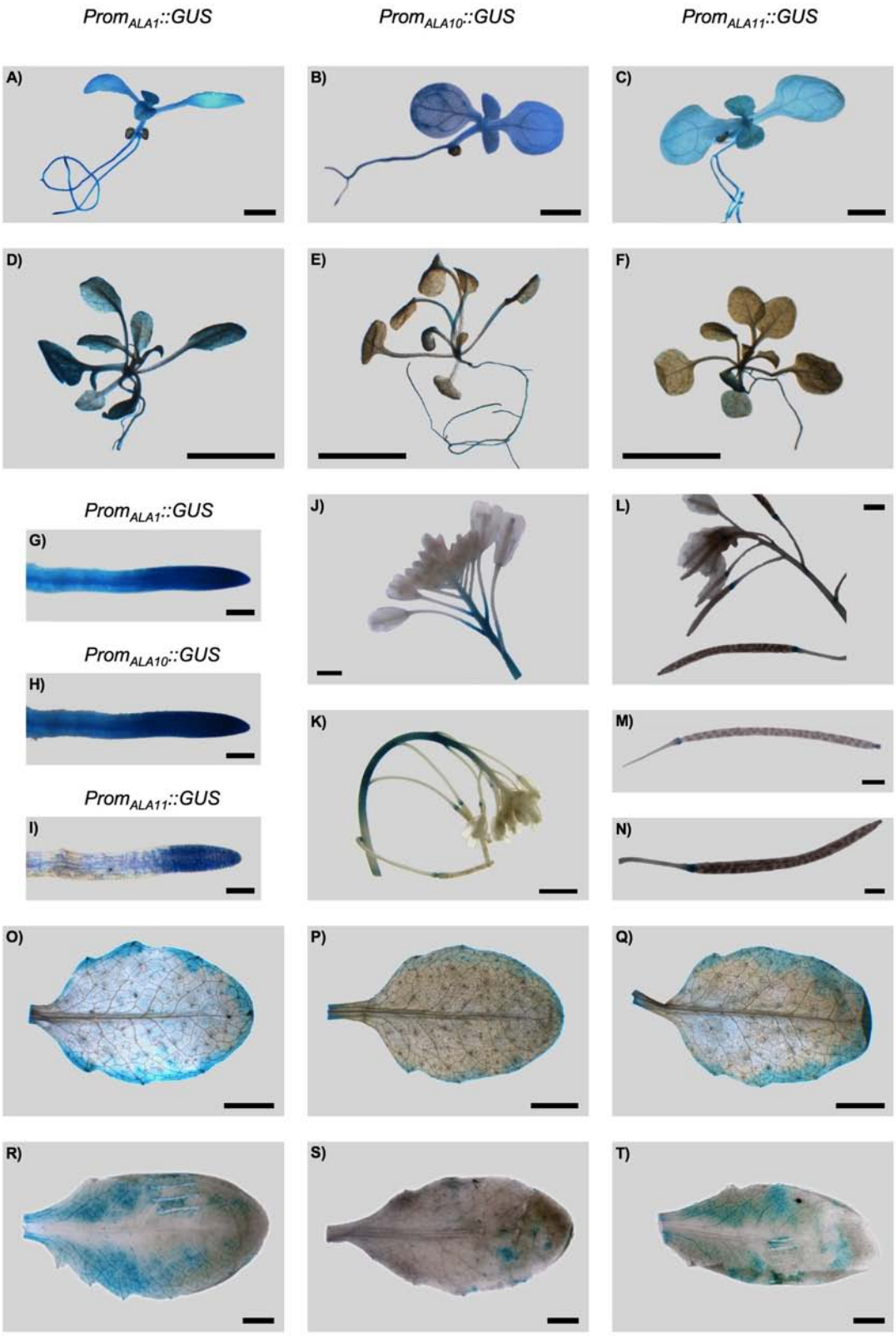

Figure 10: Analysis of *ALA* promoter activity using *Prom$_{ALA1}$::GUS*, *Prom$_{ALA10}$::GUS* and *Prom$_{ALA11}$::GUS* transgenic plants. Depicted are GUS staining from A-C) seedlings at 10 DAG, D-F) seedlings at 25 DAG, G-I) root tips at 10 DAG, J-L) flowers and inflorescences at 40 DAG, L-M) siliques, O-T) 6th rosette leaves at 35 DAG (O-Q) and 3 h after wounding by forceps at 45 DAG (R-T). Scale bars: A-C, J, L-N) 1 mm, D-F, K, O-T) 5 mm, G-I) 100 µm.

3.3 Subcellular localization of ALA1, ALA10 and ALA11

3.3.1 Prediction via bioinformatic tools

Information on the subcellular localization of P_4-type ATPases *in planta* is still very limited. Nevertheless, to elucidate the function of a protein its localization is indispensable. Various bioinformatic tools are available for assigning proteins computationally to their subcellular localization. Eleven selected individual programs summarized at the Aramemnon database (Schwacke *et al.*, 2003) were applied to calculate the subcellular location of ALA1, 10 and 11 proteins (Figure 11). Some of the programs are only capable of predicting the localization probability for a certain cellular compartment, e.g. ChloroP for plastids and Mitopred for mitochondria.

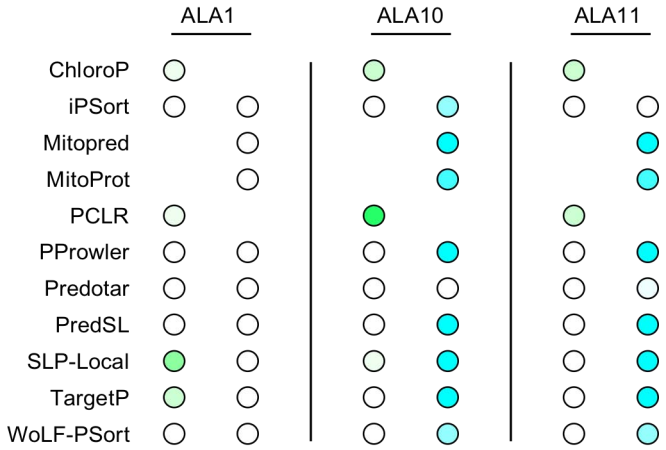

Figure 11: Prediction of the subcellular localization of ALA proteins. Depicted are calculated probabilities for ALA1, 10 and 11 by various localization prediction tools. Plastidial localization is displayed in green (left row) and mitochondrial localization in blue (right row). Higher probability is indicated by color intensity. Data from the Aramemnon database (Schwacke *et al.*, 2003).

No obvious tendency for a specific cellular compartment for ALA1 was found. However, four tools (SLP-Local, TargetP, ChloroP and PCLR) predicted a very weak probability of a plastidial localization for the protein (absolute value 0.9; values below 10 indicate only weak localization probabilities). ALA10 and ALA11 were recognized as mitochondrial localized proteins by 8 and 7 prediction tools (iPSort [only ALA10], Mitopred, Mitoprot, PProwler, PredSL, SLP-Local, TargetP and WoLF-PSort), respectively (absolute

values 13.1 and 12.4). Additionally, three programs (PCLR, ChloroP and SLP-Local) calculated a weak plastidial localization for ALA10 (absolute value 1.0). Two programs (ChloroP and PCLR) predicted a very unprobable plastidial localization for ALA11 (absolute value below 0.1). None of the tested ALA proteins were predicted by the used set of tools to the secretory pathway, including endoplasmatic reticulum (ER), Golgi apparatus, vesicles and the vacuole.
In order to confirm the calculated predictions empirically and, thus, assuring the intracellular localization of ALA proteins *in planta*, confocal microscopy was applied using ALA-GFP fusion proteins expressed in tobacco and *Arabidopsis* (chapter 2.11).

3.3.2 Localization of ALA_{TM1-4}-eGFP fusion proteins

C-terminal fusions of *eGFP* behind the first four transmembrane spanning regions of *ALA1*, *10* and *11* under transcriptional control of the *CaMV35S* (*35S*) promoter were generated (chapter 2.8.3). The constructs were introduced in tobacco leaves leading to transient expression and transformed into *Arabidopsis* resulting in *35S::ALA1$_{TM1-4}$-eGFP*, *35S::ALA10$_{TM1-4}$-eGFP* and *35S::ALA11$_{TM1-4}$-eGFP* transgenic plant lines with constitutive expression. Fluorescence signals emitted by the fusion proteins expressed in *Nicotiana* and *Arabidopsis* tissues were observed via confocal microscopy through specific stimulation with monochromatic laser light. Additionally, protein markers specific for plasma membrane, tonoplast, ER, mitochondria, peroxisomes and Golgi vesicles fused to the fluorescent protein mCherry (Nelson *et al.*, 2007) were co-expressed with the ALA_{TM1-4}-eGFP proteins to confirm the subcellular localization by overlapping fluorescence signals. Although the *35S*-promoter was used to drive expression, stable transgenic *Arabidopsis* plants (*35S::ALA$_{TM1-4}$-eGFP*) showed weak fluorescence signals (data not shown). Stronger fluorescence signals were obtained using tobacco epidermal cells expressing *35S::ALA$_{TM1-4}$-eGFP* constructs and are described as follows: GFP fluorescence signals of all tested fusion proteins were excluded from the nucleus. Fluorescence signals emitted by $ALA1_{TM1-4}$-eGFP fusion proteins were observed in chloroplasts. The obtained signals matched with the chloroplast autofluorescence resulting in a colocalization of both signals (Figure 12 A). These findings emphasize a plastidial localization of ALA1, for which only a low probability of plastidial localization was predicted by bioinformatic tools (chapter 3.3.1).
Cells expressing $ALA10_{TM1-4}$-eGFP fusion proteins displayed fluorescence signals in the cell wall proximity. In order to specifically assign the signal to a subcellular compartment, co-localization experiments with co-expressed fluorescently labeled marker proteins were carried out. Fluorescence signals obtained by plasma membrane and

tonoplast marker proteins resulted both in overlapping signals with ALA10$_{TM1-4}$-eGFP (Figure 12 B). Several repetitions of the colocalization experiments resulted always in a localization of ALA10$_{TM1-4}$-eGFP to both the plasma membrane and the tonoplast. It was not possible to localize the fusion proteins specifically to one of the membranes. However, fluorescence signals emitted by ER and mitochondria marker proteins did not match with the ALA10$_{TM1-4}$-eGFP fluorescence (data not shown) and a localization of ALA10 to the ER can be excluded. As a conclusion, the predicted mitochondrial or plastidial localization of ALA10 by bioinformatic tools (chapter 3.3.1) has to be rejected. Fluorescence signals of ALA11$_{TM1-4}$-eGFP fusion proteins were unevenly distributed within the cytoplasm of the cells and formed particle-like structures (Figure 12 C). The size of the structures varied in a range between mitochondrial and peroxisomal sizes. None of the tested fluorescently labeled marker proteins (ER, mitochondria, peroxisomes and Golgi vesicles) was able to match the fluorescence signals of ALA11$_{TM1-4}$-eGFP (data not shown). The localization of ALA11 within the cell remains elusive due to the aggregation of the ALA11$_{TM1-4}$-eGFP fusion proteins.

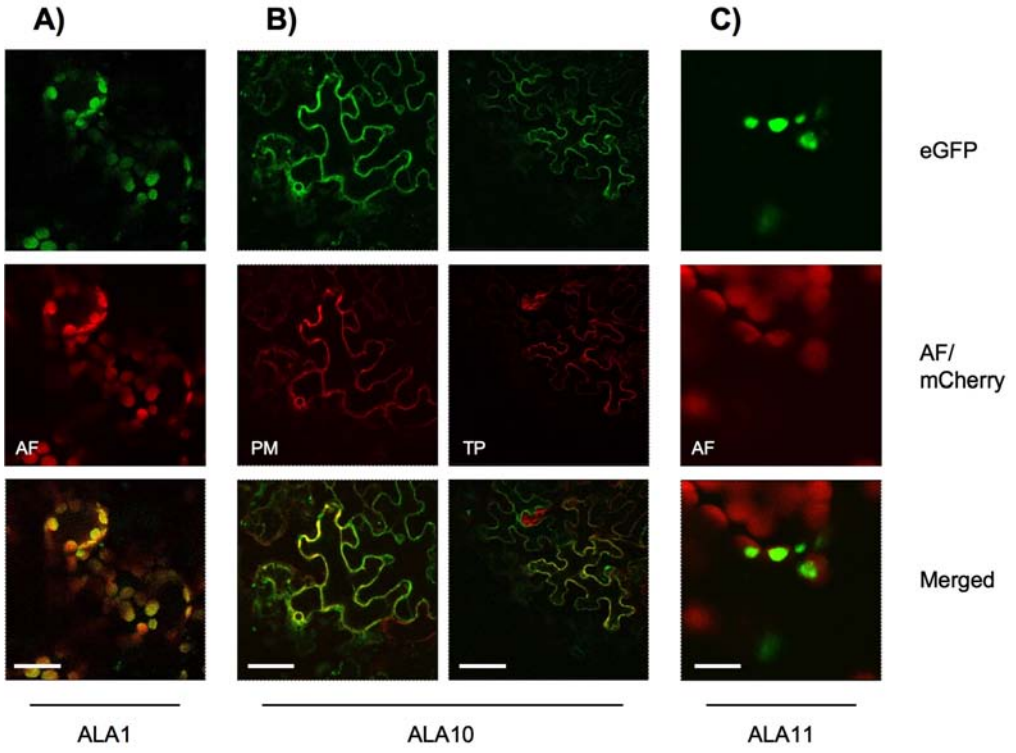

Figure 12: Fluorescence of ALA$_{TM1-4}$-eGFP fusion proteins transiently expressed in *Nicotiana benthamiana*. Depicted are images of adaxial epidermal cells obtained via confocal laser scanning microscopy. ALA$_{TM1-4}$-eGFP fusion proteins of A) ALA1, B) ALA10 and C) ALA11 are either expressed alone or in combination with marker proteins fused to mCherry: PM plasma membrane represented by PIP2A, TM tonoplast represented by γTIP, AF chlorophyll autofluorescence. Scale bar: A) 20 µm, B) 50 µm (left), 70 µm (right) and C) 10 µm.

3.3.3 Localization of eGFP-ALA$_{full\text{-}length}$ fusion proteins

In order to confirm the localization of ALA1 and ALA10 by an additional experiment, confocal microscopy was carried out using the full-length *ALA* coding regions fused to *eGFP*. Therefore, eGFP was fused N-terminally in front of *ALA1* and *10* full-length cDNA. Constructs under transcriptional control of the *35S*-promoter were generated (chapter 2.8.3) and used for transient expression in tobacco leaves and stable transformation of *Arabidopsis* resulting in *35S::eGFP-ALA1*$_{full\text{-}length}$ and *35S::eGFP-ALA10*$_{full\text{-}length}$ transgenic plants. eGFP-ALA1 and eGFP-ALA10 full-length fusion proteins resulted in identical fluorescence signals as ALA1$_{TM1\text{-}4}$-eGFP and ALA10$_{TM1\text{-}4}$-eGFP, respectively, when expressed in tobacco epidermal cells (Figure 13 A). In case of eGFP-ALA1$_{full\text{-}length}$ the fluorescence signals fitted to the chloroplast autofluorescence, while in case of eGFP-ALA10$_{full\text{-}length}$ the fluorescence was similar to the patterns of tonoplast and plasma membrane markers. Stably transformed *Arabidopsis* plants showed weaker but identical fluorescence signals for eGFP-ALA1$_{full\text{-}length}$ and eGFP-

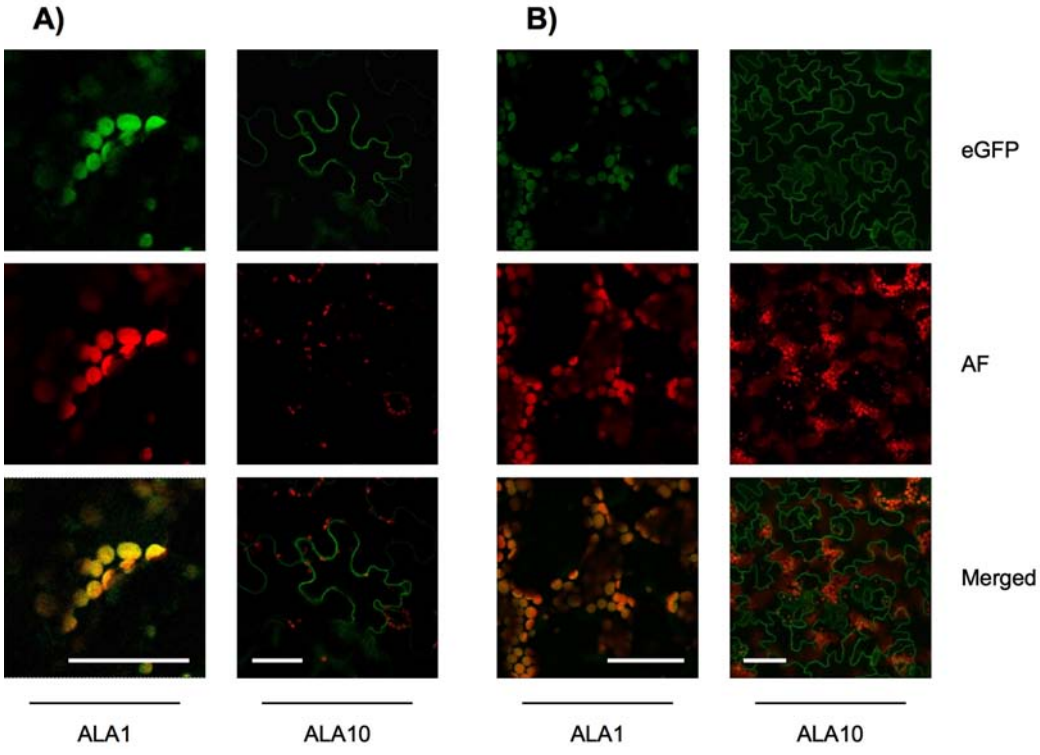

Figure 13: Fluorescence of eGFP-ALA$_{full\text{-}length}$ fusion proteins in *Nicotiana benthamiana* and *Arabidopsis thaliana*. Depicted are images of A) tobacco and B) *Arabidopsis* adaxial epidermal cells expressing eGFP proteins fused with ALA1 and 10 (full-length) obtained via confocal laser scanning microscopy. AF chlorophyll autofluorescence. Scale bar: 50 µm.

$ALA10_{full\text{-}length}$ fusion proteins (Figure 13 B). These experiments confirm the plastidial localization of ALA1 and point out a localization of ALA10 in both the plasma membrane and the tonoplast. Potentially ALA10 circulates between the two membrane systems. Furthermore, it can be assumed that the fused eGFP tag has no influence on the localization of the proteins, as C- and N-terminal fusions of eGFP to the ATPase proteins produced identical fluorescence signals.

3.4 T-DNA insertion lines for *ALA* genes

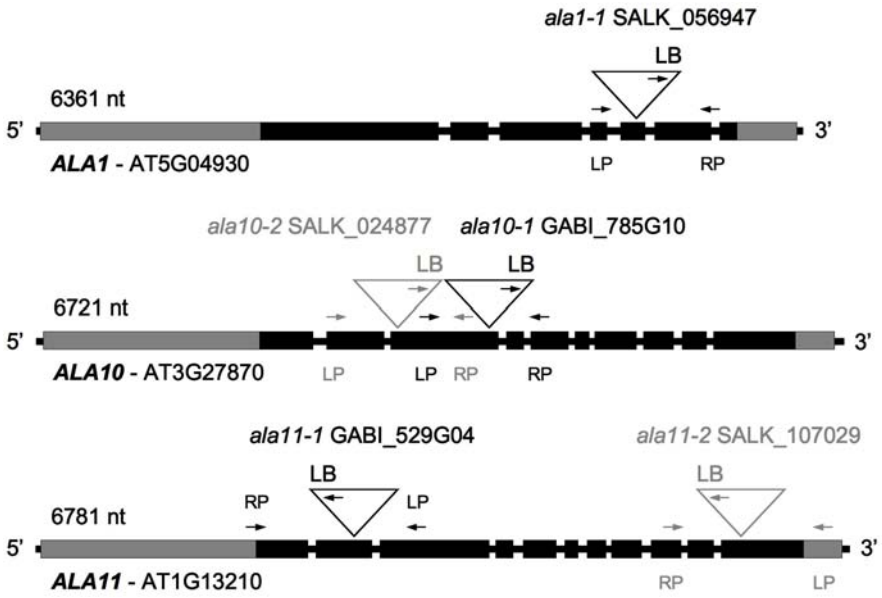

Figure 14: Organization of *ALA1*, *10* and *11* genes with T-DNA insertion sites and orientation and primer positions. Exons are represented by black boxes and UTR in grey. T-DNA insertion sites are indicated with triangles. LB left border of T-DNA (left border primer), LP left primer, RP right primer. Grey triangles indicate second, alternative T-DNA insertion lines.

T-DNA insertions have become a common tool in plant mutant analysis and are extremely useful to unravel gene functions (Bouche and Bouchez, 2001). In order to examine the role of the senescence-associated genes *ALA1*, *ALA10* and *ALA11* within the plant, a reverse genetics approach was applied and T-DNA insertion lines in the corresponding *ALA* genes in the background of ecotype Columbia (Col-0) selected (Figure 14). The corresponding *ALA* genes were interrupted by the insertion of a T-DNA (chapter 3.4.3) and should therefore result in the generation of knockout mutants (Bouche and Bouchez, 2001). The T-DNA lines were ordered from the Salk Institute Genomic

Analysis Laboratory (SIGnAL; http://signal.salk.edu/; La Jolla, CA, USA) and the GABI-Kat project (Genomanalyse im biologischen System Pflanze, http://www.gabi-kat.de/, Cologne, Germany) mutant collections (Alonso *et al.*, 2003; Rosso *et al.*, 2003). T-DNA insertion lines with an exon located T-DNA were favored and when possible a second, independent insertion line was ordered (*ALA10* and *ALA11*). Positions of the T-DNA insertions and the *ALA* gene structures are shown in Figure 14.

3.4.1 Isolation of T-DNA insertion lines in *ALA* genes

In order to test the ordered mutant plants on their T-DNA insertion, genomic DNA was extracted from leaf samples and used for PCR analyses (chapter 2.6.8). Homozygous

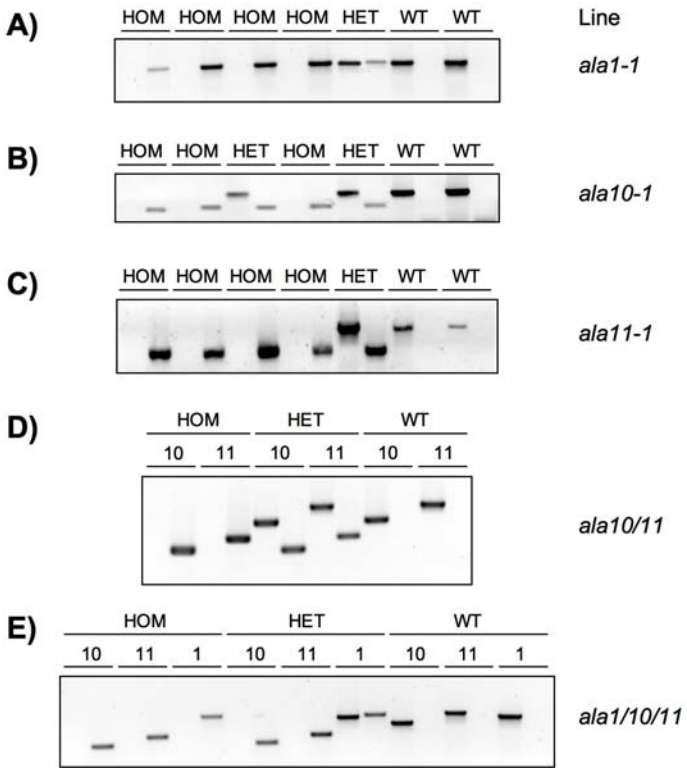

Figure 15: PCR analysis of *ala* mutant lines. Images of electrophoretically separated PCR products in an ethidium bromide stained 1% agarose gel. A)-C) Analysis of mutant line *ala1-1*, *ala10-1* and *ala11-1*. Depicted are two lanes per tested mutant plant. First lane: Intact genomic DNA sequence was detected with a gene specific primer pair (LP and RP). Second lane: Inserted T-DNA was detected with a left border specific primer (LB) combined with an *ALA* specific primer (RP). D) Analysis of generated double mutant line *ala10/11*. Depicted are two lanes for both genes (*ALA10* and *ALA11*) per plant line in the same way as for A-C). E) Analysis of generated triple mutant line *ala1/10/11*. Depicted are two lanes for the three *ALA* genes (*10*, *11* and *1*) similarly to D). HOM homozygous, HET heterozygous insertion line, WT wild type control.

insertion lines *ala1-1*, *ala10-1*, *ala10-2*, *ala11-1*, *ala11-2* were identified that way (Figure 15 A-C, data for *ala10-2* and *ala11-2* not shown). Two PCR reactions per T-DNA insertion and plant were performed. The first reaction tested for an intact gene and was performed with two gene specific primers, located up- and down-stream of the T-DNA insertion site (LP and RP; primers positions are indicated in Figure 14). The second reaction detected integrated T-DNA using one gene specific primer (RP) and a T-DNA specific primer (LB). No gene specific PCR products could be generated with an elongation step of 1 min in homozygous T-DNA insertion lines due to the large amplification product of approximately 4-5 kb. PCR on wild type material served as a control.

Two independent T-DNA insertion lines for *ALA10* and *ALA11* genes were isolated (*ala10-1*, *ala10-2* and *ala11-1*, *ala11-2*) representing two different mutant alleles for these genes. Both mutant lines displayed identical phenotypes for each gene, respectively (data not shown). Thus, it can be assumed that the observed phenotype of *ala10* and *ala11* lines was caused by a mutation of the *ALA10* and *ALA11* gene, respectively. All following experiments and analyses were therefore carried out only with mutant line *ala10-1* and *ala11-1*.

3.4.2 Isolation of double and triple T-DNA insertion lines

It is a known fact that many single knockout plants of large gene families often display no obvious phenotype (Bouche and Bouchez, 2001). In order to recognize effects of possible functional redundancy among ALA family members *in planta*, double and triple mutant lines *ala10/11* and *ala1/10/11* were generated. This was achieved by crossing *ala10-1* with *ala11-1* resulting in the *ala10/11* double mutant line. Homozygous plant lines were isolated via PCR analysis from an F2 population in the same way as for the single mutant lines *ala1-1*, *10-1* and *11-1* (Figure 15 D). The *ala1/10/11* triple mutant was generated in similar fashion by crossing *ala10/11* with *ala1-1* and homozygous plants were identified via PCR (Figure 15 E).

3.4.3 Genotyping of T-DNA insertion sites

The exact T-DNA integration position of *ala1-1*, *ala10-1* and *ala11-1* mutants was verified by sequencing from the left T-DNA border reaching into the genomic neighborhood of the *ala* mutant lines. Therefore, a PCR on extracted genomic DNA of the *ala* mutant

lines was applied using the T-DNA specific LB primer in combination with the corresponding *ALA* gene right primer (RP). The products were blunt-cloned into *EcoR*V digested pBlueScript II KS+ and sequenced. T-DNA insertion sites in *ALA10* and *ALA11* (*ala10-1* and *ala11-1*) were confirmed as stated by SIGnAL (http://signal.salk.edu/; La Jolla, CA, USA) in the 3rd and 2nd exon at position 1884 and 698, respectively (Figure 16; position given in nucleotides from the A of the ATG start-codon on genomic DNA). The T-DNA integrated in *ALA1* (*ala1-1*) was detected in the 5th exon at position 5001 and not within the 6th exon as indicated by SIGnAL. The other end (right border) of the T-DNA insertion in *ala1-1*, *ala10-1* and *ala11-1* was not determined via sequencing.

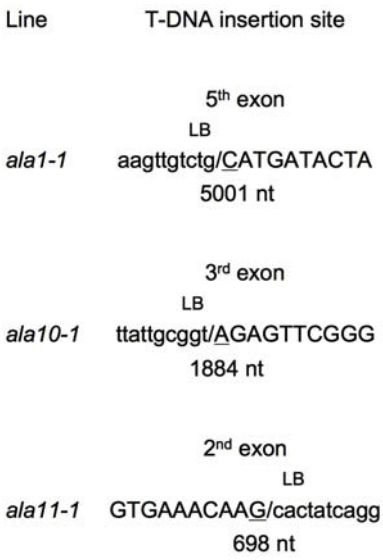

Figure 16: Position of T-DNA insertions of *ala1-1*, *ala10-1* and *ala11-1*. Depicted are the orientation and exact position within the corresponding ALA gene indicated by an underlined letter [nt from ATG start-codon]. LB left border sequence of T-DNA, lowercase: T-DNA sequence, uppercase: genomic sequence, underlined: integration position.

3.4.4 *ala* mutants possess a single T-DNA insertion

Approximately 50% of the T-DNA insertion lines obtained from the SIGnAL or GABI-Kat project (http://signal.salk.edu/ or http://www.gabi-kat.de/) contain more than one T-DNA insert (Alonso *et al.*, 2003; Rosso *et al.*, 2003). If further gene products than the desired one are affected by T-DNA insertions, unspecific pleiotropic effects might be provoked affecting the phenotype of the plants. In order to overcome the problem of multiple T-DNA insertions, *ala* single mutants (*ala1-1*, *ala10-1* and *ala11-1*) had been twice backcrossed with wild type. Homozygous identified *ala* mutant plants were then screened for the number of T-DNA insertion within their genome via Southern hybridization (chapter 2.7.5). Therefore, genomic DNA of leaf material of single homozygous mutant plants was extracted, digested with restriction endonucleases (*ala1-1*: *Kpn*I,

ala10-1: *Sac*I, *ala11-1*: *Hind*III), electrophoretically separated in a gel, blotted onto a membrane and finally probed with DIG-labeled sequences homologous to a region within the T-DNA (Figure 17). The hybridization pattern revealed one band in the expected size for each single *ala* mutant: *ala1-1*: 4002 bp, *ala10-1*: 3559 bp and *ala11-1*: 7228 bp indicating only one T-DNA insertion within the genome in the corresponding

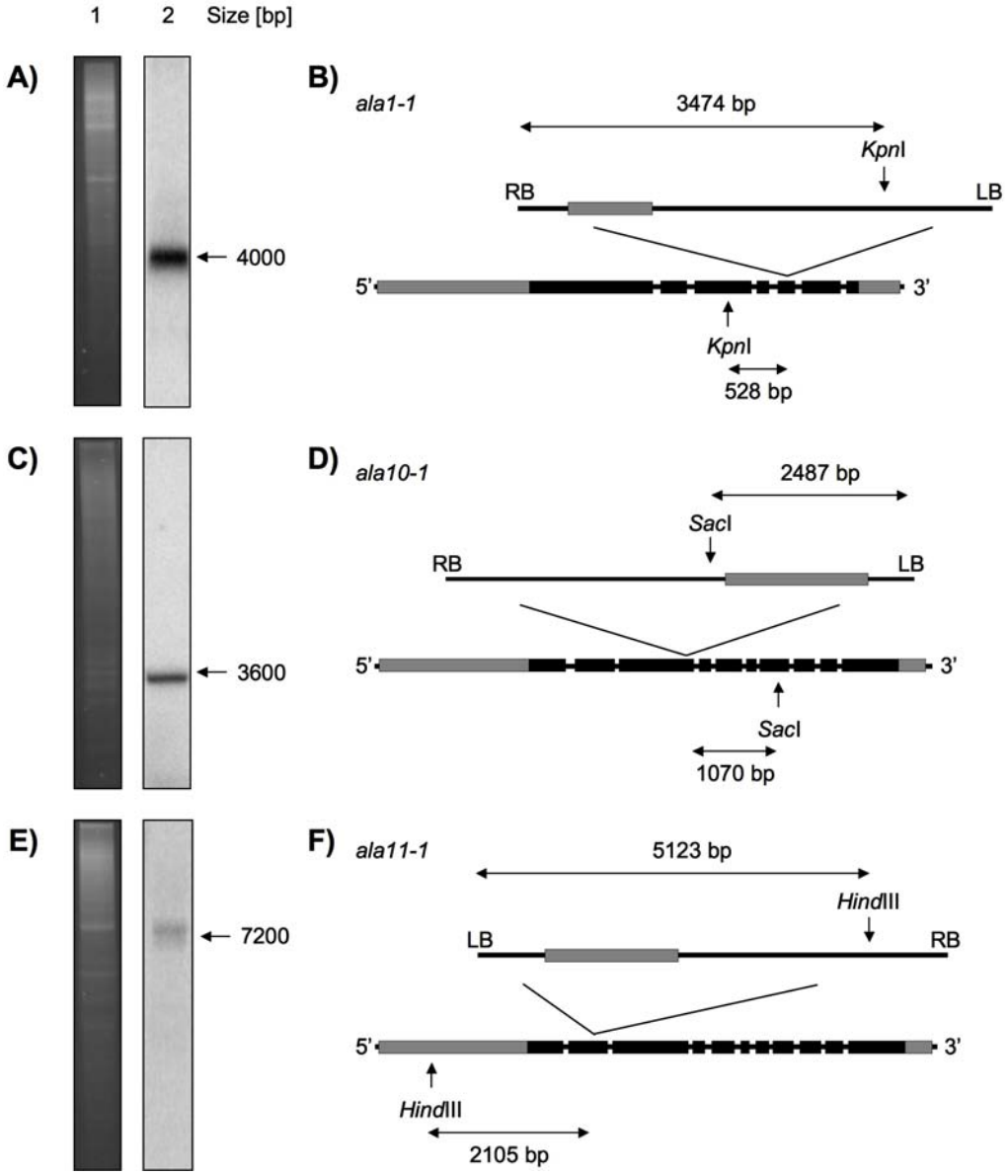

Figure 17: Quantitative analysis of T-DNA insertions in *ala* mutant lines. Ethidium bromide stained gel (lane 1) of digested genomic DNA of *ala* mutant lines and corresponding Southern blot (lane 2). A) *ala1-1* digested with *Kpn*I, C) *ala10-1* digested with *Sac*I and E) *ala11-1* digested with *Hind*III. Numbers to the right indicate expected fragment sizes. Sketch of T-DNA integration within B) *ALA1*, D) *ALA10* and F) *ALA11*. Hybridization site of the used probe located on the T-DNA indicated in grey, arrows indicate restriction sites by endonucleases and fragment lengths, LB left border, RB right border of T-DNA.

ALA gene of each tested single *ala* mutant. Repeated or rearranged integrated T-DNA as often observed in T-DNA mutagenized populations (Feldmann *et al.*, 1989; Herman and Marks, 1989) could be excluded in the tested plants. It can be assumed that the observed phenotype of *ala* mutant plants (chapter 3.5) is caused by the T-DNA integration within the corresponding *ALA* genes.
Due to the absence of additional T-DNA insertions in the tested *ala1-1*, *ala10-1* and *ala11-1* mutants, all further experiments were performed with seeds originating from these plants.

3.4.5 Altered *ALA* expression in *ala1-1*, *ala10-1* and *ala11-1*

The insertion of T-DNA into a gene leads to a mutation (Feldmann, 1991), which might result in the disruption of the corresponding gene. QRTPCR was applied in order to test whether the T-DNA insertion in *ala1-1*, *ala10-1* and *ala11-1* affects *ALA* gene expression (chapter 2.7.10). Expression of the senescence marker gene *SAG12* (Weaver *et al.*, 1998) was additionally analyzed to determine the effect of the T-DNA insertion on the senescence process within the mutant lines. Total RNA of 30-day-old 6th rosette leaves of *ala1-1*, *ala10-1* and *ala11-1* as well as wild type plants was extracted and converted to cDNA that was subsequently analyzed regarding transcript amounts. Primer pairs for the amplification were designed to hybridize within the last (at the 3' end) exon of the analyzed transcripts. The relative transcription rate of *ALA1*, *10, 11* and *SAG12* of *ala1-1*, *ala10-1* and *ala11-1* mutants was calculated, compared to wild type and visualized as expression change (Figure 18).
Expression of *ALA1*, *ALA10* and *ALA11* was reduced to very low, barely detectable levels in mutant line *ala1-1*, *ala10-1* and *ala11-1*, respectively: *ALA1* expression was 22-fold lower in the *ala1-1* mutant line compared to wild type levels. Reduction of *ALA10* expression was 14-fold in mutant line *ala10-1* and the expression of *ALA11* was 46-fold reduced in *ala11-1*. These results clearly indicate a negative effect on *ALA* gene expression by the T-DNA insertion of the *ala* mutant lines.
Besides an influence on the gene, where the T-DNA was integrated no additional effects on *ALA* gene expression were observed in the tested *ala* mutant lines (Figure 18): The expression of *ALA10 and ALA11* was comparable to wild type in *ala1-1* mutants. Likewise, the expression of *ALA1* and *ALA11* was not altered in *ala10-1* and no effect on the expression of *ALA1* and *ALA10* was observed in *ala11-1* mutants. These measurements point out that the negative effect on gene expression of the T-DNA was specific to the gene where it was integrated.

At the same time, compared to wild type the expression of the senescence marker *SAG12* was 34-, 10-, and 82-fold induced in *ala1-1*, *ala10-1* and *ala11-1*, respectively, indicating an advanced senescence status of the mutant lines as leaf senescence is generally accompanied by an expression increase of the senescence-associated gene *SAG12* (Weaver *et al.*, 1998; Grbic, 2003). Phenotypical observation of *ala* mutants revealed premature senescence (chapter 3.5).

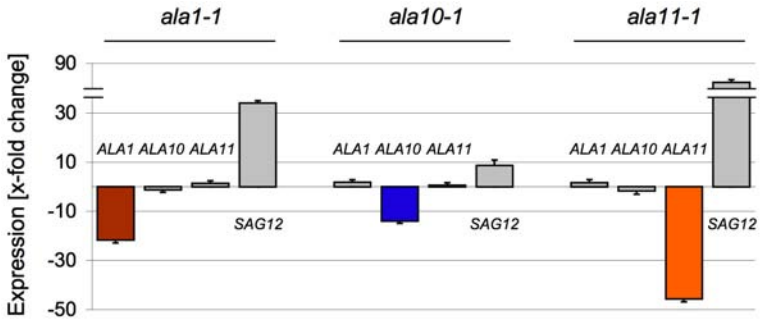

Figure 18: Expression analysis of T-DNA insertion lines *ala1-1*, *ala10-1* and *ala11-1* conducted with QRTPCR. Depicted are changes in relative transcript amounts of *ALA1*, *10* and *11* genes and *SAG12* at 30 DAG in the 6th rosette leaf compared to wild type. Data are means of five technical replicates ± S.D.

3.4.6 T-DNA integration causes different expression levels 5' and 3' to the integration site in *ala1-1*, *ala10-1* and *ala11-1*

Regarding the nomenclature from Krysan *et al.* (1999) the *ala1-1*, *ala10-1* and *ala11-1* plants could be described best as knock-about mutants. Transcript amounts of *ALA1*, *10* and *11* within *ala1-1*, *ala10-1* and *ala11-1*, respectively, were strongly reduced in comparison to wild type but still detectable by QRTPCR (Figure 18) so that the question of their nature arose. The T-DNA containing vectors pROK2 and pAC161 that were used to generate the mutant populations by the Salk Institute Genomic Analysis Laboratory and the GABI-Kat project, respectively, carry a full-lenght *CaMV35S*-promoter in proximity to the T-DNA border (Alonso *et al.*, 2003; Rosso *et al.*, 2003). The initial intention of this was to design an activation-tagging element that could be used after successful T-DNA integration into the plant genome (Alonso *et al.*, 2003; Rosso *et al.*, 2003). The *CaMV35S*-promoters, located inside the T-DNA region, can cause an expression extending into the genomic neighborhood of the integration site. In case of interference of integrated T-DNA with natural occurring expression of the affected gene its transcript amounts should vary 5' and 3' to the T-DNA insertion site. In order to

prove that detected *ALA* expression in *ala* mutant lines was due to an interference caused by the T-DNA insertion, a reverse transcription PCR (RTPCR) analysis was set up (chapter 2.7.9). Total RNA was extracted from 30-day-old plants and reverse transcribed into cDNA that was analyzed. Detection of *ALA* transcripts was investigated upstream (in the 5' region), downstream (in the 3' region) and spanning the T-DNA integration site (O; Figure 19). Band intensity of PCR products 5' and 3' to the integration site varied in mutant line *ala1-1*, *ala10-1* and *ala11-1*, thus, indicating semi-quantitatively different amounts of *ALA* transcripts 5' and 3' to the T-DNA integration. Additionally, the band intensities differed from those of wild type, which indicates an impact of the integrated T-DNA on the gene expression. Primer pairs for transcript detection 5' and 3' to the T-DNA insertion in *ALA10* and 5' in *ALA11* resulted in double bands due to an unknown but reproducible effect. These primers were designed to amplify a 690, 718 and 502 bp region, respectively, represented by the smaller band. *ACT2* expression served as an internal control for same cDNA amounts and resulted in comparable band intensities for the tested mutant lines as well as for wild type. Band sizes of 303 bp for *ACT2* indicated an absence of genomic DNA and, thus, ideal conditions for the RTPCR. *ACT2* primers were designed spanning an intron and would

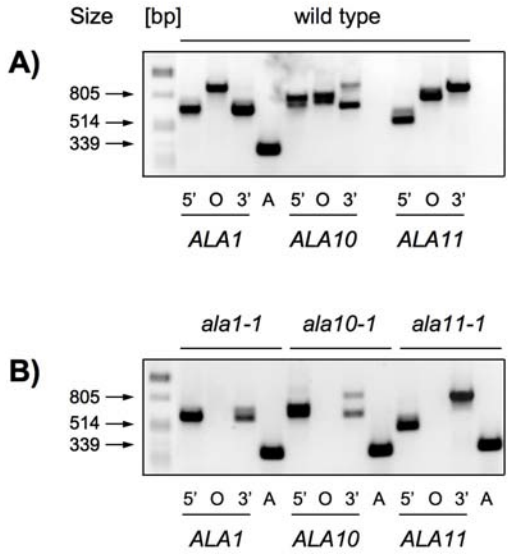

Figure 19: Effect of T-DNA integration on *ALA* transcripts in *ala* mutant lines analyzed with RT-PCR. RNA was extracted from 6th rosette leaves at 30 DAG and reverse transcribed into cDNA for PCR analysis. Depicted are images of electrophoretically separated PCR products in an ethidium bromide stained 1% agarose gel using A) wild type B) mutant lines *ala1-1*, *ala10-1* and *ala11-1*. Detection of transcript amounts was performed for *ALA1*, *ALA10* and *ALA11* genes upstream (5') and downstream (3') of the T-DNA integration site as well as spanning the T-DNA integration site (O). Transcript amounts of *ACT2* (A) served as control for equal amount of mRNA. Size marker: *Pst*I digested λ-phage DNA.

result in a larger amplification product (382 bp) in case of genomic DNA contamination. No amplification product was detectable using cDNA from *ala1-1*, *ala10-1* and *ala11-1* plants with primers spanning the T-DNA integration sites. These results demonstrate that the T-DNA is successfully transcribed and present in *ala1*, *ala10* and *ala11* transcripts. In order to test whether the detected *ALA1*, *10* and *11* transcripts in *ala1-1*, *ala10-1* and *ala11-1* plants, respectively, might result from a transcription initiation 3' to the T-DNA insertion, Northern hybridization was performed. Shortened *ala* transcripts representing truncated mRNA versions would verify this hypothesis. However, it was not possible to detect *ALA1*, *10* and *11* transcripts in *ala1-1*, *ala10-1* and *ala11-1* plants, respectively, with the Northern hybridization technique (data not shown), which indicates very low transcript amounts in the mutant plants. An additional RTPCR experiment with primers homologous to the T-DNA and the 3' flanking genomic region would answer the hypothesis.

3.5 Phenotype of *ala* mutant lines

All following experiments and analyses were carried out only with mutant line *ala10-1* and *ala11-1* and subsequently these lines are called *ala10* and *ala11*. Mutant line *ala1-1* is referred to as mutant line *ala1* from now on.

3.5.1 *ala* mutant lines exhibit reduced rosette growth and premature senescence symptoms

Expression of *ALA1*, *10* and *11* was induced during leaf senescence of *Arabidopsis thaliana* (chapter 3.1). Mutants of these genes should therefore display an altered senescence progression. In order to confirm this hypothesis, rosettes of soil-grown *ala* mutant lines and wild type plants (16 h light of 120 µmol*m^{-2}*sec^{-1} per day at 21° C) were observed during natural development (Figure 20 A). Leaf yellowing is a convenient visible indicator of leaf senescence (Lim *et al.*, 2007) and was first observed in wild type rosette leaves around 40 DAG. Rosette leaves of *ala* mutant lines exhibited earlier yellowing at 35 DAG (*ala1*), 38 DAG (*ala10*), 39 DAG (*ala11*) and 30 DAG (*ala10/11* and *ala1/10/11*). Cotyledons of the investigated *ala* mutants aged more rapidly. By 25 DAG cotyledons were completely yellow, whereas wild type cotyledons became yellow around 30 DAG. It has to be mentioned that no visible leaf yellowing was observed

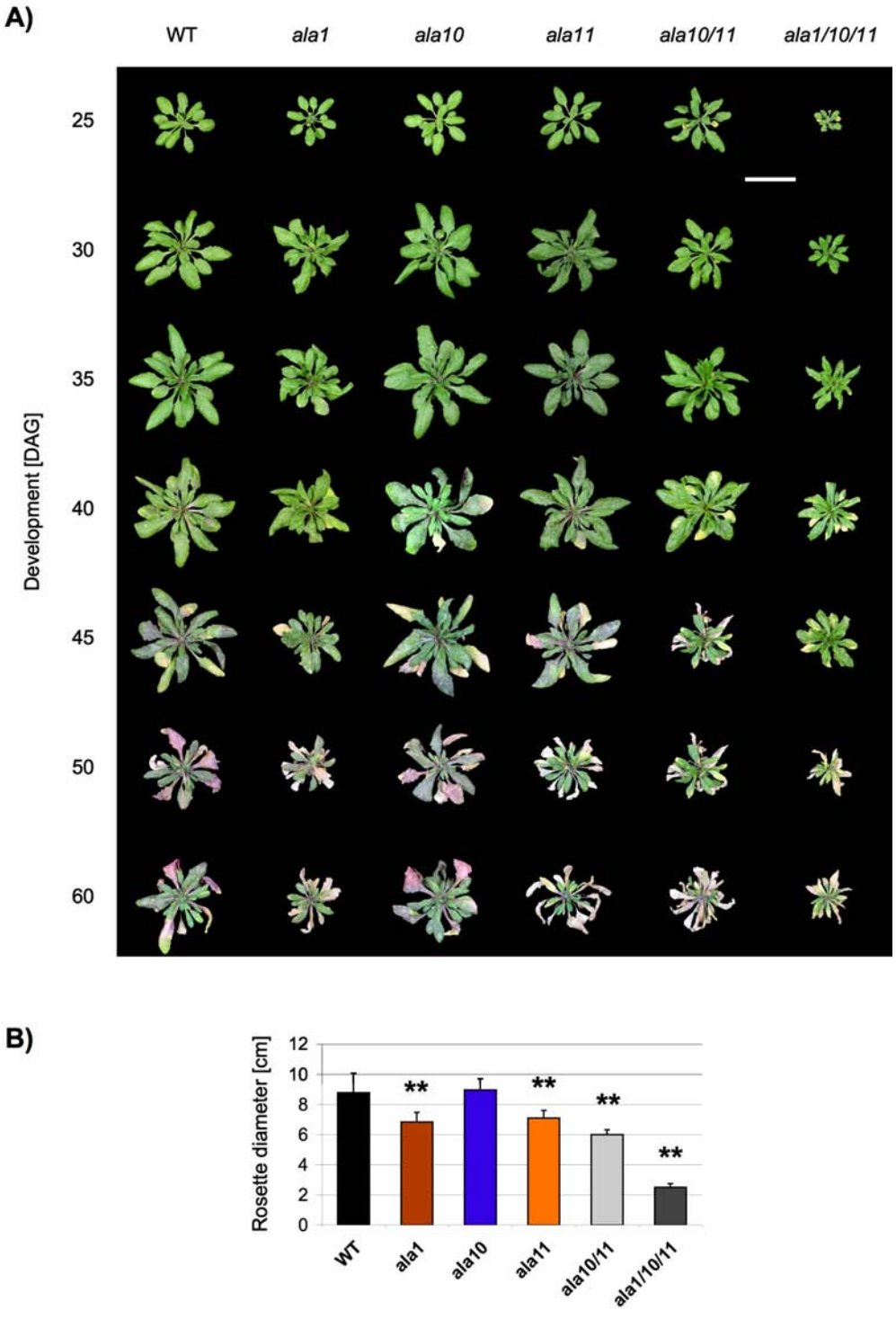

Figure 20: Phenotype of *ala* mutant lines. A) Images of whole rosettes during development of wild type and *ala* mutant lines, respectively. Depicted are representative examples grown under 16 h light/d, 120 µmol*m^{-2}*sec^{-1} photosynthetically active radiation, 21 °C and 70% humidity. Scale bar: 5 cm. B) Diagram of rosette diameter (mean values ± S.D., n=106) of wild type and *ala* mutant lines at 30 DAG. Significant differences to wild type are marked with asterisks (**), *P* < 0.01.

before 20 DAG in the investigated *ala* mutants and wild type plants. After this time point senescent cotyledons of *ala* mutant lines became visible, especially in the triple and double mutant line *ala1/10/11* and *ala10/11*. It seemed furthermore, that all investigated ala lines did not accumulate anthocyanins to the same extent as wild type by the end of their developmental phase. These observations clearly point out a positive effect on the progression of senescence caused by mutations in *ALA* genes. The described effect seems to be additive because *ala* double and triple mutants displayed more severe premature senescence than *ala* single mutants. As a conclusion, *ALA* genes are necessary for a controlled progression of leaf senescence.
Additionally, to premature senescence, mutant lines *ala1*, *ala11*, *ala10/11* and *ala1/10/11* showed a reduction in rosette size (Figure 20 B) to 78%, 80%, 68% and 28% of wild type level, respectively. Mutant line *ala10* showed no reduction in rosette size compared to wild type. The effect correlates with the severity of the premature senescence phenotype of the mutants. Again, it is an additive effect as the reduction in rosette size was more prominent in the double and triple mutant line. It seems that leaf senescence and growth are interconnected and that *ALA* genes (*1*, *10* and *11*) influence these processes.
The average rosette leaf number at bolting was 16 for *ala* mutant lines as well as wild type. However, bolting time of *ala* mutant lines varied in comparison to wild type: 50% of the observed wild type plants bolted after 23.6 DAG. Mutant line *ala10* and the double mutant line *ala10/11* displayed slightly delayed bolting around 24 DAG. The single mutant line *ala11* and the triple mutant line *ala1/10/11* were more delayed in bolting and displayed bolting at 26 and 28 DAG, respectively. In contrast, *ala1* plants bolted earlier than wild type after 20.8 DAG (Appendix, Figure 42). Regarding these data it can be assumed that ALA1 negatively influences bolting time whereas ALA11 accelerates the process. ALA10 seems to have no effect on plant bolting. The effect of *ALA* genes on plant bolting seems to be dependent on the plant size (except *ALA1*) and not on the senescence status so that it is more likely that bolting is controlled by other factors than *ALA* genes.

Each *Arabidopsis* leaf starts to senesce at a different time point depending on its emergence (leaf age) and the developmental phase of the plant (plant age; Zentgraf *et al.*, 2004). In order to observe the premature senescence phenotype of *ala* mutant lines more precisely a focus was set on the 6th rosette leaf (Figure 21 A). Additionally, by the observation of single rosette leaves faint distinctive phenotypes become more obvious as covering by other leaves of the rosette is eliminated (Zentgraf, 2006; personal communications). No visible senescence symptoms were observed in 6th rosette leaves until 30 DAG during natural development of wild type and *ala* mutant lines. Past that time point leaf yellowing was observed first in the triple mutant line (31 DAG) followed by *ala10/11* (33 DAG), *ala1* (35 DAG), *ala11* (38 DAG), and *ala10* (42 DAG). Wild type

leaves started to show visible senescence symptoms around 44 DAG. Furthermore, leaf sizes of *ala1*, *ala11*, *ala10/11* and *ala1/10/11* were reduced to 58%, 59%, 33% and 17% of wild type level, respectively (Figure 21 A and Figure 22 B). Mutant line *ala10* displayed no significantly altered leaf size compared to wild type. Accompanied by the reduction

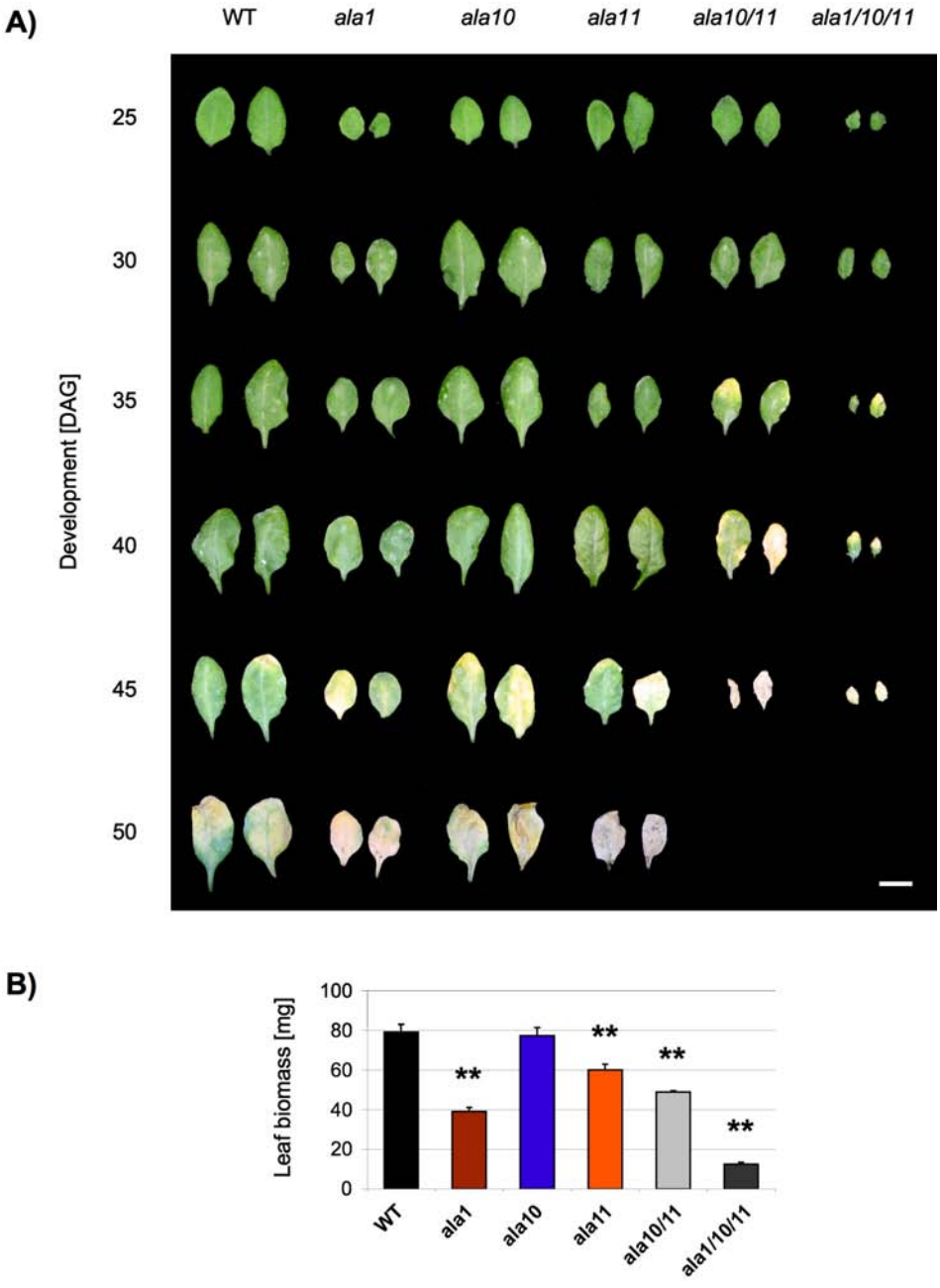

Figure 21: A) Accelerated leaf senescence of *ala* mutant lines visible by leaf yellowing. Depicted are two representative examples of the 6th rosette leaf during development of wild type and *ala* mutant lines, respectively. Scale bar: 1 cm. B) Leaf evaluation of *ala* mutant lines. Diagrams show average leaf weight ± S.D. (n=120) of 6th rosette leaves. Significant differences between wild type and mutant lines are marked with asterisks: ** *P* < 0.01.

in leaf size, weight of the 6th rosette leaf was decreased in *ala1*, *ala11*, *ala10/11* and *ala1/10/11* by 51%, 24%, 38% and 84%, respectively (Figure 21 B). The protein content of the investigated *ala* mutant lines was not significantly altered and resulted in a protein content of approximately 9 mg/g FW. The observation of single leaves show more strikingly a correlation between the senescence-inducing and growth-inhibiting effect of mutations in *ALA* genes and *Arabidopsis* 6th rosette leaves were therefore analyzed in more detail in the following chapters.

3.5.2 Reduction in cell size and cell number in *ala* mutant lines

To determine the basis of the reduced size of *ala* mutants, the adaxial epidermis of rosette leaf number six from 30-day-old plants was microscopically examined (chapter 2.10.6) and compared with wild type (Figure 22 A and C). Smaller epidermal cell sizes were observed in the single mutant line *ala1* (reduction 17%) and *ala11* (reduction by 30%). Epidermal cells of mutant line *ala10* displayed no alteration in size and were indistinguishable from wild type. The *ala10/11* double and *ala1/10/11* triple mutant line displayed an even greater reduction in cell size (by 53% and 69%, respectively). The reduction in cell size correlated with the reduction in leaf growth of the mutant lines (Figure 22 B and C). Compared with wild type, no alteration in the stomata index was found for any of the tested mutant lines (data not shown). By combining leaf and cell sizes, the total epidermal cell number per adaxial leaf side was estimated (Figure 22 D). Mutant lines *ala1*, *ala11*, *ala10/11* and *ala1/10/11* resulted in a lower cell number per leaf than wild type plants (reduced by 30%, 18%, 29% and 34%, respectively). Thus, leaves of *ala* mutant lines were not only smaller and possessed smaller cells; their cell number was also decreased. The obtained results clearly indicate a negative effect of the mutated *ALA* genes (except *ala10*) on leaf development inhibiting proper leaf and cell growth. It seems that ALA gene products are necessary for a proper leaf development and especially for a proper progression of leaf senescence.

3.5.3 Seed biomass production and quality of *ala* mutant lines

Mutant line *ala1*, *ala11* as well as the *ala10/11* double and *ala1/10/11* triple mutant line showed reduced rosette sizes under standard growth conditions (21 °C, long day of 120 µmol*m^{-2}*sec^{-1}, chapter 3.5.1). The reduction in rosette size might have influences on the seed biomass production of the plants. In order to prove this hypothesis, the

total seed biomass of *ala* mutant lines was observed (Figure 23). The single mutant lines *ala1*, *ala10* and *ala11* produced seed amounts comparable to wild type. Solely the double and triple mutant lines *ala10/11* and *ala1/10/11* produced less seeds. Their seed biomass production was reduced by 58% and 78%, respectively. As the seed biomass of single *ala* mutant lines is not altered, the effect in the double and triple mutant lines might be indirectly caused by the reduced plant size and premature senescence.

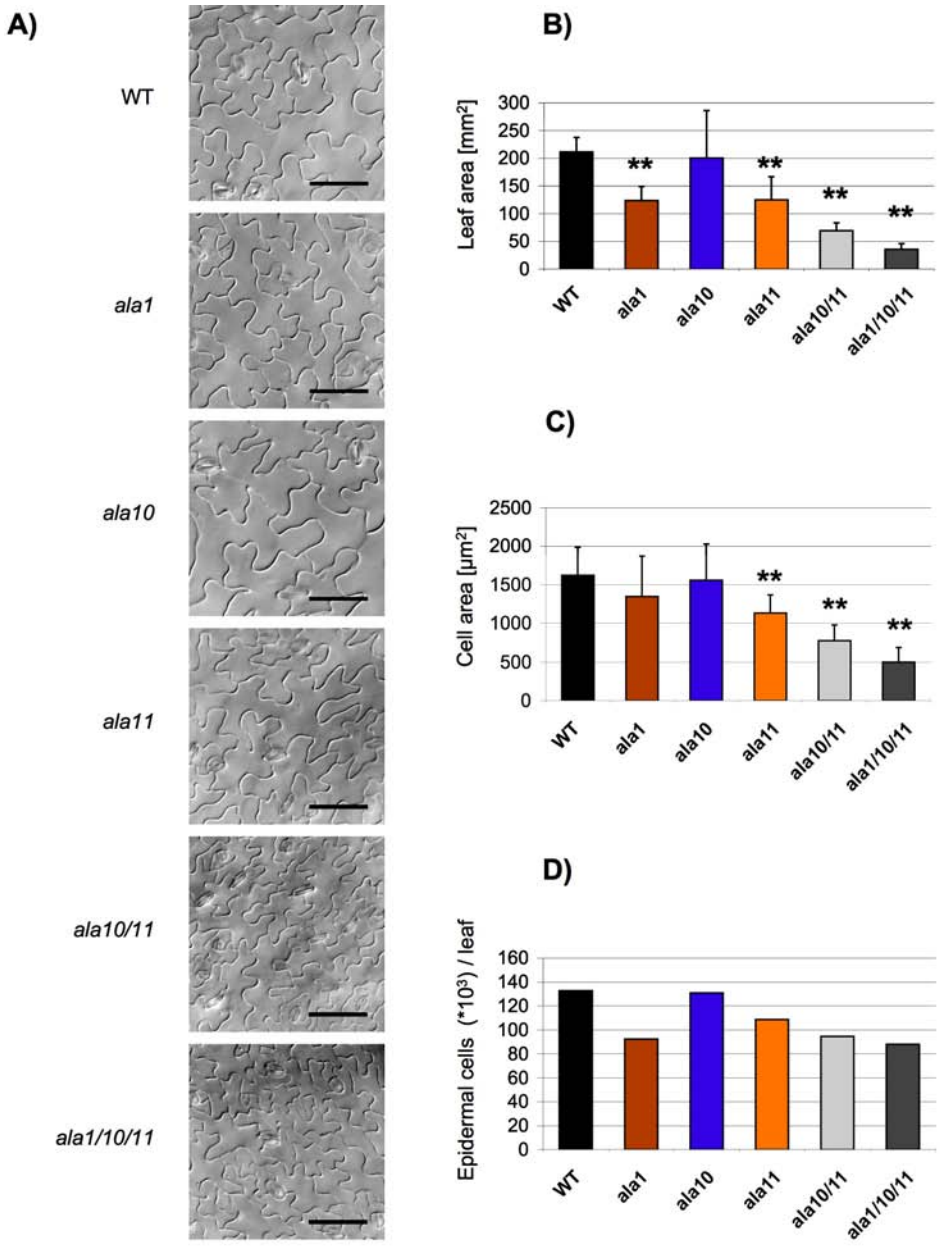

Figure 22: Microscopic analysis of 6th rosette leaves of wild type and *ala* mutant lines. A) Overview of destained adaxial epidermal cells. Depicted are representative examples at 30 DAG. Scale bar: 50 µm. B) Diagrams of leaf area (means ± S.D., n=10), C) area of epidermal cells (means ± S.D., n=800) and D) number of epidermal cells per adaxial leaf side for wild type and *ala* mutant lines, respectively. Significant differences to wild type control are denoted with asterisks (*P* < 0.01).**

Noticeable, the seed size of the *ala* mutant lines was indistinguishable from that of wild type. The observation was confirmed by macroscopic analysis of approximately 1000 seeds per plant line (data not shown), which indicates an undisturbed seed development of *ala* mutant lines.

In order to reveal any additional effects on the seed quality of *ala* mutant lines, the germination rate of the seeds was tested on soil as well as MS-medium containing agar plates and compared with the germination rate of wild type seeds. No difference in the germination rate of any of the mutants was observed (data not shown). Considering these data, an undisturbed embryogenesis has to be assumed and a regulatory system must exist ensuring proper and complete seed formation. Once the system is initiated it guarantees reproductive success of the plant avoiding incomplete, not fully developed and, thus, non-viable seeds.

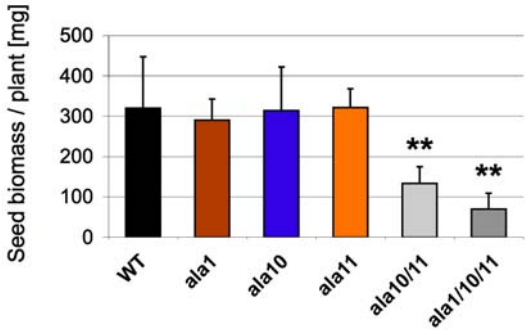

Figure 23: Seed biomass production of wild type and *ala* mutant lines. Diagram depicts mean (n=9) seed biomass per plant ± S.D. Statistically significant differences to the wild type control are denoted with asterisks (*P* < 0.01).**

3.5.4 Reduction in root growth

Due to the phenotypic alterations of *ala* mutants in the aerial, above ground and visible parts, it was interesting to know whether the underground parts of the plants were also affected. Therefore, *ala* mutant seeds were stratified and grown on vertically arranged half-strength MS-medium containing agar plates for 20 days under standard conditions (21 °C, long day of 120 µmol*m^{-2}*sec^{-1}). Root length of *ala* mutants and wild type plants was measured at two different times points (10 and 20 DAG, Figure 24). Roots of the investigated *ala* mutants were indistinguishable from wild type in terms of length and branching until 7 DAG. After that time point *ala1* plants displayed shorter roots (approximately 80% of wild type length at 10 and 20 DAG). Contrary to the reduction in rosette size, root length was not affected in any other investigated *ala* mutant line at 10 DAG. Later during development (20 DAG), root length was decreased to a minor extent in *ala10* as well as the double and triple mutant line (approximately 80-90% of wild type length). Regarding these data, ALA1 might have a positive regulatory effect on root growth, whereas ALA10 and 11 rather have no effect on the regulation of root length

and the minor reduction in root length in the corresponding mutant lines might be due to secondary effects.

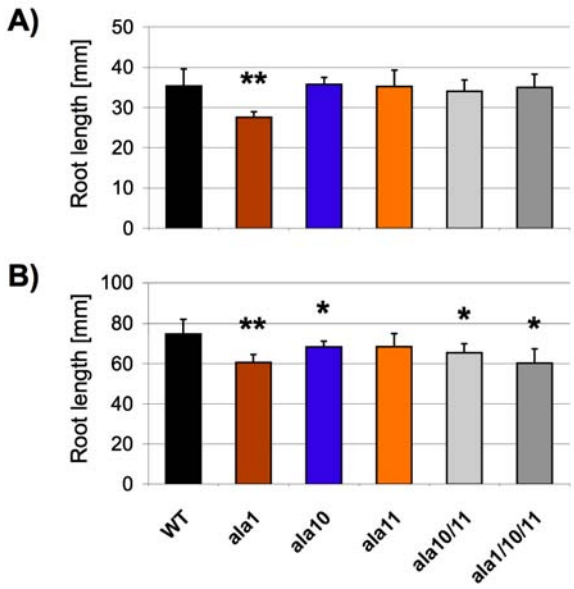

Figure 24: Root growth of wild type and *ala* mutant lines. Diagrams of root length at A) 10 DAG and B) 20 DAG (mean values ± S.D., n=20). Significant differences between wild type and mutant lines are marked with asterisks (* *P* < 0.05, ** *P* < 0.01).

3.6 Physiological parameters

Typical senescence-associated physiological markers are chlorophyll content, photochemical efficiency of photosystem II (F_v/F_{max}), and membrane ion leakage (Lohman *et al.*, 1994; Fan *et al.*, 1997; Oh *et al.*, 1997; Weaver *et al.*, 1998; Woo *et al.*, 2001). Measuring these parameters the premature senescence phenotype of *ala* mutant lines was physiologically assessed. Therefore, the following analyses were performed with pooled 6th rosette leaves of *ala* mutant lines as well as wild type grown in soil under standard conditions (16 h light of 120 µmol*m^{-2}*sec^{-1} per day at 21° C).

3.6.1 Chlorophyll and anthocyanin content in *ala* mutant lines

3.6.1.1 Chlorophyll content

To follow the ana- and catabolism of chlorophyll during development of *ala* mutant lines, 6th rosette leaves were subjected to chlorophyll measurements (chapter 2.10.4) during a time course of 25 d (Figure 25 A). Single *ala* mutant lines displayed nearly the same chlorophyll amount as wild type (1.1 mg/g FW chlorophyll a+b) at the beginning

of the observation period. 9% and 23% higher chlorophyll levels were recorded for the double and triple mutant line, respectively. After 25 DAG all *ala* mutant lines revealed a continuous decrease in chlorophyll content during development, whereas wild type chlorophyll levels increased in the following five days until 30 DAG and declined thereafter. Past 30 DAG chlorophyll levels of all tested *ala* mutant lines were below wild type level. At the end of the observation period (50 DAG) *ala1/10/11* had the lowest (0.01 mg/g FW) chlorophyll amount, followed by *ala10/11* (0.06 mg/g FW), *ala11* (0.1 mg/g FW), *ala1* (0.11 mg/g FW) and *ala10* (0.14 mg/g FW). Wild type leaves possessed the highest chlorophyll amount at 50 DAG with 0.17 mg/g FW. Lower chlorophyll content is an indicator for beginning senescence (Lohman *et al.*, 1994; Oh *et al.*, 1997) and confirms on a physiological level the described premature senescence phenotype of the *ala* mutants (chapter 3.5.1). The higher chlorophyll content of the *ala10/11* double and *ala1/10/11* triple mutant lines at 25 DAG might suggest a larger number of chloroplasts per cell in these lines.

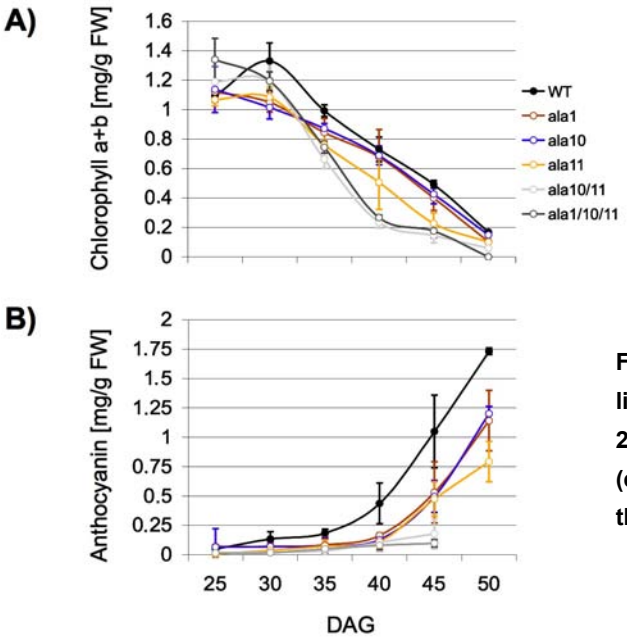

Figure 25: Pigment analyses of *ala* mutant lines and wild type during development (DAG 25-50). Diagrams depict A) chlorophyll content (chlorophyll a and b) and B) anthocyanin in the 6th rosette leaf. Mean values ± S.D. (n=5).

3.6.1.2 Anthocyanin content

Leaves of *ala* mutant lines senesced earlier than wild type (chapter 3.5.1) and did not show the typical accumulation of anthocyanins by end of the vegetative stage. Therefore, a focus was set on these pigments and changes in anthocyanin levels within the 6th rosette leaf of *ala* mutant lines and wild type were recorded (chapter 2.10.5) during development (25-50 DAG, Figure 25 B). Anthocyanin amounts increased in all tested plant lines during development but the accumulation occurred in *ala* mutant lines to a

lesser extent. By end of the time-course experiment wild type leaves had 1.73 mg/g anthocyanins per g FW. In contrast, *ala1* and *ala10* single mutant lines possessed 70% of the wild type anthocyanin amounts at that time point. More strikingly, anthocyanin amounts were reduced to 45% of wild type level in *ala11* and the double and triple mutant lines accumulated scarcely anthocyanins (14% and 6% of wild type level at 45 DAG, respectively). The low anthocyanin content in *ala* mutants during development points out that *ALA* genes are necessary for a proper and regulated progression of leaf senescence and that effects caused by mutated *ala* genes (*1*, *10* and *11*) accumulate in an additive manner.

3.6.2 Photochemical efficiency of photosystem II

The reduced chlorophyll content of *ala* mutant lines (chapter 3.6.1.1) might indicate an earlier decline of photosynthetic efficiency. To quantify the PSII efficiency, *ala* mutant lines were subjected to fluorescence measurements (chapter 2.10.1). F_v/F_{max} values reflecting photosynthetic efficiency of *ala* mutant lines were recorded over a time course of 25 days within the 6th rosette leaf (Figure 26). The measurements began after the emergence of the 6th rosette leaf at 25 DAG. The F_v/F_{max} ratio of all tested mutant lines

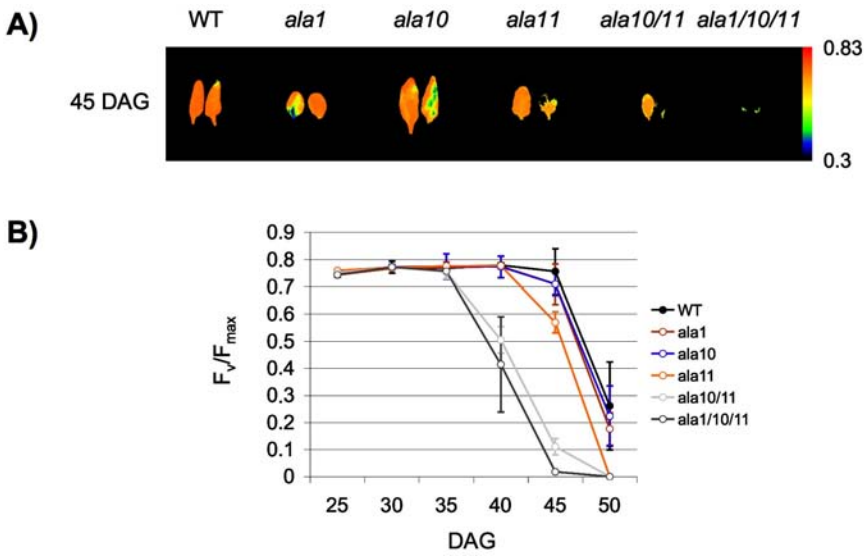

Figure 26: Photochemical efficiency of *ala* mutant lines and wild type. A) False color images of maximum quantum efficiency of photosystem II photochemistry (F_v/F_{max}) obtained via PAM fluorometry. Depicted are two representative 6th leaves at 45 DAG per plant line. B) Diagram of averaged F_v/F_{max} per 6th rosette leaf during development (DAG 25-50). Data are means ± S.D. (n=8).

were indistinguishable from wild type until 35 DAG. Past this time point the photochemical efficiency dropped first in the triple and double mutant line, followed by the single mutant lines past 40 DAG (first *ala11*, followed by *ala10* and *ala1*). In contrast to the premature reduction in photochemical efficiency of photosystem II of *ala* mutant lines, the wild type F_v/F_{max} ratio was maintained at a value of 0.79 since the beginning of the time course experiment and decreased not before 45 DAG. The F_v/F_{max} ratio is often used as a physiological senescence marker (Wingler *et al.*, 2004) and the early decrease in photochemical quantum efficiency of photosystem II in *ala* mutant lines, especially in the *ala10/11* double and *ala1/10/11* triple mutants, underline the premature senescence phenotype of these plants. However, the F_v/F_{max} ratio is maintained until late during development although chlorophyll content of the plants started to decrease (chapter 3.6.1.1) and senescence symptoms became visible (chapter 3.5.1). This finding suggests that the efficiency of photosystem II and, thus, the electron transport rates are important for the fitness of *ala* mutant lines.

3.6.3 Ion leakage

Senescence is accompanied by structural changes within cells including sequential disintegration of organelles and cellular membranes (Thomas and Stoddart, 1980; Thompson *et al.*, 1998). To observe the senescence status and plasma membrane integrity of *ala* mutants, membrane ion leakage was monitored (chapter 2.10.3). Compared to wild type, the membrane ion leakage of the 6th rosette leaves of all investigated *ala* mutants was not altered at 25 DAG and 28 DAG (data not shown). However, at 30 DAG, membrane ion leakage was approximately 43% higher in the tested *ala* mutant lines compared to wild type level (Figure 27), although visible senescence symptoms were not observed at this developmental stage (chapter 3.5.1). The higher membrane ion leakage in *ala* mutant leaves suggests an advanced deterioration of cellular membranes within these plants even at a time point when no senescence symptoms are visible.

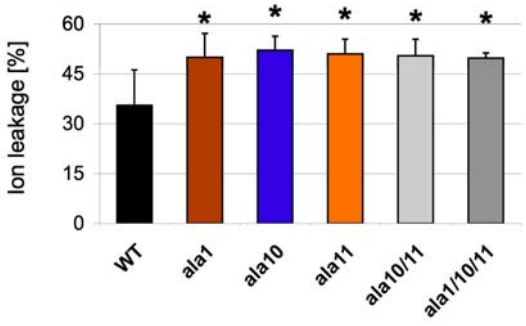

Figure 27: Ion leakage of *ala* mutant lines compared to wild type at 30 DAG. Diagram shows percentage of ion loss within 6th rosette leaves (means ± S.D., n=6). Asterisk denotes statistically significant differences to wild type (* *P* < 0.05).

3.7 Morphological parameter of *ala* mutant lines

In order to further characterize *ala* mutants and to gain information about subcellular processes within the plants, transmission electron microscopy was carried out (chapter 2.14) using soil-grown plants (16 h light of 120 µmol*m^{-2}*sec^{-1} per day at 21° C), 4 h after the begin of the photosynthetic period. To ensure that senescence did not affect leaf architecture of the plants, 6th rosette leaves from 28-day-old *ala* mutants were compared with wild type as no visible senescence symptoms (chapter 3.5.1) or altered membrane ion leakage (chapter 3.6.3) were detected at this developmental stage in these leaves. The ultrastructure of mesophyll cells situated in the middle of the leaf blade in between midrib and leaf edge was microscopically analyzed (Figure 28).

3.7.1 *ala1* has an altered plastid morphology

Transmission electron microscopy revealed a dramatically altered plastid morphology for *ala1* mutants: Whereas wild type chloroplasts possessed large starch grains (1-9, ø 6 per plastid), normal large grana stacks and rarely plastoglobuli (Figure 28 A-C) 4 h after the photosynthetic period, plastids of *ala1* mutants contained only rarely starch grains (approximately 1 per plastid, Figure 28 D-F). This observation may point out a lowered photosynthetic capacity of the mutant plants. Another striking abnormality of *ala1* plastids was the lack of grana stacks and an increased number of plastoglobuli. The majority (approximately 65%) of the observed plastids displayed a diffuse, electron dense structure similar to thylakoid lamellae lacking the typical grana stacks (Figure 28 D and F). Electron microscopy of chloroplasts from senescing leaves revealed structural changes within these organelles such as an increase in the number and size of plastoglobuli, a disorientation of grana stacks and a swelling of thylakoid membranes (Smart, 1994). It is assumed that the formation of plastoglobuli is associated with the degradation of thylakoid membranes (del Río *et al.*, 1998), which is in concordance with the ultrastructure found in *ala1* plastids. In addition to that, plastid-like structures were found in approximately 15% of *ala1* mesophyll cells. These structures were similar to wild type plastids but they did not possess the outer membrane envelope as a characteristic feature (Figure 28 E). It seems that the structures are formed due to an instant plastid breakdown, as the inner structure was still intact. Moreover, the structures contained a high number of enlarged plastoglobuli. The remaining 20% of the

observed plastids had wild type appearance and displayed grana stacks, starch grains and only few plastoglobuli. Apart from *ala1*, plastid-like structures were only found in the triple mutant *ala1/10/11* but to a lesser extent (in approximately 5% of the cells, Figure 28 Q). The altered plastidial morphology of *ala1* mutants is in line with the plastidial localization of ALA1 (chapter 3.3) and points out that the protein is probably required for proper plastid development.
Another peculiarity of *ala1* mesophyll cells was a displacement of plasma membrane from the cell wall, which was observed in approximately 60% of the cells. The phenomena occurred only to a small extent (less than 5%) in cells of the other tested *ala* mutants and never in wild type cells. These cellular changes may indicate a beginning senescence progress within cells of *ala* mutants even before senescence symptoms were detected (chapter 3.7.1). It is known that the plasma membrane undergoes structural changes during senescence and becomes more permeable (Thomas and Stoddart, 1980; Thompson *et al.*, 1998; Woo *et al.*, 2001), which affects tissue specific properties leading to preparational artifacts of senescent tissue prior to electron microscopy. This assumption is strengthened by the fact that membranes of wild type cells of the same age were never displaced from the cell wall.

3.7.2 *ala10* and *ala11* accumulate abnormal membrane structures

The single mutant lines *ala10* and *ala11* shared a striking ultrastructural feature: Both plant lines accumulated abnormal membrane structures within mesophyll cells (Figure 28 G-I and Figure 28 J-L, respectively). The abnormalities had a vesicle-like structure, varied in size between 100 and 500 nm and were either cytoplasmatically located or partly fused with the tonoplast of the central vacuole. Similar membrane abnormalities were observed in mesophyll cells of the *ala10/11* double (Figure 28 M-O) and *ala1/10/11* triple mutants (Figure 28 P-R), where the vesicle-like structures were often additionally intensely interspersed with smaller membrane abnormalities (Figure 28 M and Q). In contrast, wild type and *ala1* mutants did not accumulate abnormal membrane structures and cellular membranes were similar in appearance to wild type (Figure 28 A-C and D-F, respectively). The localization of ALA10 and ALA11 to the plasmamembrane or the tonoplast (chapter 3.3) and the occurrence of misshaped membranes either originating from the plasma membrane or the tonoplast in *ala10* and *ala11* mutant lines suggests an important role of these proteins in establishing and maintaining membrane asymmetry or curvature as it has been discussed for other P_4-type ATPases (Zachowski, 1993; Daleke, 2003; Pomorski *et al.*, 2004).

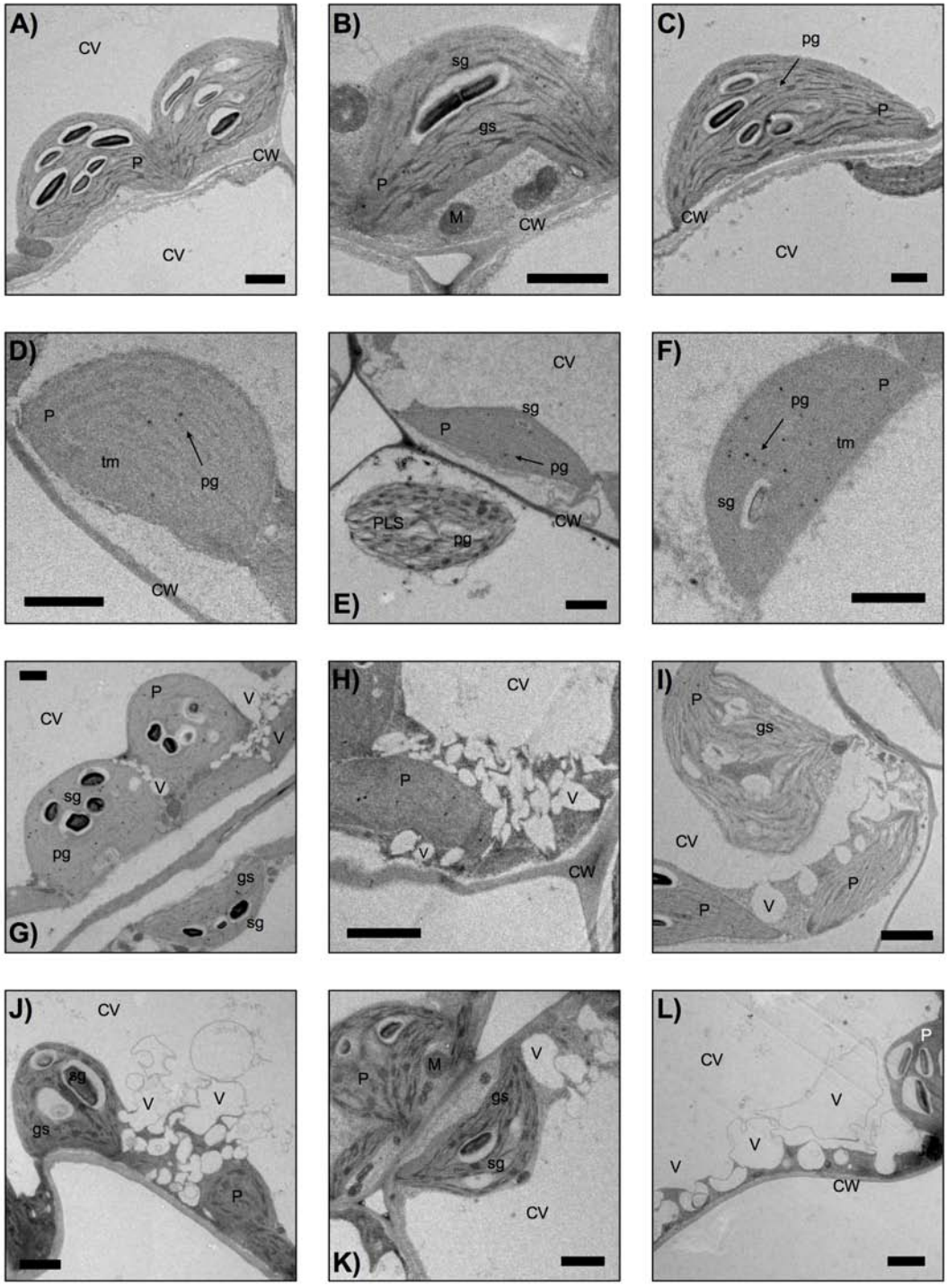

Figure 28 (continued on next page): Subcellular morphology of *ala* mutant lines and wild type. Depicted are transmission electron microscopic images of mesophyll cells from 6th rosette leaves at 28 DAG: A-C) wild type, D-F) *ala1*, G-H) *ala10*, J-L) *ala11*, M-O) *ala10/11* and P-Q) *ala1/10/11*. CV central vacuole, CW cell wall, M mitochondrion, P plastid, PLS plastid-like structure, V vesicle-like structure (not fully fused to membrane), gs grana stacks, pg plastoglobule, sg starch grain, tm thylakoid membranes. Scale bars: 1 µm.

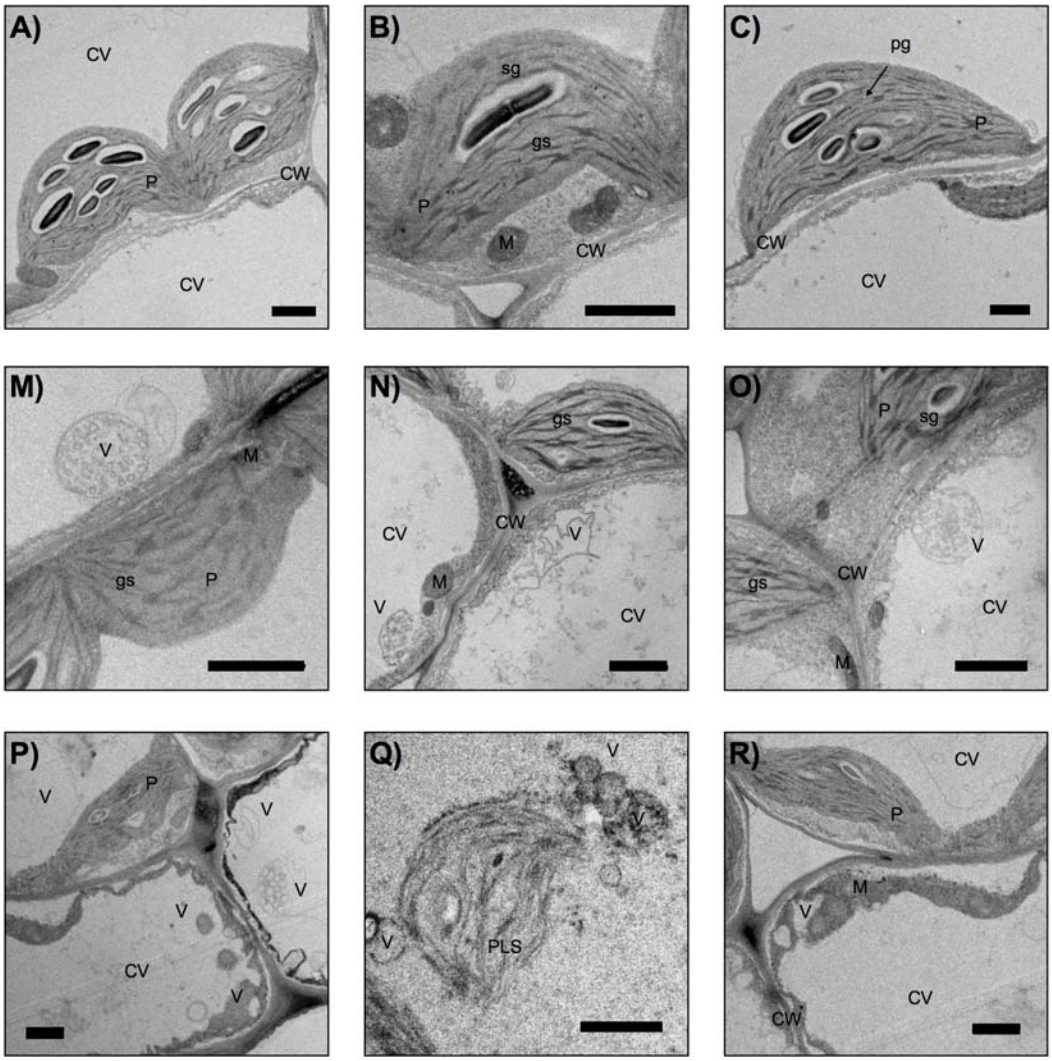

Figure 28 (continued from previous page): Subcellular morphology of *ala* mutant lines and wild type. Depicted are transmission electron microscopic images of mesophyll cells from 6th rosette leaves at 28 DAG: A-C) wild type, D-F) *ala1*, G-H) *ala10*, J-L) *ala11*, M-O) *ala10/11* and P-Q) *ala1/10/11*. CV central vacuole, CW cell wall, M mitochondrion, P plastid, PLS plastid-like structure, V vesicle-like structure (not fully fused to membrane), gs grana stacks, pg plastoglobule, sg starch grain, tm thylakoid membranes. Scale bars: 1 µm.

It has to be mentioned that plastids with a diffuse structure similar to those of *ala1* mutants (Figure 28 D-F) were only occasionally found in leaf cells of *ala10* (less than 3% of the cells, Figure 28 H) and might resemble artifacts. A reduction in the averaged plastidial starch grain number from 6 (wild type) to 2-3 was found for plastids of *ala10* (Figure 28 G-I), *ala11* (Figure 28 J-L), as well as *ala10/11* (Figure 28 M-O] and *ala1/10/11* (Figure 28 P-R) but not to the same extend as for *ala1* (chapter 3.7.1). A lower photosynthetic capacity of the mutant plants might be the reason for the reduction in plastidial starch grains.

3.7.3 Plastid sizes of *ala* mutant lines

Aside from membrane abnormalities, and alteration in plastid morphology, plastids of *ala* mutants varied in size. Wild type mesophyll cells displayed an average plastid length (measured following the thylakoid lamellar structure) of approximately 6610 nm (Figure 29). Mutant lines *ala1* and *ala10* possessed approximately 15% larger plastids (7560 and 7650 nm, respectively). Plastid sizes of the single mutant line *ala11*, the *ala10/11* double and *ala1/10/11* triple mutant lines and were smaller (8% [6060 nm], 16% [5550 nm] and 18% [5440 nm], respectively). These results make it likely that mutations in *ALA* genes affect plastid development. However, the altered plastid sizes in *ala* mutant lines could be indirectly caused by other cellular deregulations (e.g. premature senescence, reduced cell size and lower chlorophyll content).

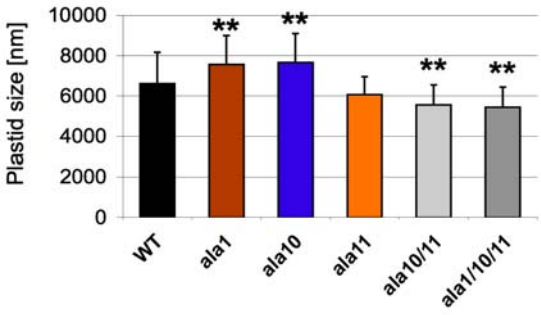

Figure 29: Plastid length of *ala* mutant plants compared to wild type. Depicted is the average size of plastids ± S.D. (n=42) in mesophyll cells of the 6th rosette leaf at 28 DAG. Asterisks indicate statistically significant differences to wild type (*P* < 0.01).**

3.8 Induction of senescence in *ala* mutant lines

Senescence can be induced by various factors, such as light, nutrient and water availability and temperature (Gan and Amasino, 1997). So far, *ala* mutant lines and wild type were investigated during natural development. The following experiments were performed to study how *ala* mutants responded to different treatments regarding their senescence process.

3.8.1 Senescence induction via glucose addition combined with nitrogen limitation

Leaf senescence of *Arabidopsis thaliana* is induced by plant cultivation in medium containing high sugar concentration (2% glucose) combined with nitrogen limitation

(≤4.7 mM nitrogen, compared to full nourishing medium with 30 mM nitrogen; Wingler *et al.*, 2004). In order to test whether senescence can be artificially induced in *ala* mutant lines by nitrogen limiting conditions, the plants were grown in sterile culture on agar plates with senescence-inducing medium (half-strength MS [chapter 2.6.5.3] with 4.7 mM nitrogen and 2% glucose) under standard conditions (16 h light of 120 µmol*m^{-2}*sec^{-1} per day at 21° C). Senescence was equally accelerated in the tested *ala* mutants and wild type plants (data not shown) and all tested *ala* mutant lines displayed the described premature senescence phenotype of soil-grown plants (chapter 3.5.1). However, all plants (including wild type) had a smaller appearance, which was due to the cultivation conditions. As a conclusion, the senescence inducing effect of low nitrogen in combination with glucose addition is not dependent on *ALA* genes. ALA proteins are of great importance during the senescence process, but it is likely that they are not responsible for its induction.

3.8.2 Influence of phosphorus limitation on *ala* mutant lines

Phosphorus is an important macronutrient to the plant. Furthermore, the element is an essential component of phospholipids (PL). Limitation in phosphorus to the plant causes a shift from PL to non-phosphorus lipids like glycolipids to support membrane functionality and allowing photosynthesis (Yu *et al.*, 2002; Andersson *et al.*, 2003). Plants of *ala* mutant lines and wild type were hydroponically grown (16 h light of 120 µmol*m^{-2}*sec^{-1} per day at 21° C, chapter 2.6.5.4) in full nourishing medium (500 µM phosphorus) and phosphorus limiting medium (10 µM phosphorus) to investigate a possible influence of limiting phosphorus on the plant phenotype and the senescence pattern. When grown under phosphorus limiting conditions rosette size of all tested *ala* mutant lines including wild type was reduced by approximately 60% compared to non-limiting conditions. Apart from the finding that all tested plant lines including wild type started to senesce approximately 5 days earlier under phosphorus limiting conditions compared to non-limiting conditions, a variation of the found premature senescence pattern (chapter 3.5.1) amongst *ala* mutant lines was not observed (Appendix, Figure 43). Thus, it has to be assumed that effects caused by low phosphorus in plants are not dependent on *ALA* genes.

3.8.3 *ala* mutant plants are unable to recover after darkening

In contrast to individually darkened leaves, darkening of whole plants does not induce senescence in rosette leaves (Weaver and Amasino, 2001). However, darkening of

whole plants induces chlorophyll and protein loss in rosette leaves (Blank and McKeon, 1991a, b; Oh *et al.*, 1996; Weaver *et al.*, 1998), which is reversible (regreening effect) by returning the plants to light within several days of the dark treatment (Blank and McKeon, 1991a, b). To investigate the effect of darkness on the regreening ability of *ala* mutant lines darkening for five days was applied: Wild type and *ala* mutant lines were grown under standard conditions (16 h light of 120 µmol*m^{-2}*sec^{-1} per day at 21° C) for 25 days, before the onset of visible senescence symptoms in rosette leaves occurs. Plants were then subjected to complete darkness. After 5 days the chlorophyll loss was visually observed (Figure 30). All plants displayed a 45° angle leaf position typical for dark-treated plants, which disappeared within the next two days when plants were grown again under light. Thus far, all tested *ala* mutant lines displayed enhanced leaf paleness and chlorophyll loss, whereas wild type leaves stayed green and showed no obvious loss of chlorophyll. When plants were again grown under standard conditions following the dark-treatment, *ala* mutants were unable to recover pale leaves. Instead, these leaves wilted completely during the next 5 days (Figure 30 B). The effect had the same intensity in single mutants (*ala1*, *ala10* and *ala11*) and was more prominent in the double and triple mutant line (*ala10/11* and *ala1/10/11*, respectively). When the same treatment was conducted with plants in a later stage of development (starting point of dark-treatment: 30 DAG) paleness and yellowing of rosette leaves was even more pronounced. However, wild type responded with leaf yellowing to the treatment; yet not to the same extent than the tested *ala* mutant lines (data not shown). Furthermore, wild type plants were still able to fully recover pale leaves after the darkness treatment. These experiments point out that ALA proteins might be required for a proper execution of the darkness recovering program.

Figure 30: Induction of leaf paleness via dark treatment. Depicted are representative plants of *ala* mutant lines and wild type at 30 DAG A) grown without treatment and B) grown for 25 d followed by complete darkness for five days. Scale bar: 5 cm.

3.8.4 Short day conditions intensify premature senescence of *ala* mutant lines

Plant development is controlled by the availability of light. Short-day photoperiods decelerate plant development. Therefore, minor changes in premature senescence between different plant lines (e.g. *ala10* and wild type, chapter 3.5.1) should be easier detectable. In order to test this hypothesis *ala* mutant lines were soil-grown under short-day (8 h light) photoperiodic length (120 µmol*m^{-2}*sec^{-1}) at 21° C. The plants showed an approximately 3-times greater life span compared to plants grown under long-day conditions (16 h light). Additionally, the leaf biomass (larger leaf blades and higher leaf number) of all plants was increased (Figure 31 A and B). The average leaf number at bolting was 45 for all tested plant lines. Under short day conditions *ala* mutant lines exhibited earlier yellowing of rosette leaves compared to wild type. Premature senescence symptoms, i.e. yellowing of rosette leaves and cotyledons, found under long-day conditions (chapter 3.5.1) were enhanced under short-day conditions. First yellow rosette leaves appeared on wild type plants around 60 DAG. In contrast, *ala* mutant lines exhibited first yellow rosette leaves 14 d (*ala10*), 15 d (*ala11*), 19 d (*ala1*), 24 d (*ala10/11*) and 30 d (*ala1/10/11*) earlier than wild type. The observations point out that *ALA* genes are necessary for a controlled progression of leaf senescence and plant growth.

3.8.5 Temperature positively influences growth of *ala* mutant lines

Ambient temperature influences vegetative growth. Gomès *et al.* (2000) reported reduced growth for *Arabidopsis thaliana ala1* antisense plants when grown at 12 °C. To investigate the impact of temperature on plant growth and senescence patterns of *ala* mutant lines, the plants were grown under low (16 °C) and elevated (24 °C) temperature conditions and compared to wild type.

3.8.5.1 Low temperature intensifies premature senescence symptoms of *ala* mutants

WT and *ala* mutants grown under low temperature (16 °C, 16 h light per day) showed a prolonged life span (Figure 31 C) that was approximately 2.5-times longer compared to plants grown under standard conditions (21 °C, 16 h light per day; Figure 31 A). The leaf number of all plant lines was increased to approximately 49 at bolting compared to 16 at bolting under standard conditions (chapter 3.5.1). At the same time, senescence symptoms of all plants cultivated under low temperature appeared earlier during devel-

opment compared with plants grown under standard conditions: Wild type plants displayed first yellow rosette leaves around 35 DAG. In contrast, leaf yellowing of *ala1* started at 30 DAG. Leaf yellowing in *ala10* occurred at 33 DAG, in *ala11* at 31 DAG, in *ala10/11* at 28 DAG and in *ala1/10/11* at 25 DAG. Similar results (prolonged life span and premature senescence symptoms) were recorded when *ala* mutants were grown at 12 °C (data not shown). Additionally, *ala* mutants displayed a reduction in rosette growth of approximately 25 % compared to plants grown under standard conditions. However, the life span of the mutant plants was longer than 140 days and for that reason not suitable for further experiments. Thus, it can be concluded that low temperature induces senescence in *ala* mutant lines, which might be due to an alteration in membrane characteristics as the proteins are supposed to flip lipids in biological membranes (Tang *et al.*, 1996; Ding *et al.*, 2000; Gomès *et al.*, 2000; Poulsen *et al.*, 2008b; Puts and Holthuis, 2009). These observations are consistent with the notion that ALA proteins are responsible for plant cold stress adaptation as suggested by Gomès *et al.* (2000).

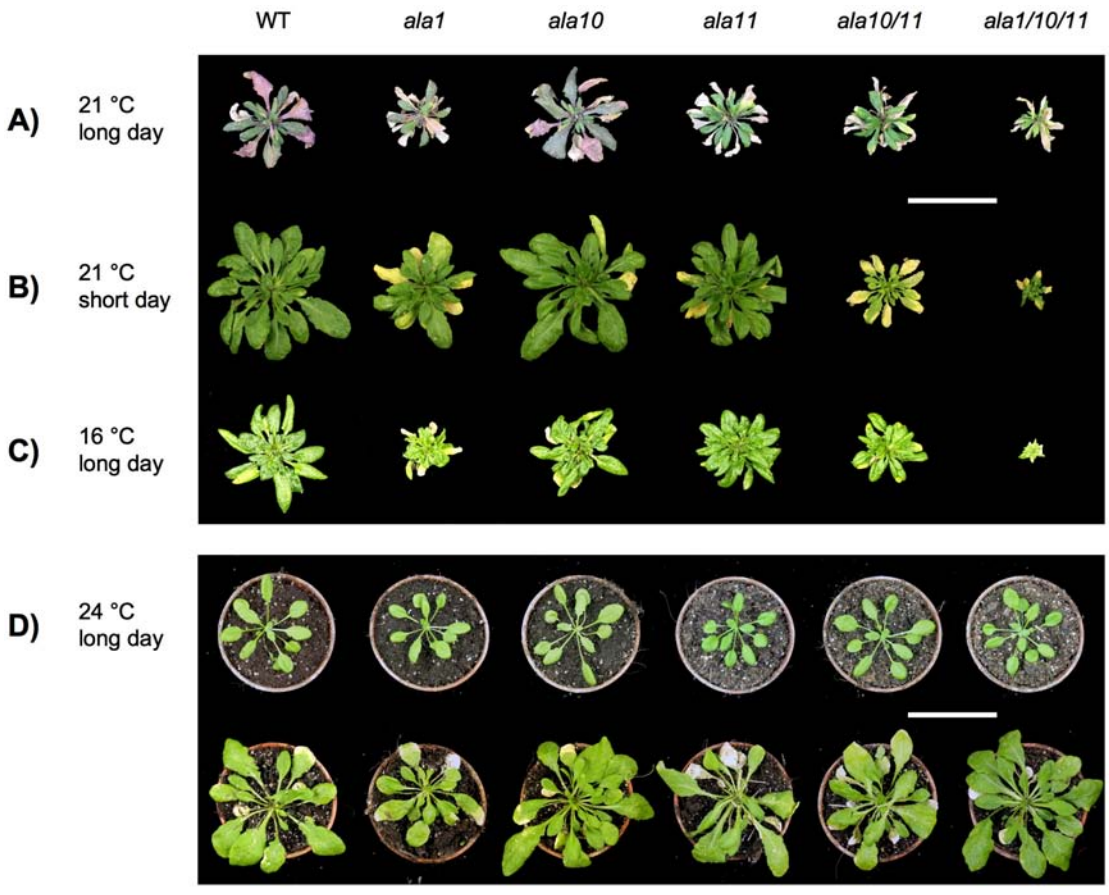

Figure 31: Phenotypes of *ala* mutant lines and wild type under different growing conditions. Depicted are rosettes of representative examples at 50 DAG grown under A) long day (standard conditions), B) short day, C) low temperature (16 °C). Scale bar: 5cm. D) Plants at 25 and 50 DAG of representative examples under elevated temperature (24 °C). Scale bar: 5cm. Long day = 16 h light per day, Short day = 8 h light per day (120 µmol*m^{-2}*sec^{-1}).

3.8.5.2 *ala* mutants display a transient phenotype occurring below 24 °C

When low temperature positively influenced the progression of senescence in *ala* mutant lines it was interesting to know if elevated temperature had the opposite effect on the plants. For that reason *ala* mutants and wild type were grown in soil at 24 °C (16 h light per day). The described premature senescence symptoms as well as the reduction in rosette size of *ala* mutant lines (chapter 3.5.1) diminished largely (Figure 31 D). At 25 DAG all investigated mutant plants were indistinguishable from wild type. Later during development (50 DAG) *ala1* plants displayed a reduction in rosette size by 20% compared to wild type. Differences in the onset and progression of leaf senescence were not found for any *ala* mutant line in comparison with wild type. When the experiment was repeated with an ambient temperature of 28 °C, *ala* mutants as well as wild type displayed obvious stress symptoms and thinner elongated leaf blades (data not shown). However, all *ala* mutant plants were indistinguishable from wild type. The experiments clearly point out that *ala* mutants display a phenotype only occurring at temperatures below 24 °C. Lower temperatures influence the senescence process and plant growth of *ala* mutant plants suggesting a role of ALA proteins in the adaptation to cold.

3.9 Lipid measurements of *ala* mutant lines

P_4-type ATPases are supposed to act as flippases that shuffle phospholipids (PL) between the two leaflets of biological membranes (Devaux *et al.*, 2006; Pérez-Victoria *et al.*, 2006; Lenoir *et al.*, 2007; Paulusma *et al.*, 2008). To gather more information on effects on membranes caused by ALA proteins *in planta* lipid analyses were conducted using soil-grown *ala* mutant lines and wild type (16 h light per day, 120 µmol*m^{-2}*sec^{-1}, 21° C). In order to avoid senescence dependent changes in membrane lipid composition of the plants and thus assuring comparability, the experiments focused on the 6^{th} rosette leaf of soil-grown 30-day-old plants (16 h light per day of 120 µmol*m^{-2}*sec^{-1}, 21° C) when no visible senescence symptoms were detectable.

3.9.1 Total fatty acid analysis

Fatty acids (FA) are essential components of PL and lipids in general. As FA are only indirectly measurable via gas chromatography (GC) by their corresponding fatty acid

methyl esters (FAME; chapter 2.9.5), FA were first extracted from pooled 6th rosette leaves (chapter 2.9.1) and then converted to FAME (chapter 2.9.4). Measurements of corresponding FAME from total FA (i.e. the sum of 16:0, 16:1, 16:2, 16:3, 18:0, 18:1, 18:2, 18:3, 20:0, 20:1, 22:0 and 22:1 FA) deriving from total lipid extracts resulted in 6.528 µmol/g FW in wild type. Slightly higher FA levels were detected in single *ala* mutant lines (*ala1*: 3%, *ala10*: 4%, *ala11*: 18% more FA compared to wild type) and notably higher FA levels in the double and triple mutant line (*ala10/11*: 28%, *ala1/10/11*: 58%; Figure 32 A). The higher total FA content of the single mutant *ala11* and especially the *ala10/11* double and *ala1/10/11* triple mutant correlated negatively with the reduction in cell size of the mutants (chapter 3.5.2) and underlines the finding of smaller cells within these mutant lines. Smaller cells exhibit a higher membrane/cell lumen ratio and consequently more membranes and, thus, more total FA per gram fresh weight are measured. Eliminating the water, which accounts for the majority of cell weight, all *ala* mutants have an equal FA amount per gram material. The analysis of total FA via FAME measurement performed on dry, lyophilized material revealed no statistically significant alterations in total FA levels between *ala* mutants and wild type. Absolute FA amounts of approximately 100 µmol/g dry weight were detected (Figure 32 B).

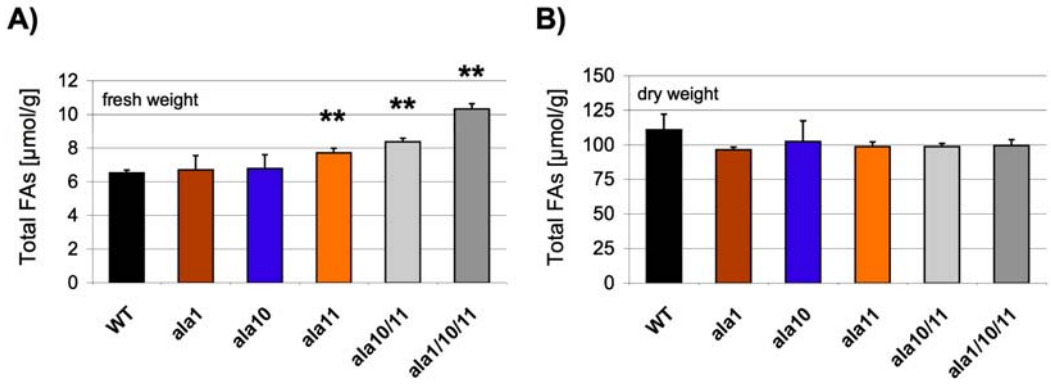

Figure 32: Total FA content in 6th rosette leaves at 30 DAG from *ala* mutant lines and wild type. Diagrams depict absolute amounts of FA (mean ± S.D., n=3) from A) fresh material (fresh weight) and B) lyophilized material (dry weight). Amounts were calculated as µmol FAME per g material. Statistically significant differences compared to wild type are indicated with asterisks (*P* < 0.01).**

P_4-type ATPases are supposed in lipid flipping (Devaux *et al.*, 2006; Lenoir *et al.*, 2007; Paulusma *et al.*, 2008), however, to date it is not known whether the proteins show specificity for lipids with a certain FA composition. Mutants with a disruption in *ALA* genes should display a deregulated FA composition in case such specificity exists. To test this hypothesis, FA profiles from total lipids of *ala* mutants were analyzed for their FA composition and compared with wild type. Analyzing the FAME profiles, and thus, the FA profiles, no differences between *ala* mutant lines and wild type were found

(Figure 33). The main FA was 18:3 (linolenic acid) representing approximately 50% of total FA in the plants. 16:0 (palmitic acid), 18:2 (linoleic acid) and 16:3 (hexadecatrienoic acid) FA were less prominent, constituting approximately 18%, 15% and 12% of the totality of FA, respectively. It seems that the investigated ALA proteins do not prefer lipids with certain acyl chains as substrates.

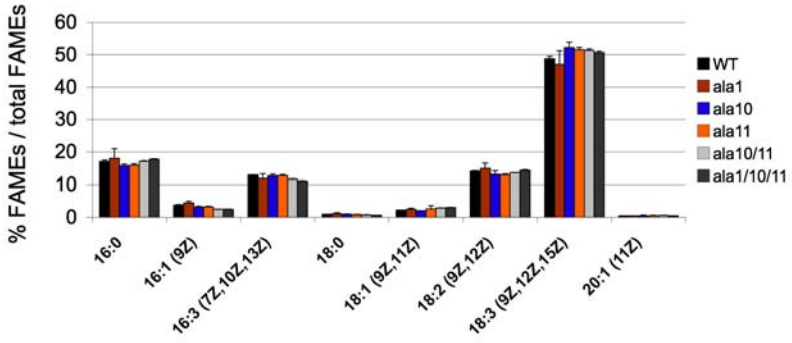

Figure 33: Total FAME profiles of *ala* mutant lines and wild type. Diagram shows FAME profiles (mean values ± S.D., n=3) derived from a total lipid extraction of 6th rosette leaves at 30 DAG given in relative percentage of total FAME. Portions below 1% are not shown. 16:0 palmitic acid, 16:1 palmitoleic acid, 16:3 hexadecatrienoic acid, 18:0 stearic acid, 18:1 oleic acid, 18:2 linoleic acid, 18:3 linolenic acid, 20:1 eicosenoic acid.

3.9.2 Lipid class profiles

P_4-type ATPases are supposed to flip PL (Devaux *et al.*, 2006; Pérez-Victoria *et al.*, 2006; Lenoir *et al.*, 2007; Paulusma *et al.*, 2008) and analyzing the total FA composition might be an improper way to unravel a deregulated lipid composition in P_4-type ATPase mutant plants as PL count only for a minor part of plant lipids. In general, neutral lipids and glycolipids (GL) represent the major fractions of lipids in green plant tissues. In order to gain deeper insights in the FA composition of different lipid groups, especially PL, total lipids of *ala* mutant and wild type plants were extracted (chapter 2.9.1) and fractionated via solid-phase extraction into neutral lipids, GL and PL (chapter 2.9.2). Subsequently, FAME profiles deriving from FA of PL and GL were determined (chapter 2.9.4 and chapter 2.9.5). The comparison of FAME profiles deriving from PL (Figure 34 A) revealed linolenic acid with approximately 37% as the main PL-bound FA. Palmitic acid, linoleic acid and 18:0 (stearic acid) represented approximately 26%, 18% and 8%, respectively. Among the FA deriving from GL, linolenic acid and 20:1 (eicosenoic acid) occupied each approximately one third of the FA within this lipid class (Figure 34 B). Hexadecatrienoic acid, palmitic and stearic acid represented ap-

proximately 15%, 8% and 8%, respectively. Comparing FAME profiles of *ala* mutant lines revealed no statistically significant alterations among the mutant lines, regardless whether FAME derived from PL or GL. The FAME profiles of total PL and GL were identical to wild type profiles and no net change occurred. Thus, it has to be assumed, that there is no substrate specificity of ALA proteins for certain FA acyl chains in PL.

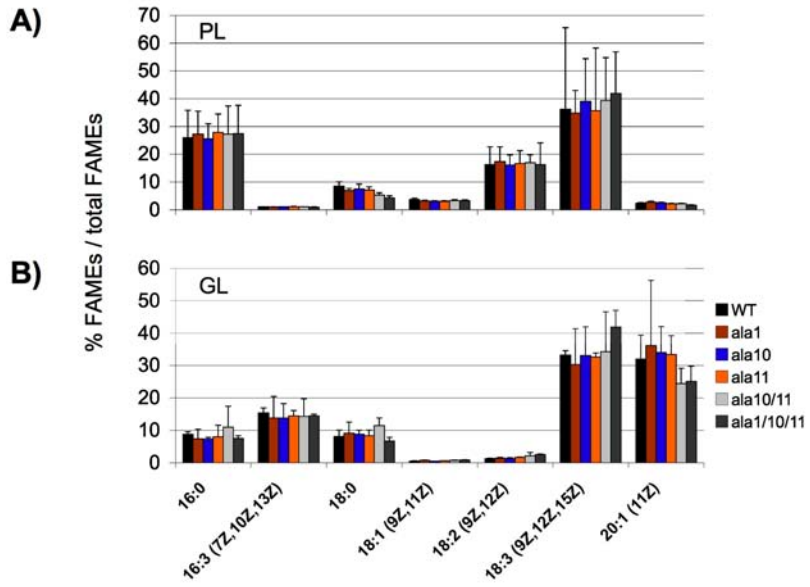

Figure 34: FAME profiles of *ala* mutant lines in comparison to wild type. Depicted are averaged FAME profiles ± S.D. of A) phospholipids and B) glycolipids of pooled 6th rosette leaves at 30 DAG. The amount of FAME is given in relative percentage of total PL/GL FAME. Portions of FAME below 3% are not depicted (n=3). 16:0 palmitic acid, 16:3 hexadecatrienoic acid, 18:0 stearic acid, 18:1 oleic acid, 18:2 linoleic acid, 18:3 linolenic acid, 20:1 eicosenoic acid.

3.9.3 Analysis of phospholipids

As PL are the supposed substrates for P_4-type ATPases (Tang *et al.*, 1996; Pomorski *et al.*, 2003; Poulsen *et al.*, 2008a) this lipid class was analyzed in more detail in P_4-type ATPase mutants. In order to reveal the single lipid species composition of PL in *ala* mutants and wild type plants, total lipids were extracted (chapter 2.9.1), PL fractionated via solid-phase extraction (chapter 2.9.2) and separated on silica plates via thin layer chromatography (TLC; chapter 2.9.3) into single PL species. PL standards were used to locate single lipid species on the chromatography plates, which were subsequently scraped off, converted into FAME (chapter 2.9.4) and analyzed (chapter 2.9.5). It has to be mentioned, that PI and PS have similar running characteristics and the two lipids were therefore analyzed together. Phosphatidylethanolamine (PE) was the most

prominent lipid species among PL with approximately 35% in wild type 6th rosette leaves. Phosphatidylcholine (PC), phosphatidylglycerol (PG) and phosphatidic acid (PA) reached 28%, 25.5% and 9%, respectively. Phosphatidylinositol (PI) together with phosphatidylserine (PS) represented the smallest fraction with 3.5% within the PL classes. As for the analysis of total PL, no significant changes between *ala* mutant lines and wild type were found when comparing amounts of single PL classes (Table 28). Statistics could not be applied to the obtained results as the measurements were carried out only once, however, a tendency among the *ala* mutant lines in comparison to wild type was noticeable. It seemed that the relative amount of PC was reduced in all tested *ala* mutant lines (Table 28). Additionally, mutant lines *ala10*, *ala11* and the double mutant line *ala10/11* seemed to display reduced relative amounts in PI + PS and in return increased relative amounts of PA (*ala10* and *ala10/11*) or PG (*ala11*). Apart from a reduction in the relative PC amount in *ala1*, the mutant line displayed reduced relative amounts of PE and PA. Relative amounts of PG were increased in return and no changes were observed in the amount of PA. The triple mutant line *ala1/10/11* displayed reduced relative amounts in PE aside from PC. In return relative amounts of PI + PS, PA and PG were increased. As a conclusion from these measurements, it seems that ALA proteins prefer to flip certain PL across biological membranes due to a deregulation of PL species in the corresponding *ala* mutants. However, this result requires reconfirmation by biological replicates.

Table 28: PL species in wild type and *ala* mutant lines. Table lists relative proportions of six identified PL species (PC, PE, PI [+ PS], PA and PG) within 6th rosette leaves at 30 DAG. Values are given in percentages and represent the proportions of a specific lipid species per total identified PL. PA phosphatidic acid, PC phosphatidylcholine, PE phosphatidylethanolamine, PG phosphatidylglycerol, PI phosphatidylinositol, PS phosphatidylserine. Data were obtained from one experiment.

	Phospholipid species				
Line	PC	PE	PI + PS	PA	PG
WT	29.65	34.93	3.43	8.71	23.38
ala1	27.36	30.09	3.65	6.69	32.12
ala10	28.28	34.35	2.01	11.58	23.68
ala11	25.49	34.21	2.85	8.10	28.34
ala10/11	25.74	38.19	2.91	11.17	21.99
ala1/10/11	28.19	30.87	7.70	9.41	23.83

Furthermore, the individual PL species in 6th rosette leaves of *ala* mutants and wild type at 30 DAG were analyzed regarding their FA composition. Comparing FAME profiles derived from different PL species, variations within the FA composition were detectable (wild type data, Table 29). However, no alterations in FAME profiles of any

tested PL species (PC, PE, PI + PS, PA and PG) were found between *ala* mutant lines and wild type (data not shown). The main FA in PC was palmitic acid (44% of total FA, approximately) followed by stearic acid, linolenic and linoleic acid (approximately 16%, 14% and 14% of total FA, respectively). FA bound to PE were mainly linolenic acid (approximately 54% of total FA), palmitic acid (approximately 26% of total FA) and linoleic acid (approximately 11% of total FA). PI- and PS-bound FA were palmitic acid (approximately 35% of total FA), linolenic and linoleic acid (approximately 27% and 24% of total FA, respectively.) The main FA in PA were palmitic acid (approximately 42%), linoleic acid (approximately 19%), linolenic acid (approximately 17%) and stearic acid (approximately 15% of total FA). FA deriving from PG were mainly palmitic acid (approximately 32% of total FA), linolenic acid (approximately 26% of total FA) and palmitoleic acid (19% of total FA, approximately). The measurements point out once more that the FA composition of lipids seems to be of no importance to P_4-type ATPases.

Table 29: FAME profiles of single PL species in wild type 6th rosette leaves at 30 DAG. Relative amounts of FAME are given in percentages of total FAME within the same lipid species. 16:0 palmitic acid, 16:1 palmitoleic acid, 18:0 stearic acid, 18:1 oleic acid, 18:2 linoleic acid, 18:3 linolenic acid, 20:2 eicosadienoic acid. Data were obtained from one measurement.

	Fatty acid methyl esters						
Lipid species	16:0	16:1 (9Z)	18:0	18:1 (9/11Z)	18:2 (9Z,12Z)	18:3 (9Z,12Z,15Z)	20:2 (11Z,14Z)
PC	43.59	1.37	15.95	8.45	13.58	13.80	2.65
PE	26.08	1.69	4.49	1.64	11.43	53.75	<1
PI + PS	34.52	<1	6.78	4.70	24.00	27.12	1.33
PA	41.56	2.61	15.02	2.83	19.19	16.52	1.91
PG	31.75	18.82	8.06	5.32	9.18	26.11	<1

3.9.4 *ala* mutants show a retarded desaturation of PL during cold adaptation

Plants respond to cold stress with an increase in unsaturated FA bound to PL and thus maintain membrane fluidity at lower temperature (Hugly and Somerville, 1992; Nishida and Murata, 1996). The level of unsaturation of membrane FA in *Arabidopsis thaliana* correlates inversely with the growth temperature (Falcone *et al.*, 2004). Furthermore, it has been suggested that P_4-type ATPases are involved in plant cold stress adaptation (chapter 3.8.5; Gomès *et al.*, 2000). To determine, whether cold stress had an influence on the saturation degree of PL-bound FA, *ala* mutants and wild type plants (soil-

grown, 16 h light of 120 µmol*m^{-2}*sec^{-1} per day at 21° C) were subjected to a cold-treatment of 12 °C for 4 and 8 h at 30 DAG of their development. Pooled 6th rosette leaf material was sampled before (0 h) and after the cold-treatment (4 and 8 h). Total lipids were extracted (chapter 2.9.1), PL fractionated (chapter 2.9.2) and profiles of total PL-derived FA determined (chapter 2.9.4 and chapter 2.9.5). No statistically significant differences between FA profiles of total PL in wild type and *ala* mutant lines were observed before subjection of the plants to 12 °C (Figure 35 A, comparable to previous measurements in chapter 3.9.2): Among the FA derived from PL of wild type plants approximately 48% were saturated while 52% were unsaturated. After 4 h of cold adaptation, no differences in PL derived FA profiles of wild type and *ala* mutant plants were observed and *ala* plants were indistinguishable from each other and wild type (data not shown). After the 8 h cold-treatment differences in FA composition among PL between *ala* mutants and wild type plants were detectable (Figure 35 B): Wild type plants displayed a reduction in saturated FA (palmitic and stearic acid) and in return an increase in poly-unsaturated FA (linoleic and linolenic acid) resulting in approximately 38% saturated and 62% unsaturated FA. In contrast, *ala* mutant plants did not display that tendency; the degree of unsaturated PL-derived FA was maintained over the duration of the experiment and resulted in similar relative amounts before and after the

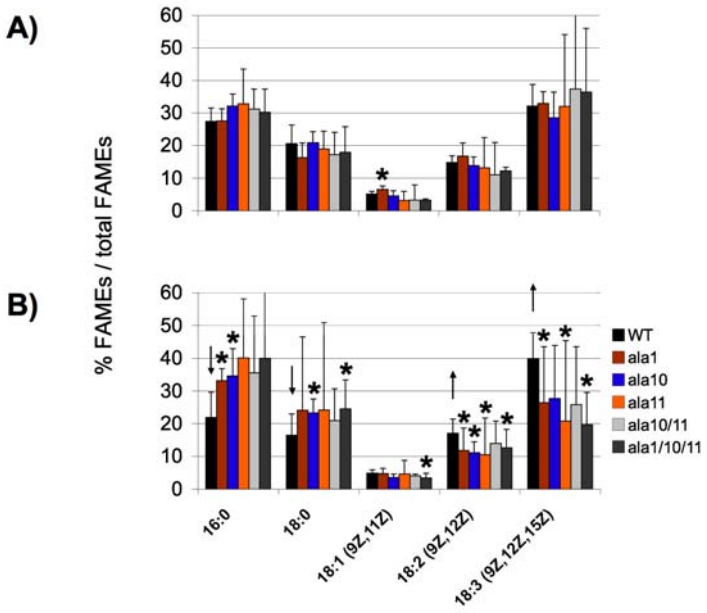

Figure 35: FAME profiles derived from PL of *ala* mutant lines and wild type during cold adaptation. Depicted are mean FAME profiles ± S.D. of pooled rosette leaf 6. Plants were grown until 30 DAG at 21 °C and analyzed A) before (0 h) and B) after subjection to 12 °C for 8 h. Data represent two measurements with averaged values ± S.D., statistically significant differences to wild type are marked with an asterisk (* *P* < 0.05). Arrows indicate changes, i.e. increase or decrease (*P* < 0.1) in the relative amount of FAME before and after the plants were subjected to cold. 16:0 palmitic acid, 18:0 stearic acid, 18:1 oleic acid, 18:2 linoleic acid, 18:3 linolenic acid.

application of cold to the plants. In order to test if the FA composition of wild type and *ala* mutants differs under prolonged exposure to cold, an additional adaptation experiment with 25-day-old plants (soil-grown at 21 °C) was performed. Wild type and *ala* mutant plants were subjected to 12 °C for 10 days and FA of total PL extracts were analyzed from pooled 6th rosette leaves. However, no differences between FA profiles of total PL were observed in wild type and *ala* mutant lines (data not shown). A temperature shift to lower temperatures clearly induces unsaturation in FA of PL in wild type plants as described by Falcone *et al.* (2004). However, *ala* mutants present a delayed response to cold treatment by a retarded unsaturation of FA. Thus, it seems that ALA proteins are necessary for a quick response to cold treatment via the reallocation of PL with newly desaturated FA. The delay in membrane lipid reallocation might be responsible for the cold-sensitive phenotype of *ala* mutants (chapter 3.8.5).

3.10 Characterization of ALA1, ALA10 and ALA11

A direct biochemical characterization of plant membrane proteins within the plant might be difficult to realize when dealing with protein families as in the case of P_4-type ATPases (chapter 3.9). The *Saccharomyces cerevisiae* triple mutant strain ZHY709 (Δ*drs2*-Δ*dnf1*Δ*dnf2*) represents a suitable tool for the functional characterization of ALA proteins as it lacks three endogenous P_4-type ATPases (Dnf1p, Dnf2p and Drf2p) causing sensitivity to temperatures below 23 °C (Hua *et al.*, 2002) and deficiencies in the uptake of fluorescently labeled PL (Poulsen *et al.*, 2008b). A successful suppression of the cold-sensitive Δ*drs2*Δ*dnf1*Δ*dnf2* phenotype by inducible heterologous expression of *Arabidopsis* ALA1, ALA10 and ALA11 proteins in the mutant cells would suggest these P_4-type ATPases as functional lipid flipping enzymes.

3.10.1 ALA expression in Δ*drs2*Δ*dnf1*Δ*dnf2* yeast cells

Recently, Poulsen *et al.* (2008b) identified ALIS subunits that interact with ALA3. ALIS1, 3 or 5 expressed in combination with ALA3 are necessary to complement the cold-sensitive phenotype of Δ*drs2*Δ*dnf1*Δ*dnf2* cells. In order to analyze the capability of ALA1, ALA10 and ALA11 alone or in combination with ALIS1, 3 or 5 to complement the cold-sensitive phenotype of Δ*drs2*Δ*dnf1*Δ*dnf2*, the proteins need to be heterologously expressed in these cells. Equally strong expression of both ALA and ALIS proteins in

yeast was aimed using the expression plasmid pRS423-GAL1-10 containing a bidirectional galactose-inducible promoter (GAL1-10; Johnston and Davis, 1984; Poulsen *et al.*, 2008b). The laboratory of Dr. M. G. Palmgren, University of Copenhagen, Denmark, kindly provided the plasmids used in this section (Table 11). cDNA of *Arabidopsis thaliana ALA1*, *ALA10* and *ALA11* (without stop codon) were cloned to the 5' end of the GAL1-10 promoter to express single ALA proteins. In case of ALA1 an HA-tag was introduced 3' to the cDNA. In addition, plasmids were generated carrying *ALA1*, *ALA10* or *ALA11* at the 5' end of the GAL1-10 promoter and *A. thaliana ALIS1*, *ALIS3* or *ALIS5* cDNA (without stop codon) at the 3' end of the GAL1-10 promoter in order to express ALA and ALIS proteins together at the same time. An $RGSH_6$-tag was added to the 3' end of the ALIS cDNA. The plasmids were transformed into Δ*drs2*Δ*dnf1*Δ*dnf2* mutant cells (chapter 2.6.4) and positive transformants were selected on selective SD media plates. Cells were then grown in selective media under non-inducing conditions. The media was replaced with protein-inducing media while the cells were within the exponential phase (chapter 2.13.2) and cells were then incubated for 12 h. Total cell lysates and total membranes of Δ*drs2*Δ*dnf1*Δ*dnf2* cells were examined for expressed protein traces via immunodetection (chapter 2.13.3). No signal was obtained for ALA1 in total membrane extracts or total cell lysate (Figure 36 A). Nevertheless, expression of

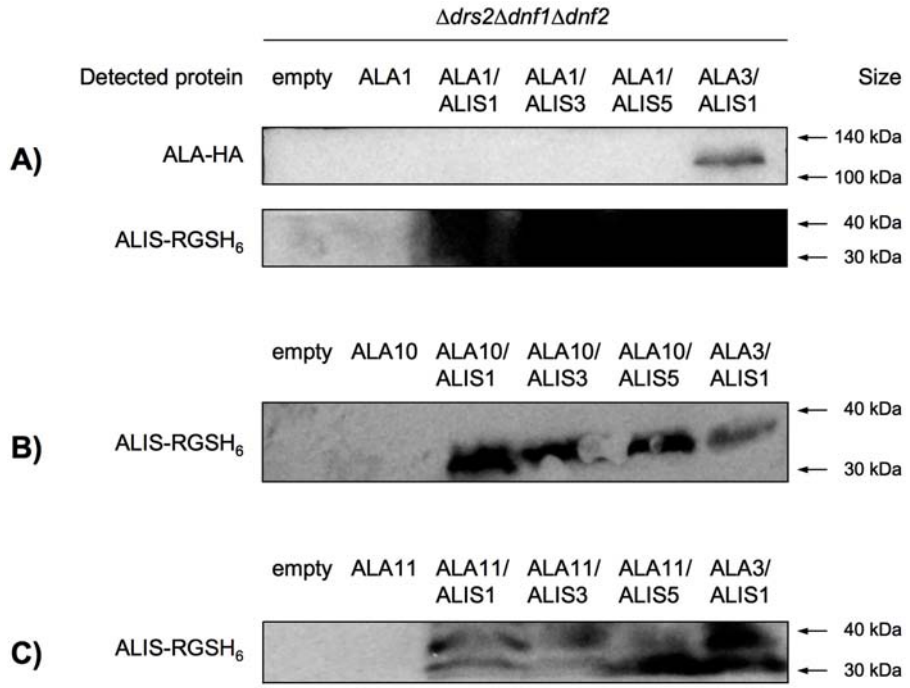

Figure 36: Immunodetection of ALA and ALIS proteins in yeast. Total membrane extraction from Δ*drs2*Δ*dnf1*Δ*dnf2* cells expressing A) ALA1, B) ALA10 and C) ALA11 alone and in combination with ALIS proteins 1, 3 or 5. Detection was carried out with monoclonal mouse anti-HA AB (for HA-tagged ALA proteins, dilution 1:1000), monoclonal mouse anti-$RGSH_6$-AB (for $RGSH_6$-tagged ALIS proteins, dilution 1:5000) and peroxidase-linked goat anti-mouse AB (secondary AB, dilution 1:5000).

ALIS proteins resulted in strong positive signals within the expected range of approximately 39 kDa. A fragmentation of ALIS bands was observed in the western blot arguing for posttranslational modifications of the proteins that might be carried out by glycosylation. Weaker detection signals were observed when the immunodetection was conducted on total cell lysate (data not shown). Δ*drs2*Δ*dnf1*Δ*dnf2* cells co-expressing ALA3 and ALIS1 served as a positive control and resulted in detectable signals for ALA3 (approximately 130 kDa) and ALIS1 proteins, again fragmentation of ALIS1 signals was observed. Expression plasmids carrying tagged versions of *ALA10* and *ALA11* were not available and an immunodetection of these proteins was therefore not practicable. However, ALIS1, 3 or 5 proteins were detected successfully in total membrane extracts from cells transformed with an expression plasmid containing either *ALA10* or *ALA11* in combination with *ALIS1*, *3* or *5* under protein inducing conditions (Figure 36 B and C). The results show that at least ALA1 is not properly expressed or rapidly degraded after its translation in yeast cells.

3.10.2 Complementation of Δ*drs2*Δ*dnf1*Δ*dnf2* cells by ALA expression

It is known that the *Arabidopsis* P_4-type ATPase ALA1 complements the cold-sensitive phenotype of yeast mutant strain Δ*drs2*, which is deficient in the Golgi-localized P_4-type ATPase Drs2p (Gomès *et al.*, 2000). Additionally, ALA3 in combination with ALIS proteins (ALIS1, 3 or 5) as an interacting subunit complements the cold-sensitive phenotype of the Δ*drs2*Δ*dnf1*Δ*dnf2* mutant strain (Poulsen *et al.*, 2008b), which is deficient in the two plasma membrane localized P_4-ATPases Dnf1p and Dnf2p and in the Golgi-localized Drs2p (Hua *et al.*, 2002). In order to test whether ALA1, ALA10 and ALA11 alone or in combination with ALIS1, 3 or 5 have the ability to complement the cold-sensitive phenotype of the triple mutant strain Δ*drs2*Δ*dnf1*Δ*dnf2*, drop-tests under standard conditions (30 °C) and low temperature (20 °C) were conducted (chapter 2.13.1). pRS423-GAL1-10 expresssion vectors carrying *ALA1*, *ALA10* and *ALA11* alone or in combination with *ALIS1*, *3* or *5* (chapter 3.10.1; Table 11) were transformed into Δ*drs2*Δ*dnf1*-Δ*dnf2* cells. Positive transformants were selected, grown and spotted in a dilution series onto agar plates with or without inductive media. Yeast wild type cells transformed with an empty pRS423-GAL1-10 vector served as negative control and Δ*drs2*Δ*dnf1*Δ*dnf2* cells transformed with the pRS423-GAL1-10 vector carrying Drs2 from *S. cerevisiae* as positive control. One set of plates was incubated at 30 °C for 2-3 days serving as a control under standard conditions (Appendix, Figure 44 A), the other set was incubated at 20 °C for 5-7 d in order to see effects of the expressed proteins on the cold-sensitive Δ*drs2*Δ*dnf1*Δ*dnf2* phenotype under low temperature (Appendix, Figure 44 B). Cells of

the Δ*drs2*Δ*dnf1*Δ*dnf2* mutant strain displayed nearly wild type growth under standard conditions. When harboring an expression plasmid with *ALA1* alone and in combination with *ALIS1*, *3* or *5* subunits, the cells displayed a minor reduction in growth. The same growth rates were observed for normal (GLU) and protein expression inducing (GAL) conditions (Appendix, Figure 44 A). Yeast wild type cells displayed a 2-3-fold reduction in doubling time when grown at low temperature compared to standard conditions. In contrast, growth of the Δ*drs2*Δ*dnf1*Δ*dnf2* mutant strain was reduced 10-15-fold. The Δ*drs2*Δ*dnf1*Δ*dnf2* cells were barely able to grow when harboring an expression plasmid with *ALA1* alone and in combination with *ALIS1*, *3* or *5* subunits indicating an altered metabolism and a possible malfunction at the translational level. The same growth behavior was observed under protein expression inducing conditions (Appendix, Figure 44 B). Δ*drs2*Δ*dnf1*Δ*dnf2* control cells expressing yeast Drs2p were able to grow under protein expression inducing conditions at low temperature to the same extent as wild type cells indicating a successful complementation of the cold-sensitive phenotype of Δ*drs2*Δ*dnf1*Δ*dnf2* cells by Drs2p. These results were confirmed by threefold repetition of the drop-test using freshly transformed yeast cells each time. Drop-tests conducted with cells harboring expression plasmids carrying *ALA10* or *ALA11* either alone or in combination with *ALIS* subunits displayed similar results (data not shown). Excluding technical difficulties, it must be assumed that the complementation of the cold-sensitive phenotype of Δ*drs2*Δ*dnf1*Δ*dnf2* cannot be achieved either by single ALA proteins (ALA1, ALA10 or ALA11) or by the combination of ALA proteins with their ALIS subunits 1, 3 or 5. Using the Δ*drs2*Δ*dnf1*Δ*dnf2* system, no background from endogenous P_4-ATPase activity is expected at the plasma membrane level (Poulsen *et al.*, 2008b) and, thus, even trace amounts of functional ALA/ALIS protein complexes reaching the plasma membrane should eventually result in a detectable internalization of fluorescently labeled PL analogs. The obtained results underline the previoulsly found expression difficulties of ALA1, ALA10 and ALA11 proteins in Δ*drs2*Δ*dnf1*Δ*dnf2* cells (chapter 3.10.1) and the ability of ALA1, ALA10 and ALA11 to complement the cold-sensitive phenotype of Δ*drs2*Δ*dnf1*Δ*dnf2* cells remains elusive.

3.10.3 Inward lipid translocase activity test of ALA1

Several reports suggest a lipid inward transport activity for P_4-type ATPases from the outer to the inner membrane leaflet (Zachowski *et al.*, 1989; Tang *et al.*, 1996; Pomorski *et al.*, 2003; Alder-Baerens *et al.*, 2006; Natarajan and Graham, 2006). An internalization of PS using reconstituted yeast microsomes was shown for ALA1 (Gomès *et al.*, 2000). Studies with ALA3 demonstrated an internalization of PE in yeast cells when expressed

in combination with the interacting subunit ALIS1 (Poulsen *et al.*, 2008b). To test whether ALA1 alone or in combination with its supposed interacting subunit is capable of internalizing PL in yeast cells, the same set of expression plasmids as for the complementation analysis (3.10.2) was used to transform the ∆*drs2*∆*dnf1*∆*dnf2* mutant strain. The lipid internalization assay from Poulsen *et al.* (2008b) was adapted and internalization of fluorescently labeled PE, PS and PC of the cells was observed via fluorescence-assisted cell sorting (FACS; chapter 2.13.2). Yeast wild type and the triple mutant strain ∆*drs2*∆*dnf1*∆*dnf2* served as positive and negative control (respectively, both transformed with the empty expression vector pRS423-GAL1-10). Fluorescence histograms of wild type cells revealed a significant increase in fluorescence signals when incubated with NBD-PE, -PS or -PC (Appendix, Figure 45). In contrast, ∆*drs2*∆*dnf1*∆*dnf2* cells showed no increase in fluorescence independently from incubation with NBD-labeled lipids. Comparable results were obtained for ∆*drs2*∆*dnf1*∆*dnf2* cells harboring an expression plasmid either with *ALA1* alone or in combination with *ALIS1*, *3* or *5* indicating no significant internalization of exogenously applied NBD-labeled PE, PS and PC (Appendix, Figure 45). The result was validated by two independent repetitions of the experiment. Due to the described expression difficulties of ALA1 (chapter 3.10.1) no conclusions can be drawn from the performed experiments regarding the PL internalization capability of ALA1 in ∆*drs2*∆*dnf1*∆*dnf2* cells. However, it can be concluded, that ALIS1 and ALIS3 have an impact on the cells as small populations of ∆*drs2*∆*dnf1*∆*dnf2* cells displayed an increase in fluorescence signal intensity when harboring an pRS423-GAL1-10 expression plasmid containing *ALA1* in combination with *ALIS1* or *ALIS3* (Appendix, Figure 45). This observation suggests an altered growth rate for ∆*drs2*∆*dnf1*∆*dnf2* cells when expressing ALIS1 and ALIS3.

4 DISCUSSION

4.1 Relation of ALA proteins to senescence

The main purpose of leaf senescence is nutrient recycling. Sugars, amino acids and anions derived from protein degradation are the major targets of nutrient remobilization during senescence supporting the growth of young tissues (Diaz *et al.*, 2005; Wingler *et al.*, 2005; Diaz *et al.*, 2006; Masclaux-Daubresse *et al.*, 2008). Long-distance transport of these nutrients is thought to take place via the phloem (Hill, 1980). However, the substances have to leave their sites of origin reaching the sites where long-distance transport originates. In order to overcome cellular membrane barriers, membrane localized transport proteins are thought to be necessary. Little is known of the genes whose products facilitate nutrient remobilization from senescing tissue and only a few senescence-associated transport proteins have been reported so far (Himelblau and Amasino, 2001). Quirino *et al.* (2001) related SFP1, a monosaccharide transporter, to the senescence process and found increased *SFP1* transcript amounts during *Arabidopsis* leaf senescence. More recently, Fan *et al.* (2009) identified NRT1.7 as an inorganic nitrate transporter with a special role in the remobilization of nitrate from older, senescing leaves into nitrogen-demanding tissues like younger leaves and developing seeds.

With the help of expression profiling studies it was possible to identify more senescence-associated transport proteins (Buchanan-Wollaston *et al.*, 2003; Buchanan-Wollaston *et al.*, 2005). Van der Graaff *et al.* (2006) found increased expression levels for 153 genes coding for transmembrane proteins with more than three transmembrane spans during natural leaf senescence pointing out that transmembrane proteins play a vital role within this process. The number of up-regulated transport proteins during senescence was approximately 2.5 times higher than that of down-regulated transport proteins indicating an increased demand for transport processes across membranes within this process. Not surprisingly, the number of amino acid and oligopeptide transporter correlated with protein degradation taking place during senescence and the resulting need for an export of the degradation products (Hörtensteiner and Feller, 2002; van der Graaff *et al.*, 2006). For example PTR3, a peptide transporter, so far known to be salt- and wounding-inducible (Karim *et al.*, 2007), displayed increased transcripts in leaves during aging (van der Graaff *et al.*, 2006). Similarly, *ECA3* transcript amounts were induced during senescence. ECA3 is known as a Ca^{2+}/Mn^{2+} transporter and belongs to

the P_2A-type ATPases. Li *et al.* (2008) localized the protein to the endoplasmatic reticulum (ER) and described for three independent *eca3* T-DNA insertion mutants a severe reduction in root growth and altered secretory processes in root cells. However, the senescence-associated role of these proteins has yet to be proven experimentally. The same is true for RAN1, a P_1B-type ATPase involved in the the import of copper ions in the post-Golgi compartment (Hirayama *et al.*, 1999; Woeste and Kieber, 2000), which showed increased transcript amounts during senescence (van der Graaff *et al.*, 2006). Based on the expression data from van der Graaff *et al.* (2006) three members of the *ALA* gene family displayed a more than 4.5-fold higher transcript amounts during natural occurring leaf senescence of *Arabidopsis thaliana* (*ALA1*: 4.7-fold [absolute values: 4034 – 18828], *ALA10*: 5.3-fold [absolute values: 1750 – 9222] and *ALA11*: 9.7-fold [absolute values: 2491 – 24283]). These data were verified in this work and partly resulted in even higher changes in transcript levels of these P_4-type ATPase genes (chapter 3.1; *ALA1*: 20-fold, *ALA10*: 6-fold and *ALA11*: 225-fold) suggesting a vital role for ALA1, ALA10 and ALA11 within the leaf senescence program. Publicly available expression data from independent experiments performed on specific tissues and organs at the Arabidopsis Membrane Protein Library (AMPL; http://wardlab.cbs.umn.edu/

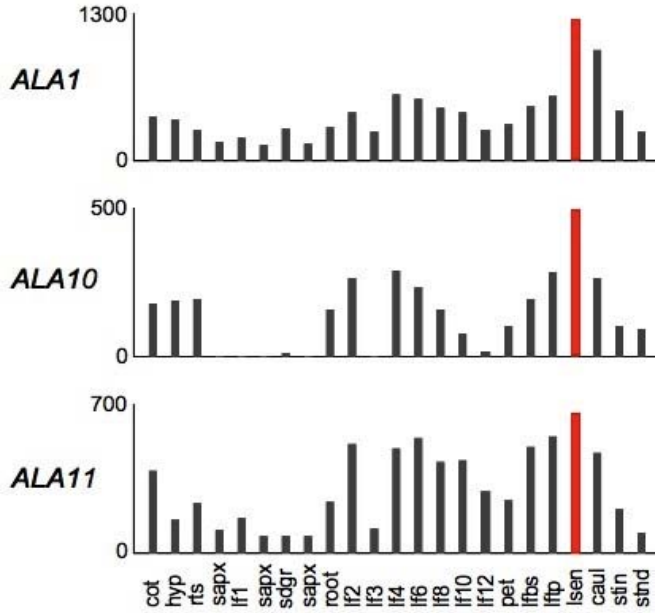

Figure 37: Microarray expression data of *ALA1*, *10* and *11* from the Arabidopsis Membrane Protein Library during development of *Arabidopsis* ecotype Col-0. Y-axis of the bar graphs represents the absolute signal strength. The data follow a developmental series from left to right with samples from seedling on the left through developing seeds on the right and are presented as means of three hybridizations. cot cotyledons, hyp hypocotyl, rts roots, sapx shoot apex, lf leaves, sdgr green seedling, pet petiole, lfbs proximal leaf half, lftp distal leaf part, lsen senescing leaves, caul cauline leaves, stin/stnd stem (1st/2nd internode).

arabidopsis/) also link *ALA1*, *10* and *11* to senescence (Ward, 2001; Figure 37). Comparable expression results are obtained using the Electronic Fluorescent Pictograph (eFP; http://bar.utoronto.ca/efp/ cgi-bin/efpWeb.cgi; Winter *et al.*, 2007; Appendix, Figure 46)

It has been shown that WRKY transcription factors play a key role in the regulation of senescence (Robatzek and Somssich, 2001; Miao *et al.*, 2004; Eulgem and Somssich, 2007). WRKY transcription factors recognize W-boxes (TTGAC) and such *cis*-elements were found in the promoters of many senescence-associated genes (Miao *et al.*, 2004). Although a single W-box within a promoter might be sufficient for a WRKY-mediated gene expression, a clustering of W-boxes is often observed (Eulgem *et al.*, 2000) and can be applied to the 2 kb promoter regions of *ALA1*, *10* and *11*, where 4, 3 and 7 W-boxes, respectively, are located. The fact that three quarter of the *ALA* gene family show at least a two-fold expression increase during the senescence program (Figure 7; van der Graaff *et al.*, 2006) suggests an important role of the ALA family during this developmental process.

Poulsen *et al.* (2008b) identified interacting partners for ALA proteins and named them ALIS (ALA interacting subunit). The proteins might serve as chaperones for newly synthesized ALA proteins due to their homology with the yeast Cdc50p protein family, which is a prerequisite for proper trafficking of yeast P_4-type ATPases to their membrane destination (Saito *et al.*, 2004; Pérez-Victoria *et al.*, 2006). Future experiments will identify preferences of different ALA proteins for their subunits (ALIS1-ALIS5). However, one member, *ALIS1*, presents increased transcript levels during senescence of *Arabidopsis thaliana* (Figure 38) indicating a possible preferred interaction of ALA proteins with ALIS1 during the senescence program.

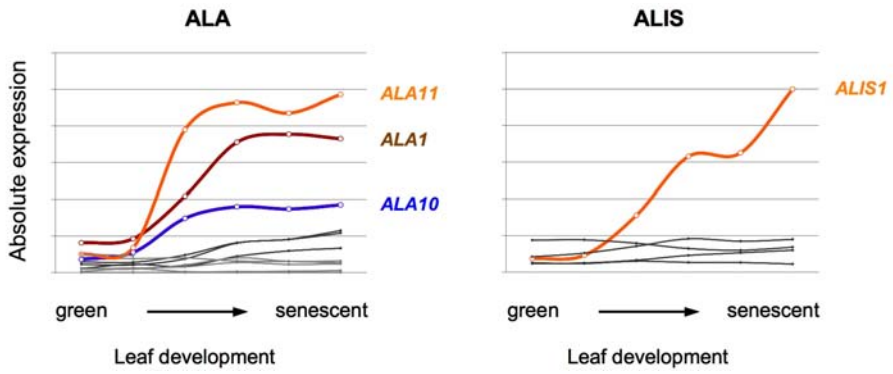

Figure 38: Expression of *ALA* (aminophospholipid ATPase) and *ALIS* (ALA interacting subunit) genes during natural development in leaves of *Arabidopsis thaliana* ecotype Col-0. Depicted are absolute expression values obtained from gene chip hybridization with pooled material from 5th and 6th rosette leaves at 4, 5 and 6 weeks and when displaying 25%, 50% and 75% yellowing of the leaf blade. (Data from van der Graaff *et al.*, 2006).

4.2 *ALA* genes are required for an orderly progression of the senescence program

Often knock out mutants of a single gene in a gene family produce no detectable phenotype (Bouche and Bouchez, 2001) due to a redundant function by other family members. This observation does not apply to mutants of the *ALA* gene family. *ala1* antisense plants and *ala3* T-DNA insertion mutants showed reduced growth and morphological alterations (Gomès *et al.*, 2000; Poulsen *et al.*, 2008b). The single T-DNA insertion lines *ala1*, *ala10* and *ala11* identified in this work, also display these symptoms and exhibit additionally premature senescence symptoms (chapter 3.5). The premature senescence phenotype was further strengthened genetically by increased transcript amounts of *SAG12* (chapter 3.4.5), which is exclusively expressed during age-dependent senescence (Gan and Amasino, 1997). In addition, the F_v/F_{max} ratio, dropped earlier at the end of leaf development (chapter 3.6.2) reflecting an earlier lowered photochemical quantum efficiency of photosystem II that is typical for senescence. Another interesting feature of *ala* mutants was a significantly higher membrane ion leakage (chapter 3.6.3) indicating an advanced deterioration of cellular membranes. Surprisingly, plastids of the investigated *ala* mutants displayed a lower number of starch grains even at a time point before visible senescence symptoms were detectable (chapter 3.7.1 and 3.7.2) underlining the premature senescence phenotype of the mutants by a reduced capability to synthesize assimilatory starch. These findings together underline the important role of *ALA* genes for a controlled progression of leaf senescence.

Furthermore, it seems that the senescence process in *ala* mutants was not carried out properly and appeared to be accelerated. Especially after a darkness period the mutants were unable to recover pale leaves (chapter 3.8.3). By end of a natural occurring senescence *ala* mutants displayed drastically reduced amounts of anthocyanins (chapter 3.6.1) Anthocyanins are accumulated in leaves in order to protect them from light and reactive oxygen during a natural, undisturbed senescence ensuring the finalization of this developmental phase (Lee *et al.*, 1987; Noodén *et al.*, 1996; Diaz *et al.*, 2006). Considering the low anthocyanin levels in the mutants it is likely that ALA proteins are necessary for a regulated, undisturbed senescence program. Strengthening this assumption, the amount of chlorophyll in *ala* mutants did not reach wild type maximum level and started to decrease earlier (chapter 3.6.1).

Senescence in *Arabidopsis thaliana* is induced under low nitrogen concentrations in combination with glucose supply (Wingler *et al.*, 2004). However, the investigated mutants in *ALA* genes did not show an alteration in the senescence pattern when grown

under low nitrogen plus glucose (chapter 3.8.1). In conclusion, ALA proteins are not primarily involved in the induction or regulation of the senescence program rather the proteins are required for a proper execution of the senescence program.

4.3 ALA proteins are viable for proper plant growth

It appears that ALA expression is triggered by cellular mechanisms even before the senescence process starts. These proteins must therefore play a role not only during senescence but also earlier during plant development. Corroborating this assumption, the expression of *ALA1*, *10* and *11* was detectable in cotyledons, young leaves and roots (Figure 37) and *Prom::GUS* plants displayed an intense staining in young seedlings and young developing tissues, which weakened later in development but intensified again during senescence (chapter 3.2). The only reported P_4-type ATPase mutants in plants are the *Arabidopsis ala3-1* and *ala3-4* T-DNA insertion lines (Poulsen *et al.*, 2008b). Expression data from van der Graaff *et al.* (2006) revealed a 3.7-fold increase in transcript amounts of *ALA3* during natural occurring leaf senescence (absolute values: 1451 – 5376). However, a senescence phenotpye is not known for both mutants. The authors rather reported reduced growth and shortened primary roots for *ala3* plants. A reduction in root growth was also found for *ala1* (chapter 3.5.4) indicating overlapping functions for ALA1 and ALA3. General growth reduction was also observed for the single mutants *ala1*, *ala10* and *ala11* and especially in the *ala10/11* and *ala1/10/11* mutants (chapter 3.5). The reduced growth of these *ala* mutant lines gives rise to speculations of its nature. The mutants possessed not only smaller leaves and a reduced leaf number, in addition they exhibited a reduction in epidermal cell size (chapter 3.5.2). Thus, it seems that ALA proteins are necessary for plant vitality and proper growth. There is evidence that the P_4-type ATPase function is evolutionary conserved as yeast P_4-type ATPase mutants also display reduced growth rates (Ripmaster *et al.*, 1993; Chen *et al.*, 1999; Hua *et al.*, 2002; Pomorski *et al.*, 2003). Chen *et al.* (1999) explained the reduction in growth for ∆*drs2* cells by an altered vesiculation resulting in impaired protein transport. Likewise, the growth defect in *ala* mutant lines might be based on an impaired vesiculation leading to a dysfunction in cellular protein transport.

P_4-type ATPases are supposed to translocate phospholipids (PL) between the two leaflets of biological membranes and help to maintain their asymmetry (Tang *et al.*, 1996; Pomorski *et al.*, 2003; Poulsen *et al.*, 2008a). Membrane asymmetry is critical to normal cell function assuring among other features proper functioning of membrane-associated proteins (Quinn, 2002; Balasubramanian and Schroit, 2003). The need for P_4-type ATP-

ases in young, developing tissues can be explained by the necessary establishment of an asymmetric PL distribution of membranes within these cells. Once the membrane asymmetry is established, it has to be maintained during development. Asymmetric membranes are thought to be a vital prerequisite for membrane proteins modulating their activity (Devaux, 1991; Falcone *et al.*, 2004). Consequently, it can be assumed that asymmetric membranes are of special importance during senescence when many transport processes take place and the need of operating and active transmembrane proteins is high. ALA1, 10 and 11 may contribute to the maintenance of an asymmetric PL distribution in cellular membranes and, thus, maintain the viability of senescent cells until the mobilization of nutrients is fully completed.

4.4 Involvement of ALA proteins in cold-tolerance

The expression of many genes with changed transcript levels during senescence is further affected by environmental stresses (Hensel *et al.*, 1993; Smart, 1994; Noodén and Penney, 2001). Expression data from the AMPL support these findings by displaying affected transcript levels for *ALA1*, *ALA10* and *ALA11* besides senescence under cold and salt stress though mainly in roots (Ward, 2001; Figure 39). Nonetheless, these altered transcript amounts suggest that the proteins also play a prominent role in cold and salt adaptation. Confirming these assumptions, Gomès *et al.* (2000) linked *Arabidopsis* ALA1 to cold stress adaptation and described reduced growth for *ala1* antisense plants when grown at 12 °C. Similarly, *ala1*, *ala10* and *ala11* mutants showed a stronger growth reduction than wild type plants when cultivated at 12 and 16 °C (chapter 3.8.5). The effect was more pronounced in the double and triple mutant lines *ala10/11* and *ala1/10/11*, respectively.

Masclaux-Daubresse *et al.* (2007) described a possible relation between senescence and cold due to altered metabolites of cold-adapted plants that subsequently induce senescence. Similarly, the senescence program might be induced in *ala* mutants due to an altered membrane lipid composition as discussed above. In fact, the investigated mutants displayed a lower desaturation degree in fatty acids (FA) originating from PL during cold adaptation (chapter 3.9.4; Figure 35). As a conclusion, missing P_4-type ATPase function in the mutants results in reduced shuffling of lipids comprising of either saturated or unsaturated FA between membrane leaflets especially during cold adaptation. Reports on poikilothermal organisms support the importance of an asymmetric PL distribution especially during cold adaptation (Hazel, 1995; Miranda and Hazel, 1996). In plants, an asymmetric PL distribution has also been demonstrated for differ-

ent cellular membranes, however the role of the lipid asymmetry is yet not understood (Cheesebrough and Moore, 1980; Rawyler and Siegenthaler, 1981; Dorne *et al.*, 1985; Tavernier and Pugin, 1995). Alternatively, the asymmetric distribution of PL might indirectly influence the plant membrane fluidity over signal transduction pathways. Phosphatidylserine (PS) has been suggested to interfere with elements of signal transduction pathways involved in cold adaptation (Gomès *et al.*, 2000). Indeed, it has been shown that PS is able to activate kinase C, a signal transduction protein in animals (Nishizuka, 1992) and a calcium-dependent protein kinase in plants (Szczegielniak *et al.*, 2000).

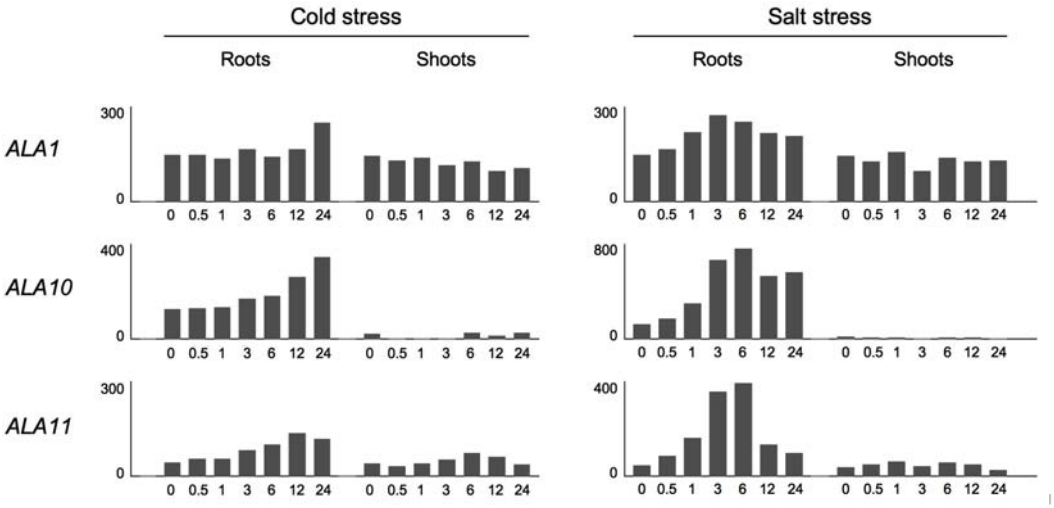

Figure 39: Expression data of *ALA1*, *ALA10* and *ALA11* in roots and shoots of *Arabidopsis thaliana* (Col-0) upon cold and salt stress. Data from the *Arabidopsis* Membrane Protein Library, y-axis of the graphs represents the absolute signal strength. The data follow a time-course series from left to right with samples 0 hours on the left through 24 h on the right and are presented as means of three replicates.

It is known that membranes with unsaturated acyl chains in PL remain fluid at lower temperatures turning out the degree of unsaturated membrane lipids in cellular membranes into a major factor determining membrane fluidity and, thus, a key determinant for cold tolerance (Kates *et al.*, 1984; Cevc, 1991; Cossins, 1994). Consequently, ALA proteins that modify the membrane structure via PL flipping should be important for a successful cold adaptation of plants. Altered membrane fluidity due to a missing distribution of PL with unsaturated acyl chains affects the activity of important membrane-associated proteins as it is the case for proteins of the photosynthetic apparatus (Falcone *et al.*, 2004). Thus, the altered distribution of PL within *ala* mutants might reduce the cold adaptation capability of the plants and lead furthermore to an induction of the senescence program.

The reduction in rosette sizes of cold-grown *ala* mutants compared to wild type disappeared to great extent when cultivated at elevated temperatures. Especially the *ala10/11*

double and *ala1/10/11* triple mutant line resembled wild type appearance at 24 °C (chapter 3.8.5). It seems, that asymmetric membranes and, thus, P_4-type ATPase activity are less important at elevated temperatures. Additionally, biological membranes are more fluid at higher temperatures supporting proper enzymatic activity or higher stability of membrane-associated proteins leading to positive effects on the whole plant growth (Falcone *et al.*, 2004).

4.5 Substrates of P_4-type ATPases

So far no lipid measurements *in planta* on P_4-type ATPase mutants have been performed. Surprisingly, all investigated *ala* mutants in this work displayed no alteration in their FA composition (deriving from total lipids, phospho- or glycolipids; chapter 3.9.1 and 3.9.2) indicating no changes in the FA biosynthesis in favor of the prokaryotic or eukaryotic pathway (Ohlrogge and Kuo, 1985). As mentioned above, ALA proteins are believed to translocate PL via PL shuffling between the two leaflets of a membrane (Tang *et al.*, 1996; Pomorski *et al.*, 2003; Poulsen *et al.*, 2008a) and are therefore responsible for the establishment and maintenance of membrane asymmetry (Figure 40 A). Mutants in *ALA* genes should consequently display deregulations within the PL class. Nevertheless, *ala* mutants revealed only minor alterations within their PL composition (chapter 3.9.3). The enrichment of PL in one membrane leaflet, which is not assessable by the analysis of whole membranes (both leaflets), might be one possible explanation for this finding. The net amount of PL within whole membranes (both leaf-

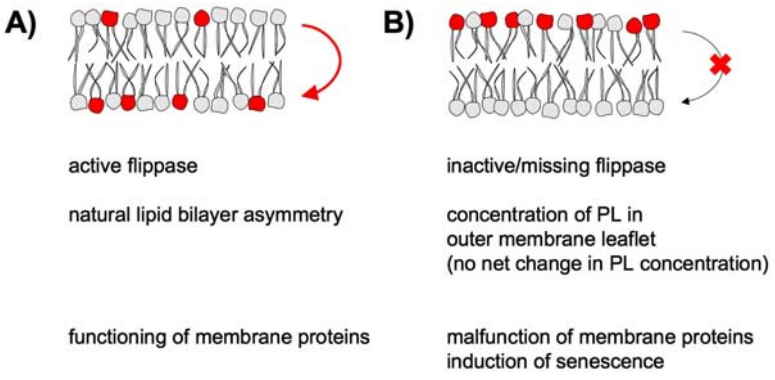

Figure 40: Schematic model of membrane lipid asymmetry established by P_4-type ATPases. Membrane with A) functional and B) nonfunctional ATPase. PL substrates for P_4-type ATPases are indicated in red. Upper membrane part illustrates exoplasmatic (outer) leaflet, lower membrane part cytoplasmatic (inner) leaflet.

lets) would appear to be not affected (Figure 40 B). Furthermore, it seems that there is no feedback regulation from ALA proteins to the origins of FA synthesis.

Based on the slightly deregulated PL composition in *ala* mutant lines one might speculate that ALA proteins have different PL substrates. The relative amount of phosphatidylethanolamine (PE) and phosphatidylcholine (PC) were mainly reduced in *ala1* plants indicating a specificity of ALA1 for PE and PC. Likewise, relative PS and PC amounts were reduced in *ala10* and *ala11* mutants suggesting both lipids as possible substrates for ALA10 and ALA11. Nonetheless, these conclusions must be taken with caution and verified by additional plant lipid analyses and lipid internalization studies as performed by Gomès *et al.* (2000), Pomorski *et al.* (2003), Saito *et al.* (2004), Poulsen *et al.* (2008b) and Stevens *et al.* (2008). However, studies with heterologously expressed ALA proteins identified PS and PE as substrates for ALA1 (Gomès *et al.*, 2000) and PE and PC for ALA3 (Poulsen *et al.*, 2008b) supporting at least partly the conclusions on ALA substrate specificity and, thus, pointing out PL flipping as a common feature of P_4-type ATPases.

Possibly the plastidial localization of ALA1 (chapter 3.3) might be the reason for the failure expression within the Δ*drs2*Δ*dnf1*Δ*dnf2* cells (chapter 3.10.1). Yeast, which does not possess plastids or similar organelles, might consequently be incapable of synthesizing the plant protein ALA1 properly resulting in unstable RNA, arrested protein synthesis or digestion via proteases. Other factors that might lead to failures when dealing with heterologously expressed membrane proteins are unknown structural features involved in protein targeting and special lipid composition requirements that are necessary for proper protein folding and functioning (reviewed in Opekarová and Tanner, 2003). Therefore, Δ*drs2*Δ*dnf1*Δ*dnf2* cells lacking three of five P_4-type ATPases might not be suitable for the investigation of some P_4-type ATPase because of the high probability of an altered membrane lipid composition of the cells evoked by the missing ATPases that negatively affects heterologously expressed membrane proteins. Gomès *et al.* (2000), aiming the functional characterization of ALA1, heterologously expressed the protein in yeast Δ*drs2* cells. These cells might display only minor changes in their natural membrane lipid asymmetry allowing therefore proper expression, folding and function of ALA1. In fact, Δ*drs2* cells expressing ALA1 were phenotypically restored to wild type level and did not display their cold-sensitive phenotype any longer. Furthermore, the authors revealed an internalization of fluorescently labeled PS and PE analogs, yet the experiments were performed using reconstituted yeast microsomes originating from ALA1 expressing Δ*drs2* cells. An activity of the remaining four P_4-type ATPases Dnf1p, Dnf2p, Neo1p and Dnf3p could not be excluded.

4.6 ALA proteins and their site of action

To date the ultrastructure of only one P_4-type ATPase mutant in plants has been analyzed. The *ala3* mutant displays very few slime vesicles and large vacuole-like structures in root tip cells compared to wild type (Poulsen *et al.*, 2008b). The authors argue that vesiculation in root tip cells is vital for proper root and plant development and that the disturbed formation of vesicles in *ala3* mutants is responsible for the reduction in root growth and presumable in rosette size of these plants. Observation of the ultrastructure of additional *ala* mutants (*ala1*, *ala10*, *ala11*, *ala10/11* and *ala1/10/11*) in this work allows deeper insights into physiological processes where P_4-type ATPases might be involved.

4.6.1 ALA1

Keeping in mind the plastidial localization of ALA1 (chapter 3.3; Figure 41), this organelle is in focus for the following discussion. The most striking morphological feature of *ala1* mutant plants was degenerated plastids with diffuse inner structure lacking the typical grana stacks of wild type plastids (chapter 3.7.1). It has to be assumed that the reduction in grana stacks might be caused by a disturbance in their formation caused by the mutation in *ALA1*. Thylakoids are formed during chloroplast development by the invagination of the inner chloroplast membrane (Brown and Weier, 1968). Alternatively or additionally, thylakoids are formed by fusion of vesicles produced in the inside of pro-

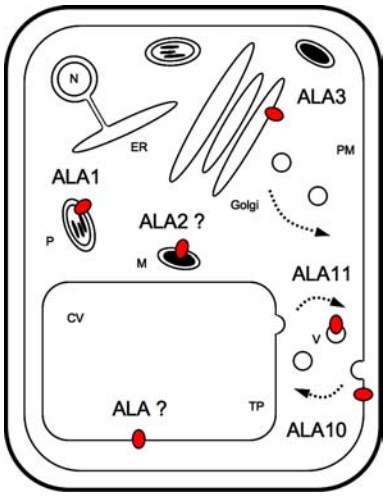

Figure 41: ALA proteins in *Arabidopsis thaliana*. Sketch of a plant cell with its P_4-type ATPases indicated by red circles. CV central vacuole, ER endoplasmatic reticulum, Golgi Golgi network, M mitochondrion, N nucleus, P plastid, PM plasma membrane, TP tonoplast, V vesicles/ endosomes.

plastids (Tripodi and Gargiulo, 1984). In both cases the inner plastidial membrane must bend in order to form thylakoids or bud thylakoid-forming vesicles. Transbilayer movement of lipids has been discussed to induce the bending of membranes in order to facilitate vesicle budding (Devaux, 1991). A possible function of the plastid localized P_4-type ATPase ALA1 might be the initiation of the curvature of the inner plastid membrane in order to facilitate thylakoid formation by translocation of lipids during plastid maturation. It is furthermore conceivable that ALA1 is specifically involved in the recycling of degradation products within the senescing plastid and might play a role in exporting thylakoid membrane degradation products. This process also requires the formation of vesicles that subsequently bud from the membrane. ALA1 might therefore represent a necessary factor for vesiculatory processes in this cellular compartment.

Another peculiarity of *ala1* plants was the enrichment of phosphatidylglycerol (PG; chapter 3.9.3). Thylakoid membranes of chloroplasts differ in their lipid composition from other cellular membranes and contain largely glycolipids such as monogalactosyldiacylglycerol (MGD), digalactosyldiacylglycerol (DGD), sulfoquinovosyldiacylglycerol (SQD; Sato and Tsuzuki, 2004). However, missing asymmetry of the less occurring PL due to a disturbed lipid translocation in the *ala1* mutant might induce structural consequences for these membranes and affect proper functioning of other membrane-localized proteins such as the light-harvesting complexes, the electron transport chain from photosystem I and II, the cytochrome b/f complex and the ATP-synthase. Asymmetric distribution of PL across the outer envelope membrane of spinach chloroplasts has been shown (Cline *et al.*, 1981; Block *et al.*, 1983). The absence of a proper thylakoid membrane system and the low content of assimilatory starch in plastids from *ala1* plants evidence this hypothesis. Furthermore, Masclaux-Daubresse *et al.* (2007) suggest the existence of complex interactions between chloroplasts and cold acclimation. Functional chloroplasts are required for cold acclimation and the regulation of the majority of cold-responsive genes, which might depend on photosystem II excitation pressure (Ensminger *et al.*, 2006). Disturbed thylakoid membranes lead to malfunctioning or reduced functioning of photosystem II, which might cause the cold-sensitive phenotype of *ala1* plants. Supporting this argumentation, the *ala1* phenotype is not fully recovered to wild type under elevated temperature as shown for the other *ala* lines (chapter 3.8.5). Finally, one possible explanation for the higher PG content in *ala1* plants might be an incorporation of PG, which is synthesized within plastids (Rawyler and Siegenthaler, 1981; Unitt and Harwood, 1982), into plastidial membranes due to a disturbed PL translocation in this cellular compartment.

PL asymmetry is vital for eukaryotic cells and a loss in plasma membrane lipid asymmetry marks the cell apoptotic resulting in its clearance (Williamson and Schlegel, 1994; Balasubramanian and Schroit, 2003). Transferred to cellular organelles the same principle might apply and plastids with a disturbed outer membrane asymmetry might be

marked for degradation explaining the existence of plastid-like structures within mesophyll cells of *ala1*. An alternative explanation for the existence of such structures might be a repulsion of the outer membrane due to a disturbed membrane lipid asymmetry followed by a degradation of thylakoids and the formation of plastoglobuli. However, the appearance of plastid-like structures can be related to a mutation in *ALA1* as the triple mutant line *ala1/10/11* likewise displayed this peculiarity (chapter 3.7.1). As a conclusion from this, the plastid-localized ALA1 represents an essential component for the establishment or maintenance of proper plastid morphology. The protein might be localized in the outer as well as the inner chloroplast membrane regulating the lipid composition and, thus, being responsible for membrane bending and vesiculation in both membrane systems.

4.6.2 ALA10 and ALA11

The single P_4-type ATPase mutants *ala10* and *ala11* exhibited a massive accumulation of abnormal membrane structures within leaf mesophyll cells (chapter 3.7.2). The membrane structures were similar to vesicles but larger in size (100-500 nm; whereas the normal vesicle size is 50-250 nm; Winkler *et al.*, 2005). The structures were either fully surrounded by cytoplasm or partly fused with the tonoplast of the central vacuole. Involvement of P_4-type ATPases in vesicle budding has been discussed intensely (Devaux, 1991; Chen *et al.*, 1999; Chantalat *et al.*, 2004; Pomorski *et al.*, 2004; Wicky *et al.*, 2004) and one might speculate that ALA10 and ALA11 are also involved in vesicle budding and/or in vesicle fusion with other cellular membranes. The discovery of abnormal membrane structures in *ala10* and *ala11* plants is in agreement with abnormal membrane-bound structures in the yeast P_4-type ATPase mutant ∆*drs2* (Chen *et al.*, 1999). However, the structures in ∆*drs2* cells represent double membrane rings with an average diameter of 240 nm and contain Golgi enzymes. Their morphology is comparable to Berkeley bodies that only occur in yeast due to a mutation in the secretory genes *sec7* and *sec14* (Novick *et al.*, 1980). Drs2p was localized to the late Golgi network affecting Golgi and endosome function (Chen *et al.*, 1999). *Arabidopsis thaliana* ALA3 is the closest Drs2p homolog (BLASTP at TAIR; http://www.arabidopsis.org; Altschul *et al.*, 1990) and was localized to the late Golgi network (Poulsen *et al.*, 2008b; Figure 41). Correspondingly, a mutant of this P_4-type ATPase displayed altered vesicle formation at the trans side of the Golgi apparatus. Furthermore, yeast mutants of the endosomal localized P_4-type ATPase Neo1p accumulated extremely aberrantly shaped membrane structures, such as multi-vesicular and ring-like tubular structures pointing out an important role of Neo1p in membrane trafficking (Wicky *et al.*, 2004). The yeast double

mutant Δ*drs2*Δ*dnf1*, where a late Golgi and a plasma membrane located P_4-type ATPase are affected revealed an even pronounced accumulation of membrane-bound structures compared to Δ*drs2* cells (Hua *et al.*, 2002). The closest *Arabidopsis* homologs to the plasma membrane localized Dnf2p protein are ALA8, ALA12 and ALA10 (BLASTP). ALA10 and ALA11 are very similar and cluster phylogenetically with ALA8, ALA12 and ALA9 in one subgroup (Baxter *et al.*, 2003). Transferring these observations to P_4-type ATPases in plants that are putatively localized to the plasma membrane, the prominent alterations in membrane-bound structures in cells of *ala10* and *ala11* mutants seem plausible and indicate an important role of these proteins in membrane trafficking. Yet the process leading to the formation of the abnormal membrane structures is not understood. The double mutant *ala10/11* as well as the triple mutant *ala1/10/11* displayed even more unusual and bizarre membrane structures that were often similar to multi-vesicular structures extending into the lumen of the vacuole. It seemed that these vesicle-like structures were ingested into the vacuole by a process similar to protrusion autophagy (Bassham *et al.*, 2006) involving multiple membrane fusion events that lead to the found intensely membrane interspersed structures. Alternatively, ALA10 and ALA11 might circulate between the plasma membrane and the tonoplast (Figure 41). Circulation of P_4-type ATPases between different membranes was shown for yeast Drs2p, which oscillates between the trans Golgi, endosomes and the plasma membrane (Saito *et al.*, 2004). Additionally, there is evidence that the closely related Dnf1p might oscillate between the plasma membrane and endosomal membranes.

One may furthermore speculate about the origin of the vesicle-like structures. Very likely cellular membranes are delivered via vesicles from the ER, where lipids are synthesized, through the Golgi network to their final destination, i.e. to a great extent the plasma membrane but also the tonoplast (reviewed in van Meer, 2000; Quinn, 2002). Additionally, the plasma membrane invaginates forming endosomes, which are transported to the central vacuole. Moreover, the central vacuole is the destination of final products of chlorophyll catabolism during senescence (Matile *et al.*, 1999; Thomas *et al.*, 2001) via endosomal structures named Rubisco-containing or Rubisco-vesicular bodies (Chiba *et al.*, 2003; Otegui *et al.*, 2005; Prins *et al.*, 2008). Currently, it is impossible to rule out which of these vesicular processes is deregulated in *ala10* and *ala11* mutants. Yeast Δ*drs2* cells display an endocytic defect attributable to a deregulation in the endosome-to-vacuole pathway rather than the clathrin-dependent endocytosis from the plasma membrane (Chen *et al.*, 1999). Although further details on vesicular alterations in *ala10* and *ala11* mutants are missing, it can be assumed that ALA10 and ALA11 are contribute to the maintenance of normal membrane structure and function.

As discussed above, *ala10* and *ala11* plants show premature senescence. Interestingly, mutants in autophagy genes (*ATG*) also display these symptoms (Doelling *et al.*, 2002; Hanaoka *et al.*, 2002; Yoshimoto *et al.*, 2004; Thompson and Vierstra, 2005;

Xiong *et al.*, 2005). The premature senescence phenotype of *atg* mutants is still unexplainable and has been interpreted as a mechanism to compensate for the failure to remobilize cytosolic nitrogen under stress conditions, indicating that autophagy is not essential for the senescence program but plays an important role in nutrient remobilization. Similarly, it can be argued that ALA10 and ALA11 proteins are not essential for the senescence program but are crucial for remobilization processes that take place during senescence involving massive vesiculation. In concordance with *atg* mutants exhibiting increased chlorosis and enhanced dark-induced senescence (Doelling *et al.*, 2002; Hanaoka *et al.*, 2002; Xiong *et al.*, 2005), *ala* mutants failed to regreen senescent leaves after dark treatment (chapter 3.8.3). Cell activities such as endocytosis and autophagy involve multiple membrane fusion events and are likely to induce transient lipid intermixing between membrane leaflets (Balasubramanian and Schroit, 2003). In order to correct these potential imbalances, lipid translocating P_4-type ATPases such as ALA10 and ALA11 might be one mechanism to restore and maintain an appropriate asymmetric aminophospholipid distribution of cellular membranes.

4.6.3 Other ALA members

Cellular organelles are relatively early affected during senescence and become degraded. Mitochondria, however, remain intact until late during the process in order to fulfill the energy requirements of the senescence program (Thomson and Platt-Aloia, 1987; Noodén, 1988). Daum and Vance (1997) and Shiao *et al.* (1998) propose a mitochondrial membrane protein that is required for the translocation of PS and PE from mitochondria-associated ER membranes to the organelles that is stimulated by magnesium. Furthermore, Quinn (2002) stated that this PL translocating enzyme belongs to the group of P-type ATPases. ALA2 might be designated to this function (Figure 41) due to its isolated position in the phylogenetic tree (Figure 6). Furthermore, expression data revealed a 6-fold increase in transcript amounts during senescence (van der Graaff *et al.*, 2006).

Lipid asymmetry has been furthermore reported for the outer membrane leaflet of other cellular organelles, e.g. peroxisomes (Cheesebrough and Moore, 1980; Dorne *et al.*, 1985) suggesting the existence of PL translocating enzymes in these organelles as well. To date, no P_4-ATPase has been identified in the ER and the characterization of P_4-type ATPases, which is the largest subfamily of P-type ATPases in eukaryotes, remains the least characterized group of these pumps in all systems.

4.7 Conclusion

The results presented in this thesis indicate that three aminophospholipid translocases, ALA1, ALA10 and ALA11, play a role within the senescence process of *Arabidopsis thaliana*. The genes display an up-regulation during the senescence process in rosette leaves but are also expressed in young seedlings. Mutants of the genes present pleiotropic phenotypical alterations but most strikingly premature senescence. The symptoms are confirmed at a genetical, physiological and molecular level. The enzymes may be responsible for the establishment of proper asymmetric membranes in young cells and, more importantly, the maintenance of cellular membrane asymmetry during the senescence process. It is assumed that the pleiotropic phenotypes of *ala* mutants are caused by a deregulated membrane asymmetry.

Mutants of *ala1* display an altered plastid morphology matching the plastidial localization of ALA1 and, thus, rendering the protein as an essential component for the maintenance of proper plastid development. It is conceivable that ALA1 is specifically involved in the maintenance of asymmetric plastidial membranes and the recycling of degradation products within senescing plastids via vesiculation. In deviation to that, *ala10* and *ala11* mutants display abnormal membrane structures within mesophyll cells demonstrating an important role of these P_4-type ATPases in the establishment and maintenance of cellular membrane asymmetry. Localization experiments indicate that the proteins may localize to the plasma membrane or the tonoplast. The proteins may possibly oscillate between the two membrane systems. ALA10 and ALA11 are thought to be responsible for the restoration and maintenance of an appropriate asymmetric aminophospholipid distribution especially during vesiculatory processes. However, their exact role remains unclear. The obtained results indicate furthermore that there is a causative relation between cultivation temperature and *ala* mutant phenotype most likely via an altered membrane asymmetry, which influences in return plant growth and senescence. The investigations revealed that the three ALA proteins play a role in cold tolerance and plant growth via the distribution of phospholipids (PL) with unsaturated fatty acids (FA). Additionally, the results evidence that ALA proteins do not display any substrate specificity for lipids with certain acyl chains.

Concluding it can be said that ALA proteins integrate several factors affecting plant fitness, thus, rendering the proteins as a necessary component for proper cell growth, adaptation to various stresses and an unimpaired progression of the senescence program. The proteins participate in these highly complex processes most probably via regulation of the cellular membrane lipid asymmetry and, thus, influencing vesiculation.

5 SUMMARY

Foliar senescence is an essential aspect within the development of plant leaves. During the past years, scientific research has been focusing on the understanding of the molecular mechanisms underlying senescence. Membrane localized transporters are thought to be necessary items during this highly regulated developmental program. Expression profiling of genes coding for membrane proteins revealed increased transcript amounts of three *ALA* genes (*ALA1*, *ALA10* and *ALA11*) during leaf senescence of *Arabidopsis thaliana*. The genes represent P_4-type ATPases that are supposed to translocate aminophospholipids between the two leaflets of biological membranes and, thus, generating asymmetric membranes and inducing vesiculation.

In order to characterize ALA1, ALA10 and ALA11, a reverse genetic approach was applied using T-DNA insertional mutants. In this work, the corresponding insertion lines were isolated and identified (*ala1*, *ala10* and *ala11*) and, to recognize functional redundancy among the ALA members, multiple mutant lines were generated (*ala10/11* and *ala1/10/11*). The mutant lines were phenotypically analyzed regarding their development with a special focus on the nature and progression of senescence.

Surprisingly, all investigated mutants displayed premature senescence symptoms at a genetical, physiological and molecular level revealing an important role of the three ALA members for a controlled and unimpaired progression of the senescence process. The premature senescence was accompanied by reduced growth at the plant and cellular level most probably due to deregulated membrane asymmetry.

ALA1 localized to plastids and confirming this finding, *ala1* displayed an altered plastid morphology lacking grana stacks. It is assumed that the protein is an essential component for proper plastid development. Mutants of *ala10* and *ala11* displayed abnormal membrane structures within mesophyll cells hinting for an important role of these P_4-type ATPases in the maintenance of proper membrane function. Experiments indicated that the proteins might localize to the plasma mebrane or the tonoplast, possibly oscillating between the two membrane systems.

Lipid analysis indicated that ALA proteins have no specificity for lipids with certain acyl chains. Moreover, the investigations revealed that the proteins play a role in cold tolerance and plant growth via the distribution of lipid-bound fatty acids within cellular membranes.

In summary, the investigation of ALA1, ALA10 and ALA11 gave new indications for processes in which P_4-type ATPases are involved most probably via regulations of the membrane lipid asymmetry and, thus, contribute to the actual limited knowledge of this protein family in plants.

6 ZUSAMMENFASSUNG

Die Seneszenz stellt eine wesentliche Entwicklungsphase von pflanzlichen Blättern dar. In den vergangenen Jahren begann sich die wissenschaftliche Forschung auf das Verständnis der molekularen Mechanismen zu konzentrieren, die diesem hoch regulierten Prozess zugrunde liegen. Hierbei wird membranassoziierten Transportern eine besondere Rolle zugeschrieben. Durch die Untersuchung von Genen, die für Transmembranproteine kodieren, stellte sich heraus, dass drei Gene der *ALA* Familie (*ALA1*, *ALA10* und *ALA11*) während der Blattseneszenz von Arabidopsis thaliana besonders erhöhte Transkriptmengen aufweisen. Die Gene stellen P_4-Typ ATPasen dar, welche vermutlich für die Translokation von Aminophospholipiden innerhalb der beiden Hälften von biologischen Membranen verantwortlich sind und somit asymmetrische Membranen generieren und vesikuläre Prozesse induzieren.

Um ALA1, 10 und 11 näher zu charakterisieren, wurde ein revers-genetischer Ansatz basierend auf T-DNA Insertionsmutanten gewählt. In dieser Arbeit wurden die entsprechenden Insertionslinien isoliert, identifiziert (*ala1*, *10* und *11*) und, um funktionelle Redundanzen unter den ALA Mitgliedern aufzuzeigen, Mehrfachmutanten (*ala10/11* und *ala1/10/11*) erzeugt. Die Mutanten wurden bezüglich ihres Phänotyps untersucht, wobei ein besonderes Augenmerk auf die Art und Weise sowie den Verlauf der Seneszenz gelegt wurde.

Überraschenderweise zeigten die untersuchten Mutanten eine verfrüht einsetzende Seneszenz, welche auf genetischer, molekularer und physiologischer Ebene nachgewiesen werden konnte. Dies lässt auf eine wichtige Rolle der drei ALA Mitglieder für einen kontrollierten und ungestörten Ablauf der Seneszenz schließen. Die verfrühte Seneszenz der Mutanten wurde von einer Wachstumsreduktion begleitet, welche auch auf zellulärer Ebene zu verzeichnen war und vermutlich durch deregulierte Membranasymmetrie hervorgerufen wird.

ALA1 konnte plastidär lokalisiert werden und es liegt nahe, dass das Protein eine essentielle Komponente für eine ungestörte Plastidentwicklung darstellt. Fehlende Granastapel in Plastiden von *ala1* Mutanten sowie weitere Störungen in der Plastidmorphologie stützen diesen Befund. *ala10* und *ala11* Mutanten wiesen abnormale Membranstrukturen in Mesophyllzellen auf, was auf eine wichtige Rolle von P_4-Typ ATPasen in der Aufrechterhaltung der normalen Membranfunktion schließen lässt. Die Untersuchungen deuten darauf hin, dass die Proteine in der Plasmamembran oder im Tonoplasten lokalisieren und möglicherweise zwischen beiden Membransystemen oszillieren.

Lipidanalysen ergaben, dass ALA Proteine keine Spezifität für Lipide mit bestimmten Acylketten aufweisen. Weiterhin konnte gezeigt werden, dass die Proteine in Kältetoleranz und Pflanzenwachstum involviert sind, indem sie die Verteilung von lipidgebundenen Fettsäuren in zellulären Membranen steuern.

Zusammenfassend ergaben die Untersuchungen an ALA1, 10 und 11 neue Einsichten in Prozesse, an welchen P_4-Typ ATPasen beteiligt sind, was mit großer Wahrscheinlichkeit über die Regulation der Membranlipidasymmetrie erfolgt, wodurch das aktuell verfügbare Wissen über diese Proteinfamilie erweitert werden konnte.

7 REFERENCES

Alder-Baerens, N., Lisman, Q., Luong, L., Pomorski, T., and Holthuis, J.C. (2006). Loss of P4 ATPases Drs2p and Dnf3p disrupts aminophospholipid transport and asymmetry in yeast post-Golgi secretory vesicles. Molecular Biology of the Cell **17,** 1632-1642.

Alonso, J.M., Stepanova, A.N., Leisse, T.J., Kim, C.J., Chen, H., Shinn, P., Stevenson, D.K., Zimmerman, J., Barajas, P., Cheuk, R., Gadrinab, C., Heller, C., Jeske, A., Koesema, E., Meyers, C.C., Parker, H., Prednis, L., Ansari, Y., Choy, N., Deen, H., Geralt, M., Hazari, N., Hom, E., Karnes, M., Mulholland, C., Ndubaku, R., Schmidt, I., Guzman, P., Aguilar-Henonin, L., Schmid, M., Weigel, D., Carter, D.E., Marchand, T., Risseeuw, E., Brogden, D., Zeko, A., Crosby, W.L., Berry, C.C., and Ecker, J.R. (2003). Genome-wide insertional mutagenesis of *Arabidopsis thaliana*. Science **301,** 653-657.

Altschul, S.F., Gish, W., Miller, W., Myers, E.W., and Lipman, D.J. (1990). Basic local alignment search tool. Journal of Molecular Biology **215,** 403-410.

An, Y.Q., McDowell, J.M., Huang, S.R., McKinney, E.C., Chambliss, S., and Meagher, R.B. (1996). Strong, constitutive expression of the *Arabidopsis ACT2/ACT8* actin subclass in vegetative tissues. The Plant Journal **10,** 107-121.

Andersson, M.X., Stridh, M.H., Larsson, K.E., Liljenberg, C., and Sandelius, A.S. (2003). Phosphate-deficient oat replaces a major portion of the plasma membrane phospholipids with the galactolipid digalactosyldiacylglycerol. FEBS Letters **537,** 128-132.

Apell, H.J. (2004). How do P-type ATPases transport ions? Bioelectrochemistry **65,** 149-156.

Arnon, D.I., and Hoagland, D.R. (1940). Crop production in artificial culture solutions and in soils with special reference to factors influencing yields and absorption of inorganic nutrients. Soil Science **50,** 463-485.

Ausubel, F.M., Brent, R., Kingston, R.E., Moore, D.D., Seidman, J.G., Smith, J., A., and Struhl, K. (1989). Short protocols in molecular biology: A compendium of methods from "Current Protocols in Molecular Biology". (New York City, NY, USA: John Wiley and Sons).

Axelsen, K.B., and Palmgren, M.G. (1998). Evolution of substrate specificities in the P-type ATPase superfamily. Journal of Molecular Evolution **46,** 84-101.

Balasubramanian, K., and Schroit, A.J. (2003). Aminophospholipid asymmetry: A matter of life and death. Annual Review of Physiology **65,** 701-734.

Balazadeh, S., Riaño-Pachón, D.M., and Mueller-Roeber, B. (2008). Transcription factors regulating leaf senescence in *Arabidopsis thaliana*. Plant Biology **10,** 63-75.

Balhadere, P.V., and Talbot, N.J. (2001). *PDE1* encodes a P-type ATPase involved in appressorium-mediated plant infection by the rice blast fungus *Magnaporthe grisea*. The Plant Cell **13,** 1987-2004.

Barber, R.F., and Thompson, J.E. (1980). Senescence-dependent increase in the permeability of liposomes prepared from bean cotyledon membranes. Journal of Experimental Botany **31,** 1305-1313.

Bassham, D.C., Laporte, M., Marty, F., Moriyasu, Y., Ohsumi, Y., Olsen, L.J., and Yoshimoto, K. (2006). Autophagy in development and stress responses of plants. Autophagy **2,** 2-11.

Baulcombe, D.C., Saunders, G.R., Bevan, M.W., Mayo, M.A., and Harrison, B.D. (1986). Expression of biologically active viral satellite RNA from the nuclear genome of transformed plants. Nature **321,** 446-449.

Baulcombe, D.C., Chapman, S., and Santa Cruz, S. (1995). Jellyfish green fluorescent protein as a reporter for virus infections. The Plant Journal **7,** 1045-1053.

Baxter, I., Tchieu, J., Sussman, M.R., Boutry, M., Palmgren, M.G., Gribskov, M., Harper, J.F., and Axelsen, K.B. (2003). Genomic comparison of P-type ATPase ion pumps in *Arabidopsis* and rice. Plant Physiology **132,** 618-628.

Becker, W., and Apel, K. (1993). Differences in gene expression between natural and artificially induced leaf senescence. Planta **189,** 74-79.

Bell, R.M., Ballas, L.M., and Coleman, R.A. (1981). Lipid topogenesis. Journal of Lipid Research **22,** 391-403.

Berleth, T., and Jurgens, G. (1993). The role of the monopteros gene in organizing the basal body region of the *Arabidopsis* embryo. Development **118,** 575-587.

Bertani, G. (1951). Studies on lysogenesis 1. The mode of phage liberation by lysogenic *Escherichia coli*. Journal of Bacteriology **62,** 293-300.

Bevers, E.M., Comfurius, P., Dekkers, D.W., and Zwaal, R.F. (1999). Lipid translocation across the plasma membrane of mammalian cells. Biochimica et Biophysica Acta **1439,** 317-330.

Birnboim, H.C., and Doly, J. (1979). Rapid alkaline extraction procedure for screening recombinant plasmid DNA. Nucleic Acids Research **7,** 1513-1523.

Bishop, W.R., and Bell, R.M. (1985). Assembly of the endoplasmic reticulum phospholipid bilayer: The phosphatidylcholine transporter. Cell **42,** 51-60.

Biswal, U.C., Biswal, B., and Raval, M.K. (2003). Chloroplast biogenesis: From plastid to gerontoplast. (Dodrecht, The Netherlands: Kluwer Academic Publishers).

Blank, A., and McKeon, T.A. (1991a). Three RNases in senescent and nonsenescent wheat leaves: Characterization by activity staining in sodium dodecyl sulfate polyacrylamide gels. Plant Physiology **97,** 1402-1408.

Blank, A., and McKeon, T.A. (1991b). Expression of three RNase activities during natural and dark-induced senescence of wheat leaves. Plant Physiology **97,** 1409-1413.

Bleecker, A.B. (1998). The evolutionary basis of leaf senescence: Method to the madness? Current Opinion in Plant Biology **1,** 73-78.

Block, M.A., Dorne, A.J., Joyard, J., and Douce, R. (1983). Preparation and characterization of membrane fractions enriched in outer and inner envelope membranes from spinach chloroplasts. II. Biochemical characterization. Journal of Biological Chemistry **258,** 13281-13286.

Borochov, A., Halevy, A.H., and Shinitzky, M. (1982). Senescence and the fluidity of rose petal membranes - relationship to phospholipid-metabolism. Plant Physiology **69,** 296-299.

Bouche, N., and Bouchez, D. (2001). *Arabidopsis* gene knockout: phenotypes wanted. Current Opinion in Plant Biology **4,** 111-117.

Boyes, D.C., Zayed, A.M., Ascenzi, R., McCaskill, A.J., Hoffman, N.E., Davis, K.R., and Görlach, J. (2001). Growth stage-based phenotypic analysis of *Arabidopsis*: A model for high troughput functional genomics in plants. The Plant Cell **13,** 1499-1510.

Bradford, M.M. (1976). Rapid and sensitive method for quantitation of microgram quantities of protein utilizing principle of protein-dye binding. Analytical Biochemistry **72,** 248-254.

Bretscher, M.S. (1972). Asymmetrical lipid bilayer structure for biological membranes. Nature-New Biology **236,** 11-12.

Brown, D.L., and Weier, T.E. (1968). Chloroplast development and ultrastructure in the freshwater red alga *Batrachospermum*. Journal of Phycology **4,** 199-206.

Browse, J., and Somerville, C. (1991). Glycerolipid synthesis: Biochemistry and regulation. Annual Review of Plant Physiology and Plant Molecular Biology **42,** 467-506.

Browse, J., and Somerville, C.R. (1994). Glycerolipids. In Arabidopsis, E.M. Meyerowitz and C.R. Somerville, eds (Cold Spring Harbor, NY, USA: Cold Spring Harbor Laboratory Press), pp. 881-912.

Browse, J., Mccourt, P.J., and Somerville, C.R. (1986). Fattyacid composition of leaf lipids determined after combined digestion and fattyacid methyl-ester formation from fresh tissue. Analytical Biochemistry **152,** 141-145.

Buchanan-Wollaston, V., and Ainsworth, C. (1997). Leaf senescence in *Brassica napus*: Cloning of senescence related genes by subtractive hybridisation. Plant Molecular Biology **33,** 821-834.

Buchanan-Wollaston, V., Earl, S., Harrison, E., Mathas, E., Navabpour, S., Page, T., and Pink, D. (2003). The molecular analysis of leaf senescence – a genomics approach. Plant Biotechnology Journal **1,** 3-22.

Buchanan-Wollaston, V., Page, T., Harrison, E., Breeze, E., Lim, P.O., Nam, H.G., Lin, J.F., Wu, S.H., Swidzinski, J., Ishizaki, K., and Leaver, C.J. (2005). Comparative transcriptome analysis reveals significant differences in gene expression and signalling pathways between developmental and dark/starvation-induced senescence in *Arabidopsis*. The Plant Journal **42,** 567-585.

Burton, X., Morrot, G., Fellmann, P., and Seigneuret, M. (1996). Ultrafast glycerophospholipid-selective transbilayer motion mediated by a protein in the endoplasmic reticulum membrane. Journal of Biological Chemistry **271,** 6651-6657.

Canut, H., Alibert, G., and M., B.A. (1985). Hydrolysis of intracellular proteins in vacuoles isolated from *Acer pseudoplatanus* L. cells. Plant Physiology **79,** 1090-1093.

Cao, J., Jiang, F., Sodmergen, and Cui, K. (2003). Time-course of programmed cell death during senescence in *Eucommia ulmoides*. Journal of Plant Research **116,** 7-12.

Cevc, G. (1991). How membrane chain-melting phase-transition temperature is affected by the lipid chain asymmetry and degree of unsaturation: An effective chain-length model. Biochemistry **30,** 7186-7193.

Chalfie, M., Tu, Y., Euskirchen, G., Ward, W.W., and Prasher, D.C. (1994). Green Fluorescent protein as a marker for gene-expression. Science **263,** 802-805.

Chantalat, S., Park, S.K., Hua, Z., Liu, K., Gobin, R., Peyroche, A., Rambourg, A., Graham, T.R., and Jackson, C.L. (2004). The Arf activator Gea2p and the P-type ATPase Drs2p interact at the Golgi in *Saccharomyces cerevisiae*. Journal of Cell Science **117,** 711-712.

Cheesebrough, T.M., and Moore, T.S. (1980). Transverse distribution of phospholipids in organelle membranes from *Ricinus communis* L. var. Hale endosperm: Mitochondria and glyoxysomes. Plant Physiology **65,** 1076-1080.

Chen, C.Y., Ingram, M.F., Rosal, P.H., and Graham, T.R. (1999). Role for Drs2p, a P-type ATPase and potential aminophospholipid translocase, in yeast late Golgi function. Journal of Cell Biology **147,** 1223-1236.

Chiba, A., Ishida, H., Nishizawa, N.K., Makino, A., and Mae, T. (2003). Exclusion of ribulose-1,5-bisphosphate carboxylase/oxygenase from chloroplasts by specific bodies in naturally senescing leaves of wheat. Plant and Cell Physiology **44,** 914-921.

Chomczynski, P., and Sacchi, N. (1987). Single-step method of RNA isolation by acid guanidinium thiocyanate-phenol-chloroform extraction. Analytical Biochemistry **162,** 156-159.

Cline, K., Andrews, J., Mersey, B., Newcomb, E.H., and Keegstra, K. (1981). Separation and characterization of inner and outer envelope membranes of pea chloroplasts. Proceedings of the National Academy of Sciences of the United States of America **78,** 3595-3599.

Clough, S.J., and Bent, A.F. (1998). Floral dip: a simplified method for *Agrobacterium*-mediated transformation of *Arabidopsis thaliana*. The Plant Journal **16,** 735-743.

Cossins, A.R. (1994). Temperature adaptation of biological membranes. (London, UK: Portland Press).

Costanzo, M.C., Crawford, M.E., Hirschman, J.E., Kranz, J.E., Olsen, P., Robertson, L.S., Skrzypek, M.S., Braun, B.R., Hopkins, K.L., Kondu, P., Lengieza, C., Lew-Smith, J.E., Tillberg, M., and Garrels, J.I. (2001). YPD, PombePD and WormPD: Model organism volumes of the BioKnowledge library, an integrated resource for protein information. Nucleic Acids Research **29,** 75-79.

Dai, N., Schaffer, A., Petreikov, M., Shahak, Y., Giller, Y., Ratner, K., Levine, A., and Granot, D. (1999). Overexpression of *Arabidopsis* hexokinase in tomato plants inhibits growth, reduces photosynthesis, and induces rapid senescence. The Plant Cell **11,** 1253-1266.

Daleke, D.L. (2003). Regulation of transbilayer plasma membrane phospholipid asymmetry. Journal of Lipid Research **44,** 233-242.

Daleke, D.L. (2007). Phospholipid flippases. Journal of Biological Chemistry **282,** 821-825.

Daleke, D.L., and Huestis, W.H. (1985). Incorporation and translocation of aminophospholipids in human erythrocytes. Biochemistry **24,** 5406-5416.

Daum, G., and Vance, J.E. (1997). Import of lipids into mitochondria. Progress in Lipid Research **36,** 103-130.

De Block, M., Botterman, J., Vandewiele, M., Dockx, J., Thoen, C., Gosselé, V., Rao Movva, N., Thompson, C., Van Montagu, M., and Leemans, J. (1987). Engineering herbicide resistance in plants by expression of a detoxifying enzyme. EMBO Journal **6,** 2513-2518.

De Veylder, L., Beeckman, T., Beemster, G.T.S., Krols, L., Terras, F., Landrieu, I., Van Der Schueren, E., Maes, S., Naudts, M., and Inze, D. (2001). Functional analysis of cyclin-dependent kinase inhibitors of *Arabidopsis*. The Plant Cell **13,** 1653-1668.

del Río, L.A., Pastori, G.M., Palma, J.M., Sandalio, L.M., Sevilla, F., Corpas, F.J., Jiménez, A., López-Huertas, E., and Hernández, J.A. (1998). The activated oxygen role of peroxisomes in senescence. Plant Physiology **116,** 1195-2000.

Dellaporta, S.L., Wood, J., and Hicks, J.B. (1983). A plant DNA minipreparation: Version II. Plant Molecular Biology Reporter **1,** 19-21.

Desai, U.J., and Pfaffle, P.K. (1995). Single-step purification of a thermostable DNA polymerase expressed in *Escherichia coli*. Biotechniques **19,** 780, 782, 784.

Devaux, P.F. (1991). Static and dynamic lipid asymmetry in cell membranes. Biochemistry **30,** 1163-1173.

Devaux, P.F., López-Montero, I., and Bryde, S. (2006). Proteins involved in lipid translocation in eukaryotic cells. Chem Phys Lipids **141,** 119-132.

Devaux, P.F., Herrmann, A., Ohlwein, N., and Kozlov, M.M. (2008). How lipid flippases can modulate membrane structure. Biochimica et Biophysica Acta **1778,** 1591-1600.

Diaz, C., Purdy, S., Christ, A., Morot-Gaudry, J.F., Wingler, A., and Masclaux-Daubresse, C. (2005). Characterization of markers to determine the extent and variability of leaf senescence in *Arabidopsis*. A metabolic profiling approach. Plant Physiology **138,** 898-908.

Diaz, C., Saliba-Colombani, V., Loudet, O., Belluomo, P., Moreau, L., Daniel-Vedele, F., Morot-Gaudry, J.F., and Masclaux-Daubresse, C. (2006). Leaf yellowing and anthocyanin accumulation are two genetically independent strategies in response to nitrogen limitation in *Arabidopsis thaliana*. Plant and Cell Physiology **47,** 74-83.

Ding, J.T., Wu, Z., Crider, B.P., Ma, Y.M., Li, X.J., Slaughter, C., Gong, L.M., and Xie, X.S. (2000). Identification and functional expression of four isoforms of ATPase II, the putative aminophospholipid translocase - Effect of isoform variation on the ATPase activity and phospholipid specificity. Journal of Biological Chemistry **275,** 23378-23386.

Döbereiner, H.G., Käs, J., Noppl, D., Sprengler, I., and Sackmann, E. (1993). Budding and fission of vesicles. Biophysical Journal **65,** 1396-1403.

Doelling, J.H., Walker, J.M., Friedman, E.M., Thompson, A.R., and Vierstra, R.D. (2002). The APG8/12-activating enzyme APG7 is required for proper nutrient recycling and senescence in *Arabidopsis thaliana*. Journal of Biological Chemistry **277,** 33105-33114.

Don, R.H., Cox, P.T., Wainwright, B.J., Baker, K., and Mattick, J.S. (1991). Touchdown PCR to circumvent spurious priming during gene amplification. Nucleic Acids Research **19,** 4008.

Dormann, P., Voelker, T.A., and Ohlrogge, J.B. (1995a). Cloning and Expression in *Escherichia coli* of a novel thioesterase from *Arabidopsis thaliana* specific for long-chain acyl-acyl carrier proteins. Archives of Biochemistry and Biophysics **316,** 612-618.

Dormann, P., Hoffmannbenning, S., Balbo, I., and Benning, C. (1995b). Isolation and characterization of an *Arabidopsis* mutant deficient in the thylakoid lipid digalactosyl diacylglycerol. The Plant Cell **7,** 1801-1810.

Dorne, A.J., Joyard, J., Block, M.A., and Douce, R. (1985). Localization of phosphatidylcholine in outer envelope membrane of spinach chloroplasts. Journal of Cell Biology **100,** 1690-1697.

Dower, W.J., Miller, J.F., and Ragsdale, C.W. (1988). High efficiency transformation of *Escherichia coli* by high voltage electroporation. Nucleic Acids Research **16,** 6127-6146.

Ensminger, I., Busch, F., and Huner, N.P.A. (2006). Photostasis and cold acclimation: Sensing low temperature through photosynthesis. Physiologia Plantarum **126,** 28-44.

Eulgem, T., and Somssich, I.E. (2007). Networks of WRKY transcription factors in defence signalling. Current Opinion in Plant Biology **10,** 366-371.

Eulgem, T., Rushton, P.J., Robatzek, S., and Somssich, I.E. (2000). The WRKY superfamily of plant transcription factors. Trends in Plant Science **5,** 199-206.

Falcone, D.L., Ogas, J.P., and Somerville, C.R. (2004). Regulation of membrane fatty acid composition by temperature in mutants of *Arabidopsis* with alterations in membrane lipid composition. BMC Plant Biology **17,** 17.

Fan, L., Zheng, S., and Wang, X. (1997). Antisense suppression of phospholipase D retards abscisic acid- and ethylene-promoted senescence of postharvest *Arabidopsis* leaves. The Plant Cell **9,** 2183-2196.

Fan, S.C., Lin, C.S., Hsu, P.K., Lin, S.H., and Tsay, Y.F. (2009). The *Arabidopsis* nitrate transporter NRT1.7, expressed in phloem, is responsible for source-to-sink remobilization of nitrate. The Plant Cell **21,** 2750-2761.

Farge, E. (1995). Increased vesicle endocytosis due to an increase in the plasma membrane phosphatidylserine concentration. Biophysical Journal **69,** 2501-2506.

Feldmann, K.A. (1991). T-DNA insertion mutagenesis in *Arabidopsis*: Mutational spectrum. The Plant Journal **1,** 71-82.

Feldmann, K.A., Marks, M.D., Christianson, M.L., and Quatrano, R.S. (1989). A dwarf mutant of *Arabidopsis* generated by T-DNA insertional mutagenesis. Science **243,** 1351-1354.

Feller, U., Anders, I., and Mae, T. (2008). Rubiscolytics: Fate of Rubisco after its enzymatic function in a cell is terminated. Journal of Experimental Botany **59,** 1615-1624.

Frentzen, M. (1990). Comparison of certain properties of membrane bound and solubilized acyltransferase activities of plant microsomes. Plant Science **69,** 39-48.

Friedrich, J.W., and Huffacker, R.C. (1980). Photosynthesis, leaf resistances, and ribulose-1,5-bisphosphate carboxylase degradation in senescing barley leaves. Plant Physiology **65,** 1103-1107.

Gall, W.E., Goething, N.C., Hua, Z.L., Ingram, M.F., Liu, K., Chen, S.I., and Graham, T.R. (2002). Drs2p-dependent formation of exocytic clathrin-coated vesicles *in vivo*. Current Biology **12,** 1623-1627.

Gan, S. (2003). Mitotic and postmitotic senescence in plants. Science of Aging Knowledge Environment **38,** RE7.

Gan, S., and Amasino, R.M. (1997). Making sense of senescence - Molecular genetic regulation and manipulation of leaf senescence. Plant Physiology **113,** 313-319.

Geering, K. (2001). The functional role of beta subunits in oligomeric P-type ATPases. Journal of Bioenergetics and Biomembranes **33,** 425-438.

Gepstein, S. (2004). Leaf senescence--not just a 'wear and tear' phenomenon. Genome Biology **5,** 212-212.213.

Gietz, R.D., and Woods, R.A. (2002). Transformation of yeast by lithium acetate/ single-stranded carrier DNA/polyethylene glycol method. Methods in Enzymology **350,** 87-96.

Gomès, E., Jakobsen, M.K., Axelsen, K.B., Geisler, M., and Palmgren, M.G. (2000). Chilling tolerance in *Arabidopsis* involves *ALA1*, a member of a new family of putative aminophospholipid translocases. The Plant Cell **12,** 2441-2454.

Graham, I.A., and Eastmond, P.J. (2002). Pathways of straight and branched chain fatty acid catabolism in higher plants. Progress in Lipid Research **41,** 156-181.

Graham, T.R. (2004). Flippases and vesicle-mediated protein transport. Trends in Cell Biology **14,** 670-677.

Grbic, V. (2003). SAG2 and SAG12 protein expression in senescing *Arabidopsis* plants. Physiologia Plantarum **119,** 263-269.

Grover, A. (1993). How do senescing leaves lose photosynthetic activity? Current Science **64,** 226-233.

Guiamét, J.J. (2004). Whole plant senescence. In Plant Cell Death Processes, L.D. Noodén, ed (Amsterdam, The Netherlands: Elsevier Academic Press), pp. 227-244.

Guiulietti, A., Overbergh, L., Valckx, D., Decallonne, B., Bouillon, R., and Mathieu, C. (2001). An overview of real-time quantitative PCR: Applications to quantify cytokine gene expression. Methods **25,** 386-401.

Guo, Y., and Gan, S. (2005). Leaf senescence: Signals, execution, and regulation. Current Topics in Developmental Biology **71,** 83-112.

Guo, Y., and Gan, S. (2006). AtNAP, a NAC family transcription factor, has an important role in leaf senescence. The Plant Journal **46,** 601-612.

Guo, Y., Cai, Z., and Gan, S. (2004). Transcriptome of *Arabidopsis* leaf senescence. Plant, Cell and Environment **27,** 521-549.

Hajdukiewicz, P., Svab, Z., and Maliga, P. (1994). The small, versatile pPZP family of *Agrobacterium* binary vectors for plant transformation. Plant Molecular Biology **25,** 989-994.

Hanahan, D. (1983). Studies on transformation of *Escherichia coli* with plasmids. Journal of Molecular Biology **166,** 557-580.

Hanaoka, H., Noda, T., Shirano, Y., Kato, T., Hayashi, H., Shibata, D., Tabata, S., and Ohsumi, Y. (2002). Leaf senescence and starvation-induced chlorosis are accelerated by the disruption of an *Arabidopsis* autophagy gene. Plant Physiology **129,** 1181-1193.

Hanfrey, C., Fife, M., and Buchanan-Wollaston, V. (1996). Leaf senescence in Brassica napus: Expression of genes encoding pathogenesis-related proteins. Plant Molecular Biology **30,** 597-609.

Haritatos, E., Ayre, B.G., and Turgeon, R. (2000). Identification of phloem involved in assimilate loading in leaves by the activity of the galactinol synthase promoter. Plant Physiology **123,** 929-937.

Hazel, J.R. (1995). Thermal adaptation in biological membranes: Is homeoviscous adaptation the explanation? Annual Review of Physiology **57,** 19-42.

He, Y., Tang, W., Swain, J.D., Green, A.L., Jack, T.P., and Gan, S. (2001). Networking senescence-regulating pathways by using *Arabidopsis* enhancer trap lines. Plant Physiology **126,** 707-716.

Heinz, E. (1993). Biosynthesis of polyunsaturated fatty acids. In Lipid metabolism in plants, T.S. Moore, ed (Boca Raton, FL, USA: CRC Press), pp. 33-90.

Hennegan, K.P., and Danna, K.J. (1998). pBIN20: An improved binary vector for shape *Agrobacterium*-mediated transformation. Plant Molecular Biology Reporter **16,** 129-131.

Hensel, L.L., Grbic, V., Baumgarten, D.A., and Bleecker, A.B. (1993). Developmental and age-related processes that influence the longevity and senescence of photosynthetic tissues in *Arabidopsis*. The Plant Cell **5,** 553-564.

Herman, P.L., and Marks, M.D. (1989). Trichome development in *Arabidopsis thaliana*. II. Isolation and complementation of the *GLABROUS1* gene. The Plant Cell **1,** 1051-1055.

Hill, J. (1980). Remobilization of nutrients from leaves. Journal of Plant Nutrition **2,** 407-444.

Himelblau, E., and Amasino, R.M. (2001). Nutrients mobilized from leaves of *Arabidopsis thaliana* during leaf senescence. Plant Physiology **158,** 1317-1323.

Hinderhofer, K., and Zentgraf, U. (2001). Identification of a transcription factor specifically expressed at the onset of leaf senescence. Planta **213,** 469-473.

Hirayama, T., Kieber, J.J., Hirayama, N., Kogan, M., Guzman, P., Nourizadeh, S., Alonso, J.M., Dailey, W.P., Dancis, A., and Ecker, J.R. (1999). RESPONSIVE-TO-ANTAGONIST1, a Menkes/Wilson disease-related copper transporter, is required for ethylene signaling in *Arabidopsis*. Cell **97,** 383-393.

Hornung, E., Pernstich, C., and Feussner, I. (2002). Formation of conjugated Delta11 Delta13-double bonds by Delta12-linoleic acid (1,4)-acyl-lipid-desaturase in pomegranate seeds. European Journal of Biochemistry **269,** 4852-4859.

Hörtensteiner, S. (2006). Chlorophyll degradation during senescence. Annual Review of Plant Biology **57,** 55-77.

Hörtensteiner, S., and Feller, U. (2002). Nitrogen metabolism and remobilization during senescence. Journal of Experimental Botany**,** 927-937.

Hua, Z.L., Fatheddin, P., and Graham, T.R. (2002). An essential subfamily of Drs2p-related P-type ATPases is required for protein trafficking between Golgi complex and endosomal/vacuolar system. Molecular Biology of the Cell **13,** 3162-3177.

Huala, E., Dickerman, A.W., Garcia-Hernandez, M., Weems, D., Reiser, L., LaFond, F., Hanley, D., Kiphart, D., Zhuang, M.Z., Huang, W., Mueller, L.A., Bhattacharyya, D., Bhaya, D., Sobral, B.W., Beavis, W., Meinke, D.W., Town, C.D., Somerville, C., and Rhee, S.Y. (2001). The *Arabidopsis* Information Resource (TAIR): A comprehensive database and web-based information retrieval, analysis, and visualization system for a model plant. Nucleic Acids Research **29,** 102-105.

Huang, A.H.C. (1992). Oil Bodies and Oleosins in Seeds. Annual Review of Plant Physiology and Plant Molecular Biology **43,** 177-200.

Hudak, K., Yao, K., and Thompson, J.E. (1995). Release of fluorescent peroxidized lipids from membranes in senescing tissue by bledding of lipid-protein particles. American Society for Horticultural Science **30,** 209-213.

Hudak, K.A., and Thompson, J.E. (1996). Flotation of lipid-protein particles containing triacylglycerol and phospholipid from the cytosol of carnation petals. Physiologia Plantarum **98,** 810-818.

Hugly, S., and Somerville, C. (1992). A role for membrane lipid polyunsaturation in chloroplast biogenesis at lower temperature. Plant Physiology **99,** 197-202.

Inada, N., Sakai, A., and Kuroiwa, H. (1998). Three-dimensional analysis of the senescence program in rice (*Oryza sativa* L.) coleoptiles. Investigations of tissues and cells by fluorescence microscopy. Planta **205,** 153-164.

Ish-Horowicz, D., and Burke, J.F. (1981). Rapid and efficient cosmid cloning. Nucleic Acids Research **9,** 2989-2998.

Jefferson, R.A., Kavanagh, T.A., and Bevan, M.W. (1987). GUS fusions: β-glucuronidase as a sensitive and versatile gene fusion marker in higher plants. EMBO Journal **6,** 3901-3907.

Jing, H.C., Schnippers, J.H., Hille, J., and Dijkwel, P.P. (2005). Ethylene-induced leaf senescence depends on age-related changes and *OLD* genes in *Arabidopsis*. Journal of Experimental Botany **56,** 2915-2923.

Johnston, M., and Davis, R.W. (1984). Sequences that regulate the divergent GAL1-GAL10 promoter in *Saccharomyces cerevisiae*. Molecular and Cellular Biology **4,** 1440-1448.

Joyard, J., Block, M.A., Malherbe, A., Marechal, E., and Douce, R. (1993). Origin and synthesis of galactolipid and sulfolipid head groups. In Lipid metabolism in plants, T.S. Moore, ed (Boca Raton, FL, USA: CRC Press), pp. 231-258.

Karim, S., Holmstrom, K.O., Mandal, A., Dahl, P., Hohmann, S., Brader, G., Palva, E.T., and Pirhonen, M. (2007). AtPTR3, a wound-induced peptide transporter needed for defence against virulent bacterial pathogens in *Arabidopsis*. Planta **225,** 1431-1445.

Karimi, M., Inze, D., and Depicker, A. (2002). GATEWAY vectors for *Agrobacterium*-mediated plant transformation. Trends in Plant Science **7,** 193-195.

Karnovsky, M.J. (1965). A formaldehyde-glutaraldehyde fixative of high osmolality for use in electron microscopy. Journal of Cell Biology **27,** 137-138.

Kates, M., Pugh, E.L., and Ferrante, G. (1984). Regulation of membrane fluidity by lipid desaturases. Biomembranes **12,** 379-395.

Kato, U., Emoto, K., Fredriksson, C., Nakamura, H., Ohta, A., Kobayashi, T., Murakami-Murofushi, K., Kobayashi, T., and Umeda, M. (2002). A novel membrane protein, Ros3p, is required for phospholipid translocation across the plasma membrane in *Saccharomyces cerevisiae*. Journal of Biological Chemistry **277,** 37855-37862.

Katoh, Y., and Katoh, M. (2004). Identification and characterization of *CDC50A*, *CDC50B* and *CDC50C* genes *in silico*. Oncology Reports **12,** 939-943.

Kean, L.S., Fuller, R.S., and Nichols, J.W. (1993). Retrograde lipid traffic in yeast: Identification of two distinct pathways for internalization of fluorescent-labeled phosphatidylcholine from the plasma membrane. Journal of Cell Biology **123,** 1403-1419.

Koncz, C., and Schell, J. (1986). The promoter of TL-DNA gene 5 controls the tissue-specific expression of chimeric genes carried by a novel type of *Agrobacterium* binary vector. Molecular and General Genetics **204,** 383-396.

Kornberg, R.D., and McConnel, H.M. (1971). Inside-outside transitions of phospholipids in vesicle membranes. Biochemistry **10,** 1111-1120.

Krysan, P.J., Young, J.C., and Sussman, M.R. (1999). T-DNA as an insertional mutagen in *Arabidopsis*. The Plant Cell **11,** 2283-2290.

Kühlbrandt, W. (2004). Biology, structure and mechanism of P-type ATPases. Nature Reviews Molecular Cell Biology **5,** 282-295.

Kuroiwa, H., Mori, T., Takahara, M., Miyagishima, S., and Kuroiwa, T. (2002). Chloroplast division machinery as revealed by immunofluorescence and electron microscopy. Planta **215,** 185-190.

Laemmli, U.K. (1970). Cleavage of structural proteins during the assembly of the head of bacterio phage T-4. Nature **227,** 680-685.

Lee, D.W., Bremmeier, S., and Smith, A.P. (1987). The selective advantage of anthocyanins in developing leaves of mango and cocoa. Biotropica **19,** 40-49.

Lee, R.H., and Chen, S.C.G. (2002). Programmed cell death during rice leaf senescence is nonapoptotic. New Phytologist **155,** 25-32.

Leigh, R.A. (1979). Do plant vacuoles degrade cytoplasmic components. Trends in Biochemical Sciences **4,** N37-N38.

Lenoir, G., Williamson, P., and Holthuis, J.C. (2007). On the origin of lipid asymmetry: The flip side of ion transport. Current Opinion in Chemical Biology **11,** 654-661.

Lenoir, G., Williamson, P., Puts, C.F., and Holthuis, J.C. (2009). Cdc50p plays a vital role in the ATPase reaction cycle of the putative aminophospholipid transporter drs2p. Journal of Biological Chemistry **284,** 17956-17967.

Leopold, A.C. (1961). Senescence in plant development: The death of plants or plant parts may be of positive ecological or physiological value. Science **134,** 1727-1732.

Leshem, Y.Y., Sridhara, S., and Thompson, J.E. (1984). Involvement of calcium and calmodulin in membrane deterioration during senescence of pea foliage. Plant Physiology **75,** 329-335.

Li, X., Chanroj, S., Wu, Z., Romanowsky, S.M., Harper, J.F., and Sze, H. (2008). A distinct endosomal Ca2+/Mn2+ pump affects root growth through the secretory process. Plant Physiology **147,** 1675-1689.

Lichtenthaler, H.K. (1987). Chlorophylls and carotenoids: Pigments of photosynthetic biomembranes. Methods in Enzymology **148,** 350-382.

Lim, P.O., Woo, H.R., and Nam, H.G. (2003). Molecular genetics of leaf senescence in *Arabidopsis*. Trends in Plant Science **8,** 272-278.

Lim, P.O., Kim, H.J., and Nam, H.G. (2007). Leaf senescence. Annual Review of Plant Biology **58,** 115-136.

Lin, J.F., and Wu, S.H. (2004). Molecular events in senescing *Arabidopsis* leaves. The Plant Journal **39,** 612-628.

Liu, K., Surendhran, K., Nothwehr, S.F., and Graham, T.R. (2008). P4-ATPase requirement for AP-1/clathrin function in protein transport from the trans-Golgi network and early endosomes. Molecular Biology of the Cell **19,** 3526-3535.

Lohman, K.N., Gan, S., John, M.C., and Amasino, R.D. (1994). Molecular analysis of natural leaf senescence in Arabidopsis thaliana. Physiologia Plantarum **92,** 322-328.

Makino, A., Mae, T., and Ohira, B. (1991). Differences between wheat and rice in the enzymatic properties of ribulose-1,5-bisphosphate carboxylase oxygenase and the relationship to photosythetic gas-exchange. Planta **174,** 30-38.

Masclaux-Daubresse, C., Reisdorf-Cren, M., and Orsel, M. (2008). Leaf nitrogen remobilisation for plant development and grain filling. Plant Biology **10,** 23-36.

Masclaux-Daubresse, C., Purdy, S., Lemitre, T., Pourtau, N., Taconnat, L., Renou, J.P., and Wingler, A. (2007). Genetic variation suggests interaction between cold acclimation and metabolic regulation of leaf senescence. Plant Physiology **143,** 434-446.

Matile, P. (1975). The lytic compartment of plant cells. In Cell biology monographs, M. Alfert, ed (Berlin, Germany: Springer-Verlag.

Matile, P. (1997). The vacuole and cell senescence. Advances in Botanical Research **25,** 87-112.

Matile, P., Hörtensteiner, S., and Thomas, H. (1999). Chlorophyll degradation. Annual Review of Plant Physiology and Plant Molecular Biology **50,** 67-95.

Matyash, V., Liebisch, G., Kurzchalia, T.V., Shevchenko, A., and Schwudke, D. (2008). Lipid extraction by methyl-tert-butyl ether for high-throughput lipidomics. Journal of Lipid Research **49,** 1137-1146.

McKeon, T.A., and Stumpf, P.K. (1982). Purification and characterization of the stearoyl-acyl carrier protein desaturase and the acyl-acyl carrier protein thioesterase from maturing seeds of safflower. Journal of Biological Chemistry **257,** 12141-12147.

Mckersie, B.D., and Thompson, J.E. (1975). Cytoplasmic membrane senescence in bean cotyledons. Phytochemistry **14,** 1485-1491.

Menon, A.K., Watkins, W.E.r., and Hrafnsdottir, S. (2000). Specific proteins are required to translocate phosphatidylcholine bidirectionally across the endoplasmic reticulum. Current Biology **10,** 241-252.

Miao, Y., Laun, T., Zimmerman, P., and Zentgraf, U. (2004). Targets of the WRKY53 transcription factor and its role during leaf senescence in *Arabidopsis*. Plant Molecular Biology **55,** 853-867.

Millar, A.A., Smith, M.A., and Kunst, L. (2000). All fatty acids are not equal: Discrimination in plant membrane lipids. Trends in Plant Science **5,** 95-101.

Miquel, M., and Browse, J. (1992). *Arabidopsis* mutants deficient in polyunsaturated fatty acid synthesis. Biochemical and genetic characterization of a plant oleoyl-phosphatidylcholine desaturase. Journal of Biological Chemistry **267,** 1502-1509.

Miranda, E.J., and Hazel, J.R. (1996). Temperature-induced changes in the transbilayer distribution of phosphatidylethanol-amine in mitoplasts of rainbow trout (*Oncorhynchus mykiss*) liver. Journal of Experimental Zoology **274,** 23-32.

Moore, T.S. (1982). Phospholipid biosynthesis. Annual Review of Physiology **33,** 235-259.

Morth, J.P., Pedersen, B.P., Toustrup-Jensen, M.S., Sørensen, T.L., Petersen, J., Andersen, J.P., Vilsen, B., and Nissen, P. (2007). Crystal structure of the sodium-potassium pump. Nature **450,** 1043-1049.

Mudd, S.H., and Datko, A.H. (1989). Synthesis of methylated ethanolamine moieties: Regulation by choline in soybean and carrot. Plant Physiology **90,** 306-310.

Mullis, K., Faloona, F., Scharf, S., Saiki, R., Horn, G., and Erlich, H. (1986). Specific enzymatic amplification of DNA *in vitro* - the Polymerase Chain Reaction. Cold Spring Harbor Symposia on Quantitative Biology **51,** 263-273.

Murashige, T., and Skoog, F. (1962). A revised medium for rapid growth and bioassays with tobacco tissue cultures. Physiologia Plantarum **15,** 473-497.

Murphy, D.J. (1990). Storage lipid bodies in plants and other organisms. Progress in Lipid Research **29,** 299-324.

Murphy, D.J. (1993). Structure, function and biogenesis of storage lipid bodies and oleosins in plants. Progress in Lipid Research **32,** 247-280.

Murray, H.G., and Thompson, W.F. (1980). Rapid isolation of high molecular weight plant DNA. Nucleic Acids Research **8,** 4321-4325.

Nair, S.J., and Ramaswamy, N.K. (2004). Chloroplast proteases. Biologia Plantarum **48,** 321-326.

Nam, H.G. (1997). The molecular genetic analysis of leaf senescence. Current Opinion in Biotechnology **1,** 200-207.

Natarajan, P., and Graham, T.R. (2006). Measuring translocation of fluorescent lipid derivatives across yeast Golgi membranes. Methods **39,** 163-168.

Neff, M.M., and Chory, J. (1998). Genetic interactions between phytochrome A, phytochrome B, and cryptochrome 1 during *Arabidopsis* development. Plant Physiology **118,** 27-36.

Nelson, B.K., Cai, X., and Nebenfuhr, A. (2007). A multicolored set of in vivo organelle markers for co-localization studies in *Arabidopsis* and other plants. The Plant Journal **51,** 1126-1136.

Nicolson, T., and Mayinger, P. (2000). Reconstitution of yeast microsomal lipid flip-flop using endogenous aminophospholipids. FEBS Letters **476,** 277-281.

Nishida, I., and Murata, N. (1996). Chilling sensitivity in plants and cyanobacteria: The crucial contribution of membrane lipids. Annual Review of Plant Physiology and Plant Molecular Biology **47,** 541-568.

Nishijima, M., Kuge, O., and Akamatsu, Y. (1986). Phosphatidylserine biosynthesis in cultured Chinese hamster ovary cells. I. Inhibition of *de novo* phosphatidylserine biosynthesis by exogenous phosphatidylserine and its efficient incorporation. Journal of Biological Chemistry **261,** 5784-5789.

Nishizuka, Y. (1992). Intracellular signaling by hydrolysis of phospholipids and activation of protein kinase C. Science **258,** 607-614.

Noodén, L.D. (1988). Senescence and ageing in plants. In Whole plant senescence, L.D. Noodén and A.C. Leopolds, eds (San Diego, CA, USA: Academic Press), pp. 391-439.

Noodén, L.D., and Penney, J.P. (2001). Correlative controls of senescence and plant death in *Arabidopsis thaliana* (Brassicaceae). Journal of Experimental Botany **52,** 2151-2159.

Noodén, L.D., Hillsberg, J.W., and Schneider, M.J. (1996). Induction of leaf senescence in *Arabidopsis thaliana* by long days through a light-dosage effect. Physiologia Plantarum **96,** 491-495.

Novick, P., Field, C., and Schekman, R. (1980). Identification of 23 complementation groups required for post-translational events in the yeast secretory pathway. Cell **21,** 205-215.

Odell, J.T., Knowlton, S., Lin, W., and Mauvais, C.J. (1988). Properties of an isolated transcription stimulating sequence derived from the Cauliflower Mosaic Virus *35S* promoter. Plant Molecular Biology **10,** 263-272.

Oh, S.A., Lee, S.Y., Chung, I.K., Lee, C.H., and Nam, H.G. (1996). A senescence-associated gene of *Arabidopsis thaliana* is distinctively regulated during natural and artificially induced leaf senescence. Plant Molecular Biology **30,** 739-754.

Oh, S.A., Park, J.H., Lee, G.I., Paek, K.H., Park, S.K., and Nam, H.G. (1997). Identification of three genetic loci controlling leaf senescence in *Arabidopsis thaliana*. The Plant Journal **12,** 527-535.

Ohlrogge, J.B., and Kuo, T.M. (1985). Plants have isoforms for acyl carrier protein that are expressed differently in different tissues. Journal of Biological Chemistry **260,** 8032-8037.

Opekarová, M., and Tanner, W. (2003). Specific lipid requirements of membrane proteins -- A putative bottleneck in heterologous expression. Biochimica et Biophysica Acta **1610,** 11-22.

Otegui, M.S., Noh, Y.S., Martínez, D.E., Vila Petroff, M.G., Staehelin, L.A., Amasino, R.M., and Guiamet, J.J. (2005). Senescence-associated vacuoles with intense proteolytic activity develop in leaves of *Arabidopsis* and soybean. The Plant Journal **41,** 831-844.

Paulusma, C.C., Folmer, D.E., Ho-Mok, K.S., de Waart, D.R., Hilarius, P.M., Verhoeven, A.J., and Oude Elferink, R.P. (2008). ATP8B1 requires an accessory protein for endoplasmic reticulum exit and plasma membrane lipid flippase activity. Hepatology **47,** 268-278.

Pedersen, P.L. (2007). Transport ATPases into the year 2008: a brief overview related to types, structures, functions and roles in health and disease. Journal of Bioenergetics and Biomembranes **39,** 349-355.

Pedersen, P.L., and Carafoli, E. (1987). Ion motive ATPases. I. Ubiquity, properties, and significance to cell function. Trends in Biochemical Sciences **4,** 146-150.

Pérez-Victoria, F.J., Sánchez-Cañate, M.P., Castanys, S., and Gamarro, F. (2006). Phospholipid translocation and miltefosine potency require both *L. donovani* mitefosine transforter and the new protein LdRos3 in *Leishmania* parasites. Journal of Biological Chemistry **281,** 23766-23775.

Pomorski, T., and Menon, A.K. (2006). Lipid flippases and their biological functions. Cellular and Molecular Life Sciences **63,** 2908-2921.

Pomorski, T., Holthuis, J.C., Herrmann, A., and van Meer, G. (2004). Tracking down lipid flippases and their biological functions. Journal of Cell Science **117,** 805-813.

Pomorski, T., Lombardi, R., Riezman, H., Devaux, P.F., van Meer, G., and Holthuis, J.C. (2003). Drs2p-related P-type ATPases Dnf1p and Dnf2p are required for phospholipid translocation across the yeast plasma membrane and serve a role in endocytosis. Molecular Biology of the Cell **14,** 1240-1254.

Porra, R.J., Thompson, W.A., and Kriedemann, P.E. (1989). Determination of accurate extinction coefficients and simultaneous equations for assaying chlorophylls a and b extracted with four different solvents verification of the concentration of chlorophyll standards by atomic absorption spectroscopy. Biochimica et Biophysica Acta **975,** 384-394.

Poulsen, L.R., López-Marqués, R.L., and Palmgren, M.G. (2008a). Flippases: Still more questions than answers. Cellular and Molecular Life Sciences **65,** 3119-3125.

Poulsen, L.R., Lopez-Marques, R.L., McDowell, S.C., Okkeri, J., Licht, D., Schulz, A., Pomorski, T., Harper, J.F., and Palmgren, M.G. (2008b). The *Arabidopsis* P4-ATPase ALA3 localizes to the golgi and requires a beta-subunit to function in lipid translocation and secretory vesicle formation. The Plant Cell **20,** 658-676.

Pourtau, N., Jennings, R., Pelzer, E., Pallas, J., and Wingler, A. (2006). Effect of sugar-induced senescence on gene expression and implications for the regulation of senescence in *Arabidopsis*. Planta **224,** 556-568.

Prins, A., van Heerden, P.D., Olmos, E., Kunert, K.J., and Foyer, C.H. (2008). Cysteine proteinases regulate chloroplast protein content and composition in tobacco leaves: A model for dynamic interactions with ribulose-1,5-bisphosphate carboxylase/ oxygenase (Rubisco) vesicular bodies. Journal of Experimental Botany **59,** 1935-1950.

Puts, C.F., and Holthuis, J.C.M. (2009). Mechanism and significance of P4 ATPase-catalyzed lipid transport: Lessons from a Na+/K+ -pump. Biochimica et Biophysica Acta **1791,** 603-611.

Quinn, P.J. (2002). Plasma membrane phospholipid asymmetry. Subcellular Biochemistry **36,** 29-60.

Quirino, B.F., Reiter, W.D., and Amasino, R.D. (2001). One of two tandem *Arabidopsis* genes homologous to monosaccharide transporters is senescence-associated. Plant Molecular Biology **46,** 447-457.

Quirino, B.F., Noh, Y.S., Himmelblau, E., and Amasino, R.M. (2000). Molecular aspects of leaf senescence. Trends in Plant Science **5,** 278-282.

Rawyler, A., and Siegenthaler, P.A. (1981). Transmembrane distribution of phospholipids and their involvement in electron transport, as revealed by phospholipids A2 treatment of spinach thylakoids. Biochimica et Biophysica Acta **635,** 348-358.

Reynolds, E.S. (1963). Use of lead citrate at high Ph as an electron-opaque stain in electron microscopy. Journal of Cell Biology **17,** 208-212.

Ripmaster, T.L., Vaughn, G.P., and Woolford, J.L.J. (1993). *DRS1* to *DRS7*, novel genes required for ribosome assembly and function in *Saccharomyces cerevisiae*. Molecular & Cellular Biology **13,** 7901-7912.

Robatzek, S., and Somssich, I.E. (2001). A new member of the *Arabidopsis* WRKY transcription factor family, AtWRKY6, is associated with both senescence- and defence-related processes. The Plant Journal **28,** 123-133.

Rose, A.B., and Broach, J.R. (1990). Propagation and expression of cloned genes in yeast: 2-microns circle-based vectors. Methods in Enzymology **185,** 234-279.

Rosso, M.G., Li, Y., Strizhov, N., Reiss, B., Dekker, K., and Weisshaar, B. (2003). An *Arabidopsis thaliana* T-DNA mutagenized population (GABI-Kat) for flanking sequence tag-based reverse genetics. Plant Molecular Biology **53,** 247-259.

Roughan, P.G., and Slack, C.R. (1982). Cellular organization of glycerolipid metabolism. Annual Review of Plant Physiology **33,** 97-132.

Roughan, P.G., Holland, R., and Slack, C.R. (1980). The role of chloroplasts and microsomal fractions in polar-lipid synthesis from [1-14C]acetate by cell-free preparations from spinach (*Spinacia oleracea*) leaves. Biochemical Journal **188,** 17-24.

Rozen, S., and Skaletsky, H.J. (2000). Primer3 on the WWW for general users and for biologist programmers. In Bioinformatics Methods and protocols: Methods in molecular biology, S. Krawetz and S. Misener, eds (Totowa, NJ, USA: Humana Press), pp. 365-386.

Saito, K., Fujimura-Kamada, K., Furuta, N., Kato, U., Umeda, M., and Tanaka, K. (2004). Cdc50p, a protein required for polarized growth, associates with the Drs2p P-type ATPase implicated in phospholipid translocation in *Saccharomyces cerevisiae*. Molecular Biology of the Cell **15,** 3418-3432.

Sambrook, J., Fritsch, E.F., and Maniatis, T. (1989). Molecular cloning: A laboratory manual. (Cold Spring Harbor, NY, USA: Cold Spring Harbor Laboratory Press).

Sato, N., and Tsuzuki, M. (2004). Isolation and identification of chloroplast lipids. Methods in Molecular Biology **274,** 149-157.

Scholl, R.L., May, S.T., and Ware, D.H. (2000). Seed and molecular resources for *Arabidopsis*. Plant Physiology **124,** 1477-1480.

Schulz, A., Kuhn, C., Riesmeier, J.W., and Frommer, W.R. (1998). Ultrastructural effects in potato leaves due to antisense-inhibition of the sucrose transporter indicate an apoplasmic mode of phloem loading. Planta **206,** 533-543.

Schwacke, R., Schneider, A., van der Graaff, E., Fischer, K., Catoni, E., Desimone, M., Frommer, W.B., Flügge, U.I., and Kunze, R. (2003). Aramemnon, a novel database for *Arabidopsis* integral membrane proteins. Plant Physiology **131,** 16-26.

Seigneuret, M., and Devaux, P.F. (1984). ATP-dependent asymmetric distribution of spin-labeled phospholipids in the erythrocyte-membrane - Relation to shape changes. Proceedings of the National Academy of Sciences of the United States of America **81,** 3751-3755.

Shaner, N.C., Campbell, R.E., Steinbach, P.A., Giepmans, B.N.G., Palmer, A.E., and Tsien, R.Y. (2004). Improved monomeric red, orange and yellow fluorescent protein derived from *Discosoma sp.* red fluorescent protein. Nature Biotechnology **22,** 1567-1572.

Shanklin, J., and Somerville, C. (1991). Stearoyl-acyl-carrier-protein desaturase from higher plants is structurally unrelated to the animal and fungal homologs. Proceedings of the National Academy of Sciences of the United States of America **88,** 2510-2514.

Shiao, Y.J., Balcerzak, B., and Vance, J.E. (1998). A mitochondrial membrane protein is required for translocation of phosphatidylserine from mitochondria-associated membranes to mitochondria. Biochemical Journal **331,** 217-223.

Sitte, P. (1977). Chromoplasten - bunte Objekte der modernen Zellbiologie. Biologie in unserer Zeit **7,** 65-74.

Smart, C.M. (1994). Gene expression during leaf senescence. New Phytologist **126,** 419-448.

Somerville, C., Browse, J., Jaworski, J.G., and Ohlrogge, J.B. (2000). Lipids. (Rockville, ML, USA: American Society of Plant Physiologists).

Soupene, E., Kemaladewi, D.U., and Kuypers, F.A. (2008). ATP8AI activity and phosphatidylserine transbilayer movement. Journal of Receptor, Ligand and Channel Research **1,** 1-10.

Southern, E.M. (1975). Detection of specific sequences among dna fragments separated by gel electrophoresis. Journal of Molecular Biology **98,** 503-517.

Sparkes, I.A., Runions, J., Kearns, A., and Hawes, C. (2006). Rapid, transient expression of fluorescent fusion proteins in tobacco plants and generation of stably transformed plants. Nature Protocols **1,** 2019-2025.

Sprong, H., van der Sluijs, P., and van Meer, G. (2001). How proteins move lipids and lipids move proteins. Nature Reviews Molecular Cell Biology **2,** 504-513.

Spurr, A.R. (1969). A low-viscosity epoxy resin embedding medium for electron microscopy. Journal of Ultrastructure Research **26,** 31-43.

Starling, A.P., East, J.M., and Lee, A.G. (1995). Effects of gel phase phospholipid on the Ca(2+)-ATPase. Biochemistry **34,** 3084-3091.

Stevens, H.C., Malone, L., and Nichols, J.W. (2008). The putative aminophospholipid translocases, DNF1 and DNF2, are not required for 7-nitrobenz-2-oxa-1,3-diazol-4-yl-phosphatidylserine flip across the plasma membrane of *Saccharomyces cerevisiae*. Journal of Biological Chemistry **283,** 35060-35069.

Sune, A., Bettebobillo, P., Bienvenue, A., Fellmann, P., and Devaux, P.F. (1987). Selective outside inside translocation of aminophospholipids in human platelets. Biochemistry **26,** 2972-2978.

Szczegielniak, J., Liwosz, A., Jurkowski, I., Loog, M., Dobrowolska, G., Ek, P., Harmon, A.C., and Muszyńska, G. (2000). Calcium-dependent protein kinase from maize seedlings activated by phospholipids. European Journal of Biochemistry **267,** 3818-3827.

Tang, X., Halleck, M.S., Schlegel, R.A., and Williamson, P. (1996). A subfamily of P-type ATPases with aminophospholipid transporting activity. Science **272,** 1495-1497.

Tavernier, E., and Pugin, A. (1995). Transbilayer distribution of phosphatidylcholine and phosphatidylethanolamine in the vacuolar membrane of *Acer pseudoplatanus* cells. Biochimie **77,** 174-181.

Thomas, H., and Stoddart, J.L. (1980). Leaf senescence. Annual Review of Plant Physiology and Plant Molecular Biology **31,** 83-111.

Thomas, H., and Donnison, I. (2000). Back from the brink: Plant senescence and its reversibility. In Programmed cell death in animals and plants, J.A. Bryant, S.G. Hughes, and J.M. Garland, eds (Oxford, UK: Bios), pp. 149-162.

Thomas, H., Ougham, H.J., and Hörtensteiner, S. (2001). Recent advances in the cell biology of chlorophyll catabolism. Advances in Botanical Research **35,** 1-52.

Thomas, H., Ougham, H.J., Wagstaff, C., and Stead, A.D. (2003). Defining senescence and death. Journal of Experimental Botany **54,** 1127-1132.

Thompson, A.R., and Vierstra, R.D. (2005). Autophagic recycling: Lessons from yeast help define the process in plants. Current Opinion in Plant Biology **8,** 165-173.

Thompson, J., Taylor, C., and Wang, T.W. (2000). Altered membrane lipase expression delays leaf senescence. Biochemical Society Transactions **28,** 775-777.

Thompson, J.E. (1988). The molecular basis for membrane deterioration during senescence. In Senescence and ageing plants, L.D. Noodén and A.C. Leopold, eds (San Diego, CA, USA: Academic Press), pp. 52-84.

Thompson, J.E., Legge, R.L., and Barber, R.F. (1987). The role of free radicals in senescence and wounding. New Phytologist **105,** 317-344.

Thompson, J.E., Froese, C.D., Hong, Y., Hudak, K., and Smith, M.D. (1997). Membrane deterioration during senescence. Canadian Journal of Botany **75,** 867-879.

Thompson, J.E., Froese, C.D., Madey, E., Smith, M.D., and Hong, Y. (1998). Lipid metabolism during plant senescence. Progress in Lipid Research **37,** 119-141.

Thomson, W.W., and Platt-Aloia, K.A. (1987). Ultrastructure and senescence in plants. In Plant senescence: Its biochemistry and physiology, W.W. Thomson, E. Nothnagel, and R.C. Huffacker, eds (Rockville, MD, USA: American Society of Plant Physiologists), pp. 20-30.

Towbin, H., Gordon, J., and Staehelin, T. (1979). Electrophoretic transfer of proteins from poly acrylamide gels to nitro cellulose sheets procedure and some applications. Proceedings of the National Academy of Sciences of the United States of America **76,** 4350-4354.

Toyoshima, C., and Mizutani, T. (2004). Crystal structure of the calcium pump with a bound ATP analogue. Nature **430,** 529-535.

Tripodi, G., and Gargiulo, G.M. (1984). Relationships among membranes in plastids of the red alga *Nitophyllum punctatum* (Stackh.) Grev. Protoplasma **119,** 55-61.

Unitt, M.D., and Harwood, J.L. (1982). Lipid topography of thylokoid membranes. In Biochemistry and metabolism of plant lipids, J.F.G.M. Wintermans and P.J.C. Kuiper, eds (Amsterdam, The Netherlands: Elsevier/North Holland Biomedical Press), pp. 359-362.

van der Graaff, E., Schwacke, R., Schneider, A., Desimone, M., Flügge, U.I., and Kunze, R. (2006). Transcription analysis of *Arabidopsis* membrane transporters and hormone pathways during developmental and induced leaf senescence. Plant Physiology **141,** 776-792.

van Doorn, W.G., and Woltering, E.J. (2004). Senescence and programmed cell death: substance or semantics? Journal of Experimental Botany **55,** 2147-2153.

van Meer, G. (2000). Cellular organelles: How lipids get there, and back. Trends in Cell Biology **10,** 550-552.

van Meer, G., Voelker, D.R., and Feigenson, G.W. (2008). Membrane lipids: Where they are and how they behave. Nature Reviews Molecular Cell Biology **9,** 112-124.

Vance, J.E., and Shiao, Y.J. (1996). Intracellular trafficking of phospholipids: import of phosphatidylserine into mitochondria. Anticancer Research **16,** 1333-1339.

Villalba, J.M., Palmgren, M.G., Berberián, G.E., Fergusion, C., and Serrano, R. (1992). Functional expression of plant plasma membrane H(+)-ATPase in yeast endoplasmic reticulum. Journal of Biological Chemistry **267,** 12341-12347.

Voelker, D.R. (2000). Interorganelle transport of aminoglycerophospholipids. Biochimica et Biophysica Acta **1486,** 97-107.

Wada, S., Ishida, H., Izumi, M., Yoshimoto, K., Ohsumi, Y., Mae, T., and Makino, A. (2009). Autophagy plays a role in chloroplast degradation during senescence in individually darkened leaves. Plant Physiology **149,** 885-893.

Ward, J.M. (2001). Identification of novel families of membrane proteins from the model plant *Arabidopsis thaliana*. Bioinformatics **17,** 560-563.

Weaver, L.M., and Amasino, R.M. (2001). Senescence is induced in individually darkened *Arabidopsis* leaves but inhibited in whole dark plants. Plant Physiology **127,** 876-886.

Weaver, L.M., Gan, S., Quirino, B., and Amasino, R.M. (1998). A comparison of the expression patterns of several senescence-associated genes in response to stress and hormone treatment. Plant Molecular Biology **37,** 455-469.

Weigel, D., and Glazebrook, J. (2002). Arabidopsis: A laboratory manual. (Cold Spring Harbor, NY, USA: Cold Spring Harbour Laboratory Press).

Wicky, S., Schwarz, H., and Singer-Krüger, B. (2004). Molecular interactions of yeast Neo1p, an essential member of the Drs2 family of aminophospholipid translocases, and its role in membrane trafficking within the endomembrane system. Molecular and Cellular Biology **24,** 7402-7418.

Williamson, P., and Schlegel, R.A. (1994). Back and forth: The regulation and function of transbilayer phospholipid movement in eukaryotic cells. Molecular Membrane Biology **11,** 199-216.

Wingler, A., Mares, M., and Pourtau, N. (2004). Spatial patterns and metabolic regulation of photosynthetic parameters during leaf senescence. New Phytologist **161,** 781-789.

Wingler, A., Brownhill, E., and Pourtau, N. (2005). Mechanisms of the light-dependent induction of cell death in tobacco plants with delayed senescence. Journal of Experimental Botany **56,** 2897-2905.

Winkler, K., Leneweit, G., and Schubert, R. (2005). Characterization of membrane vesicles in plant extracts. Colloids and Surfaces B: Biointerfaces **45,** 57-65.

Winter, D., Vinegar, B., Nahal, H., Ammar, R., Wilson, G.V., and Provart, N.J. (2007). An "Electronic Fluorescent Pictrograph" browser for exploring and analyzing large-scale biological data sets. PLoS ONE **2,** e718.

Woeste, K.E., and Kieber, J.J. (2000). A strong loss-of-function mutation in RAN1 results in constitutive activation of the ethylene response pathway as well as a rosette-lethal phenotype. The Plant Cell **12,** 443-455.

Woo, H.R., Chung, K.M., Park, J.H., Oh, S.A., Ahn, T., Hong, S.H., Jang, S.K., and Nam, H.G. (2001). ORE9, an F-box protein that regulates leaf senescence in *Arabidopsis*. The Plant Cell **13,** 1779-1790.

Woodson, W.R., and Handa, A.K. (1987). Changes in protein patterns and *in vivo* protein synthesis during presenescence and senescence of hibiscus petals. Journal of Plant Physiology **128,** 67-75.

Woolhouse, H.W. (1984). The biochemistry ans regulation of senescence in chloroplasts. Canadian Journal of Botany **62,** 2934-2942.

Xiong, Y., Contento, A.L., and Bassham, D.C. (2005). AtATG18a is required for the formation of autophagosomes during nutrient stress and senescence in *Arabidopsis thaliana*. The Plant Journal **42,** 535-546.

Yadegari, R., Paiva, G., Laux, T., Koltunow, A.M., Apuya, N., Zimmerman, J.L., Fischer, R.L., Harada, J.J., and Goldberg, R.B. (1994). Cell differentiation and morphogenesis are uncoupled in *Arabidopsis* raspberry embryos. The Plant Cell **6,** 1713-1729.

Yao, K., Paliayath, G., and Thompson, J.E. (1991a). Nonsedimentable microvesicles from senescing bean cotyledons contain gel phase-forming phospholipid degradation products. Plant Physiology **97,** 502-508.

Yao, K., Paliayath, G., Humphrey, R.W., Hallett, F.R., and Thompson, J.E. (1991b). Identification and characterization of nonsedimentable lipid-protein microvesicles. Proceedings of the National Academy of Sciences of the United States of America **88,** 2269-2273.

Yoo, S.Y., Bomblies, K., Yoo, S.K., Yang, J.W., Choi, M.S., Lee, J.S., Weigel, D., and Ahn, J.H. (2005). The *35S* promoter used in a selectable marker gene of a plant transformation vector affects the expression of the transgene. Planta **221,** 523-530.

Yoshida, S. (2003). Molecular regulation of leaf senescence. Current Opinion in Plant Biology **6,** 79-84.

Yoshimoto, K., Hanaoka, H., Sato, S., Kato, T., Tabata, S., Noda, T., and Ohsumi, Y. (2004). Processing of ATG8s, ubiquitin-like proteins, and their deconjugation by ATG4s are essential for plant autophagy. The Plant Cell **16,** 2967-2983.

Yu, B., Xu, C., and Benning, C. (2002). *Arabidopsis* disrupted in SQD2 encoding sulfolipid synthase is impaired in phosphate-limited growth. Proceedings of the National Academy of Sciences of the United States of America **99,** 5732-5737.

Zachowski, A. (1993). Phospholipids in animal eukaryotic membranes - transverse asymmetry and movement. Biochemical Journal **294,** 1-14.

Zachowski, A., Henry, J.P., and Devaux, P.F. (1989). Control of transmembrane lipid asymmetry in chromaffin granules by an ATP-dependent protein. Nature **340,** 75-76.

Zavaleta-Mancera, H.A., Thomas, B.J., Thomas, H., and Scott, I.M. (1999a). Regreening of *Nicotiana* leaves. II. Redifferentiation of plastids. Journal of Experimental Botany **50,** 1683-1689.

Zavaleta-Mancera, H.A., Franklin, K.A., Ougham, H.J., Thomas, H., and Scott, I.M. (1999b). Regreening of *Nicotiana* leaves. I. Reappearance of NADPH-protochlorophyllide oxidoreductase and light-harvesting chlorophyll a/b-binding protein. Journal of Experimental Botany **50,** 1677-1682.

Zentgraf, U., Jobst, J., Kolb, D., and Rentsch, D. (2004). Senescence-related gene expression profiles of rosette leaves of *Arabidopsis thaliana*: leaf age versus plant age. Plant Biology **6,** 178-183.

Zimmerman, S.B., and Pheiffer, B.H. (1983). Macro molecular crowding allows blunt end ligation by DNA ligases from rat liver or *Escherichia coli*. Proceedings of the National Academy of Sciences of the United States of America **80,** 5852-5856.

Zimmermann, P., and Zentgraf, U. (2005). The correlation between oxidative stress and leaf senescence during plant development. Cellular and Molecular Biology Letters **10,** 515-534.

8 APPENDIX

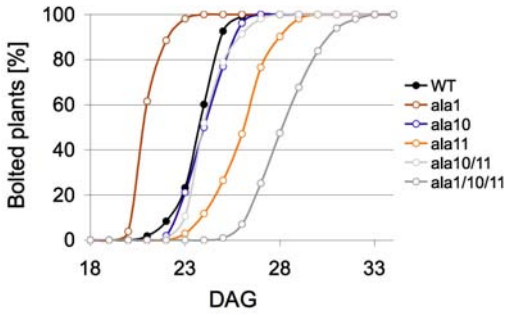

Figure 42: Bolting of *ala* mutant and wild type plants. Diagram depicts percentage of bolted plants (5.10 stadium according to Boyes *et al.*, 2001) during development (n=108).

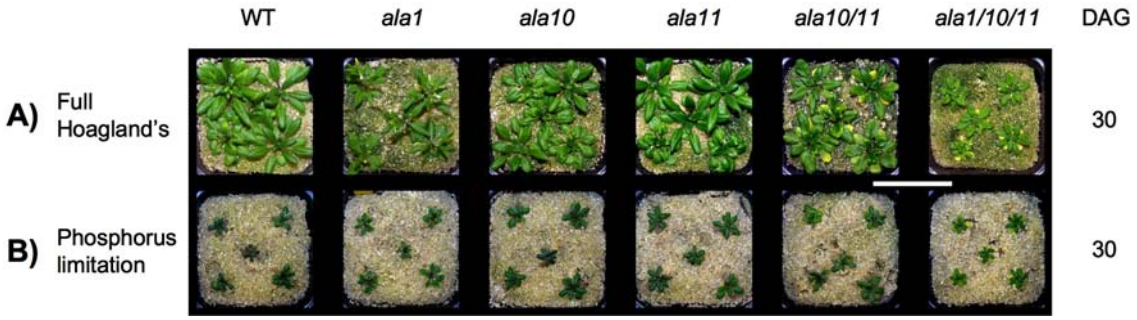

Figure 43: Phenotypes of *ala* mutant lines compared to wild type under A) full nutrition (0.5 mM P_i) and B) phosphorus limitation (10 µM P_i). Depicted are representative examples at 30 DAG (five plants per pot). Scale bar: 10 cm.

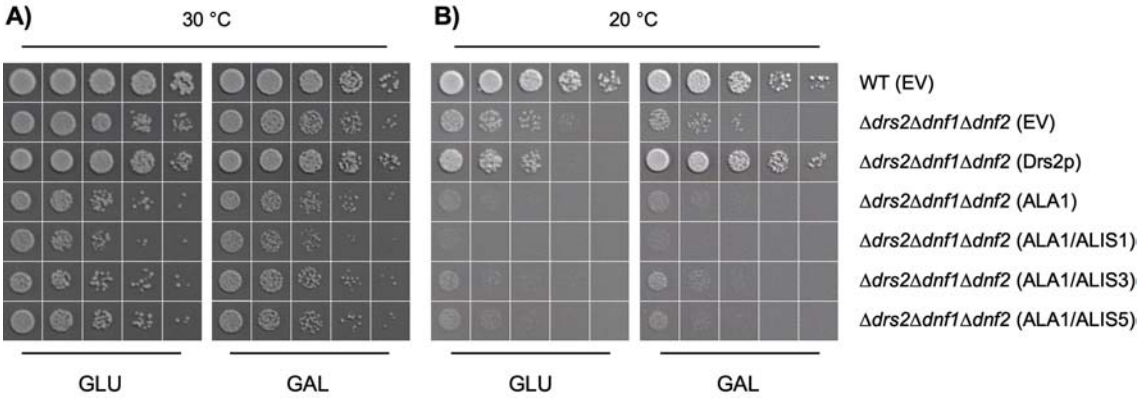

Figure 44: Drop-test with ALA1. Depicted are 1:5 dilution series (left to right) of yeast strains BY4741 (WT) and ZHY709 (Δ*drs2*Δ*dnf1*Δ*dnf2*) transformed with vectors containing ALA1 either alone or in combination with ALIS1, 3 or 5 under the control of a bidirectional galactose-inducible promoter. EV empty vector control. 3 µl drops of cells grown on SD media supplemented with 2% glucose (GLU; non-inducing condition) or 1% galactose and 1% fructose (GAL; inducing condition) for A) 2 days at 30 °C, B) 5 days at 20 °C.

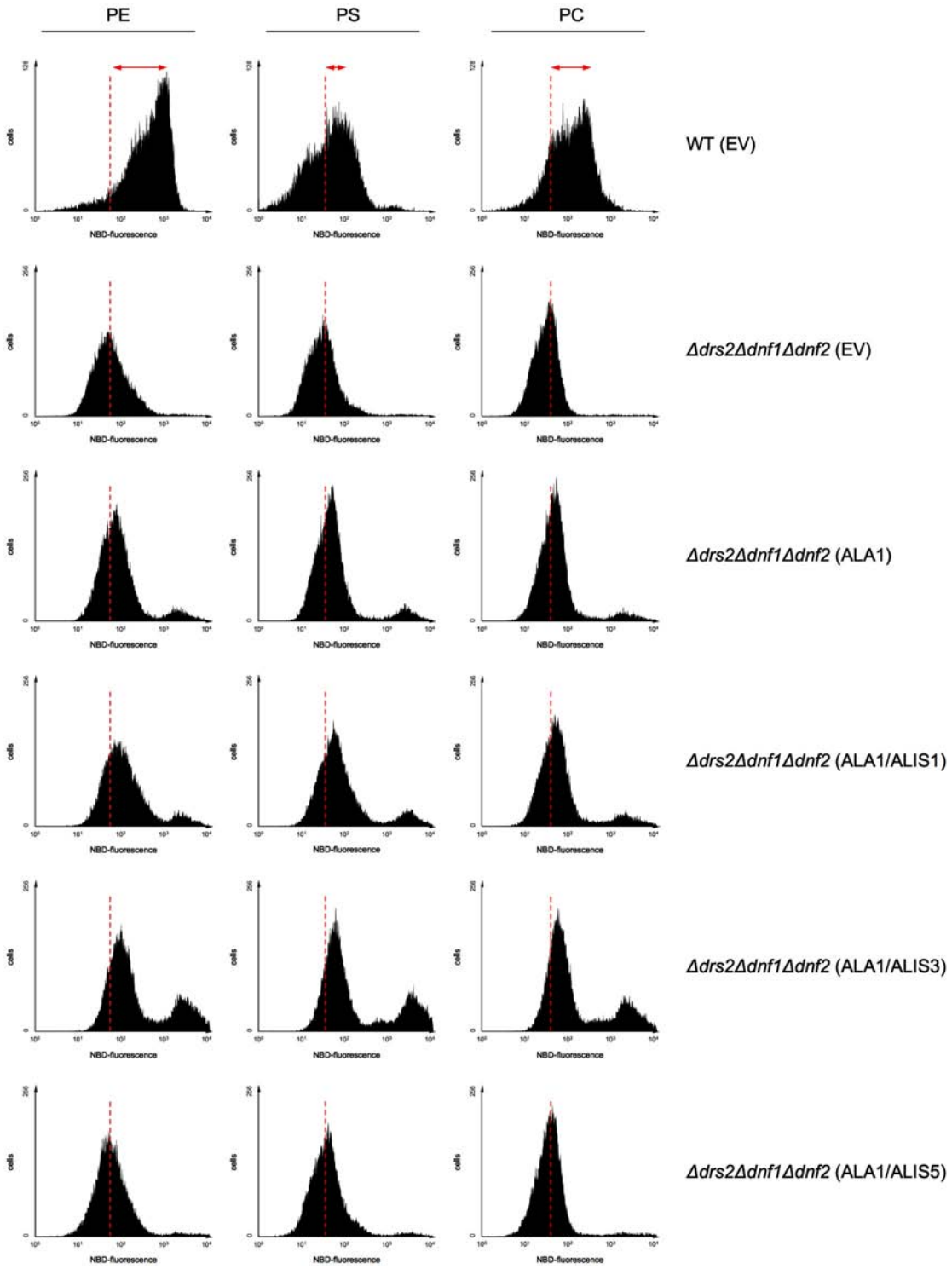

Figure 45: FACS analysis of yeast cells incubated with NBD-labeled PL. Depicted are representative histograms (cell number over fluorescence intensity) of 20000 cells (gating of PI stained dead cells) each for WT and △*drs2*△*dnf1*△*dnf2* cells harboring either the empty expression plasmid (EV) or expression plasmid with *ALA1*, *ALA1*/*ALIS1*, *ALA1*/*ALIS3* and *ALA1*/*ALIS5*. Red dotted lines indicate background fluorescence (of unlabeled cells [data not shown]), red arrows indicate cell populations with increased fluorescence.

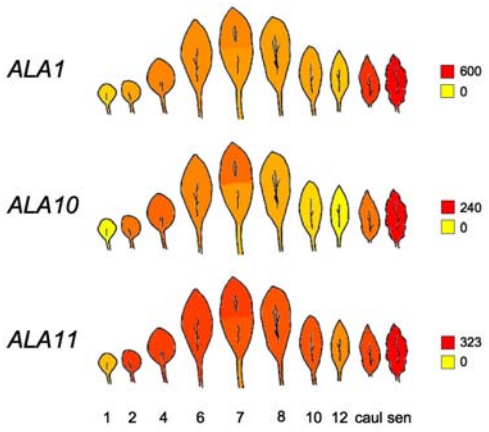

Figure 46: Visualized microarray expression data of *ALA1*, *10* and *11* in leaves of *Arabidopsis thaliana*. Depicted are different developmental leaf statuses (1-12, caul cauline leaf, senescence senescent leaf). Colors indicate expression intensity (yellow: low, red: high). Data taken from the Electronic Fluorescent Pictrograph (Winter *et al.*, 2007).

Acknowledgements

I thank Prof. Dr. Reinhard Kunze (Institut für angewandte Genetik, Freie Universität Berlin) for the opportunity to work in his group, for the supervision, the interesting research topic of foliar senescence and for the great chance to perform parts of my research in different laboratories.

In addition I thank Prof. Dr. Bernd Müller-Röber (Institut für Biologie und Biochemie, Universität Potsdam) for his offer as a second referee.

Furthermore, I'd like to thank:

Prof. Dr. Ivo Feussner and Dr. Cornelia Göbel (Zentrum für molekulare Biowissenschaften, Georg-August-Universität Göttingen) for the fruitful cooperation and the kind supervision during my stays in their group.

Prof. Dr. Thomas Pomorski (Institut für Biologie und Biophysik, Humbold Universität Berlin) for the excellent supervision and pleasant cooperation over months in his laboratory.

Dr. Rudi Lurz and Beatrix Fauler for the permission to work in their group (Max-Planck-Institut für molekulare Genetik, Berlin), for their supervision and their friendly support.

All members of the Kunze group for their help and the great atmosphere in the laboratory and encouragement whenever problems arose, especially Alexis Kasaras, My-Linh Du, Dr. Katina Lazarow and Dr. Christine Rausch.

Prof. Dr. Michael Gjedde Palmgren, Dr. Lisbeth Rosager Poulsen and Dr. Rosa Laura López Marqués (Institut for Plantebiologi og Bioteknologi, Universitet København) for their support and interest in my work providing me with yeast strains and plasmids.

Dr. Kerstin Holst and Dr. Tal Pery for the critical review of my manuscripts.

Most of all I thank my dear friends and family for their support of any kind. Without them this dissertation would have never been possible.

Eidesstattliche Erklärung

Hiermit versichere ich, die vorliegende Arbeit selbsständig angefertigt und keine anderen als die angegebenen Quellen und Hilfsmittel verwendet zu haben. Weiterhin erkläre ich, dass diese Arbeit an keiner anderen Hochschule als der Freien Universität Berlin eingereicht wurde.

Berlin, den 11. März 2010